SP-1233 (2)

REPORTS FOR MISSION SELECTION

THE FOUR CANDIDATE EARTH EXPLORER CORE MISSIONS

Gravity Field and Steady-State Ocean Circulation Mission

Land-Surface Processes and Interactions Mission

Earth Radiation Mission

Atmospheric Dynamics Mission

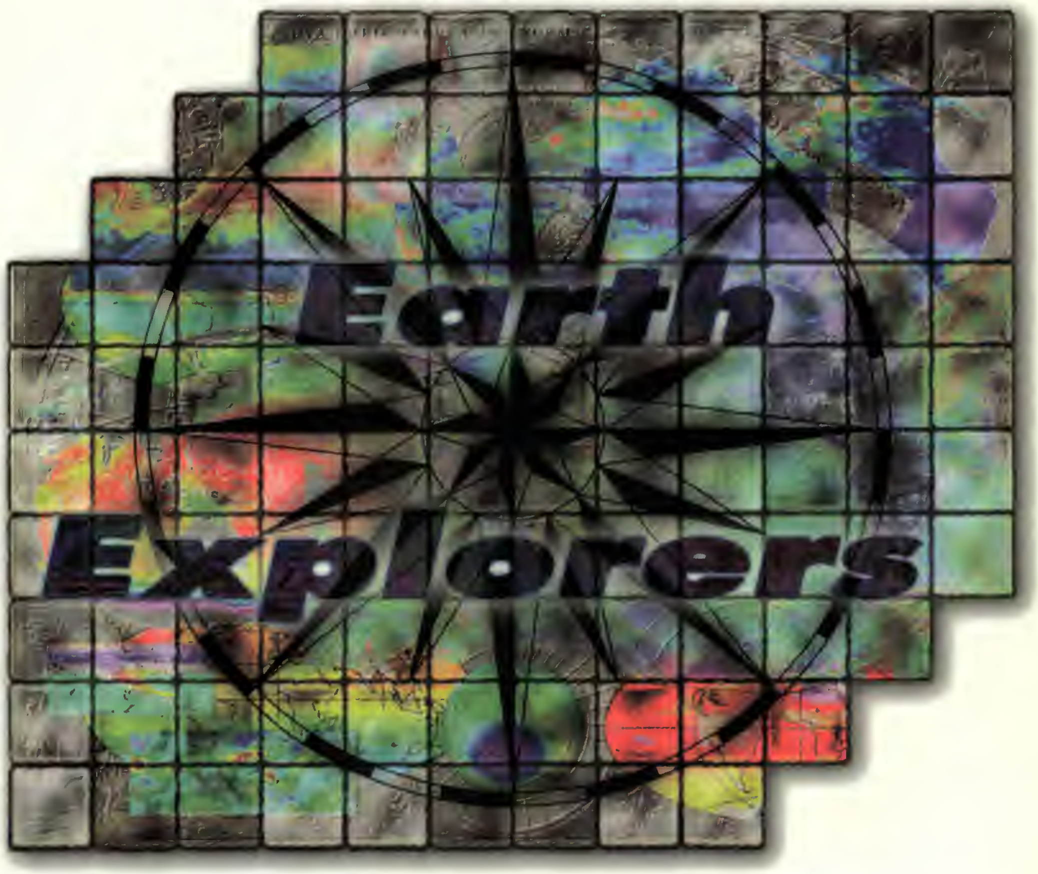

European Space Agency
Agence spatiale européenne

ESA SP-1233 (2)
July 1999

Reports for Mission Selection
THE FOUR CANDIDATE EARTH EXPLORER CORE MISSIONS

Land-Surface Processes and Interactions Mission

European Space Agency
Agence spatiale européenne

ESA SP-1233 (2) – The Four Candidate Earth Explorer Core Missions –
LAND-SURFACE PROCESSES AND INTERACTIONS

Report prepared by:	Earth Sciences Division *Scientific Co-ordinator:* Michael Rast Earth Observation Preparatory Programme *Technical Co-ordinator:* Pierluigi Silvestrin
Cover:	Richard Francis & Carel Haakman
Published by:	ESA Publications Division c/o ESTEC, Noordwijk, The Netherlands *Editor:* Bruce Battrick
Copyright:	© 1999 European Space Agency ISBN 92-9092-528-0
Price:	70 DFl

CONTENTS

… where man has gone before …

1 Introduction

The Living Planet Programme document (ESA SP-1227) describes the plans for the European Space Agency's new strategy for Earth Observation in the post-2000 time frame. It marks a new era for European Earth Observation based on smaller more focused missions and a programme that is user driven, covering the whole spectrum of interests ranging from scientific research-driven Earth Explorer missions through to application-driven Earth Watch missions. The user community is therefore now able to look forward to a programme of more frequent, but very specific missions directed at the fundamental problems of Earth system sciences.

Out of the nine Earth Explorer core missions identified in ESA SP-1196 (1-9), four core missions were selected for Phase-A studies, which began in June 1998, namely: the Land-Surface Processes and Interactions Mission; the Earth Radiation Mission; the Gravity Field and Steady-State Ocean Circulation Mission; and the Atmospheric Dynamics Mission. The Phase-A studies were all completed in June 1999 and drawing on the findings emerging from this work and complementary scientific and technical support studies, Reports for Mission Selection have been written for all four.

This Report for Mission Selection for the Land-Surface Processes and Interactions Core Mission (hereafter LSPIM) was prepared by a Core Mission Drafting Team consisting of five members of the LSPIM Mission Advisory Group (MAG): F. Baret,

W. Mauser, M. Menenti, J. Settle and M. Verstraete. They were supported by the other MAG members, V. Caselles, E. Lambin, J. Miller, M. Schaepman and M.P. Stoll. The technical content of the report (notably Chapter 6) has been compiled by the Executive based on inputs provided by the industrial Phase-A contractor. Others who, in various ways, have contributed to the report are listed in the Acknowledgements.

The primary goal of this mission is the provision of bio-geophysical variables to increase the understanding of bio-geophysical processes and land/atmosphere interactions at the local scale and advance the understanding of these processes and interactions on a global scale.

This report describes the objectives and scientific requirements of the LSPIM mission. It provides evidence of the scientific objectives and technical maturity of the mission elements and system concept, including new and advanced understanding and knowledge acquired since the User Consultation Meeting in Granada in May 1996. Moreover, it provides guidelines for the technical implementation of the mission, and defines and outlines the ground segment structure including data processing, archiving and distribution. Key inputs to this report have to some extent been provided by the outcome and findings of recent scientific and technical support studies which ESA initiated in parallel with the LSPIM Phase-A study.

This report, together with those for the other three Earth Explorer Core Missions, which recently completed their Phase-A studies, is being circulated within the Earth Observation research community in preparation for the User Consultation Workshop in Granada (Spain) in October 1999.

The information in this report is intended to give a detailed insight into the scientific and technical aspects of the proposed mission. It is structured in the following way:

- Chapter 2 introduces the processes on the land surface and their interactions with other components of the Earth system, the issues of concern, which motivate research in this field, the general and specific research needs and the role remote sensing information and land-surface process models play. In so doing it provides evidence for the need for an observing system providing the requisite data for this area of research.
- Drawing on these arguments, Chapter 3 lays out the research objectives linked to the research needs identified in Chapter 2 by giving a detailed overview of the key land-surface processes and interactions considered by the mission and the related variables and observables that need to be measured in fulfilling the missions focused aims.
- Chapter 4 addresses the mission goal and outlines the corresponding observational requirements in terms of spectral, geometric and temporal sampling and the way in which radiance measurements will be converted into variables for land-surface processes and interactions models. In that way the

framework is being laid out for a space-borne observing system that will take full account of the observation requirements that need to be satisfied to achieve the mission goal.

- Chapter 5 provides an overview of the various mission elements, including the space-, field-, and ground segment of the LSPIM.
- Based on the observational requirements and the requisite mission elements, Chapter 6 presents and explains the complete technical description of the proposed space-borne observing system and its capability to fulfil each of the previous observational requirements.
- Chapter 7 continues with a discussion of the proposed data processing and the basic algorithms that will be used to convert the spectral and directional measurements into spatially distributed fields of variables needed to improve models describing land-surface processes and interactions and the methodology to assimilate the measurements into the models.
- Chapter 8 provides by comparison the expected mission performance versus the corresponding requirements and focuses in particular on the quantitative accuracy aspired for the retrieval of the variables in relation to the requirements of process models. In that way, the link between the required observations and the land-surface process research and scaling underlying the LSPIM is being established.
- Programme implementation, including development schedule, risks and international collaboration, is discussed in Chapter 9. Drawing on the previous chapters, Chapter 9 discusses in particular the LSPIM in the context of other related missions, concluding that the proposed launch in 2004 would be of a high priority to the scientific community.

2 Background and Scientific Justification

2.1 Scientific Context

In this Chapter the underlying scientific framework for the mission is described, which is intended to help resolve essential scientific and technological issues related to the quantitative characterisation of land-surface processes. These processes include all water, energy, carbon and other bio-geochemical exchanges on the land surface and between the land surfaces and the other components of the Earth system, like atmosphere, oceans and groundwater. It covers the spotlighted area of Figure 2.1, in which a sketch of the network of processes on the Living Planet Earth is shown.

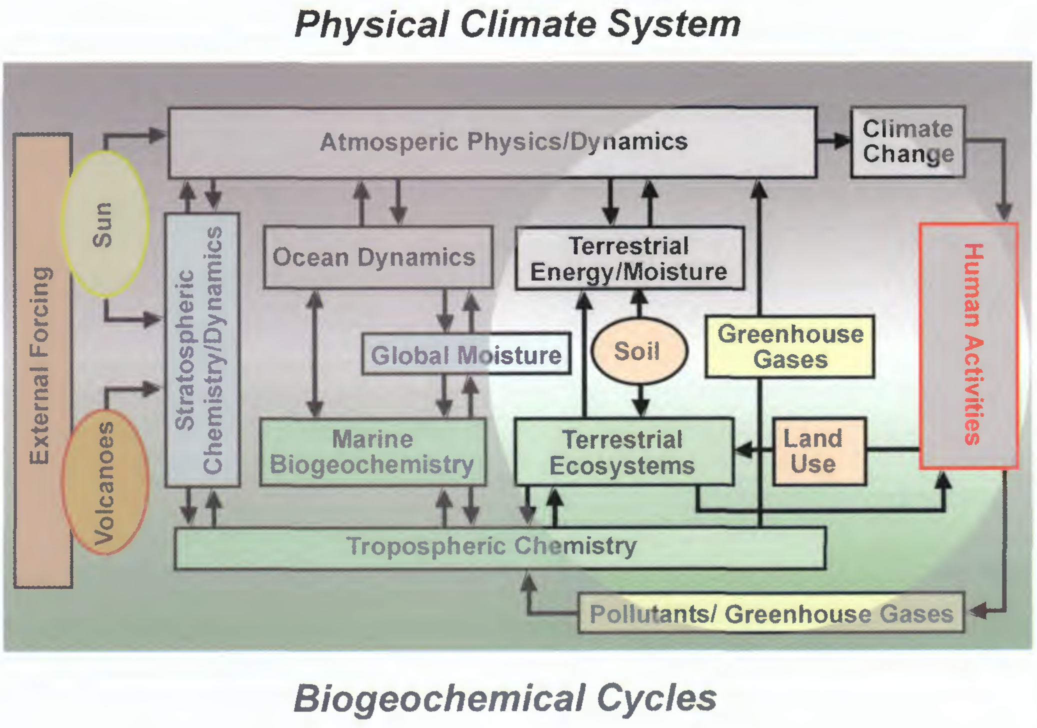

Figure 2.1. Land-surface processes and interactions as part of ESA's Living Planet Programme.

Land-surface processes constitute key scientific challenges because:

- the current crude parameterisations of the main land-surface processes constitute one of the major limitations of climate prediction models and medium-range weather forecasting. Improvements in this area are expected to significantly improve forecasting skill,
- current inaccuracies and unknowns on the fate of the terrestrial component of the carbon cycle make it difficult to pinpoint the nature and location of the

postulated missing carbon sink. Major improvements in observational data on the stocks, fluxes and processes of carbon exchange at or near continental surfaces will go a long way towards answering key questions related to the Kyoto Protocol on climate change.

To further complicate matters, it is important to remember that the land surface is constantly being transformed and adapted to meet human needs associated with basic food production, population expansion and economic development. In the medium term, the impact of regional changes due to human activities on the geosphere and biosphere is likely to be comparable to that of climate variability (National Science Foundation, 1992). The net effects of the exploitation of natural resources are land-cover or land-use change, through processes such as:

- fossil-fuel consumption
- deforestation
- agriculture
- the development of transportation and wide-scale urbanisation
- the modification of the chemical composition of the atmosphere, with the well-known side effects of inadvertent climate change
- the systematic pollution of fresh water and soil, and
- a net loss of biodiversity.

The resolution of these issues requires major advances in understanding of the nature and functioning of land-surface processes at relevant spatial and temporal scales. This depends on joint progress in advancing theoretical knowledge of the processes at work, and in the capacity to acquire adequate measurements and observations to constrain these models to actually describe the real world. The main limiting factor at this time is the lack of detailed information on the state and evolution of the environment at scales intermediate between what can be observed locally in the field and what is already measured globally by low-resolution space sensors. The proposed **L**and-**S**urface **P**rocesses and **I**nteractions **M**ission (LSPIM) is a direct response to this problem and intended to fill an important scientific and technological gap in this domain. As such, the LSPIM will provide a new, very comprehensive set of data and is thus expected to enable the discovery of new approaches and insights into so far unexplored processes and interactions.

The most dynamic component of land surfaces is vegetation. The nature, state and distribution of plants on Earth are clearly controlled by weather and climate, among other factors. However, plants also directly or indirectly control most of energy and mass exchanges between the surface and the atmosphere. Vegetation constitutes the essential link between the mineral world and all other living organisms, including humans. Agriculture, forestry, as well as large industrial sectors critically depend on the availability and qualitative state of the vegetation cover.

The over-exploitation of this renewable resource leads to significant environmental damage, including deforestation, desertification, salinisation, soil erosion and loss of biodiversity. The plant cover is in fact a sensitive and excellent indicator of environmental stress and condition. It will therefore play the key role in the development of sustainable ways to manage the environment. Figure 2.2 outlines the major biospheric interactions, the fluxes between the components and the variables, which have to be measured in order to quantify the related processes.

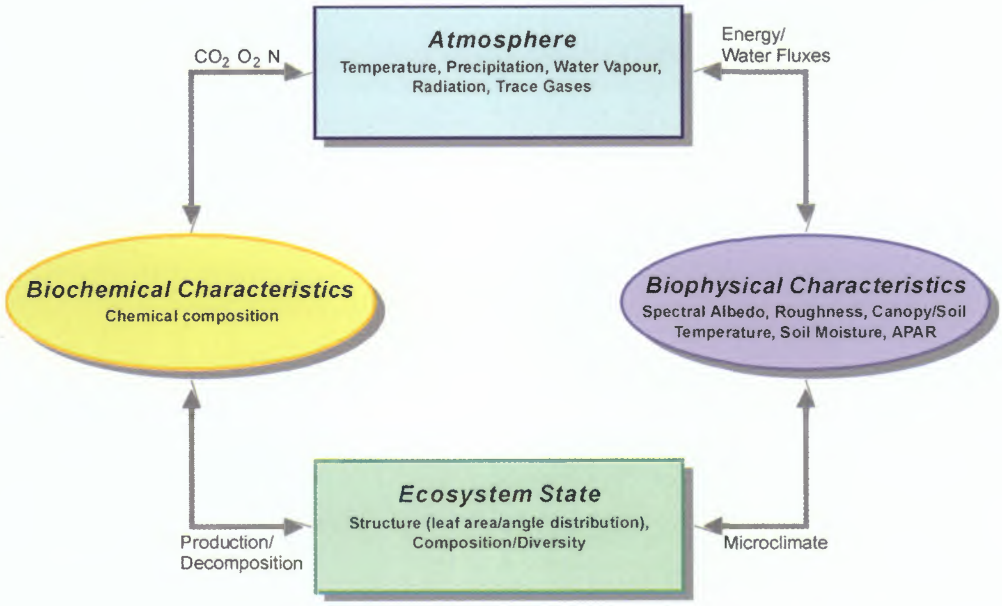

Figure 2.2. *Interactions between biosphere and atmosphere: fluxes and variables.*

2.2 Open Issues in Land-Surface Processes

The processes, which take place within the terrestrial geosphere/biosphere, play an important role in the evolution of the Earth. Climate change and environmental degradation, now commonly referred to as 'Global Change', become issues of major concern. From the multitude of changes taking place on the land surface, population increase, change in land-use, loss of biodiversity and gaseous emissions are of particular concern, as they affect water quality and availability, and the vegetation productivity.

The growth of both the global population and economy calls for a more rational utilisation of natural resources and an increase in the efficiency of key agricultural and industrial processes. This is evident when looking at the global expansion of farmland and the increase in the efficiency of farming practices across a broad range of climates and natural conditions. Forests, grasslands, lakes and rivers must be exploited in such a way as to preserve these essential resources for future generations. Unfortunately, the majority of the land and its associated natural resources have so far not been widely managed in a sustainable way. Clearly, the management of natural resources takes place at the regional and local level and under considerable economic and population pressure. Everywhere regional-scale decisions by individuals, oriented towards their own survival and well-being, lead to a broad diversity of farming practices, industrial activities, urban development or wildlife preservation measures (to mention but a few issues) directly affecting the productivity and stability of natural and man-made ecosystems (Bowler, 1992). How these decisions could be made in a manner such that at the same time they lead to sustainable management of the available resources has become a core issue motivating Global Change research. Although the latter has achieved considerable progress in the past decade, there is no satisfactory guideline for sustainable development because large gaps exist in the understanding of key land- surface processes.

In order to improve understanding of the regional impacts of such changes and their global effects, important questions related to the functioning, sensitivity and evolution of ecosystems and biomes have to be addressed in the post-2000 era:

- How will Global Change affect terrestrial ecosystems, and on which spatial and temporal scales?
- How stable are terrestrial ecosystems and are man-made changes reversible?
- How do changes in terrestrial ecosystems, including soils, affect renewable and non-renewable resources?
- What is the role of vegetation in the water and energy cycles?
- What is the magnitude of gas fluxes to and from the major carbon reservoirs (including CO_2, CH_4,...) in different natural and man-made ecosystems? What are the spatial and temporal variations of these fluxes and the corresponding uncertainties? What is the role of land-surface biological processes in the chemistry of the atmosphere and especially in the production and consumption of methane and other trace gases?

The spatially distributed character of land-surface processes, their large spatial heterogeneity and their dynamic changes with time call for remote-sensing approaches to consistently measure the variables which determine these processes, in space and time (Waring and Running, 1998). The mission presented in this report will provide critical data at high spatial, temporal, spectral, angular and radiometric resolutions for selected ecosystem study sites and significantly contribute to a better understanding of the key ecosystem-level processes and interactions.

Changes in the geosphere/biosphere system and especially the land surface are addressed within the four large Global Change research programmes of the International Council of Scientific Unions (ICSU). They consist of the International

Geosphere Biosphere Programme (IGBP, 1990), the World Climate Research Programme (WCRP), the International Human Dimensions Programme (IHDP) and the International Programme on Biodiversity (DIVERSITAS, 1996).

The large international scientific community organised around these programmes has devoted considerable effort over the past decade to investigating some of the most important natural and man-induced land-surface processes, including:

- changes in soils, vegetation and land cover (e.g. transformation of natural ecosystems into arable land, soil erosion, deforestation, desertification)
- changes in the intensity of land- and resource-utilisation (e.g. unsustainable management practices in forestry, intensive agriculture, urbanisation)
- changes in hydrological conditions to sustain agricultural and grazing activities (e.g. lack of water, overgrazing, deforestation)
- changes in atmospheric composition (e.g. increase in greenhouse gases, atmospheric aerosols, precipitation)
- natural hazards and extreme events (e.g. flooding, drought, volcanic activities)
- loss of biodiversity (in particular due to deforestation).

The sustainability of natural resource exploitation and of the related human activities has become a central issue of international discussion among scientists and policy makers. It has resulted in treaties (e.g. Kyoto Protocol, Buenos Aires Protocol, Helsinki Process, Rio-Agenda 21), which aim at the sustainable management of natural resources in the future. In this context, the cycles of carbon (essential to all life forms) and water (required for the transport of all chemical compounds over land) have attracted major attention because they pose the most serious limitations on sustainable development in terms of impact, availability and distribution (Tenhunen et al., 1998). Indeed, vegetation largely controls the exchanges of energy, water and many bio-geochemicals between the land surface and the atmosphere or the hydrosphere.

Given the importance of the carbon and water cycles, and the crucial role of vegetation in these cycles, it is possible to identify five fundamental land-surface processes that form the core theme of this mission. These are:

- heat and mass exchange at the land/atmosphere interface
- photosynthesis and primary production
- regional hydrological processes
- land-atmosphere exchange of biochemical compounds, and
- establishment and dynamics of ecosystems.

These processes are strongly interlinked through exchange of energy, water, carbon and other chemicals like nitrogen. Figure 2.3 illustrates the five fundamental processes on the land surface, which constitute the core of the LSPIM. It also emphasises the central role vegetation plays in controlling these fluxes.

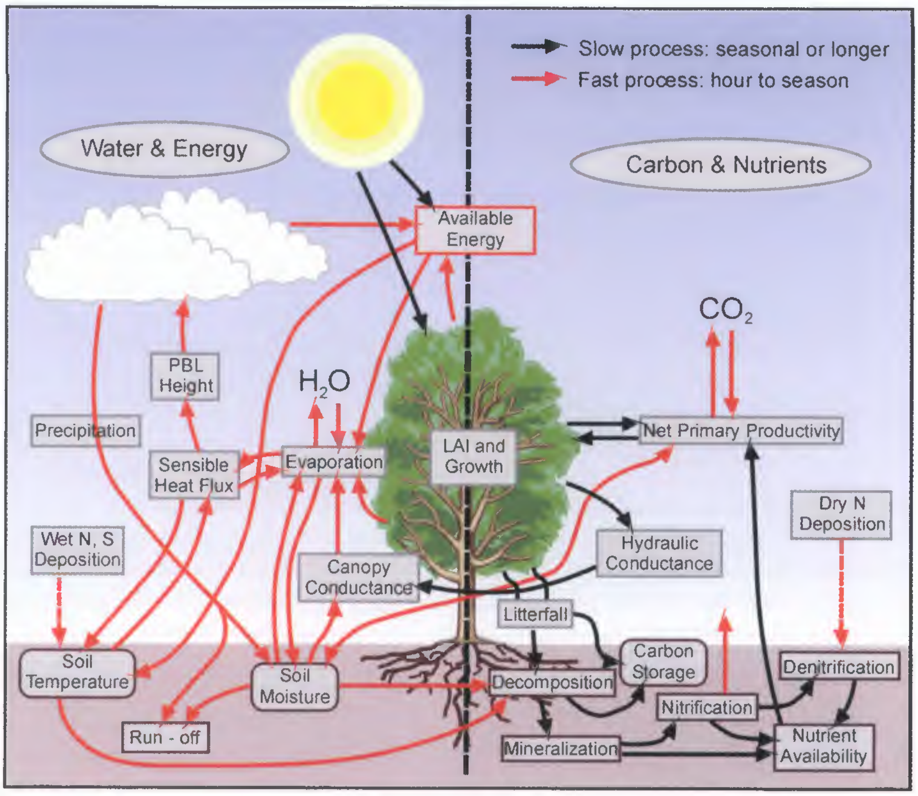

Figure 2.3. Schematic of land-surface processes, including the five core processes addressed by the LSPIM.

2.3 Fundamental Land-Surface Processes

2.3.1 Heat and Mass Exchange at the Land/Atmosphere Interface

Heat and mass exchanges between terrestrial environments and the atmosphere are essentially constrained by the energy balance at the land surface. The latter comprises the incoming and outgoing radiation fluxes at both short and long wavelengths. The latent, sensible and soil heat fluxes, and in particular their spatial distributions, are difficult to measure directly with sufficient accuracy. They vary with land cover type over a wide range of spatial and temporal scales. Currently, they represent the major unknowns of the land-surface processes and have to be observed with adequate temporal and spatial resolution.

To a significant extent, the dynamics of the convective boundary layer (CBL) of the atmosphere are determined by the land surface (Mahfouf et al., 1987; Segal et al., 1988; Hadfield et al., 1991; Xue and Shukla, 1993). Over homogeneous land surfaces the controlling factor is the partition of net radiation into sensible, latent and soil heat flux. The partition of net radiation is determined by the presence and functioning of vegetation and by the availability of soil moisture. Heterogeneous land surfaces compound the complexity of these processes, since the spatial pattern of land-surface properties determines CBL motion at small length scales (Hadfield et al., 1991; Wang and Mitsuta, 1992). Over the last 20 years, observation and modelling of land-surface processes in the context of local boundary layer dynamics has become a wide and active research field in its own right. Land use has a significant impact on local atmospheric circulation (e.g. Segal et al., 1988). Large differences in evaporation contribute to determine the spatial variability of precipitation (Fig. 2.4).

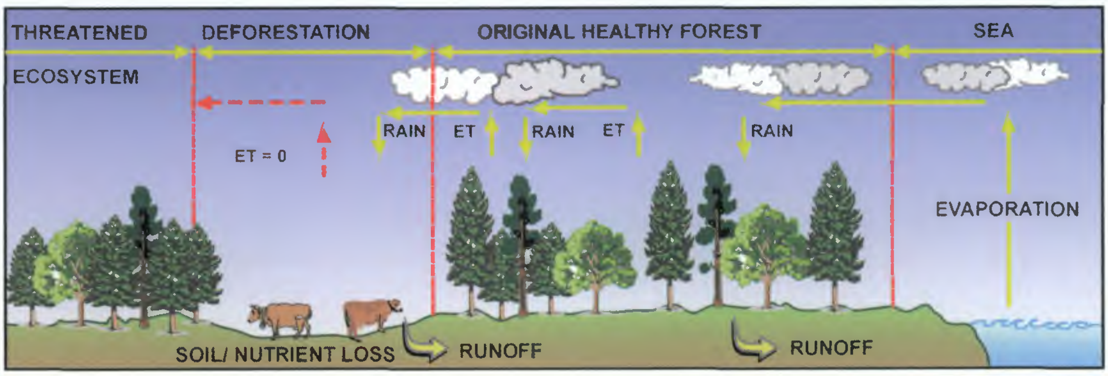

Figure 2.4. *Land use, land cover, land-surface processes and mesoscale atmospheric processes: A conceptual scheme.*

These studies have brought the attention of a wide scientific community to the need for significant improvements in models of such land-surface processes and of the interactions of land surfaces with the atmosphere (e.g. Avissar and Pielke, 1989; Pielke et al., 1991; Pielke et al., 1999; Valentini et al., 1999).

2.3.2 Photosynthesis and Primary Production

Photosynthesis is the biochemical process that converts radiative energy into chemical energy, which is stored in the form of assimilated carbon. It takes place through the action of the plant pigments (mainly chlorophyll) and forms the basis of plant growth, development and productivity. The latter is part of the metabolism of plants and strongly depends on the fraction of absorbed photosynthetically active radiation (fAPAR) and the conversion efficiency of the plants. It depends on the chlorophyll content of the vegetation, plant type and environmental conditions like temperature, soil water availability and nutrient availability. Thus, the accurate characterisation of photosynthetic processes requires the measurement of plant type, fAPAR and chlorophyll content.

Primary productivity is defined as the net photosynthesis accumulated over a period of time. It is the amount of carbon stored in structural biomass. The productivity of the various terrestrial and aquatic ecosystems and the associated bio-geochemical cycling of important elements largely determine the state of the biosphere. A clear and detailed understanding of bio-geochemical processes, and the change in vegetation state, productivity and dynamics due to climatic and anthropogenic pressure is therefore necessary.

Since leaf-area index, fractional vegetation cover, and leaf absorptive properties in the solar spectrum are most important variables controlling primary productivity, it is important to measure their spatial distribution. This information is needed by ecosystem or agricultural productivity models, which also require information on the conversion efficiency, on water or nutrient deficiencies and on the phasing of plant development in response to external forcing factors like climatic and agricultural management practices. This type of information can be derived partly from an identification of the plant and ecosystem type using classification techniques and from advanced model inversion techniques.

2.3.3 Regional Hydrologic Processes

The water cycle is the basic transport path for energy and chemical compounds on the land surface. Knowledge of the spatial and temporal distribution of major water fluxes like precipitation, evapotranspiration (latent heat flux, ET), surface runoff and ground water flow as well as of the major components like soil-moisture and snow- and ice-storage and inland waters (lakes and streams) is therefore vital. Since water flows along elevation gradients, the heterogeneity of bio-geochemical processes on the land surface is largely determined by those same gradients. The spatial and temporal heterogeneity of functional relations within the water cycle on the land surface shows similarities to the energy cycle. Therefore they should be studied as a coupled system along such gradients (Becker and Bugmann, 1997).

Water is the most intensely utilised natural resource. It is used as potable water, for irrigation and in various industrial processes. Growing populations and developing economies will increase the pressure on water utilisation and will lead to increasing pressure on water resources both regionally and globally within the next 25 years (United Nations, 1997). Therefore the accurate determination of the regional availability of fresh water in the form of lakes, soil-moisture or snow, either through direct or indirect measurements or based on land-surface models, is crucial to understand, predict, and possibly minimise the effects of water stress. Water availability to the plant cover to a large extent controls the carbon and nitrogen cycles in terrestrial ecosystems and directly influences plant growth and food production. Detailed information on soil moisture, either through accurate land-surface models or through direct observation, substantially improves the predictions of general circulation models, regional water-balance models and water-runoff models.

2.3.4 Land-Atmosphere Exchange of Biochemical Compounds

Carbon dioxide, methane and other trace gases have a well-known impact on the Earth's radiation balance, through the so-called greenhouse effect. Their increasing concentrations in the atmosphere, due to human activities, are likely to induce important climatic changes. This point of view has been largely endorsed by the scientific community (IPCC, 1996a,b) and by the majority of governments, as evidenced at major international conferences on the global environment (Rio, Kyoto, etc.). The role of the spatially-heterogeneous land surfaces in controlling the expected levels of these gases is not known quantitatively. Nevertheless it is clear that the land surface is a prime source of the major greenhouse gases and that the strength of these emissions is strongly related to human activities. Beyond the necessity to observe the effects of greenhouse gases in the atmosphere and their role within the energy balance of the planet, it is of major importance for a sustainable future management of greenhouse gas emissions to identify their precise sources and sinks on the land surface and explain their dynamics. The magnitude of these sinks, as well as their geographical distribution around the globe are largely unknown.

The concentration of the atmospheric carbon dioxide is largely controlled by sources and sinks at the Earth's surface. Presently the rate of carbon dioxide increase in the atmosphere is only about half the rate of the anthropogenic emission. The excess production is taken up by the oceans and the terrestrial biosphere, both sinks being estimated to be of similar magnitude. However, present estimates of the exchanges and uptakes leave a significant part of anthropogenic carbon unaccounted for, reflecting a lack of knowledge on the interactions and exchange processes that link the atmosphere and the terrestrial ecosystems as well as on the productivity of different terrestrial ecosystems

Trace gases such as nitrogen compounds, hydrocarbons and ozone, also play important roles in atmospheric chemistry and ecosystem processes. Increased tropospheric ozone concentrations in northern-hemispheric mid-latitudes, resulting from anthropogenic activities, affect the biosphere on regional scales. Nitrogen oxides (NO_x) and volatile organic compounds are produced biologically or by the burning of fuel and biomass.

The carbon dioxide, methane and trace-gas cycles are strongly coupled with the land-surface components of energy and water cycles through the dynamics of ecosystems. This coupling is based on the radiation balance, strongly influenced by the concentrations of greenhouse gases and water vapour in the atmosphere, and on the functioning of the plant stomatal pathways, which influence both transpiration and absorption of carbon dioxide. The understanding of these interactions is therefore critical. However, the radiative effects of greenhouse gases are partly compensated by increased aerosol concentrations originating from anthropogenic as well as from natural sources. Improved information is therefore needed to quantify the exchange processes controlling release, transport, and deposition of aerosols globally.

2.3.5 Establishment and Dynamics of Ecosystems

Ecosystems are communities of plants and vegetation patches which develop an internal structure with a set of dynamic characteristics dominated by the internal processes and interactions with their surroundings. The structure and evolution of ecosystems are strongly related to the environmental conditions (temperature, precipitation, humidity, radiation, day-length, etc.) under which they develop and the human impacts acting on them.

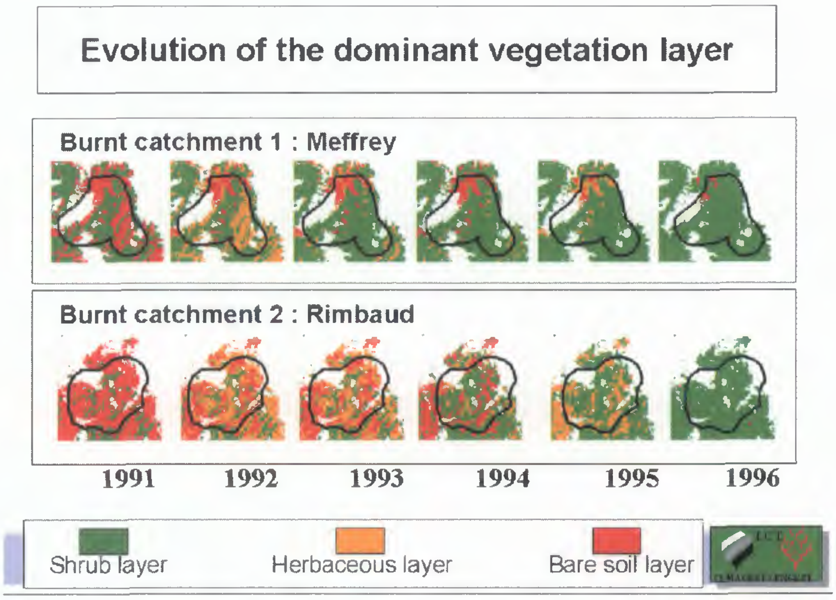

Figure 2.5. *Recovery of vegetation cover in two catchments after a wildfire in 1990; fractions of bare soil, grasses and shrubs determined with a time series of satellite images (Puech, pers. comm., 1999).*

The establishment and dynamics of ecosystems are related to their stability, which is a property of their responses to external forcing (climate, human). Understanding the stability of an ecosystem is a prerequisite to its sustainable management. This resilience determines how far an ecosystem may be moved away from natural equilibrium before it is irreversibly altered in its function and/or structure. It has been shown to be strongly related to its composition and abundance of the constituent species, biodiversity and competition (Smith et al., 1997) and determined by landscape fragmentation, disturbances and succession (Noble, 1999). In the case of man-made ecosystems, stability further involves a balance between carrying capacity in terms of livestock and agricultural production and the degree of human impact.

The study of terrestrial ecosystems and of their dynamics leads to the analysis of time- and space scales in ecological systems. Understanding of controlling factors and patterns is conducive to identifying and understanding processes. Computer models have been developed to simulate the dynamics of ecological succession and have led to the quantitative study of patterns in forestry. Aber (1992) described the dynamics of ecosystems driven by the movement of energy and mass (water, nutrients and pollutants) through elements of the landscape.

Lavabre et al. (1993) studied the recovery of a Mediterranean landscape after a wildfire and the resulting impacts on hydrological processes. Vegetation in the entire basin of the Real Collobrier was severely affected. Runoff was unusually high in the months following fires. Changes in land cover (Fig. 2.5) have a very significant impact on interception, evaporation and runoff. Distributed hydrological models help to understand these processes, but require observations of the recovery of vegetation cover, such as those provided by space-borne imaging radiometers. It appears that the key to a better understanding of the factors determining the structure and dynamics of ecosystems is the ability to observe the composition and temporal change of vegetation cover and to determine its biophysical properties.

2.4 Spatial Scale and Non-Linearity

Spatial heterogeneity is the feature that mainly distinguishes land surfaces from oceans and atmospheres. Landscapes are heterogeneous in a way apparent to any observer, and perceived spatial patterns evolve slowly. Figure 2.6 illustrates the 3-dimensional spatial complexity of land-surface processes and of the fluxes to, from and within the land surface. It also shows that the land surface is composed of separate land-surface units of different size and shape, which can be represented in a model through an ensemble of suitable spatial building blocks in a finite-element approach.

The finite elements are becoming known as proxels (process pixels) (Tenhunen et al., 1998), which are combined within land-surface process models to represent and describe complex landscapes. The proxel concept is also illustrated in Figure 2.6 and has been used by several authors (Bach, 1998; Famiglietti and Woods, 1992; Mauser, 1997; Mölders and Raabe, 1998; O'Neill et al., 1997; Schädlich, 1996; Schneider, 1999) in the fields of hydrology, landscape analysis, net primary production and mesoscale meteorology. It has been successfully tested on different scales (Cernusca et al.,1998; Mauser and Schädlich, 1998; Mölders et al., 1997; Waring and Running, 1999; Tenhunen et al., 1998) from the single plant stand to the meteorological mesoscale using remote-sensing data.

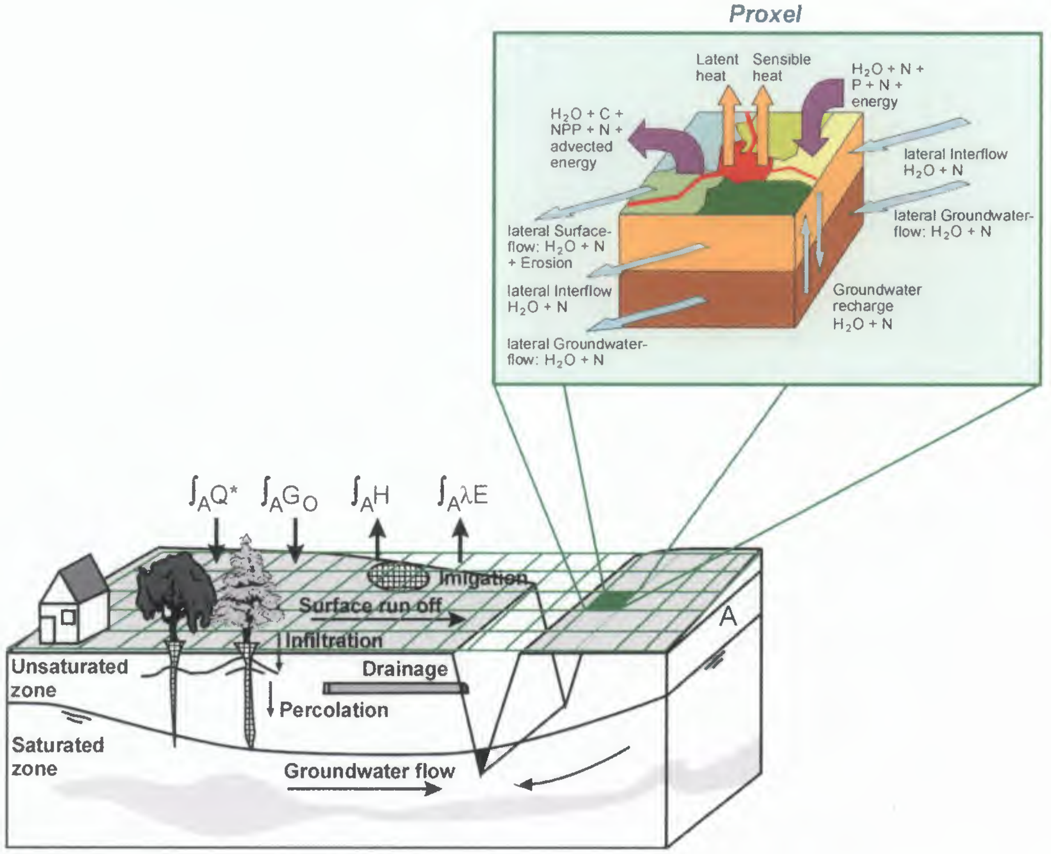

Figure 2.6. *Spatial variability of land-surface processes and interactions (Q^* = net radiation flux, Go = surface heat flux, H = sensible heat flux, λE = latent heat flux) and their representation in distributed models.*

2.4.1 Scales in Process Studies

The relative importance of different land-surface processes varies with the space- and time scales considered.

Three different scales can be identified at which land-surface processes should be studied:

- *The local scale* – this is the smallest scale to be considered in this context. On the local scale, land-surface processes can be observed, modelled and verified through direct field measurements. It is assumed that the properties of the land cover and soil (as well as the driving meteorological inputs) are homogeneous over the size of the land-use plot, which makes up the local scale. Local scale plots usually have an extension of 10-100 m and internal variability may be neglected.

- *The regional scale* – this is the scale at which single homogeneous plots of uniform land cover and soil type form ecosystems. The combination of internal exchange processes between the plots and the exchange with the atmosphere alters the environmental conditions for each plant in the community. Ecosystems consist of land-use patches and differ in the way they function from the plots of the local scale. Regional-scale ecosystems usually have an extension of 10-100 km. The length scale of the internal variability is of the order of 10-100 m.
- *The global scale* – this is the scale at which the differentiation of land-surface processes is mainly determined by the circulation pattern of the atmosphere, by the distribution of the continents and by ocean currents. For the understanding of land-surface processes on the global scale, the broad variety of global ecosystem types have to be understood in the way they function.

Figure 2.7 illustrates the passage across scales from the locally verifiable scale of processes across the regional scale to the global scale and back. It also shows the changing objects of interest on the land surface. The focus of the LSPIM is located between local and regional scales.

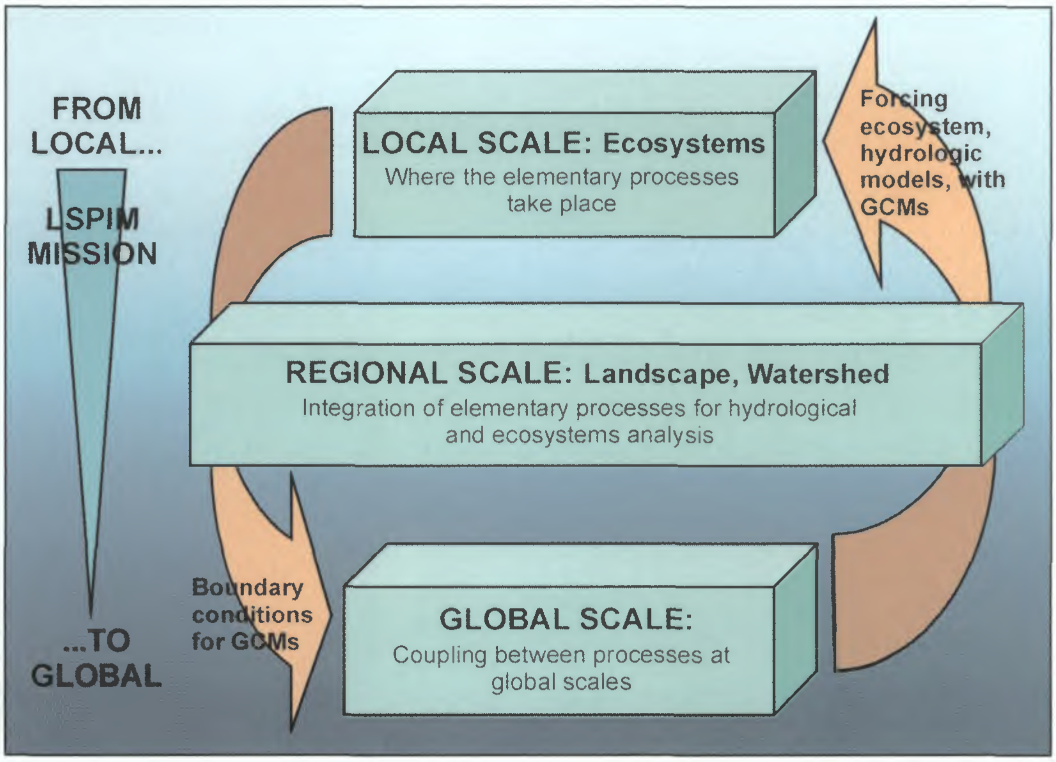

Figure 2.7. *Flow chart showing the interactions between processes occurring at different scales.*

2.4.2 Non-Linearity of Land-Surface Processes

Land-surface processes are frequently non-linear with respect to the variables by which they are determined. Non-linearity sets limits to the degree of spatial and temporal averaging of input data that can be performed for a given level of error when modelling the processes. This gives rise to differences between spatially averaged results of a distributed model using detailed input data, and the result of the same model using spatially lumped input data. This fact is illustrated in Figure 2.8. Therefore, even though some of the critical processes occurring on the land surface and at the interfaces with the other components of the Earth system, are well understood and parameterised on the scale of single land-use plots, extending that knowledge to regional and global scales is still difficult and has not yet been achieved in a proper way.

There are three different ways to proceed when modelling a process across a heterogeneous area:

- average spatial variables and apply to the aggregated variables a model identical to the one valid at high spatial resolution (top integral in Fig. 2.8)
- apply the model valid at high spatial resolution and aggregate the results (bottom integral in Fig. 2.8)
- apply an effective lumped model, which behaves in an equivalent way to the detailed model but does not need detailed spatial information. This approach is represented by the question mark in Figure 2.8.

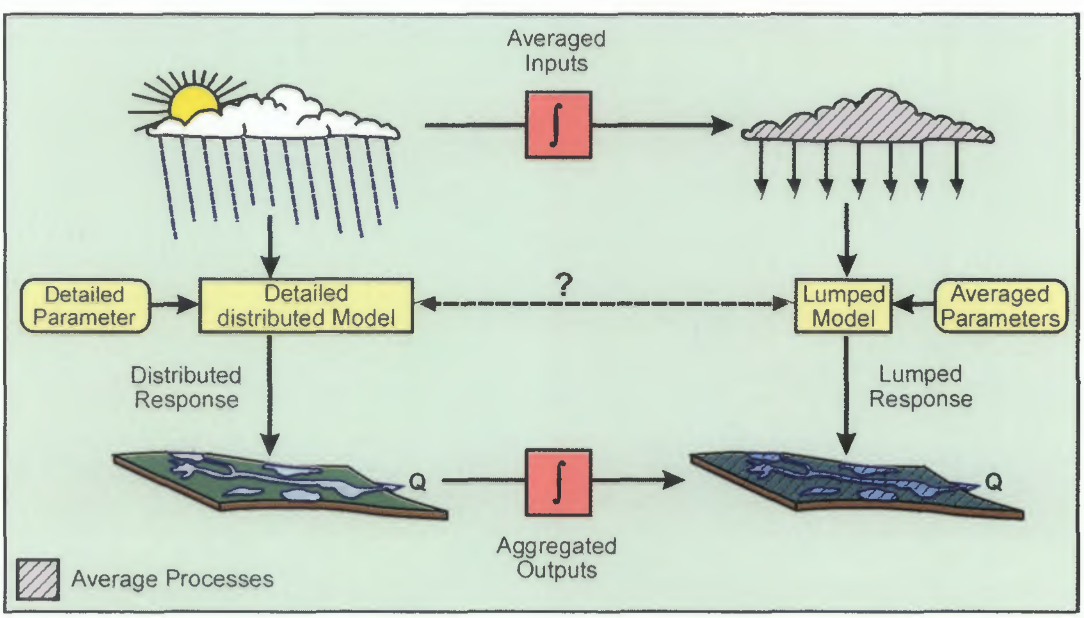

Figure 2.8. *The role of scale on the result of land-surface models (from NASA, 1988).*

To obtain a quantitative idea of the difference between the first two approaches, a simple flux F, smoothly dependent on a parameter p is assumed. The integrated flux, $\overline{F}$ is then determined over an area A, within which the parameter p varies, and compared to the flux calculated with the average value of the parameter, $\overline{p}$. These correspond to passing from top left to bottom right of Figure 2.8 in the anticlockwise and clockwise directions, respectively:

$$\overline{F} = \frac{1}{A}\int_A F(p)dA \qquad \overline{p} = \frac{1}{A}\int_A p\,dA \tag{2.1}$$

Now, by the intermediate value theorem, for any value of p in A it follows that:

$$F(p) = F(\overline{p}) + (p-\overline{p})\left.\frac{\partial F}{\partial p}\right|_{\overline{p}} + \frac{1}{2}(p-\overline{p})^2\left.\frac{\partial^2 F}{\partial p^2}\right|_{p^*} \tag{2.2}$$

where p^* lies between p and $\overline{p}$, and is a function of p. Integrating over A results in:

$$\overline{F} = \frac{1}{A}\int_A F(p)dx = \frac{1}{A}\int_A F(\overline{p})dA + \frac{1}{A}\left.\frac{\partial F}{\partial p}\right|_{\overline{p}}\int_A (p-\overline{p})dA + \frac{1}{2A}\int_A\left((p-\overline{p})^2\left.\frac{\partial^2 F}{\partial p^2}\right|_{p^*}\right)dA \tag{2.3}$$

The second term on the right-hand side of this equation is zero, by design, and the first is simply the flux corresponding to $\overline{p}$. The third term on the right-hand side of this equation is thus the error introduced by scaling up the parameter to apply to the process (top line in Fig. 2.8). To this term we can apply the mean-value theorem once again to evaluate it as:

$$\frac{1}{2}\int_A\left((p-\overline{p})^2\left.\frac{\partial^2 F}{\partial p^2}\right|_{p^*}\right)dA = \frac{1}{2}\left.\frac{\partial^2 F}{\partial p^2}\right|_{p_1}\int_A (p-\overline{p})^2 dA \tag{2.4}$$

Therefore a parameterisation of the difference is given by:

$$\overline{F} - F(\overline{p}) = \frac{1}{2}kV \quad \text{where } k = \left.\frac{\partial^2 F}{\partial p^2}\right|_{p_1} \tag{2.5}$$

$$\text{and } V = \frac{1}{A}\int_A (p-\overline{p})^2 dA \tag{2.6}$$

where p_l is a value that is realised somewhere in the given area A. The error in treating the lumped pixel in the same way as a uniform pixel may thus be regarded as a product of two terms, a non-linearity factor k depending on the degree of non-linearity of the process and a heterogeneity factor V being a direct measure of the heterogeneity of the parameter across the area. If the process is linear with respect to p, or if p does not vary, then there is no error. However, any inherent non-linearity of the process is amplified by the spatial heterogeneity of the parameter at the scale of the model.

The best way to understand and quantify the heterogeneity of complex land-surface processes is simply by direct observation (King, 1999). The non-linearity term might be found directly from the model, if the process is simple enough to define in terms of a simple physical equation, although there will be some uncertainty in the numerical value as p_l is unknown. If the flux F is determined through more complicated modelling, such as water flux determined in a Soil Vegetation Atmosphere Transfer (SVAT) model, then the non-linearity term must be found by extensive evaluation of the model. The upscaling in this simple formulation must be approached from two complementary sides, modelling and observation.

More realistically, the process will depend on more than just a single parameter, so the precise formulation of the upscaling correction is very complicated, depending on the covariances of the parameters. Nevertheless, the basic principle is the same: the difference depends quantitatively on the heterogeneity of the parameters that the process depends on and on the non-linearity of the process as a function of these parameters.

The differences in the model results caused by non-linear processes in complex landscapes apply to both radiometric variables like surface temperature (Becker and Li, 1995) and to process models of heat exchanges (Bastiaanssen et al., 1996). Surface radiometric temperature, for example:

- is measurable from space; the definition of the variable is scale-invariant
- the value is equal to the thermodynamic temperature for homogeneous pixels
- *but* an ensemble of black bodies at different temperatures *does not behave like one* black body.

Spatial and temporal sampling of the properties of terrestrial ecosystems is closely linked to questions of scale. Methods to bridge scales (as symbolised through the question mark in Fig. 2.8) from the local scale to the regional scale, and from the regional scale to the global scale, are the most critical building blocks of land-surface processes science. As Figure 2.7 demonstrates, being unable to understand land-surface processes on the regional scale prevents the causal description of the land-surface processes on the global scale, even if adequate understanding of the processes is available on the local scale.

2.5 Complexity and Accuracy of Process Models

A panoply of numerical models has been developed worldwide to model the interactions of land surface with the atmosphere. Two major international evaluations of a representative set of such models have been carried out: PILPS (Project for Intercomparison of Land Surface Parameterisation Schemes) (Pitman et al., 1993) and the Potsdam Net Primary Productivity (NPP) model intercomparison (Cramer and Field, 1999). The overall outcome of both studies is similar: results were significantly different even though all models in either study were run with the same data set and the simulations were done according to a precise protocol.

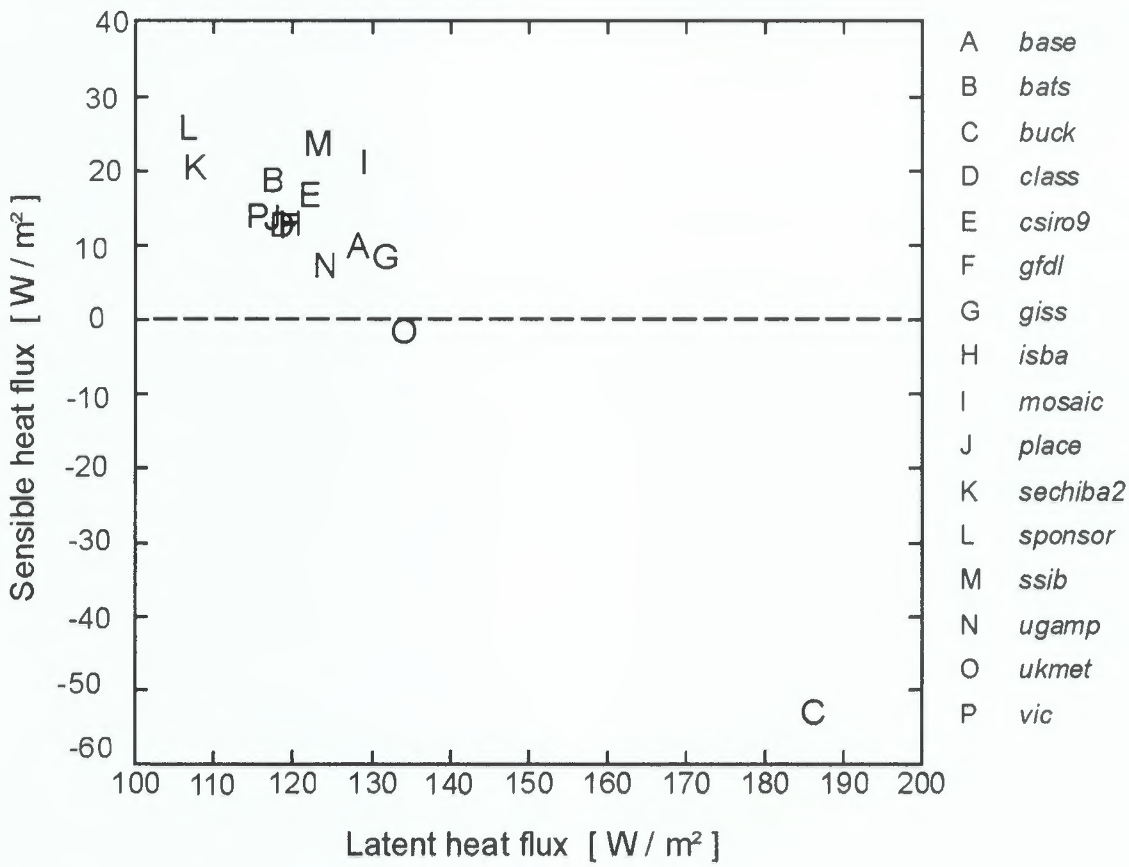

Figure 2.9. *PILPS evaluation of SVAT schemes: example of simulated latent and sensible heat fluxes for a homogeneous grass canopy (annual averages).*

The SVAT models evaluated under PILPS have different levels of complexity, from a simple bucket model to advanced schemes describing water transfer through soil, vegetation and the atmosphere with significant detail. Some schemes require estimates of some hundred variables to characterise the system. Sixteen different SVAT models were compared by means of a numerical experiment. All models were run using the same data set. Model calculations of surface temperature, sensible and latent heat fluxes were compared using: annual averages, monthly averages and instantaneous values on selected days. All results pointed to significant differences between model calculations, including the ones obtained with the most sophisticated SVAT schemes. As can be seen in Figure 2.9, differences in sensible and latent heat flux simulated for a homogeneous grass canopy were rather large.

Likewise, the NPP schemes evaluated as part of the Potsdam NPP model intercomparison gave large differences in net carbon uptake for all biomes, as can be seen in Figure 2.10.

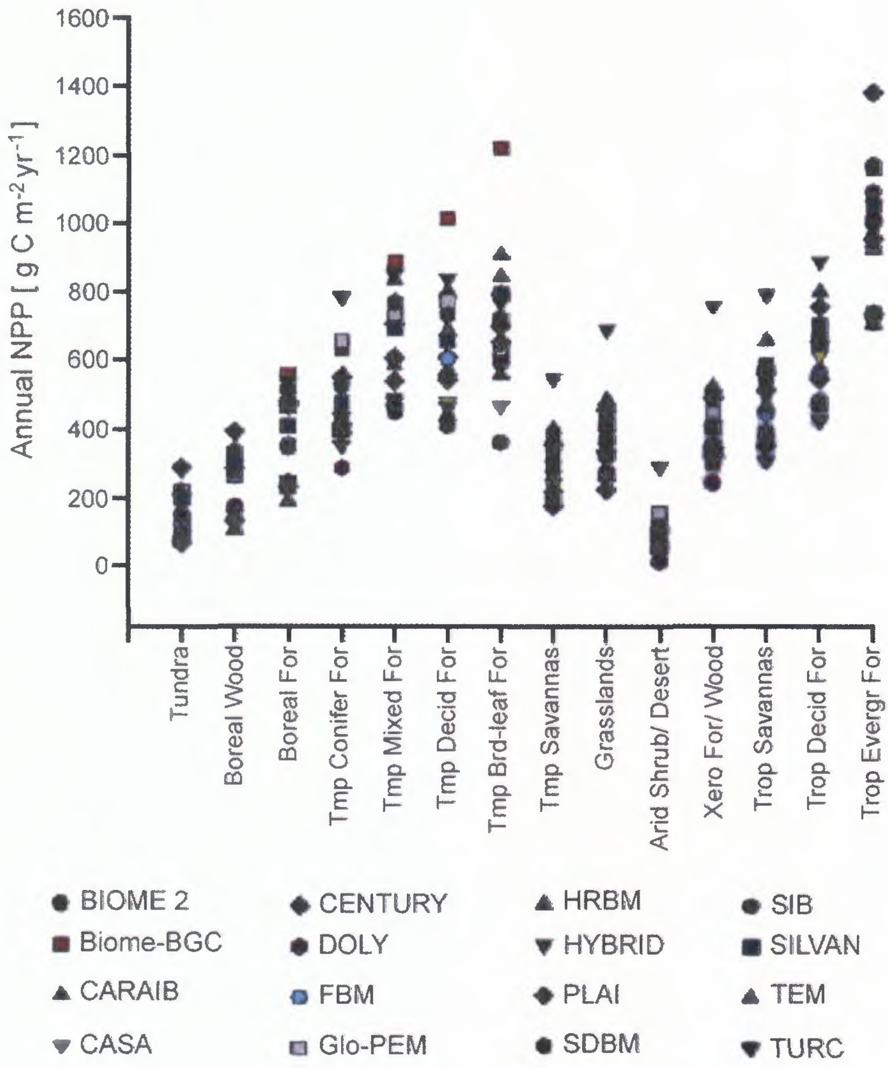

Figure 2.10. *Results of the Potsdam NPP model intercomparison study. The coloured symbols represent different NPP models, which were tested with data sets representing different ecosystems.*

Although many explanations may be put forward for the differences between the model results, a rather fundamental one was proposed by Beven and Binsley (1992) which was studied in more detail by Franks and Beven (1997). Complex models use a rather large number of variables to describe biophysical processes. The accuracy of estimates of such variables is moderate to poor. When error bounds are combined with the large number of variables, a rather large 'solutions space' (i.e. a rather large number of combinations of the values of independent variables) gives similar values of dependent variables such as latent and heat fluxes. This also implies that numerous different combinations of independent variables are likely to be observed. Simultaneous and accurate determination of as many land-surface variables as possible limits the solution space, i.e. increases the accuracy of model calculations.

As Figure 2.10 clearly shows, there is a need to improve the accuracy of current land-surface processes and interactions models to describe the energy, water and carbon cycles through improved determination of the driving variables. The aim must be to answer the questions related to the land-surface processes and to improve the reliability of their models to a level where the impact of human activities on the quality of the environment, the stability of the ecosystems (both natural and man-made), the state of the resources and climate trends can be modelled.

2.6 The International Context

The World Climate Research Programme (WCRP) and the International Geosphere Biosphere Programme (IGBP) with their core projects BAHC (1993), GCTE (Steffen et al., 1992), LUCC (Turner et al., 1995) and LOICZ (Pernetta and Milliman, 1995) have stimulated the generation of data-sets and insights into the relevant processes on local, regional and global scales (Galloway and Melillo, 1998; Walker and Steffen, 1996, 1999). The community needs the data from the proposed LSPIM to further understanding of the land-surface aspects of their research objectives.

In March 1996 the Committee on Earth Observation Satellites (CEOS) proposed an Integrated Global Observing Strategy (IGOS) which was reviewed and endorsed by the WCRP Joint Scientific Committee in March 1997. Two elements (implementation projects) of IGOS are relevant to LSPIM:

- the Global Terrestrial Observation System (GTOS) (Heal et al., 1995)
- the Global Climate Observation System (GCOS).

In comparison with the earlier IEOS (International Earth Observing System), the IGOS concept places a strong emphasis on an integrated approach to data provision, combining in-situ and remote-sensing data.

The WCRP/GEWEX Hydrometeorology Panel (JSC, 1998) has stated that *"... new problems arise in the use of models to represent large heterogeneous areas, as well as in the availability of data for testing and calibration of such models"*. GEWEX is formulating plans for co-ordinated periods of observation as part of major experiments on land-surface processes.

Data Assimilation Systems are expected to become the basic tool for synthesis of diverse satellite and in-situ observations and for the generation of the global data sets actually used for monitoring and modelling the Earth system. The data provided by LSPIM are expected to create substantial improvements in the understanding and modelling of processes on heterogeneous land surfaces and in choosing the best way to determine state variables and fluxes at the right spatial resolution of the aggregated models used for four dimensional data assimilation. It therefore provides an important keystone in preparing the scientific ground on which to build a successful and continuous GTOS.

European research activities within the Fifth Framework Programme (European Community, 1999) specifically aim at the establishment of quantifiable targets and indicators of the ecological quality of water and of ecosystem health, also taking into account socio-economic aspects. The proposed mission will make a considerable contribution to this research goal.

2.7 Conclusions

Changes in the important cycles of energy and mass through land-surface processes, and interactions with the other components of the Earth system, predominantly occur on the regional scale of (natural and man-made) ecosystems and are strongly influenced by human activities. They materialise in different ways depending on the regional combination of climate, surface conditions, soils, vegetation and human impacts. In order to develop ways to manage development in a sustainable way, it is necessary to understand regional ecosystem functioning and level of stability. This has been difficult in the past because of a lack of adequate globally distributed, regional-scale data sets of land-surface process variables, at the requisite spatial and temporal resolution.

In summary, without entering into the specific requirements of all land-related applications, basic land-surface process variables that constitute the focus of attention in a space observation strategy for the next decade can be identified. They are related to:

- Land-surface processes such as primary productivity, biochemical cycles, energy and mass transfer.
- The dynamics of land-surface changes (land-use change, erosion, land degradation, urbanisation, desertification).

- Land-surface characteristics and conditions (type and condition of land cover, vegetation morphology and biochemistry, terrain characteristics, soils and minerals, water availability and quality).

In order to deliver these variables to the next generation of sophisticated process models, observations at high spatial and temporal resolution will be necessary. The proposed LSPIM will acquire the basic radiance measurements needed to generate those fields of model variables, and will fill the important observational gap that exists in today's suite of sensors.

Therefore, two parallel elements should be pursued within the LSPIM:

- The development and implementation of an observing system ensuring the provision of measurements of derived key geo-biophysical variables characterising the state, dynamics and evolution of a broad range of representative ecosystems composing the land-surface component of the biosphere/geosphere system, taking account of the fact that a number of potentially important processes may not yet be known.
- A scientific programme leading to the derivation of more appropriate and accurate models of geosphere/biosphere processes and land-atmosphere interaction processes, formulated in terms of variables. Coupled with this there must be an improvement in assimilation procedures and processing algorithms.

Studying land-surface processes from regional to global scales leads to measurement and observation challenges still to be overcome. Remote sensing offers the possibility to consistently measure the variables, which determine the processes, in space and time on the regional scale (Waring and Running, 1998). This challenge can only be met by a carefully derived observing system that is able to provide these variables in a quantitative way, enabling the scientific community to comprehensively study land-surface processes with the appropriate tools and transfer this knowledge onto global scale.

3 Research Objectives

The study of land-surface processes on the regional scale presents measurement and observation challenges yet to be overcome. Satellite remote sensing appears to offer the opportunity to measure consistently the variables that determine regional-scale processes (Waring and Running, 1998). The main assumption underlying this assertion is that the fields of required variables can be derived through knowledge of the way the land surface interacts with electromagnetic radiation. This assumption is supported by a large body of theoretical and experimental evidence, which documents strong relations between certain process variables and, in particular, reflection and emission properties of the land surface.

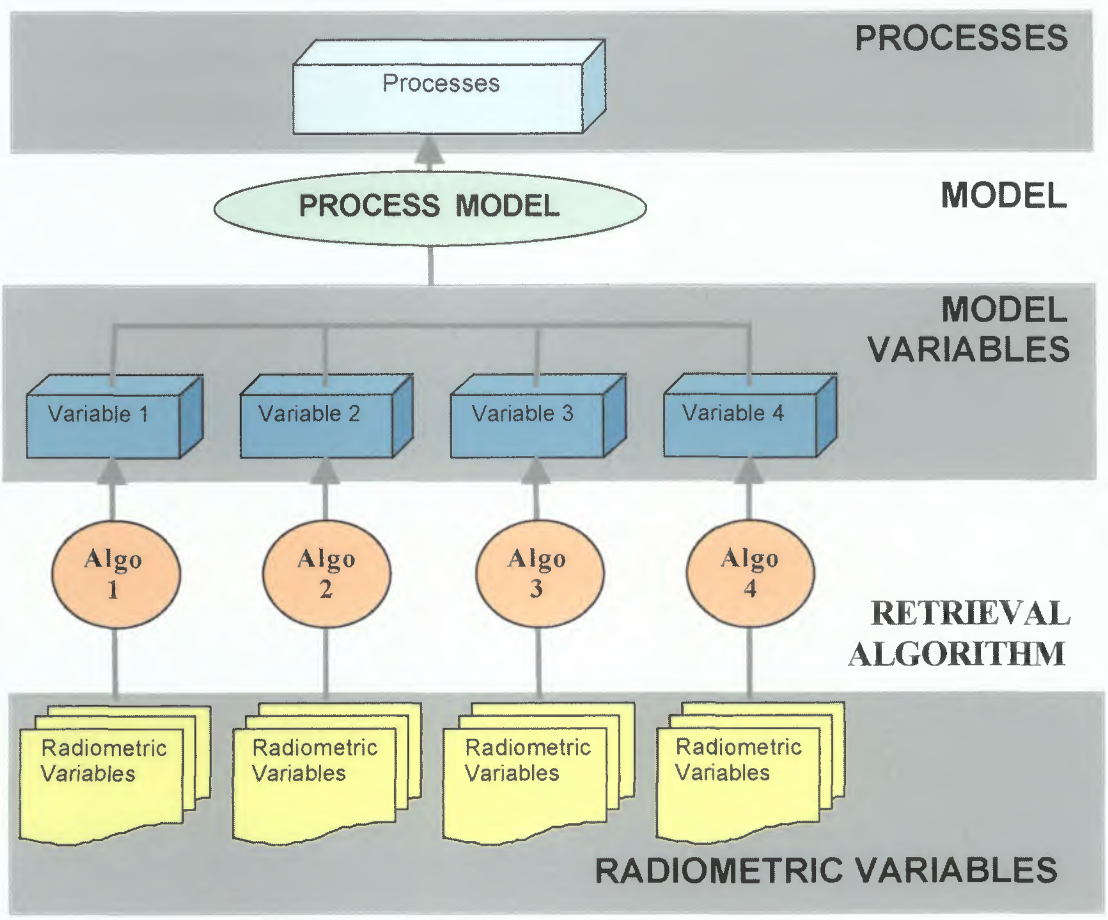

Figure 3.1. *From radiometric variables to processes through models.*

To derive observational requirements for any one of the relevant families of process studies, the processes and variables of interest must be formally associated with observations of spectral radiances. The processes relate to specific families of models, which need defining variables as input. Some of these variables, although not all, affect directly or indirectly the way in which the surface interacts with radiation. These variables feature in forward radiative-transfer models, which predict the intensity of scattered and emitted radiation in different directions and at different wavelengths. They can in principle be inferred from a well-chosen set of radiometric measurements through inversion of those radiative-transfer models which are locally verifiable through measurements on single plots. This approach is supported by recent developments of algorithms described in the literature, as well as in studies carried out to define specific aspects of the Land-Surface Processes and Interactions Mission. These algorithms will be discussed in Chapter 4, when the observational requirements are derived; the principle of these linkages is set out in Figure 3.1.

3.1 Processes and Variables

Five fundamental processes were identified in the last Chapter that are critical for understanding the way in which the land surface functions. Each process is associated with a particular set of geophysical and biophysical variables, and with families of models that operate across a range of space and time scales. The links between these processes, the associated variables and a simplified set of generic models that use them, are illustrated in Table 3.1.

This table presents a simplified outline and the true situation is somewhat more complex than is suggested there. More than one process will usually be important in a particular environmental system so the modelling activity must contain a set of sub-models representing all the process involved. For example, a crop growth modelling (and assimilation) scheme will necessarily need to model heat and water exchanges, as well as include a sub-model for photosynthesis. The colour coding introduced in Table 3.1 will enable the processes and models to be related to their key variables in other illustrations and tables shown in the report.

One of the essential objectives of the LSPIM is to enable the retrieval of the variables listed in Table 3.1 by inverting appropriate radiance measurements.

PROCESSES	MODELS	MODEL VARIABLES
Heat and mass transfer at the land/atmosphere interface	Soil vegetation atmosphere transfer models Planetary boundary layer models Global circulation model Numerical weather prediction models	Albedo Emissivity Long-wave spectrally integrated exitance Surface temperature Canopy and soil temperature Resistance to heat and mass transfer
Primary production	Efficiency models Canopy functioning models Canopy architecture dynamics models	Vegetation type Cover fraction fAPAR LAI LIDF Leaf chlorophyll content Leaf water content Stand density Phenology Soil type
Regional hydrological processes	Distributed watershed models Water conveyance and PBL dynamics Sediment removal and transport Chemicals transport and accumulation	Cover fraction Vegetation type Soil type Soil surface status (residues, moisture, roughness) Evaporation Snow cover, grain size Surface storage capacity
Land-atmosphere exchanges of biochemical species	Plant production and senescence, mineral nutrition Soil organic-matter turnover Transit and residence in soil and watershed Bio-geochemicals input to water	Relative amount of fast and slow decaying biochemicals Water-saturated soil temperature Soil moisture, water thickness Fresh-water constituents
Establishment and dynamics of ecosystems	Process models in stands Transect models Gap models Spatial models Dynamic global vegetation models	Spatial patterns of canopy architecture Fractional cover by vegetation type Soil type

Table 3.1. *Processes, models and associated variables.*

3.1.1 Heat and Mass Transfer

Heat exchange is a major part of the energy and water cycles. The energy cycle is driven by net radiation, the difference between incident and outgoing radiation at the surface. The partitioning of the shortwave component depends on the surface reflectance, and the longwave contribution on surface temperature and emissivity. These important state variables will be derived from the data generated by the LSPIM.

The heat fluxes are difficult to measure directly and are usually modelled, traditionally on either small, locally controlled experimental plots, or on very large scales with very simple representations, such as is used within General Circulation Models (GCM). Only recently has attention been turned to more complex systems, at the scale of typically a watershed, via distributed models, which are still amenable to direct observation. Even at local scales, the transport of heat and water from vegetated surfaces cannot be described as a single process and a family of schemes known as SVATs used to model the action of vegetation on mass and energy transfers at the surface. The representations of heat and mass transfer tend to be similar in different models, although the long-term consequences of slight differences may be significant. Systematic efforts to compare these land-surface schemes have been made by Henderson-Sellers and Pitman (1992), Pitman et al. (1993).

In the simplest representations, heat flux is modelled as a potential difference divided by a term that is interpreted as a resistance (Monteith and Unsworth, 1991). The potential difference is proportional to a temperature difference, or a water-vapour difference in the case of latent heat flux. Resistance varies spatially, being a strong function of surface cover, and the effective resistance of a heterogeneous area will not, in general, be an area-weighted average of the resistances of the cover types present. The link between the integrated heat flux over a heterogeneous area, and the average temperature over that area, is not then given by the same simple representation that can be used for a homogeneous area.

Given the sensitivity of regional and global climate models to surface heat fluxes, it is important to understand better how to aggregate heat fluxes over heterogeneous areas. It was shown in the previous chapter how current land-surface models disagree on how this should be achieved. The current poor state of understanding of this upscaling problem is illustrated by two contemporaneous studies focussing on the heat fluxes, one of which argued that the latent heat flux is nearly scale invariant, and another appearing to show the opposite (Bonan et al., 1992; Hall et al., 1992).

The relevant research objective of the LSPIM associated with this set of processes is to provide reliable and accurate data sets of reflectance and temperature distribution. The combination of space- and ground-based measurements over heterogeneous areas will enable the development of more accurate aggregated models.

3.1.2 Primary Production and Photosynthesis

Primary production is the conversion of atmospheric carbon and soil water into plant growth. This is achieved in a chain of processes, which include light interception by the canopy, conversion of the light energy to chemical energy (photosynthesis), and allocation of organic materials to roots, leaves and stems. Because of its role in converting atmospheric carbon to carbohydrate, photosynthesis is extremely important in the global carbon cycle.

There exists a good understanding of basic biochemical processes at the scale of a leaf, and models exist of global carbon cycling. However, these are not well matched. Current uncertainty as to what happens to anthropogenically produced carbon is quite profound, and presently only about 70% of the seven gigatons or so of carbon that are released annually through fossil-fuel burning and land-use change (Houghton, 1995), can be accounted for. Few carbon sinks, other than photosynthetic activity of the land surface, seem capable of accounting for the missing mass. The gap in the science occurs at the scale of individual landscapes, in regional biomass and growth models, where the understanding of basic plant processes, and representation of the landscape, have not been adequately brought into context. This is strikingly borne out in a recent study; in a similar exercise to the PILPS study for SVAT schemes (Henderson-Sellers and Pitman, 1992; Pitman et al, 1993), a comparison scheme was devised for Net Primary Productivity (NPP) models (Cramer and Field, 1999). The NPP was found to vary between models by more than a factor of two for all the biomes considered.

Rates of photosynthesis in a canopy depend on the concentration of chlorophyll, and on the canopy's ability to intercept light of the right wavelength (400-700nm). This in turn depends on the structure of the canopy. It is regulated also by the functioning of leaf stomata which couple photosynthesis to water transpiration. Models of primary productivity therefore require basic information on canopy geometry to determine the efficiency of light interception under different illumination conditions. They also need to know the leaf area index, chlorophyll concentration and species type (to determine conductance). For regional processes of photosynthesis, it is important to try to retrieve all of these variables, as well as the larger scale structure of the vegetation cover, to account for gap density etc. It is also necessary to determine the most appropriate averaging of the canopy conductance and how this is affected by environmental factors such as water stress.

The research objectives to be addressed by the LSPIM include the improvement of models of regional photosynthesis. This requires accurate information on canopy structure for calculating light interception and accurate identification of surface-cover types and chlorophyll concentration.

3.1.3 Regional Hydrological Processes

Water is, of course, an essential part of life and the need to secure adequate supplies of water for agriculture, and potable water to a growing population, are the main reasons to study and model the water cycle. Beyond this, however, its abundance makes it a unique component in surface and atmospheric processes. Water vapour is the major greenhouse gas and clouds are a source of great uncertainty in models of radiation balance and climate. Surface water is a strong determinant in the partitioning of surface energy and the high albedo of snow and ice are again important elements in determining surface energy budgets. Water availability in the soil is a limiting factor in plant growth models. Understanding of hydrological processes at a regional scale is thus not merely important for determining fresh-water availability, but is necessary to understanding the functioning of vegetation at the same scale, and to determining the regional scale interactions of the surface with the atmosphere. The short-term behaviour of a hydrological model is largely determined by initial conditions, but the longer term evolution of the water cycle is determined by the surface properties, particularly through feedbacks between surface behaviour and precipitation.

Simple one-dimensional treatments can be used to model the mass balance of a column of air, or the movement of water through a column of bare soil. An important boundary condition in each case is provided by the evaporation of water at the surface, so SVAT models form an important component of hydrological process modelling. Evapotranspiration is controlled by the opening and closing of plant stomata, coupling evaporation to the absorption of atmospheric carbon. This 'stomatal resistance' depends on vegetation type and condition, but is poorly modelled even for uniform cover. As evaporation is a non-linear function of stomatal resistance, there is a scaling problem with respect to regional evaporation. More accurate modelling of the water cycle over heterogeneous areas requires a distributed approach to the modelling, i.e. the explicit inclusion of the spatial variability of geophysical parameters.

Thus, the mission shall provide, in addition to variables related to surface radiation balance,

- fractional vegetation cover and soil composition for evaporation rates
- canopy structure to determine precipitation interception
- vegetation type, for surface-roughness estimates and stomatal properties, and
- snow area cover, for estimates of water storage and snowmelt prediction.

These will be used for improved model initialisation at basin scales, and hence to regional scales.

The contribution of this mission to hydrological studies is to quantify these key geophysical variables. These are needed to determine the partitioning of surface *energy and water flows, as already indicated above, and to determine fields of surface variables that modulate water flow.*

3.1.4 Land-Atmosphere Exchanges of Biochemical Species

Trace gases play an important role in atmospheric chemistry and ecosystem processes, and here specific mention must be made of methane which is an important greenhouse gas. The processes leading to the formation of methane are not well known, though intense agricultural practices and biomass burning have been identified as important sources. Fluxes of methane, CH_4, and nitrous oxide, N_2O, are controlled by terrestrial ecosystems but appear to be unrelated to climate at large length scales (Aber, 1992). Methane is, however, related to local hydrological conditions, e.g. depth of water table in wetlands, higher temperatures in wetlands and bogs and rice paddies in agricultural areas. Nitrification and denitrification depend on the impact of nitrogen limitation on biological activity. Models of these processes are in some cases at an early stage of development, and at present calculations are often done by multiplying acceptable estimates of fluxes by the area of land-cover types.

The main contribution of this mission in this area will be an improvement in the understanding of biochemical cycles.

3.1.5 Establishment and Dynamics of Ecosystems

The bio-geochemical cycles are strongly coupled to the energy and water cycles through the dynamics of ecosystems. Different species react differently to this forcing. Soils and topography are significant determinants of ecosystems. Spatial heterogeneity of ecosystems is the overall response of ecosystems to forcing. In this context it is necessary to model accurately the fluxes of carbon methane and trace gases with particular attention to the role of vegetation and litter decomposition.

As the time scale over which complex ecosystems change is longer than the lifetime of an Explorer mission, the main contribution of this mission will be to explore ecosystem spatial structures through improved ability to characterise surface cover.

3.2 Scaling

A common problem associated with the way in which all of these important processes are treated in existing models is uncertainty about the correct way to aggregate variables in heterogeneous landscapes. This uncertainty may be, in part, a failing of understanding, but is frequently caused by a general lack of knowledge on the way values are distributed spatially within a heterogeneous area. A simple stratification into land-cover classes, with acceptable values assigned to each class, is a possible approach, but this ignores the variability of values within a single cover type, such as might arise when an environmental or local climatic gradient extends across an ecosystem. It may also introduce systematic errors when parameter values taken from one observational study are applied to the same class under different conditions.

A better way to study the spatial variability of surface variables is to measure those variables more directly, through advanced model inversions. It is therefore important to be able to retrieve as many of the process variables as possible in any given case. It is also important not simply to retrieve variables, but also to characterise their variation across heterogeneous areas. This must be done with sufficient accuracy to ensure that the aggregated process is represented without bias at the appropriate scale.

A further reason to study these aggregations is to establish the relationship between process variables and radiances so that mesoscale models can assimilate satellite data of high temporal frequency. The relationships based on physical laws for homogeneous patches will not usually apply in the same way across heterogeneous areas. However, for models to operate at regional and continental level, the spatial representation of the surface must be of at least kilometric scale, and the only practical sources of satellite data for their initialisation and for assimilation must be of similar resolution given the large spatial areas involved. 'Effective parameters' need to be defined so that models can operate at the more practical resolutions, and make use of the coarser satellite data. This is the scaling problem as it applies to the use of operational satellite data, the determination of the relationships between radiances and fluxes over heterogeneous areas.

An essential element of the mission will be the preferential acquisition of data over well-instrumented test and experimental sites, covering a comprehensive range of biomes and ecosystems, at a time when measurements of a large range of ground measurements are being taken. If the mission were to start today, there are at least 100 sites around the World where such studies are being carried out to estimate fluxes and to investigate the problems of scaling. They cover a wide variety of ecosystems under different climatic conditions; all of these studies make use of satellite data where they can, usually from instruments such as the AVHRR, originally deployed for other reasons. These sites have been identified as the result of a study to assess the capabilities of the mission, which will be discussed further in Chapter 5.

The LSPIM data will enable the flux contributions from each landscape unit to be estimated and combined. This in return will establish the linearity (or non-linearity, as the case may be) of the aggregation process.

3.3 Accuracy Requirements

In many surface-process models, the values adopted for some variables may currently have quite high uncertainties associated with them. Nevertheless, for important processes it is preferable to assign to a variable an intelligently guessed value, with a large uncertainty, than to ignore completely the corresponding process (Dickinson, 1995). It is therefore not always sensible to think along the lines of accuracies required by the modelling community; an order of magnitude error would be acceptable, if no other value can be supplied. Estimates based on remotely sensed data are generally far more accurate than this. However, the main benefit of satellite-derived parameters is not that they can be more accurate than guessed or historical values, or than tabulated values for the cover type, or more accurate than values extrapolated from a small number of field measurements. The benefit lies in the fact that they are obtained across the whole of the modelled area, at the scale required by the model, in a consistent and repeatable fashion. The increased accuracy is, of course, a welcome bonus.

For variables such as soil and vegetation type there is in any case no single, sensible quantitative measure of accuracy, since the rationale for requiring these is to help determine such otherwise unobservable quantities as canopy resistance. There may therefore be no concomitant error if the mis-identification leads to no significant difference in the derived quantity. Error tolerances may also be rather difficult to assign to individual variables, since the variables are used in concert, and the total error is a complicated function of the individual errors and the way they are combined in the models. The situation with land-surface models is more complicated than for a single process depending on a single variable, where analytical treatments for error propagation may be readily applied, and a simple sensitivity study can illustrate the consequences of an error of given size. In such an active research area as land-surface process studies, it must also be expected that improved models and retrieval algorithms will be forthcoming, so it would be inappropriate to define the required accuracy solely on the basis of current practice.

For these reasons most modellers would be happy to work with, for example, LAI estimates carrying uncertainties of about 25%. However, this size of relative error could not be tolerated in surface reflectance or surface temperature. The critical importance of energy and water transfer to the functioning of surface, and the sensitivity of the processes to net radiation, means that the elements of the surface radiation budget (SRB) should be as accurate as possible. The major uncertainty in the SRB is the downwelling longwave radiation from clouds. According to Ellingson et al. (1995) this averages some 7 Wm^{-2} for each 10% of low-level cloud cover. Under slightly cloudy conditions, this uncertainty at the surface will be of the order 10-20 Wm^{-2}. This unpredictable and highly variable contribution to the SRB sets a limit to what it is probably feasible to retrieve from the satellite signal.

A sensible target is to be able to estimate other elements of the SRB, namely net short-wave radiation, and emitted longwave radiative flux, with an accuracy of 10 Wm^{-2}. A surface at 290 K emits some 400 Wm^{-2} of radiant energy, and an uncertainty of 10 Wm^{-2} in this value corresponds to an uncertainty in the surface temperature of some 2 K, or in the surface emissivity of about 0.02. For downward shortwave radiation of typical strength 500 Wm^{-2} irradiating a surface of albedo 30%, the SWR absorbed is 350 Wm^{-2}. The 10 Wm^{-2} uncertainty then corresponds to an error in surface albedo of 0.02, or about 7%. These numbers help guide the observational requirements presented in the next chapter.

As mentioned above, the real need of the modelling community is for data sets of process variables to be made available, consistently and repeatably, at the scale of the models. The models will thereby be improved and the science advanced, even if very large uncertainties attach to any given single number. Later, in Chapter 8 an attempt is made to relate the performance of the LSPIM to the accuracy requirements as identified in Table 3.2. These values are a selection corresponding to the variables as outlined in Table 3.1.

Variable	Relative Accuracy Required	Comment
Albedo	7%	Required for SRB
Emissivity	0.02	
Long-wave spectrally integrated exitance	2.5%	
Surface temperature	1 K	
Canopy and soil temperature	1 K canopy 2 K soil	Dual source heat transfer models
Cover fraction	10%	
fAPAR	10%	
LAI	20%	
LIDF	10%	5% for erectophile plants
Leaf chlorophyll content	20%	
Leaf water content	20%	
Stand density	20%	
Evaporation	10%	
Snow cover, grain size	10%	
Soil moisture	10%	
Relative amounts of fast- and slow-decaying biochemicals	10%	Elemental soil storage (C, N)
Water-saturated soil temperature	0.5 K	
Fractional cover by vegetation type	10%	Spectral un-mixing

Table 3.2. *Accuracy requirements for LSPIM variables.*

3.4 Application Potential

There is no clear dividing line between fundamental surface process research and applied science, leading to the transition from one to the other being blurred. It is apparent that by satisfying the basic requirements of this mission, to provide data to improve scientific models of surface functioning, data of direct usefulness in related fields are also being provided. These include the management of water bodies (coastal monitoring, inland waters, reservoirs), of managed semi-natural ecosystems (e.g. national parks) and of economically important systems such as agriculture and forestry. While these considerations did not constitute the prime motivation for this mission, it is evident that there will be a useful economic spin-off from this mission in many areas of interest to European national governments and international organisations.

3.5 Concluding Remarks

The performance of information processing systems (databases, and communication networks) has continued to improve drastically over recent years. These developments, coupled with major advances in numerical methods and simulation techniques, permit the design of ever more realistic environmental models. Current and near-future plans include the representation of heterogeneous ecosystems at resolutions hitherto unachievable. Parallel progress in space observation techniques now provides a unique opportunity to collect data at high spatial resolution and to address the scaling issues that have been hindering progress in furthering understanding of the environment. The next generation of environmental models must have the power to address the type of questions raised at the beginning of this document, namely to model and predict the impacts of environmental change. This will further the capability of understanding the functioning of ecosystems at the regional scale and provide a better quantification of bio-geochemical fluxes especially for elements of the carbon cycle. It will be critical that these models be evaluated, and that their accuracy and reliability be confirmed over a wide range of conditions for which field data must be collected.

The main objective of this LSPIM mission is to provide the detailed, spatially distributed, observations that are required to meet these needs. This will be achieved by:

- *deploying a satellite system capable of acquiring accurate observations in the solar and thermal spectral domains, as a function of space and time, and in multiple directions of observation,*
- *delivering to the scientific community high-quality radiometric data and products derived from these space observations to be combined with ground measurements.*

The characteristics of the proposed instrument have to be chosen so as to fill a major gap between the very high spatial resolution provided by field experiments and the much reduced resolution of existing (and planned) operational sensors which are designed to cover the entire globe every day or so.

This strategy of course also hinges on the capability of the scientific community to also bridge the gap between radiometric measurements acquired in space and the environmental information required over land. However, significant progress has been achieved in this direction. In fact, a wide diversity of solutions have been proposed and are already being implemented to exploit current and near-future sensors. Given the rates of progress of science and technology, as well as recent achievements in remote-sensing science, it is expected that the major limitation to the understanding of the environment by 2004 will be access to highly accurate, reliable data at resolutions intermediary between local and global observations. It is further anticipated that, by then, models will be capable of either ingesting the derived products as initial and boundary conditions, or of assimilating the measured calibrated reflectances themselves into comprehensive land-surface models, just as forecasting models are doing today for the weather.

4 Observation Requirements

The models linking the processes of interest to the corresponding variables characterising either canopy and soil status or mass and energy fluxes were reviewed in Chapter 3. This Chapter will derive the requirements for their retrieval from radiometric observations. Implications for the most appropriate spectral, directional, radiometric, spatial and temporal sampling strategy will then be derived.

4.1 Direct and Inverse Modelling for Estimating Biophysical Variables from Radiance Data

The radiation coming from the Sun is scattered both by the atmosphere and the Earth's surface, in particular by vegetation and soil. Part of the radiation is absorbed and contributes to increase the temperature of these elements, which will emit radiation. The spectral and directional features of the radiation observed by a sensor on-board a satellite will thus depend on:

- **The Atmosphere** – the radiative properties of the atmosphere are governed by its composition and temperature and their vertical distribution (e.g. Kaufman, 1989; Vermote et al., 1997).
- **The Vegetation** – the scattering and emission by vegetation are governed by its structural and optical properties as well as its temperature (e.g. Knyazikhin et al., 1992; Liang and Strahler, 1993b; Marshak, 1989; Myneni and Ross, 1991; Ross, 1981; Shultis and Myneni, 1988; Simmer and Gerstl, 1985). Relevant structural properties include the area, shape, orientation and position in space of the elements (leaves, stems, branches, etc.).
- **The Soil** – the scattering and emission properties of soils are mainly driven by their surface roughness, structure, texture, moisture, temperature and type of soil in terms of its biochemical composition (Irons et al., 1989; Jacquemoud et al., 1992; Pinty et al., 1989).

Several physically based models have been developed to describe the scattering properties of these components. They can be classified into three categories:

- Detailed three dimensional models of radiation transfer (e.g. Borel et al., 1991; España et al., 1999; Gastellu-Etchegorry et al., 1996; Govaerts and Verstraete, 1995; Govaerts and Verstraete, 1998; Myneni and Asrar, 1993; Peltoniemi, 1993; Ross and Marshak, 1988);
- Geometrical optical models (e.g. Begue, 1992; Li and Strahler, 1985);
- One-dimensional vertical models of radiation transport for horizontally homogeneous geophysical systems (e.g. Gobron et al., 1997b; Knyazikhin et al., 1992; Liang and Strahler, 1993a; Marshak, 1989; Nilson and Kuusk, 1989;

Pinty et al., 1990; Shultis and Myneni, 1988; Simmer and Gerstl, 1985; Suits, 1972; Verhoef, 1984; Verstraete et al., 1990).

The coupling between surface and atmospheric models allows one to compute the spectral and directional radiance field as collected by the sensor on board the satellite, as a function of the characteristics of each component. This is referred to as the direct modelling approach. However, the main issue in remote sensing is to infer characteristics of the atmosphere, vegetation and soil system from the spectral and directional variation of the radiation field measured at the satellite level. The coupled models have therefore to be inverted to provide estimates of the characteristics of the underlying objects as shown in Figure 4.1.

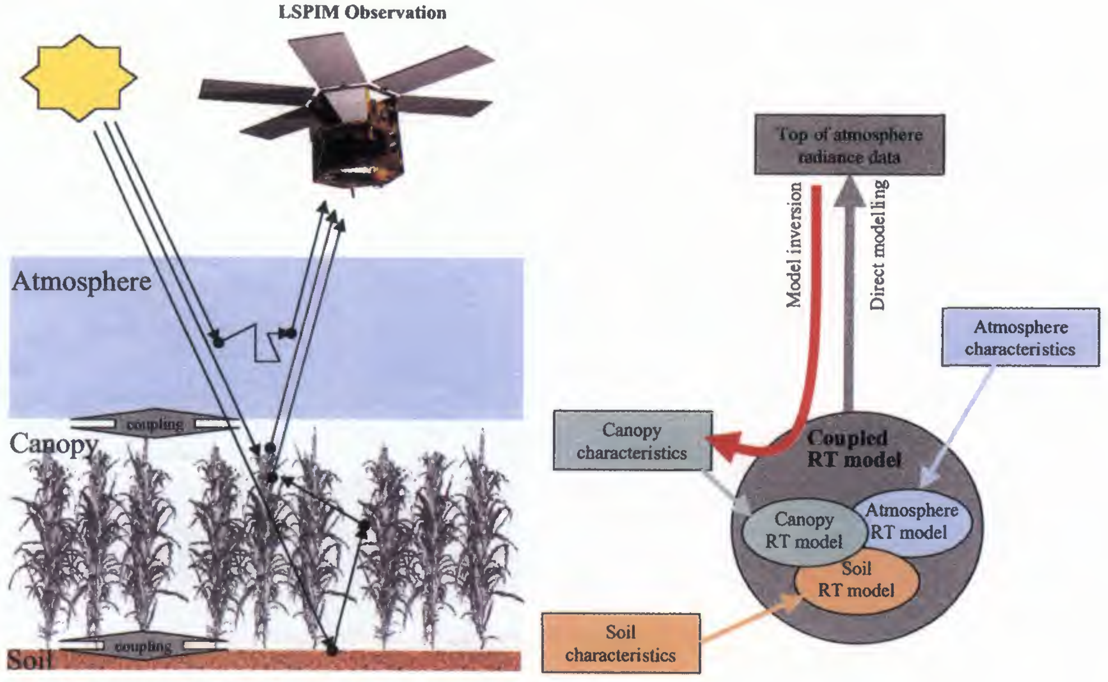

Figure 4.1. *Schematic description of the interactions of the radiation with the soil-vegetation-atmosphere showing the coupling between the radiative transfer of each of these components (left side of the Figure). The right side shows how coupled soil-canopy-atmosphere radiative transfer (RT) models simulate the top-of-atmosphere radiance data as measured from the satellite. These models can be inverted to estimate canopy characteristics from satellite data.*

Inversion of radiative transfer models is currently a very active scientific field where advanced techniques are being developed (Baret et al., 1999; Bertero and Boccacci, 1998; Pinty and Verstraete, 1991; Tarantola, 1987; Verstraete et al., 1996).

Two main approaches are classically used by the geophysical scientific community as well as by the remote-sensing community:

- *optimisation techniques* (Goel et al., 1984; Jacquemoud, 1993; Kuusk, 1991; Privette et al., 1996) where, starting from an initial set of variables, the values of the variables are iteratively updated to the point where a good match is reached between the radiance field simulated by the coupled models and that measured by the sensors. The use of look-up tables (Knyazikhin et al., 1998a) is a special case of these iterative techniques. Genetic algorithms have also been used in this context (e.g. Renders and Flasse, 1996);
- *approximation of the surface response*, uses mathematical techniques such as neural networks (Baret et al., 1995; Kimes et al., 1998; Smith, 1992) intended to approximate the inverse relationship between the radiance field and the variables of interest. Simpler relationships such as vegetation indices used to estimate several variables such as *fAPAR* have been investigated by, e.g. Baret and Guyot, 1991; Leprieur et al., 1994; Pinty and Verstraete, 1992; Sellers, 1985; Verstraete and Pinty, 1996. The split-window technique for atmospheric correction in the thermal infrared (Becker and Li, 1995; Caselles et al., 1996; Prata and Cechet, 1999) also belongs to this latter category.

The accuracy of the estimation of the canopy characteristics will mainly depend on (Gobron et al., 1997a; Myneni et al., 1995; Verstraete et al., 1996):

- The sensitivity of the radiance field to the variable considered. This depends mainly on the variables considered (Baret and Jacquemoud, 1994). For example, the relationship between *LAI* and reflectance is strongly non-linear, with a saturation of canopy reflectance for the higher *LAI* levels (Fig. 4.2). This implies that the radiance values observed from the satellite loose their sensitivity to *LAI* beyond *LAI* values of 3 to 4, depending on soil optical properties and canopy architecture (Gobron et al., 1997a).
- The capacity of the models to accurately represent the characteristics of the objects, in particular canopy structure which can be very complex. Simple radiative-transfer models are based on simple assumptions of canopy architecture which may or may not strictly apply to sparse canopies, or clumped canopies such as forests. The models used should ideally be consistent with the type of canopy considered.
- The accuracy with which the models approximate the radiative-transfer physical processes. Several assumptions are used to solve the radiative-transfer problem, mainly through directional and spatial discretisation. Some of these

approximations induce significant errors, which propagate through the inversion process up to the estimation of the biophysical variables (Baret et al., 1999).

- The amount of external information put into the system, for example in terms of the a priori distribution of the variables to be retrieved, which, for vegetation, generally identifies the type of canopy considered.
- The amount of spectral and directional information used, which mainly refers to the sampling achieved by the sensor, both in the spectral and directional domains.
- The uncertainties underlying the radiometric measurements, which are governed by the radiometric resolution and the accuracy of the absolute radiometric calibration. It should also take into account the accuracy with which the spectral bands and directions of observations are positioned as these will also effect the effective radiometric accuracy.

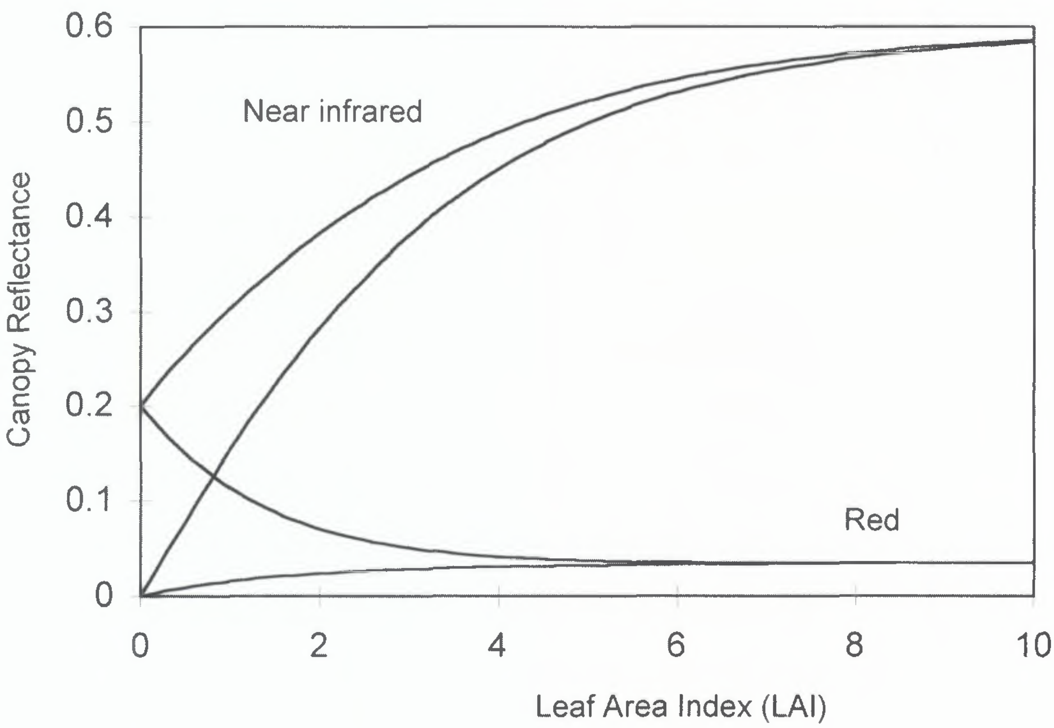

Figure 4.2. *Sensitivity of canopy reflectance to the leaf area index (LAI) in the red and near-infrared bands. For each waveband, two cases are presented: black soil (reflectance=0.0) and a soil with reflectance=0.2.*

The specification of the sensor in terms of spectral, directional, spatial and temporal sampling must be tuned to provide the best estimates of the variables of interest consistent with the description of the processes considered in the LSPIM. This is discussed in the following sections after describing the retrieval methods of the model variables from the radiance field.

4.2 From the Radiance Field to the Variables of Interest at the Local and Instantaneous Scales

At the local spatial scale, where the objects are assumed homogeneous, and at the instantaneous time scale, where objects are considered in a steady state, information on canopy characteristics will be derived from the spectral and directional variability of the radiance field observed. Figure 4.3 shows the typical directional and spectral variation of canopy reflectance.

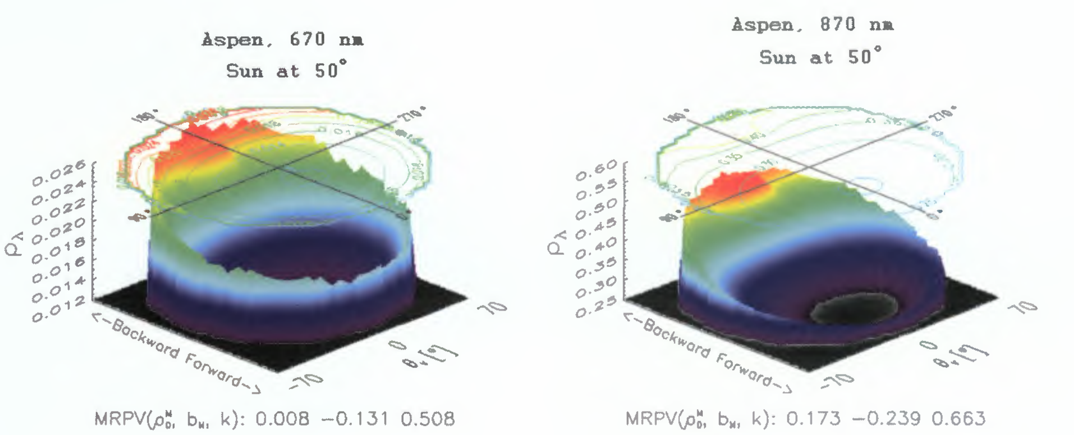

Figure 4.3. *Example of the BRDF of an aspen forest canopy in the red (left) and near infrared (right) for a Sun zenith angle at 50°. The hot-spot feature in the backward direction and the general typical bowl shape of the BRDF can clearly be observed. The BRDF appears strongly dependent on the wavelength.*

The approach will be illustrated by the two most dominant and important of the basic land-surface processes: heat and mass fluxes at the land/atmosphere interface and primary production. Similar examples could have been given for the other processes.

The algorithms that will be used to retrieve the biophysical variables of interest will be reviewed, paying particular attention to the spectral and directional sampling scheme required to get accurate estimates.

Heat and mass exchange

For the spatial and temporal scales considered here, the models associated with processes controlling the exchange of heat and mass are the Soil Vegetation Atmosphere Transfer (SVAT) models, which are generally designed to work at the local scale where horizontal homogeneity can be assumed. A few of the variables used in SVAT models (e.g. Dickinson, 1983; Menenti and Verhoef, 1998; Pitman et al., 1993; Sellers, 1985; Sellers, 1987) are closely related to radiometric variables because they are associated with radiation balance: albedo (bi-directional reflectance integrated over the hemisphere and over wide spectral bands), emissivity, surface temperature for soil and vegetation components and long-wave emittance. Other variables, such as resistance of heat and mass transfer can be parameterised using canopy structure variables and vegetation type (Menenti and Ritchie, 1994), which could be derived from radiometric data.

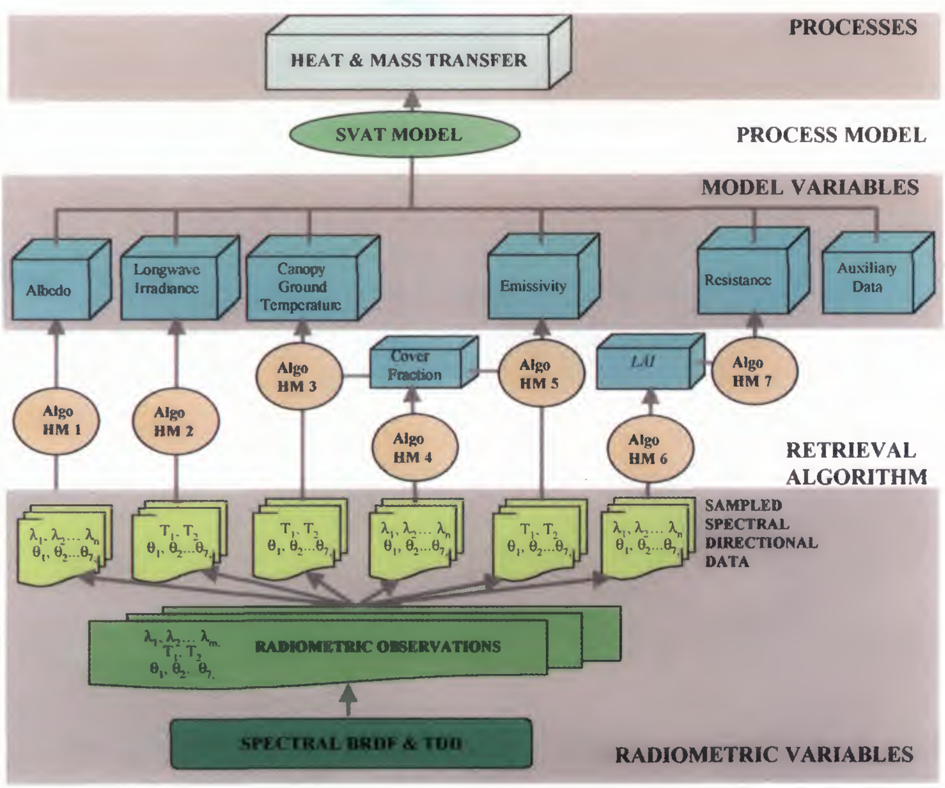

Figure 4.4. Link between processes, models, model variables, retrieval algorithms and radiometric variables in the case of heat and mass fluxes.

Some examples are given in Figure 4.4 on how the variables required as input to the SVAT model could be derived from radiometric observations both in the spectral and directional domains. The radiometric field, i.e. the spectral BRDF and TDD (Temperature Directional Distribution), is first acquired by the sensor that provides the observations. The sensor data are then corrected to feed the retrieval algorithms of each model variable involved in the process considered. Therefore defining the observational requirements for the LSPIM consists of designing the spectral and directional sampling of BRDF and TDD, as well as defining the corresponding radiometric performances that allow accurate and robust estimation of the model variables of interest.

Primary production

The associated model describes the functioning of the canopy (Brisson et al., 1998) and is generally designed to work at the local scale (where the vegetation can be assumed to be horizontally homogeneous). Such models describe elementary processes such as photosynthesis, respiration, allocation of assimilates to the several parts of the plant, and canopy structure development. In addition, they require inputs from heat and mass transfer models to specify the strong constraint imposed by water limitation. In that way, these models gain by being coupled to heat-and mass transfer-models.

Canopy functioning models have the capacity to run by themselves, using mainly meteorological and soil inputs. However, due to the complexity of the processes involved and the sometimes poor knowledge of some of the key parameter values (such as the specific leaf area, the efficiency of photosynthesis or the allocation coefficients), model simulations tend to depart progressively from reality as they do not represent the evolutions of the vegetation. Therefore, comparisons between actual canopy structure and those simulated from canopy functioning models have to be repeated frequently in order to keep the model on track (Bouman, 1992; Fisher et al., 1997; Moulin et al., 1998). This is achieved through assimilation techniques where the key variables are adjusted so that canopy structure and optical properties agree with actual observations.

Therefore, apart from the canopy type, the variables required by these models are mainly those characterising canopy structure and the optical properties of the leaves through chlorophyll and water contents. Nevertheless, part of the processes within such models could be directly driven by the provision of remote-sensing estimates of variables such as *fAPAR* that drives the potential photosynthetic production, *LAI* for vegetation phenology and heat- and mass-transfer variables providing estimates of the soil water availability that modulates the efficiency of the photosynthesis and the biomass distribution. Similar to what was shown for energy and mass exchange,

Figure 4.5 illustrates the link between primary production and radiometric observations through retrieval of the variables used by canopy functioning models.

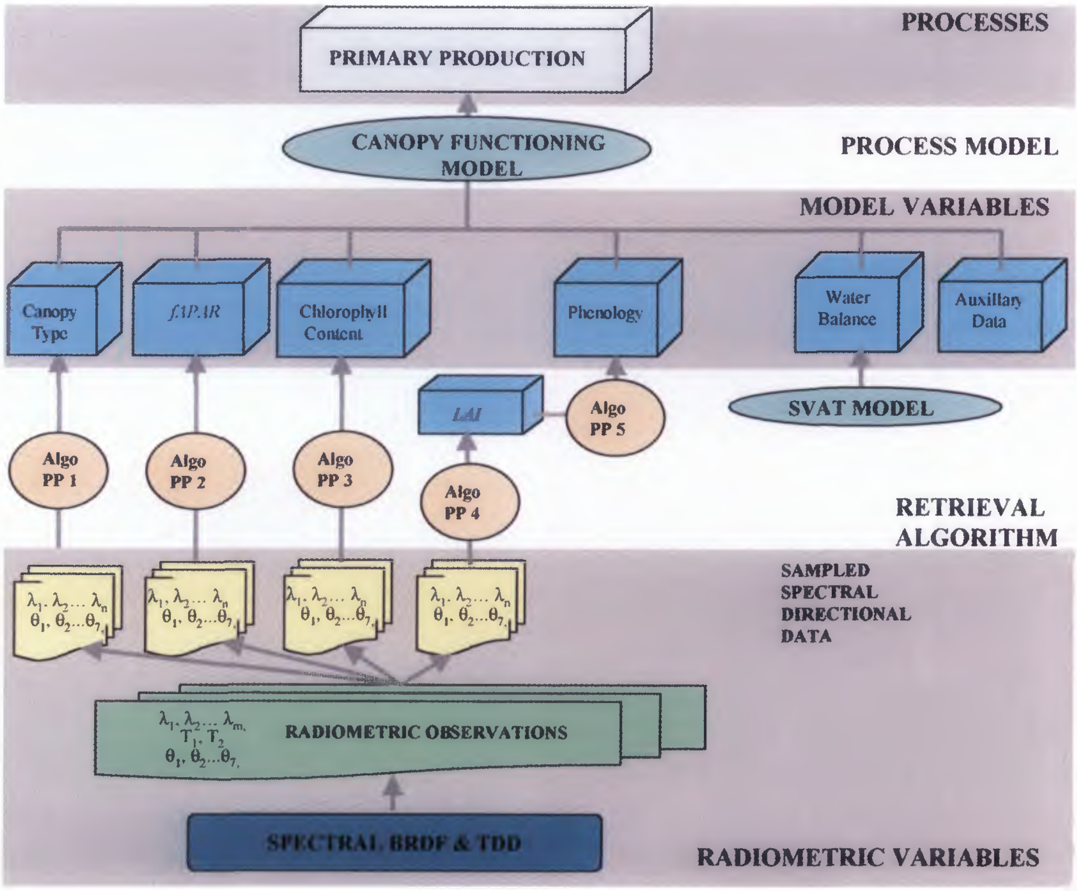

Figure 4.5. *Link between processes, models, model variables, retrieval algorithms and radiometric variables for primary production.*

The list of biophysical variables used as inputs to the models associated to the five fundamental processes are presented in Table 4.1. This Table complements Table 3.1 by going a step further and identifying already proposed retrieval algorithms and the corresponding radiometric variables required. This Table therefore provides the link between model variables and radiometric observations. Additionally, the temporal dimension is also mentioned where it is mandatory for some variables such as those describing the phenology.

The estimation of many of these variables requires both directional and spectral sampling of the radiance field. Furthermore, when all these variables are being estimated, the radiance must be observed across the whole spectral domain, i.e. in the visible, near-infrared, shortwave infrared and thermal infrared.

A selection of the algorithms proposed will be described in more detail in Chapter 7. Similar examples could also be made for other relevant land-surface processes, the approach for their analysis would be adopted in an analogous way.

MODEL VARIABLES	ALGORITHM	VIS		NIR		SWIR		TIR		Time
		λ	θ	λ	θ	λ	θ	λ	θ	
Albedo	Rahman, 1998; Lucht et al., 1998; Privette et al., 1997; Menenti, 1998; Weiss, 1999a	✓	✓	✓	✓	✓	✓			
Emissivity	MOD-11, Caselles, 1988; Becker and Li, 1995; Wan and Snyder, 1996	✓	✓	✓	✓			✓	✓	
Long-wave spectrally integrated exitance	Menenti and Verhoef, 1998							✓	✓	
Surface temperature	Caselles et al., 1998; Becker and Li, 1995	✓	✓	✓	✓			✓	✓	
Canopy and soil temperature	Francois 1997; Norman, 1990; Djepa et al.,1998	✓	✓	✓	✓	✓	✓	✓	✓	
Resistance to heat and mass transfer	Norman and Chen, 1990; Menenti and Ritchie, 1994	Estimates from LAI and Vegetation type								
Vegetation type	MOD-12, MOD-41	✓	✓	✓	✓	✓	✓	✓	✓	✓
Cover fraction	Weiss, 1999b	✓	✓	✓	✓					
fAPAR	Knyazikhin, 1998b; Weiss, 1999b; Bicheron, 1999	✓	✓	✓	✓					
LAI	Knyazikhin, 1998b; Weiss, 1999b; Menenti, 1998; Bicheron, 1999	✓	✓	✓	✓	✓	✓			
LIDF	Pinty, 1998; Weiss, 1999	✓	✓	✓	✓	✓	✓			
Leaf chlorophyll content	Weiss, 1999; Bicheron and Leroy, 1999	✓	✓	✓	✓					
Leaf water content	Gao and Goetz, 1990; Fourty and Baret, 1997; Moreno, personal correspondence			✓	✓	✓	✓			
Stand density		✓	✓	✓	✓	✓	✓			
Phenology	Duchemin et al., 1999	✓	✓	✓	✓	✓	✓			✓
Soil type	Escadafal and Huete, 1992; Mackin, 1997	✓	✓	✓	✓	✓	✓	✓		
Soil surface status (residues, moisture, roughness)	Bach and Mauser, 1994; Biard and Baret, 1996	✓	✓	✓	✓	✓	✓	✓	✓	
Evaporation	Menenti and Choudhury, 1993;	Estimates from Heat and mass transfer processes								

Snow cover, grain size	MOD-10; Painter 1998	✓	✓	✓	✓	✓	✓	✓	✓	
Surface storage capacity	Soil Conservation Service (SCS)	Estimates from LAI, LIDF and vegetation type								
Relative amount of fast- and slow-decaying biochemicals	Joffre et al., 1992	✓	✓	✓	✓	✓	✓			
Fresh-water constituents	MOD-23; MOD-24; Doerffer and Schiller, 1997; Hoogenboom et al., 1998;	✓								
Fractional cover by vegetation type	Lavabre et al., 1993; Vine et al., 1999	✓	✓	✓	✓	✓	✓	✓	✓	

Table 4.1. *Variables used in the models of processes (model variables); algorithms, spectral (λ), directional (θ) and temporal (Time) domains required for the estimation of variables. The spectral domain was split into four parts: VIS (0.4-0.7 μm); NIR (0.7-1.3 μm); SWIR (1.3-2.5 μm) and TIR (8-13.5 μm). The tick marks indicate the typical extent of spectral and directional sampling required to effectively retrieve the selected model variable with useful accuracy using the proposed algorithms.*

4.3 Requirements of the Space Segment of the LSPIM

Based on the discussion of environmental processes (identified above), the needs of the associated models and the driving variables to be extracted from the space component of the LSPIM, the observational requirements have been derived taken due account of the other components (field- and ground segment).

4.3.1 Spatial Requirements

Spatial distribution of the sites of interest

The LSPIM is intended to provide detailed observations of globally selected sites where intensive ground investigations are taking place. A typical distribution of currently maintained experimental sites that are scientifically representative for the processes and biomes to be investigated is provided in Figures 5.2 to 5.6. The actual distribution of sites to be supported during the period of exploitation of LSPIM may well evolve, but the current situation does provide an illustration of a representative set of the site locations.

The mission must be able to provide data for any site, arbitrarily selected anywhere over continental regions.

Spatial scale of the targets of interest

The field campaigns and other local investigations that will be exploited by this mission will cover a wide variety of ecosystems and watersheds of different dimensions. However, past experience shows that even during broad international campaigns, field investigations tend to concentrate on a restricted number of sites of limited extent. For instance, the HAPEX, FIFE, BOREAS and LBA in this case, have all identified dedicated sites for intensive data acquisition and characterisation. These sites vary in size, but typically cover areas of 100 to 2500 square km. Such regions exhibit the following characteristics:

- areas of that extent correspond to the typical size of a grid square of regional circulation model (10 to 50 km on the side),
- medium-sized watersheds include sufficient heterogeneities to enable the simulation of complete landscapes (this size permits the study of critical scaling issues identified earlier),
- local to regional topographic, soil and climatic gradients dominate the landscape and the distribution of ecological variables at that scale,
- meteorological and hydrological field measurement networks are designed to work at that scale, and are usually implemented on watersheds of that size,
- process studies are often conducted at that scale because the collection and processing of data for such regions of that size are operationally and logistically feasible.

The mission must be able to provide data simultaneously acquired over target areas of about 50 x 50 km.

Spatial sampling within the target of interest

As mentioned earlier, significant variabilities in physical, chemical, biological and ecological variables occur at all scales. This mission is intended to directly contribute to a better understanding of the up- and downscaling issues characteristic of climate and environmental studies.

A major attribute of the landscape is its spatial organisation, i.e. the arrangement in space of its different elements. The concept of landscape spatial pattern covers, for example, the patch size distribution of residual forests, the location of agricultural plots in relation to natural or cultural features, the shapes of fields or the number, type and configuration of landscape elements (their spatial heterogeneity). To detect changes in landscape patterns, the spatial resolution of the sensor must be sufficient to document the average size and properties of the ground elements that need to be resolved. Briggs et al. (1995) showed that there is a monotonic loss of information as the spatial resolution decreases. For complex landscapes, there is no particular spatial resolution threshold at which an abrupt loss of spatial information would occur with increasing resolution. For well-structured landscapes, the existence of a threshold would depend on the average parcel size and would therefore be different for different landscape types.

Experience with current sensors reveals that with spatial resolutions of 20 to 30 metres, the structure of complex landscapes is resolved in great detail. A slightly coarser spatial resolution would not affect the analysis of surface processes in a major way as most agricultural fields, forest plots or natural landscape units have sizes of several tens of metres. Data layers, which are used in ecological models and which are not derived by remote sensing (e.g., digital elevation models, soil maps, etc.), are generally conceived at a coarser spatial resolution. On the other hand, collection of field observations with ground instruments rarely extends beyond an area larger than one to a few hectares. A good compromise between these different constraints would therefore be found with an instrument providing a spatial resolution of about 50 metres at nadir. This requirement is clearly a compromise between the needs of various scientific groups. However, it is expected that all the key studies that this mission is designed to support will be feasible using data with that spatial resolution.

The LSPIM will take place in the context of many other existing or planned missions, which will also provide data relevant for the same geographical regions of interest. The proposed spatial resolution is complementary to those available from global Earth observing instruments, which typically operate at spatial resolutions between 250 and 1000 m, and bridges the gap between these and high-resolution instruments such as SPOT HRV and Landsat ETM (with respect to spatial resolution).

The mission must be able to provide data at a spatial sampling interval of 50 m at nadir.

Data acquisition over ground sites

The spatial distribution of sites considered in the LSPIM must be optimised to sample several processes over a range of biomes. The location of the corresponding sites then follows from (already existing) scientific studies concentrated over well-instrumented and known areas. Multiple sites should be observable during each orbit to maximise the utilisation of the sensor and to minimise the impact of cloud obscurations. This mission must be capable of acquiring data for a number of experimental sites, with a specified temporal revisit capability, the observational requirements for which are specified in Chapter 5.

Several sites should be observable during each orbit. This mission should have enough flexibility to be able to overcome cloud impacts by being able to select alternative sites.

4.3.2 Temporal Requirements

Duration of the mission

All major processes of interest exhibit significant daily, seasonal and inter-annual variations, due to such phenomena as El-Niño, major volcanic eruptions and other year-to-year climatic fluctuations. From a programmatic point of view, the detailed investigations typically undertaken in major international field campaigns last for a few years.

The mission must be able to provide data for a minimum period of 2 years, but ideally for 4 years.

Site revisit capability and temporal sampling resolution

Some scientific issues are of particular relevance only during limited periods of time. For instance, most of the research activities dedicated to the study of vegetation processes take place during the growing season. As for the spatial requirements (discussed above), bio-geophysical processes take place over a variety of time scales. For instance, plants may exhibit noticeable changes over periods of hours or more (e.g. heliotropism, changes in leaf turgor, etc). However, the most important environmental changes in the scientific context of the mission are those that take place from week to week throughout the season. Thus the maximum period between two consecutive useful observations should not be longer than about a week. This will allow efficient assimilation of the data into dynamic models of ecosystems.

Data acquisition in the thermal domain has to account for different time scales applicable for reflectance in the solar domain. Leaf and soil temperatures may vary significantly over periods of minutes to hours. Monitoring such changes would require either a geostationary platform (at a severely reduced spatial resolution), or a constellation of platforms. However, assimilation of thermal data acquired at intervals close to 3 days to one week within SVAT models allows the main terms of the energy and water balance to be evaluated through assimilation procedures.

Field measurements are often undertaken only during limited campaign periods at a given site. The proposed temporal sampling resolution would therefore permit the support of such campaigns with data being provided every few days, assuming that the weather conditions are favourable. The presence of clouds that prevent the observation of the Earth's surface is one of the main limitations of optical remote-sensing systems when high-temporal-frequency data acquisition is required. The cloud climatology shows that on, an average, half of the Earth is covered by clouds (Rossow et al., 1988) at any given moment. This limitation has to be taken into account for the site acquisition scheme.

The mission must be able to acquire data every 2 to 3 days during periods of up to a few months for any particular site.

4.3.3 Spectral Requirements

Spectral extent of the measurements

The derivation of environmental information from remote-sensing data hinges on the capability of interpreting these data with the help of radiation-transfer models. Two major spectral regions are considered critical to address the scientific issues identified earlier, namely the solar and the thermal spectral ranges.

The solar spectral range extends between 0.25 and 3.0 μm, although most of the ultraviolet radiation is absorbed in the upper atmosphere and the intensity of the incoming irradiance becomes very small beyond 2.35 μm. Thus, reliable and accurate data have to be acquired with sufficient signal-to-noise ratio in the spectral range 0.45 to 2.35 μm.

The thermal emission domain extends from 3 to 30 μm, but the radiation emitted by the surface in significant parts of this range is immediately absorbed in the atmosphere and re-emitted. This means that the surface is not observable outside the so-called atmospheric windows, which extend from 3 to 5 μm and from 8 to 13.5 μm. Measurement problems in the 3-5 μm window, arising from the combination of emitted radiation and some contributions from reflected solar radiation, make the efficient use of the information available in this window over land during day-time rather complex and difficult. The TIR window is between 8 and 13.5 μm and is thus preferred for the purpose of estimating surface temperature.

The mission must be able to provide reliable spectral reflectance data in the spectral range 0.45 to 2.35 μm, as well as allow the retrieval of surface-brightness temperatures.

Spectral resolution and sampling interval

Different materials absorb and scatter solar light differently as a function of wavelength. Absorption features are associated with the conversion of electromagnetic radiation into electronic, rotational and vibrational forms of energy at the molecular level. These quantum processes are strongly dependent on wavelength, and are thus intimately related to the chemical composition and physical status of the materials interacting with the radiation field. This feature constitutes the basis for the interpretation of the spectral variations in terms of target identification and characterisation.

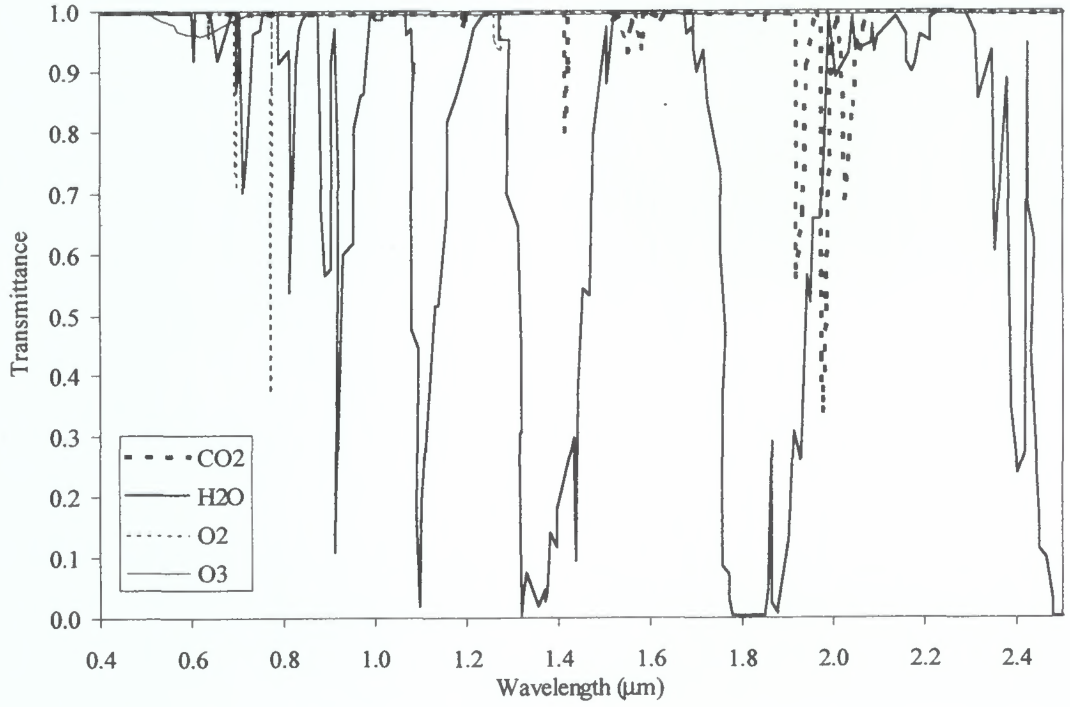

Figure 4.6. *Transmittance of the atmosphere for the main gas as derived from the 6S mode (Vermote et al., 1997).*

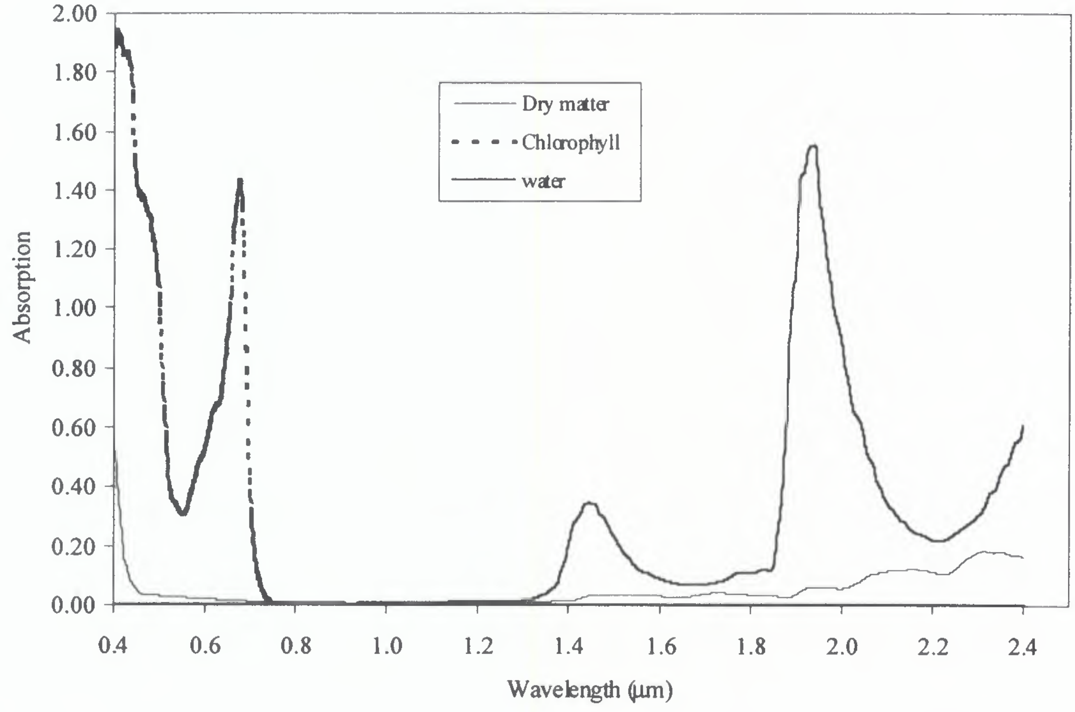

Figure 4.7. *Absorption (relative unit) of the main vegetation absorbing materials. (Baret and Fourty, 1998).*

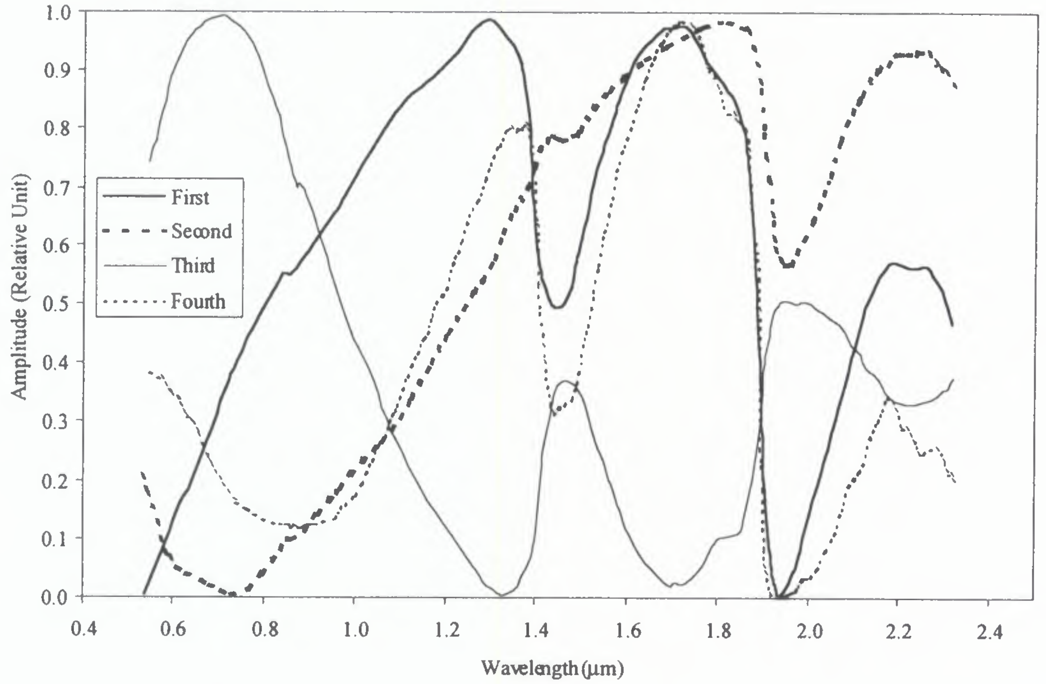

Figure 4.8. *The four end-member reflectance spectra used to describe the spectral variation of most soil types (Price, 1990).*

The simplest way of exploiting the spectral signature of a target is to measure its reflectance in a set of spectral bands which are affected differently by the absorption process. The differential response provides the desired source of information. The spectral resolution and sampling interval must therefore be high enough to locate and characterise the absorption features of targets of interest.

Most retrieval algorithms rely on the possibility to accurately simulate the absorption features of targets using radiative-transfer models. The spectral resolution and sampling interval of the instrument used to provide the data depends on the size of the absorption features used for the retrieval of surface characteristics and for the atmospheric correction. Individual absorption features vary in width from typically 1 nm in the atmosphere (Fig. 4.6 – where specific simple molecules interact with the incoming radiation field) up to 20 nm to 100 nm for broad features of plant canopies, such as the photosynthesis absorption well in the red region (Fig. 4.7) and soils (Fig. 4.8). Individual absorption bands can be broadened through a variety of physical mechanisms resulting in absorption continuum spanning a wide range of the spectrum (Fig. 4.7 and 4.8).

It is important to remember that the spectral sampling interval is linked to the spectral resolution to ensure almost continuous measurement of the absorption features. The optimal value is found when the spectral resolution is ≤ 1.5 times the spectral sampling interval.

In the thermal-infrared region, two spectral bands, positioned around 8 to 8.5 μm and 8.6 to 9.1 μm, respectively, have been found to be an optimal trade-off for surface temperature estimation (Caselles et al., 1998).

The mission must provide data at a spectral sampling interval of approximately 10 nm at the shorter wavelengths (680-769 nm-vegetation red edge) and about 15 nm, at the longer wavelengths. The spectral resolution should be better than 1.5 times the spectral sampling interval. In the thermal infrared, two spectral bands are required, namely: 8.0-8.5 μm and 8.6-9.1 μm.

Number of spectral bands transmitted per scene

This mission is intended to facilitate the study of surface processes, and different science areas have an interest in different spectral ranges. Energy-budget studies need information at visible and near-infrared ranges, and over the thermal infrared, while plant chemistry studies need narrow bands in the short-wave infrared. The sets of algorithms listed earlier in this chapter typically makes use of different amounts of spectral bands. Moreover, the scientific community is still very active in the improvement of the retrieval algorithms with an increasing number of spectral bands being used in these algorithms. It is thus likely that a larger set of bands could be used to enhance the accuracy of canopy biophysical variables estimation.

From recent advances in the analysis of the information content provided by high-spectral-resolution sensors, it appears that about 60 bands should be enough to describe accurately most canopy, snow/ice, or soil reflectance spectra from top-of-atmosphere data (Price, 1994a). The precise number of spectral bands required, and their optimal location, depend on the type of area and object studied and on the approaches used. There may also be certain applications which make use of the contiguous spectrum. A high degree of flexibility in the choice of bands should be preserved. No single application will require all of the bands across the large spectral range; however, the bands required will be different for each application and surface type. Together the individual applications span the entire optical range with their requirements for spectral coverage. Further important considerations in this context are:

- One of the foremost topics benefiting from a contiguous spectral coverage is the relative spectral calibration and the spectral stability of the observations. Calibration has become one of the most critical issues in this domain as it enables the quantitative retrieval of geophysical variables, when carried out accurately. The stability in this case ensures the compatibility of long-term and of repeat measurements. A contiguous spectral coverage is necessary to ensure the calibration throughout the spectrum using the different absorptions as calibration 'hinges' or anchor points. Only by means of contiguous spectral coverage can the whole shape of the absorption band be reconstructed and the potential sensor shifts identified.
- For the analysis (diagnosis as well as the quantification) of inorganic as well as organic matter observed with an imaging spectrometer and their separation (e.g. vegetation and soil), the symmetry and shape of absorptions are often more important than the absorption depths. This can only be ensured by a non-interrupted or contiguous spectrum.
- The separation of coupled spectral absorption features caused by a combination of different materials and/or atmospheric features often requires the analysis of secondary absorptions or absorption overtones, necessitating access to wider spectral ranges.
- A detailed observation of spectra is needed based on the principle used by algorithms to retrieve variables. Modelled or laboratory spectra are being used for the analysis of the observed spectra. The need for first an identification and further a quantification of bio-geophysical variables postulate a high spectral resolution, sampling interval and thus a large number of bands.

The mission must acquire and transmit a minimum of 60 programmable bands on a routine basis and for all directions. On some occasions, it will be desirable to be able to acquire the complete spectral domain covered by the observing system.

Accuracy of wavelength position

Due to the need for contiguous and programmable band acquisition and transmission, no strict requirement can be placed on band positioning. However, the retrieval of most biophysical variables considered in this mission relies essentially on the capability to reconstruct the spectral shape of the absorption features that occur by radiative transfer models. Even quite small errors in the actual spectral position of the channels used in the retrievals can lead to huge deviations in the derived values. For example, large errors have been reported for retrievals of canopy water content with imaging spectrometer data when the band positions were slightly shifted (Moreno, 1999, pers. comm.). Accurate knowledge of the position of the bands is thus one of the most critical issues as it enables the quantitative retrieval of geophysical variables.

The accuracy of the knowledge of wavelength position must be better than 1 nm in the solar spectral region and 0.1 μm in the thermal region.

Spectral co-registration

All algorithms referred to previously exploit the spectral variation of the reflectance of a target. It is therefore critical that those spectral observations effectively represent measurements achieved over the same location. This can be achieved either at the sensor or through specific processing of the data.

The mission must be able to provide accurately co-located spectral data, such that the energies measured in any two arbitrarily selected spectral bands correspond to the same geometric areas on the Earth's surface.

4.3.4 Directional Requirements

All remote-sensing measurements acquired with imaging sensors in the solar spectral range depend strongly on the illumination and observation zenith and azimuth angles. This means that the sampling strategy is intrinsically directional, since the data acquired for each pixel of a given scene are taken in a particular direction. In addition, most land surfaces are non-lambertian, i.e. they reflect solar light in non-isotropic fashion. Furthermore, the scattering in the atmosphere is highly anisotropic. As previously mentioned, land surfaces are always observed through the atmosphere, and the radiative coupling between the surface and the atmosphere can only be taken into account when multi-directional measurements are made (Martonchik et al., 1998). Last but not least, the anisotropy of the surface and the atmosphere is spectrally variable: it will thus be necessary to acquire directional measurements separately in a variety of spectral bands, as proposed in Figure 4.9.

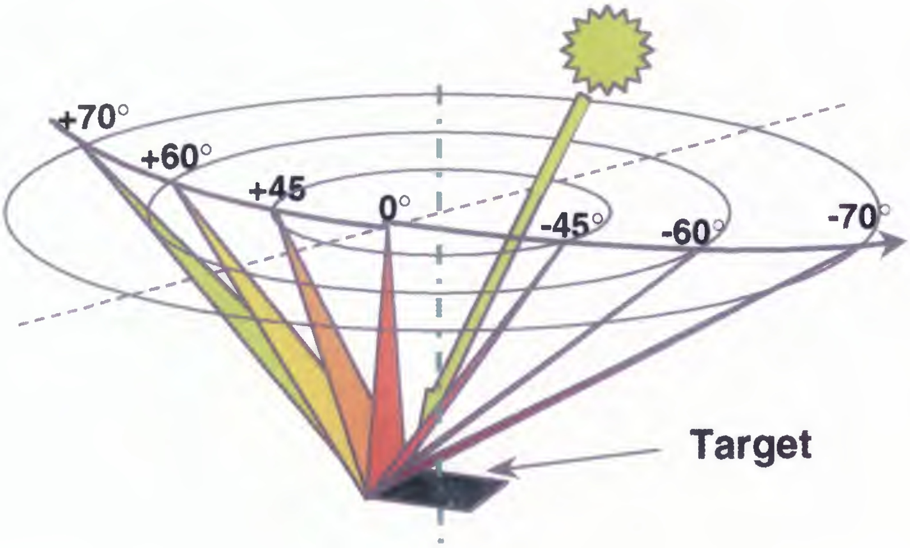

__Figure 4.9.__ LSPIM proposed angular measurements.

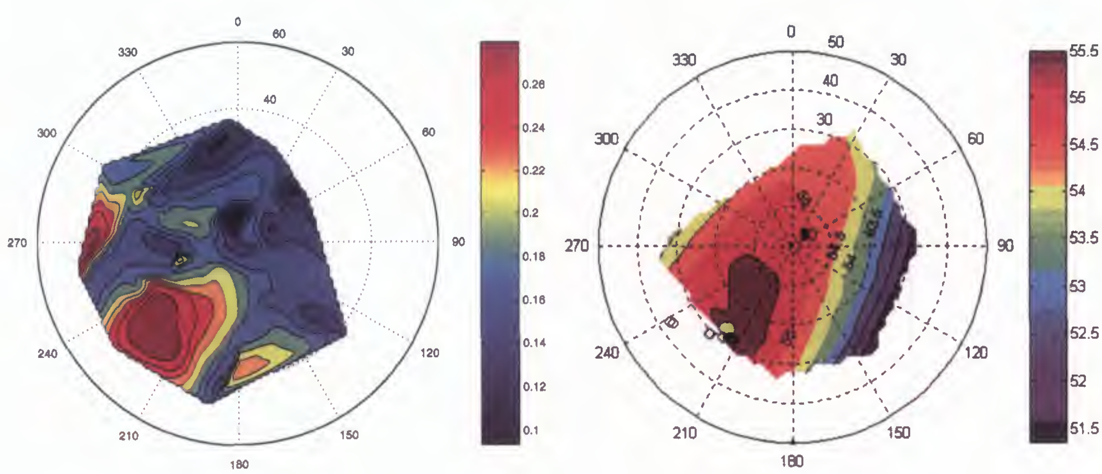

Figure 4.10. *Directional distribution of radiances over canopies. Left image corresponds to reflectance in the red obtained with airborne POLDER. Right image corresponds to brightness temperature in the 8-14 μm band obtained with thermal-infrared INFRAMETRICS camera. Data extracted from the ReSeDA experiment in 1997 (Baret et al., 1999).*

In the thermal-infrared domain, the emitted flux is also highly directional (see Balick et al., 1987; Kimes and Kirchner, 1983). The directional variation of emitted fluxes in the thermal infrared is mainly determined by the distribution of temperatures and emissivities between the elements of the canopy. This is linked to the distribution of shadowed and illuminated parts, as well as the amount of soil and vegetation viewed. Models have been developed to describe the directional variation in this spectral domain (e.g. Norman and Chen, 1990; Otterman, 1990; Smith and Goltz, 1995; François et al., 1997). Similar to the solar domain, it is critical to document the directional variation of the thermal radiance, for at least two reasons:

- to retrieve foliage and soil temperature separately
- to estimate directly the long-wave hemispheric emitted flux.

Number and distribution of observation directions

Some biophysical variables, such as radiative fluxes or albedo, correspond to integral quantities, while some others require a more detailed description of the BRDF field such as canopy structure or LAI or ground and vegetation temperatures.

The BRDF generally displays a typical 'bowl-shape' surface, with rapidly increasing reflectance at large illumination or observation zenith angles. Beyond this general trend, the most prominent anisotropic feature is the hot spot. The hot spot is observed when the view and illumination directions are close together. It corresponds to the situation where very little shadow is seen. The specular reflectance which often characterises smooth surfaces and is of greater relevance for oceanographic than for land applications, can be observed in the forward scattering direction. Although the latter is relatively sharp, the hot spot can measurably affect reflectance at significant angular ranges around the illumination direction, depending on the structure of the target. Both features require a relatively high directional sampling for full and reliable characterisation.

Therefore, directional observations are required to:

- document the anisotropy of the surface and account for these effects for the interpretation of the data; this is always necessary, but particularly when depointing the sensor across-track to improve the revisit capability
- improve significantly the atmospheric corrections, building on the work carried out for the POLDER (Leroy et al., 1997) and MISR missions (Martonchik et al., 1998)
- derive additional information on the target of interest which cannot be obtained on the basis of spectral data alone; this is obviously the case for albedo estimation, but is also true for the other canopy structural variables, as shown

recently (Bicheron and Leroy, 1999; Menenti and Verhoef, 1998; Weiss et al., 1999b).

To achieve this objective, it is necessary to document the depth and slope of the 'bowl-shaped' BRDF function, its asymmetry with respect to forward and backward scattering, and the size and width of the hot spot feature. This will be achieved using 7 angular observation directions: one at nadir, two at ± 70°, two at ± 60°, one at 45° in the forward scattering hemisphere, and the last one programmable as closely as possible to the actual hot-spot direction. When the latter observation cannot be usefully acquired, it will be acquired at 45° in the backward hemisphere as an angular default position.

As recalled above, the anisotropy of land surfaces varies with wavelength. It is thus necessary to acquire these directional measurements for all the spectral bands.

The mission must be able to provide data in at least 60 spectral bands for at least 7 along-track observation directions distributed as follows (in target-dependent zenith angles): one closest to nadir, +45°, ±60°, ±70° and one additional programmable angle which can be located within observational constraints, close to the hot spot conditions, or otherwise set to -45°.

Knowledge of the angular position of the observation directions

The reflectance change may be very high near the hot spot and at large zenith angles. It is thus critical that the actual observation geometry be precisely known, as small errors in the estimation of these angles may prevent the effective use of directional data.

The mission must provide directional data closest to the specified angles with a maximum angular error of 0.1° on the knowledge of the actual view direction.

Concomitance of measurements

Because the radiative properties of vegetation and the atmosphere change rapidly with time, the spectral and directional measurements over a given site must be acquired simultaneously for all wavelengths and for all directions. In the case of spectral measurements, this is feasible because the light coming from the target can be dispersed onto a spectrometer. Directional measurements, however, must necessarily be acquired in sequence. In this case, it is important that the period of time separating the first and the last acquisition be minimised, because the interpretation of the data will assume that the geophysical system being observed has not changed during that period. The fastest processes likely to invalidate this assumption are those associated with the effect of wind on the position and orientation of objects in the scene, such as clouds in the atmosphere or other objects at the surface. Since clouds obscure the surface and cloudy scenes would be avoided or discarded, the main concern is to ensure that the state of the surface has not changed much during the period of acquisition.

Only for very stable environments (e.g. arid areas or tropical forests), it may be more advantageous to accumulate data from multiple orbits. However, this will only be useful when the assumption that the state of the atmosphere has not changed significantly during the period of observation is valid.

All spectral measurements should be obtained simultaneously, and all directional measurements for a given site should be acquired in less than a few minutes, the time interval for which vegetation and atmosphere states could be considered steady, at least in the solar spectral domain.

4.3.5 Radiometric Requirements

The retrieval algorithms discussed earlier and described in more detail in Chapter 7 are mainly based on physical radiative-transfer models that use the spectral and directional variation of the radiance field. Therefore, the data provided by the LSPIM must be accurately calibrated in terms of physical quantities to be comparable to radiative-transfer-model outputs.

Radiometric accuracy for reflective channels

The radiometric accuracy is determined by the absolute radiometric calibration, and the radiometric noise coming from the instrument. The radiometric resolution is derived from the smallest increment of surface reflectance (Noise-Equivalent Differential Reflectance at surface, or $Ne\delta\rho$) that must be measured to accurately derive canopy or soil characteristics. In order to reduce the influence of random noise that contaminates the data, the observation must provide radiance in absolute physical quantities with a high level of accuracy.

Studies conducted for the preparation of this mission show that the radiometric accuracy must be of the order of 2% to 5%.(Fourty and Baret, 1997; Menenti and Verhoef, 1998; Weiss et al., 1999b).

The mission must be able to provide data with a radiometric resolution for the reflective channels $\mathrm{Ne}\delta\rho$ *in the range of 0.0025 with a radiometric accuracy of 2% to 5%.*

Radiometric accuracy for thermal channels

The radiometric requirements for the thermal channels are conceptually less complex than for the reflectance channels (VNIR/SWIR). The Earth is assumed to be equivalent to a black body whose minimum and maximum temperatures (about 200 K and 360 K) set the dynamic range of the input radiance seen by the sensor. Studies show that the accurate retrieval of ground and vegetation temperatures (as well as of long-wave fluxes) requires a radiometric resolution better of than 0.1 K with an absolute accuracy of better than 1.0 K (Caselles et al., 1996).

The mission must provide temperatures with a radiometric resolution NeδT *better than 0.1 K when observing a black body at 300 K. The absolute accuracy should be better than 1.0 K at 300 K.*

Polarisation sensitivity

Significant perturbations of the incoming radiant power may reflect to properties of the radiation field other than its intensity or geometry. One such possible source of error is the state of polarisation of the radiation field. The signal measured by a detector that is polarisation-sensitive is dependent upon the relative orientation of the sensor with respect to the state of polarisation of the incoming radiation field. In general, the radiance emitted by the Sun is not polarised in most parts of the spectrum. However, the interaction of this field with the atmosphere, in particular due to Rayleigh scattering processes, results in the linear polarisation of the reflected light.

The degree of polarisation depends on the type and amount of atmospheric scatterers, the phase angle, and the wavelength. Variations in the measurements of 20% of the total signal are not uncommon and can be observed solely as a result of these effects, depending on the wavelength and the reflecting objects. In some extreme cases, the degree of polarisation can reach up to 50% or more, if observations take place over water or when light is reflected near the Brewster's angle. The net impact of polarisation in remote sensing is difficult to quantify since polarisation effects do not allow for a deterministic description of the polarisation source.

Therefore, the polarisation sensitivity and the polarisation dependent loss have to be limited in the instrument in such a way that their contributions remain a minor source of uncertainty.

4.4 Summary of LSPIM Observational Requirements

In summary, the observational requirements described above point to the design and exploitation of an hyperspectral directional sensor capable of repeatedly acquiring high-spatial-resolution observations over a wide variety of experimental sites over a period of several years. The following Table synthesises these requirements, taking into account the scientific objectives of the mission and the approaches available to derive the geophysical products of interest from the radiometric measurements acquired in space.

Spatial requirements		
Accessibility		Global (1)
Scene extent		~50 km x 50 km
Resolution		~50 m
Coverage		> 2 (2)
Temporal requirements		
Mission duration		> 2 years
Revisit period for any site		2-3 days
Simultaneity of measurements		< 8 minutes
Spectral requirements		
Coverage	Solar	0.45-2.35 μm
	Thermal	8-9.1 μm
Spectral sampling interval (SSI)	0.680-0.769 μm	10 nm
	elsewhere	15nm
Spectral bandwidth	0.45-2.35 μm	< SSI x 1.5
	8-9.1 μm	0.5 μm
Number of bands observed	Solar	142 bands
	Thermal	2 bands
Number of bands downloaded	Solar	min. 60 bands (4), (5)
	Thermal	2 (5) bands
Directional requirements		
Number of directions		7
Angular positions		±70°, ±60°, ±45°, 0°
Knowledge of position		0.1°
Radiometric requirements		
Neδρ (0.45-2.35 μm)		0.0025
Radiometric accuracy		2%-5%
NeδT (8-9.1 μm)		0.1 K @ 300K
Absolute accuracy		< 1 K
Polarisation requirements resulting uncertainty		the smallest

Table 4.2. *Summary of LSPIM observational requirements.*

(1) Provided the illumination and observation zenith angles are both less than 70°.

(2) The coverage requirement is expressed in terms of the number of sites that can be visited per orbit.

(3) The goal is to operate this mission for 4 years.

(4) The solar bands are selectable in flight within the full set of 142 bands.

(5) The 60 solar and the two thermal bands are to be downloaded at all 7 observation zenith angles.

5 Mission Elements

5.1 The Essential Mission Elements

The scientific objectives as outlined in the previous chapters lead to an LSPIM concept in which space-borne directional imaging spectrometer measurements are converted into surface variables at well-characterised study sites at a pre-determined temporal revisit sequence. A mission is envisaged that comprises three key elements (Fig. 5.1):

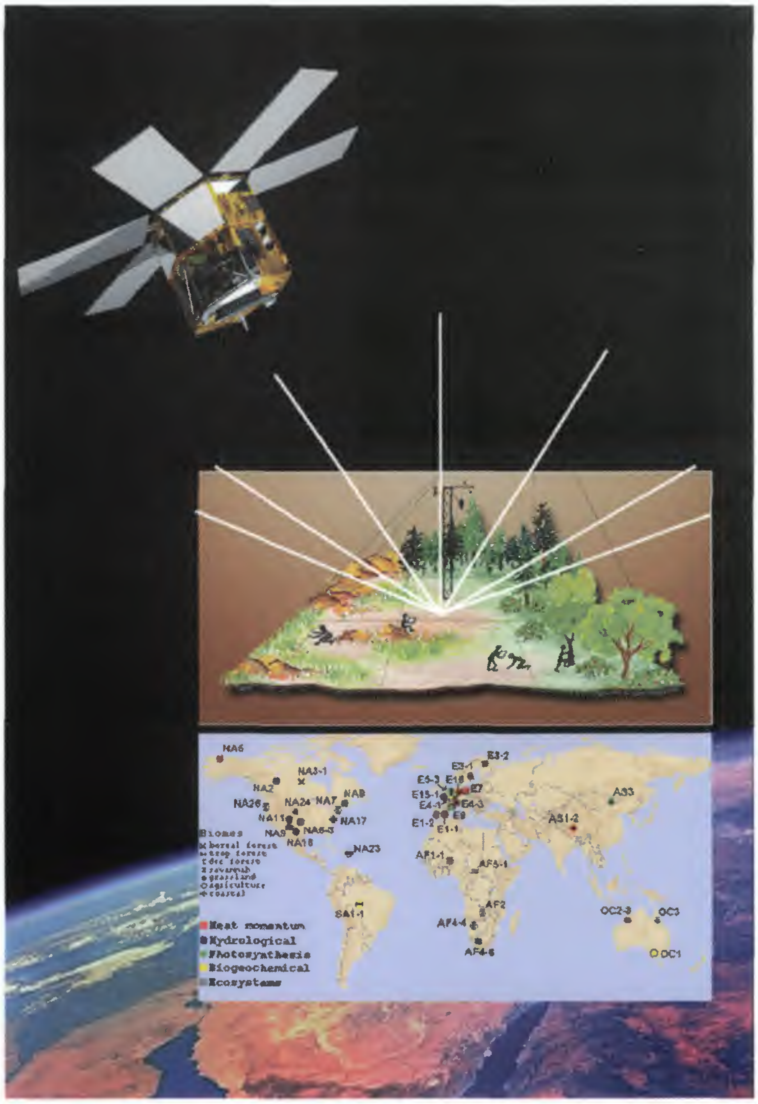

Figure 5.1. Conceptual scheme of the proposed mission elements: field, ground and space segment.

- field segment: well-documented and instrumented sites, intensively studied by the teams devoted to the scientific investigation of land-surface processes
- space segment: a single satellite with an instrument called 'Process Research by an Imaging Space Mission' (PRISM) to provide observations of the selected sites and according to the requirements stated in Chapter 4
- ground segment: satellite operation control and provision of data products.

This chapter shows how the mission science objectives can be met with the proposed space segment, in concert with well-conceived field and ground segments.

5.2 Field Segment: A Mission Experiment Plan

The mission objectives as previously discussed, imply that the success of the mission depends partly on a comprehensive programme of field experiments. To develop a mission experiment plan, a worldwide inventory of national and international experiments focussed on land-surface processes has been compiled. The activities initiated by the International Satellite Land Surface Climatology Project (ISLSCP) of ICSU, UNEP and WCRP and later by IGBP/ BAHC provide a solid base for the mission experiment plan. From these and other research programmes well-documented sites have been established in nearly every region of the World.

Data from advanced airborne sensor systems (e.g. AVIRIS and DAIS) have been acquired repeatedly in the framework of these experiments. The inventory of sites is based on information provided by the investigators involved in the experiments and supported by an intensive literature and web site investigation. Where the information on a specific site was considered too generic or insufficient, the site was excluded from the inventory.

Maps of the sites were prepared (see Fig. 5.2 through Fig. 5.6). The codes in the Figures are as follows:

CI.i: C= continent; I = project or programme; i = index of site within the project.

Furthermore, the colour coding provides a link to the land-surface processes that will be studied at the specific sites (see Table 3.1) and the symbols represent the biome present at the sites.

The information retrieved was summarised using the following key site attributes:

- biome
- period of operation

- baseline measurements
- continuity of intensive observation periods
- radiation measurements
- airborne campaigns using advanced sensors
- satellite data archive
- modelling studies.

A preliminary assessment of the relevance of all sites included in the inventory (Table 5.1) has been performed to support LSPIM operation simulations (see Chapter 8). At a later stage, a peer-reviewed selection procedure should be developed in preparation for the mission. All attributes listed above were considered in the assessment.

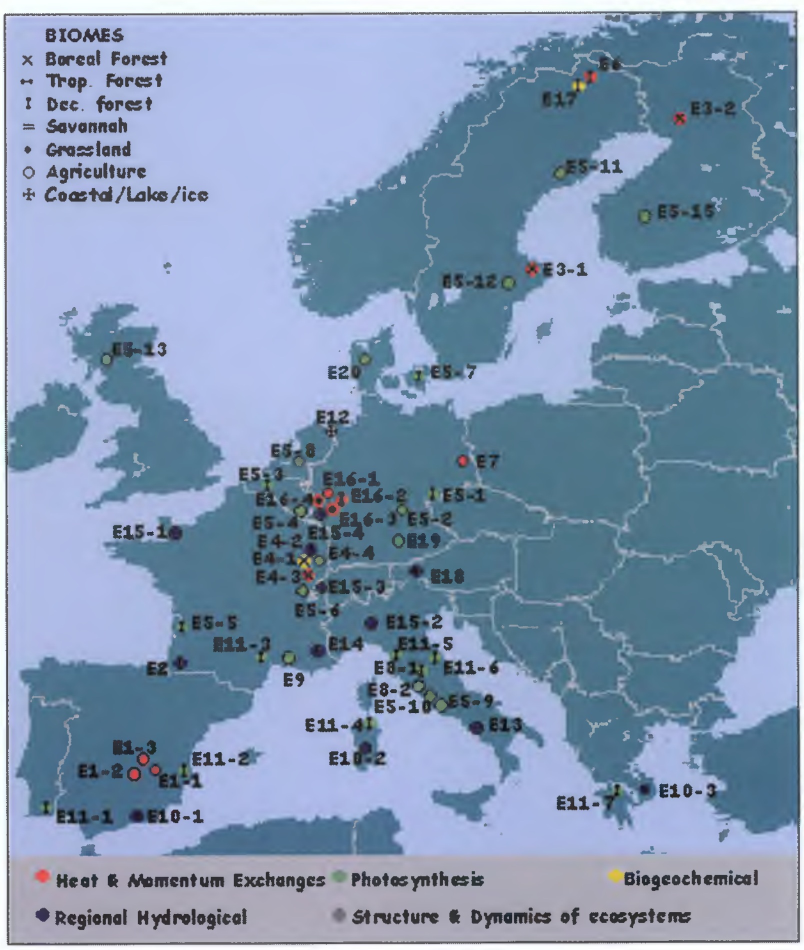

Figure 5.2. *Map of sites included in the Mission Experiment Plan: Europe.*

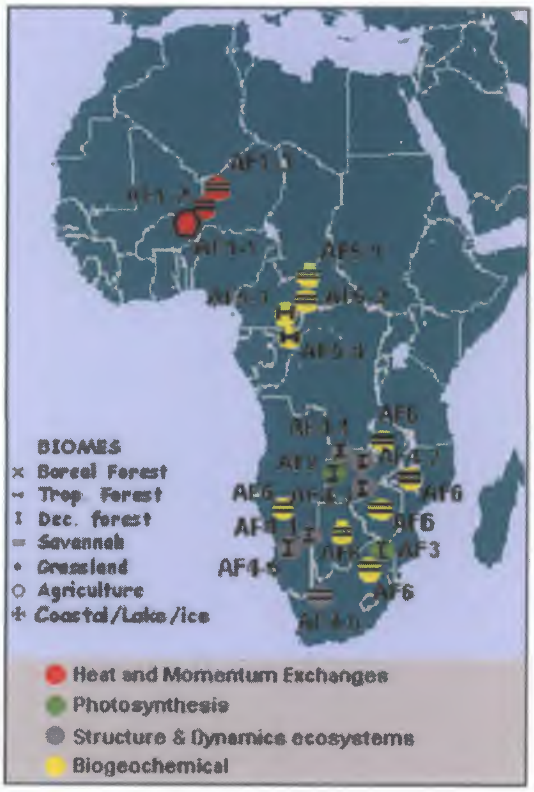

Figure 5.3. *Map of sites included in the Mission Experiment Plan: Africa.*

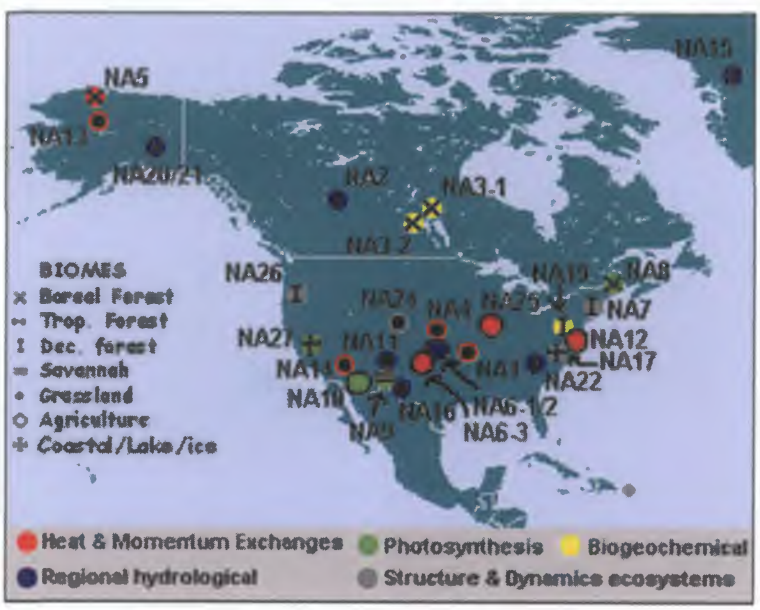

Figure 5.4. *Map of sites included in the Mission Experiment Plan: North America.*

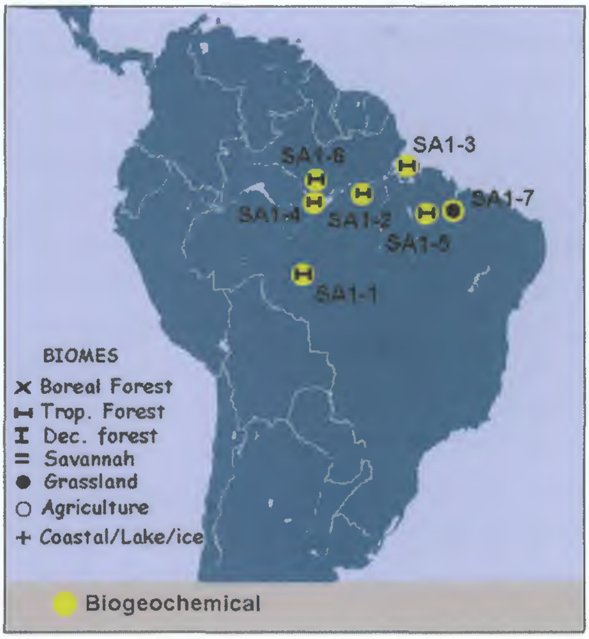

Figure 5.5. Map of sites included in the Mission Experiment Plan: South America.

Figure 5.6. Map of sites included in the Mission Experiment Plan: Asia and Oceania.

Continent/ Process	Europe	Africa	North America	South-America	Asia	Oceania
Heat and momentum exchange	(1) E1-1 *a* (2) E3-1 *bf* (5) E1-2 *a* (6) E3-2 *bf* (10) E4-3 *bf* (11) E7 *a* (13) E16-1 *a* (14) E16-2 *df* (15) E16-3 *g* (16) E16-4 *g* (21) E1-3 *a*	(26) AF1-1 *a* (27) AF1-2 *s* (28) AF1-3 *s*	(3) NA6-3 *a* (7) NA5 *bf* (8) NA4 *g* (12) NA12 *a* (24) NA13 *g* (25) NA14 *g*		(4) AS1-2 *g* (9) AS1-3 *g* (20) AS6 *bf* (22) AS2 *g* (23) AS1-1 *g*	(17) OC2-1 *g* (18) OC2-2 *g* (19) OC2-3 *s*
Photo-synthesis	(1) E5-3 *df* (2) E5-5 *df* (5) E5-7 *df* (6) E5-1 *df* (7) E11-1 *df* (8) E11-6 *df* (9) E9 *a* (10) E8-1 *df* (16) E8-2 *a* (17) E11-2 *df* (18) E11-3 *df* (21) E11-4 *df* (22) E11-7 *df* (23) E11-5 *df* (24) E4-4 *a* (25) E19 *a*	(12) AF3 *df* (15) AF2 *df*	(3) NA8 *bf* (4) NA9 *s* (11) NA10 *a*		(13) AS3 *g* (20) AS4 *g*	(14) OC3 *c* (19) OC4 *bf*
Regional hydrological	(1) E15-1 *a* (2) E15-2 *a* (5) E18 *g* (8) E15-3 *a* (9) E15-4 *a* (10) E4-2 *df* (14) E14 *df* (18) E10-1 *df* (19) E13 *g* (20) E2 *a* *df*		(3) NA16 *g* (4) NA11 *g* (6) NA2 *df* (7) NA6-1 *a* (12) NA22 *df* (13) NA6-2 *a* (15) NA18 *c* (16) NA20 / NA21 *bf* (17) NA15 *c*		(11) AS8 *a*	
Bio-geochemical	(4) E4-1 *bf* (7) E6 *df* (17) E17 *df*	(13) AF5-1 *s* (14) AF5-2 *s* (15) AF5-3 *tf* (16) AF5-4 *tf* (18) AF6 *s*	(8) NA3-1 *bf* (9) NA3-2 *bf* (10) NA19 *df*	(1) SA1-1 tf (2) SA1-2 tf (3) SA1-3 tf (6) SA1-6 tf (11) SA1-4 tf (12) SA1-5 g		(5) OC1 *a*
Structure and dynamics Ecosystems	(12) E12 *c*	(3) AF4-4 *df* (4) AF4-1 *df* (6) AF4-2 *df* (7) AF4-3 *df* (8) AF4-5 *df* (9) AF4-6 *s*	(1) NA26 *df* (2) NA7 *df* (5) NA23 *tf* (10) NA24 *g* (11) NA17 *c*		(13) AS7 *s*	

Biomes

bf	Boreal Forest	g	Grassland
tf	Tropical Forest	a	Agriculture
df	Deciduous Forest	c	Coastal / Lake / Ice
s	Savannah		

Table 5.1. *Overview of all sites included in the Mission Experiment Plan; the sequence in each cell of the table reflects the preliminary review of the information retrieved through the inventory.*

The number and geographical spread of existing field sites illustrates the high interest in this scientific field. The availability of the European sites is depicted in Figure 5.7. While continued operation cannot be guaranteed for any given site, the trend evidenced in Figure 5.8 leaves little doubt that a comprehensive field segment should exist in the time frame of the LSPIM.

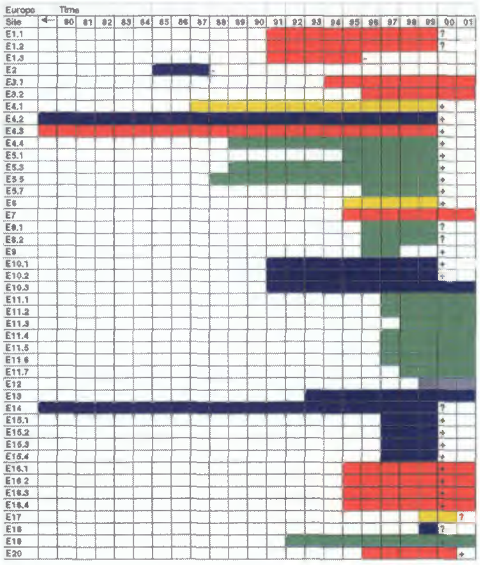

Figure 5.7. *Period of operation of sites included in the Mission Experiment Plan; + = continued operation expected; ? = continued operation not expected; - = site operation discontinued.*

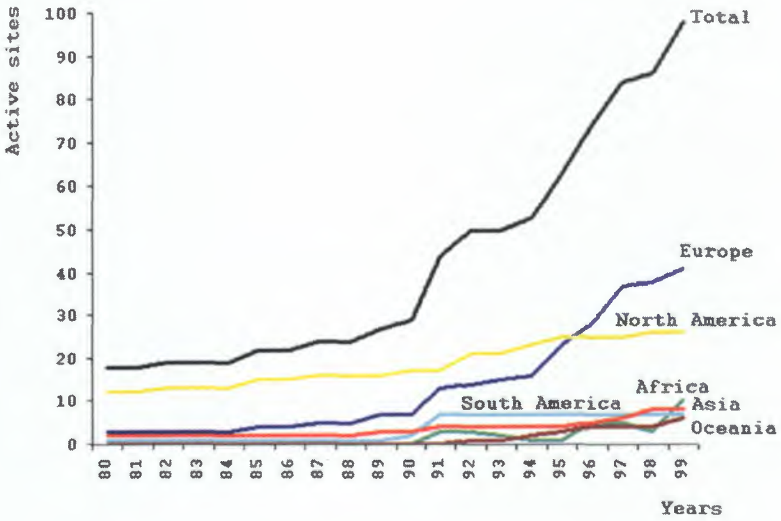

Figure 5.8. *Total number of sites in operation by continent as a function of time.*

5.3 Space Segment

The mission objectives and the related mission experiment plan place challenging requirements on the LSPIM space segment.

The space segment must guarantee coverage of all sites of interest with a revisit period of (at most) 3 days and at a local time over the equator between 10:00 am and 12:00 a.m. to ensure good illumination conditions. Even though the revisit time of the actual observations may be larger (e.g. seasonal observations) than the nominal three days, periods of intensive observations may require a revisit time as short as three days, taking also the cloud coverage statistics into account.

The algorithms listed in Table 4.1 require angular-reflectance measurements to retrieve key variables with sufficient accuracy; therefore the system must also be capable of acquiring directional measurements with an adequate pointing accuracy (0.1°, or better). The desired angular measurements should cover the following co-elevation angles: ±70°, ±60°, +45°, 0° (or as close as possible to 0° when the site is not on the satellite ground track). In addition, one programmable angle in the backward direction with the default value of -45° is desired to support the detailed study of BRDF hot-spots if viewing and illumination conditions permit this.

Spectral measurements in two wavelength regions are required. Region 1 covers the Visible-Near InfraRed (VNIR) and the Short-Wave InfraRed (SWIR) from 0.45 μm to 2.35 μm. Region 2 covers the Thermal Infra-Red (TIR) range from 8.0 to 9.1 μm. Two spectral bands with a width of 0.5 μm will be used (Caselles et al., 1996) in Region 2. Other requirements, e.g. radiometric accuracy, spatial and spectral sampling, etc., are specified in Chapter 4 and will not be repeated here.

The spectral-resolution requirements lead to more than 140 spectral bands. However, the simultaneous acquisition of all these spectral bands will only occur sporadically. Normally up to 60 bands, properly selected for each site, will be sufficient to derive the required variables.

The observations directly provided by the space segment will be TOA radiances above the selected ground sites in the form of images calibrated so as to assign an absolute radiometric value to each of the picture elements (pixel). Each image acquired in a specific direction can be seen as a 3D array of samples, where the first two dimensions cover the spatial extent of the area, and the third dimension covers the spectral domain. To be able to accurately exploit the data, each image needs to be spectrally co-registered (band-to-band), with a goal for the spectral registration accuracy of 15% of the spectral sampling interval and with a goal for the spatial co-registration accuracy of 20% of the spatial sampling interval.

As will be shown in detail in Chapter 6, the above requirements can be achieved by a single satellite carrying the PRISM instrument flying in a Sun-synchronous orbit at an altitude of approx. 670 km. The revisit requirement will be met owing to the combined pointing capabilities of both the satellite and the instrument, with basically the former providing the along-track pointing and the latter the across-track pointing. With respect to pointing capabilities, the satellite will be fully manoeuvrable in order to meet the BRDF observation objectives, and this fact will also be exploited to reduce the satellite's size and complexity.

The PRISM instrument design has been tailored to meet the mission scientific objectives with a limited complexity and with the use of well-known technologies, many of which are directly derived from previous programmes such as MERIS. It will provide observations that are accurately radiometrically, spatially and spectrally calibrated in the required spectral regions and with the desired spatial/spectral resolution.

5.4 Ground Segment

The ground segment has to have the following functional elements:

- The *command and data acquisition element,* which is in charge of direct interaction with the satellite for the uplinking of telecommands and the reception of housekeeping telemetry and scientific data. The Kiruna Salmijaervi station is proposed.
- The *mission operations and satellite control element,* which is in charge of implementing the mission plan and controlling the satellite operations.
- The *processing and archiving element,* which is in charge of processing the data to Level 1b, and providing an archiving function and user services.

The processing and archiving element distributes the data to the scientific community, identified as a virtual science data centre. It is expected that the scientific interest will be organised both around sites, and hence programmes, and around issues/processes.

The concept for the ground-segment facilities is outlined in Section 6. The data processing strategy is described in Chapter 7. Algorithms to derive the geophysical variables required to investigate the land processes have been identified in Chapter 4.

5.4.1 Higher Level Data Products

The development of retrieval algorithms requires specific expertise which may not be readily available at an operational data centre. On the other hand, the large amount of multi-temporal directional hyperspectral measurements require computing facilities to provide the scientific teams with calibrated radiances, and eventually with higher level data products.

At this point in time, the provision of higher level data products based on a Level 1b data is being considered. There are various options for the establishment of Level 2 products, which represent geophysical quantities. One of these options is to have Level 2 products produced by-data processing centres each related to a land-surface process; another option would be to establish a central geophysical data processing facility. As this is a clear task for a Phase-B ground-segment development study, the data-processing aspects of Level 2 are not discussed here in further detail. A conceptual organisational scheme is presented in Figure 5.9.

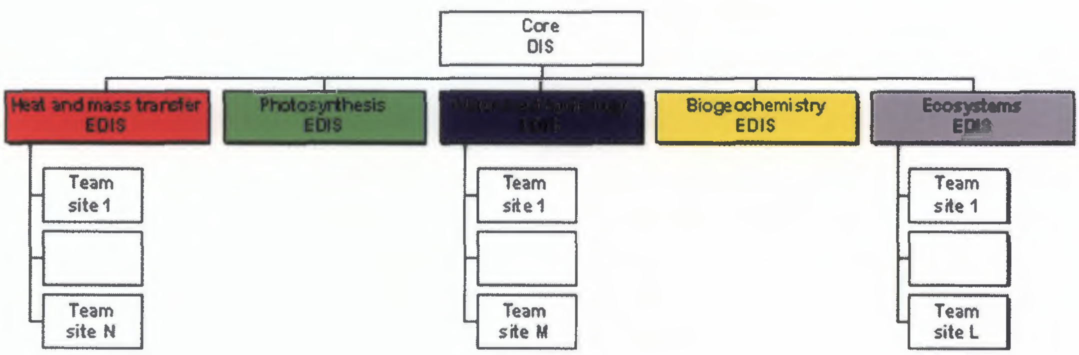

Figure 5.9. *One possibility for the conceptual organisation of a distributed LSPIM data-processing and dissemination system.*

5.4.2 Calibration and Validation

The instrument will be designed to guarantee performance stability. A comprehensive calibration system will be implemented onboard.

Specific experiments will be required to assess the accuracy of all Level 2 products. Post-launch comparison of at-satellite radiances with simulated TOA radiance, resulting from vicarious calibration experiments conducted at sites such as White Sands or the Libyan Desert, will be used to establish a high degree of confidence in the accuracy. Calibration experiments can also be carried out as AO studies, as was done for ERS-1/2 and is planned for Envisat.

The validation of retrieved variables will be a continuing activity throughout the mission and will be carried out routinely at the test sites by the scientific user community. However, not all higher level products can be validated at once.

5.4.3 Campaigns in Support of the Mission

In view of the unique and new capabilities of the LSPIM to estimate bio-geophysical land-surface variables, both remote-sensing and ground data will be used to prepare the science community and to simulate combined ground-measurement and remote sensing-data collection schemes.

The main objectives for airborne, space-borne and ground data collection campaigns in the frame of this mission are:

- to develop and validate algorithms to extract bio-geophysical model parameters and modelling approaches for different processes (see Table 3.1 and Table 4.1) at different test sites covering a broad spectrum of land-surface conditions
- to prove the efficiency of atmospheric-correction procedures
- to develop optimal ground data-collection strategies, model designs and test-site selection approaches for the actual mission
- to design LSPIM calibration activities
- to demonstrate and prove the LSPIM approach to remote-sensing application for land-surface processes.

5.5 The Mission Context

5.5.1 International Context

Over the past few years, several airborne imaging spectrometers have been designed and built (Table 5.2), but none of them satisfies the characteristics required to fulfil the scientific objectives of LSPIM. In this sense, the proposed instrument is unique. On the other hand, the rapid growth in the number and capabilities of airborne imaging spectrometers is an indication of the maturity of the technology and of the broad international interest in such observations. In this context, a dedicated LSPIM demonstrator, the Airborne PRISM Experiment (APEX), is under development.

There is a logical evolution from airborne towards space-borne systems (Table 5.3). Again none of these systems meets the requirements as developed for the LSPIM (see Chapter 4).

Acronym	Full Name	Operator	LSPIM Capabilities[1]				Operation	URL / Comments
			Reflective		Thermal			
			Nadir	BRDF	Nadir	TDD		
APEX	Airborne PRISM Experiment	ESA / RSL & VITO	XX	–	–	–	2002 – 2007	http://www.apex-esa.org
Airborne BIRD	Bispectral Infrared Detection	DLR / WS	–	–	X	–	Current	http://www.ba.dlr.de/NE-WS/projects/bird/bird.html
MAS	MODIS Airborne Simulator	NASA / JPL	X	–	X	–	Current	http://ltpwww.gsfc.nasa.gov/MAS/
MASTER	MODIS/ ASTER Airborne Simulator	NASA / JPL	X	–	X		Current	http://masterweb.jpl.nasa.gov/
AVIRIS	Airborne Visible/ Infrared Imaging Spectrometer	NASA / JPL	XX	–	–	–	Current	http://makalu.jpl.nasa.gov/aviris.html
DAIS 7915	Digital Airborne Imaging Spectrometer	DLR / OE	X	–	XX		Current	http://www.dlr.de/dais/
ASAS	Advanced Solid-state Array Spectro-radiometer	NASA / GSFC	X	X	–	–	Current	http://asas.gsfc.nasa.gov/
CASI	Compact Airborne Spectro-graphic Imager	Itres Corp. (div.)	X	–	–	–	Current	http://www.itres.com
ROSIS	Reflective Optics Imaging Spectrometer	DLR / OE	X	–	–	–	1999 – ?	http://www.op.dlr.de/ne-oe/fo/rosis/home.html
HYMAP	Airborne Hyperspectral Scanner	Intspec Corp. (div.)	XX	–	–	–	Current	http://www.intspec.com/products.htm#hymap
AISA	Airborne Imaging Spectrometer	Spectral Imaging Ltd. (div.)	X	–	–	–	Current	http://www.specim.fi/aisa.html
MIVIS (Daedalus AA5000)	Multispectral Infrared and Visible Imaging Spectrometer	CNR / LARA	X	–	XX	–	Current	n.a.
SMIFTS	Spatially Modulated Imaging Fourier Transform	Hawaii Institute of Geo-physics and Planet-ology	XX	–	–	–	Current	http://www.pgd.hawaii.edu/higp_smifts.html
AirMISR	Airborne Multi-angle Imaging Spectro-radiometer	NASA / JPL	X	X	–	–	Current	http://www-misr.jpl.nasa.gov/armain.html
TIMS	Airborne Imaging Spectro-radiometer	NASA/ JPL	–	–	XX	–	Current	
HYDICE	Hyperspectral Digital Imagery Collection Experiment	NRL (US)	X				Current	http://ltpwww.gsfc.nasa.gov/hydiceop.html

Table 5.2. *Airborne instruments having partial LSPIM capabilities.*

[1] XX = Full spectral/thermal coverage, X = Partial spectral/thermal coverage, – = No simulation capabilities

Sensor/ Platform	Spectral coverage	Spatial resolution	Angular geometry	Temporal resolution	Operation
CHRIS/ PROBA	18 bands in VNIR	25 m	6 BRDF angles	3 days	2000-2001
ARIES	32 bands in VNIR, 32 bands in SWIR (2.0 – 2.5 µm), optional coverage in 1.0µm – 2.0µm, one PAN band	PAN 10 m HSI 30 m	nadir and cross-track	7 days	planned for 2000
NEMO	contiguous VNIR/ SWIR coverage – one PAN band	PAN 5 m HSI 30/60 m	nadir and cross-track	7 days	planned for mid 2000
HYPERION	contiguous VNIR/ SWIR coverage	30 m	nadir	16 days	December 1999

Table 5.3. *Space-borne imaging spectrometers –high spatial resolution.*

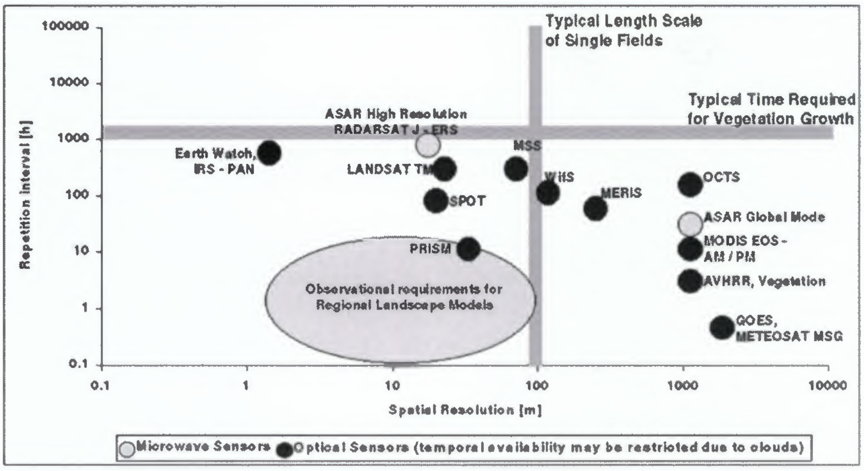

Figure 5.10. *The spatial resolution and revisit time of the LSPIM in the context of current and planned Earth observation systems (adapted from Mauser et al., 1999).*

The combination of an adequate spatial resolution with a flexible operation system makes it possible to provide short revisit times for the sites included in the experiment plan. In this sense also the observing system proposed by LSPIM is unique.

5.5.2 Synergy with Other Space Missions

The strongest synergy aspect between the LSPIM and other space-borne missions lies in the investigation of land-surface processes and related scaling issues, which will become feasible by looking at the same site with a variety of instruments acquiring data at different spatial resolutions and within short revisit times.

Contributions to Other Missions

Earth Radiation Budget:
An important element in understanding the Earth's climate is the knowledge and understanding of the Earth's Radiation Budget (ERB). A number of existing and planned instruments (e.g. ERBE, GERB, SCARAB and CERES) take measurements that directly relate to this quantity and are generally known as radiation-budget instruments, from Sun-synchronous low-altitude orbits and from geostationary satellites.

Directional reflectance models are needed to retrieve fluxes from directional radiance measurements over land areas. These models must be valid over the full range of observing and illumination geometries. Measurements of the proposed LSPIM will further the study, testing and refinement of these models, providing an important contribution to ERB studies.

Thermal heterogeneity and directional observations:
The high spatial resolution and directional capability of the LSPIM will provide measurements capable of advancing understanding of the role of radiometric heterogeneity and quantifying its impact on low-resolution sensors such as Envisat's AATSR, MSG SEVIRI, etc.

Land-cover properties and the directionality of reflectance:
Information retrieved from data acquired by the LSPIM instrument will contribute to a general description of the state and evolution of terrestrial ecosystems. The LSPIM will provide complementary data to those acquired by current and future planned Earth observation systems:

- By acquiring high spectral resolution data, LSPIM will provide complementary data to sensor systems such as Landsat ETM, Terra-1 ASTER, SPOT HRV and Vegetation, etc.).

- By acquiring multi-directional spectral data at comparably high spatial resolution. Only few instruments currently planned can acquire data at more than one observation geometry. The AATSR sensor (2 directions in 5 spectral bands and at 1 km spatial resolution), and the MISR sensor (9 directions in 4 spectral bands and at 250 m resolution) are the only instruments currently operational or planned to be launched with directional observation capability. None of these sensors is capable of providing angular measurements at the spectral and spatial detail as proposed for LSPIM. On the other hand LSPIM can benefit from the experience gained from these precursors.

Contributions from Other Missions

Optical Domain

Related to LSPIM are European sensors such as MERIS on Envisat, HRV and VEGETATION on SPOT, POLDER on ADEOS and foreign sensors such as MISR or MODIS on-board the US-Terra-1. These sensors will provide information, with generally coarser spatial resolution, in fewer spectral bands and with limited directional capability but with larger swath width. They will be complementary to the LSPIM. In particular, LSPIM would benefit from the exploitation of the contextual information provided by the other, large scale, sensors.

SAR

The relation with SAR missions has been specifically addressed in the definition of the LSPIM to benefit from the steady advances in retrieval of land properties with SAR sensors (Bach et al., 1996). It is planned to use SAR observations to further tune and calibrate particular aspects of process models.

5.6 Conclusion

The nature of land-surface process studies entails a significant effort on the part of scientists, comparing their model predictions against observations in large-scale field campaigns. This community of modellers and experimenters, together with the networks of test sites and transect studies, constitutes an important third element to the mission, beyond the usual space and ground segments (Table 5.4). The ground segment itself will do more than basic processing, and should comprise a dedicated set of processing centres, exploiting well-tested, sophisticated retrieval algorithms. A novel space element will therefore deliver a large number of geophysical data products at the scale needed by the highly diverse scientific community. This balanced combination constitutes a unique opportunity to make significant advances in surface process research, as well as enhancing the value of other missions.

Space Segment	Imaging spectrometer Thermal radiometer Versatile, pointable platform Polar orbit
Ground Segment	Possibly distributed processing and data dissemination centres
Field Segment	100+ field sites observable at any time 200+ field campaigns in mission lifetime Cal-Val activities

Table 5.4. *The three elements of the LSPIM.*

6 Technical Concept

6.1 From System Requirements to Satellite Concept

The technical concept for the LSPIM system has been defined with the goal of ensuring the best technical answers to the mission requirements based on feasible, cost-effective and, whenever possible, proven solutions. In this way, the system has been optimised as a whole, rather than separately for space and ground segments or for platform and instrument, resulting in a design meeting the required performance at well controlled cost and risk.

Figure 6.1. *Artist's impression of the LSPIM satellite in orbit.*

This chapter briefly addresses the rationale behind the technical concepts proposed for the LSPIM space and ground segments, covering in particular the selection of the mission profile and the definition of the satellite and ground-segment architectures.

The definition of the mission profile involves both orbit selection and mission planning and operations strategy. Orbit selection is driven by three requirements:

(a) to provide the required access time of 3 days for the sites of interest, which can be anywhere within the continental regions

(b) to optimise the directional sampling over these sites
(c) to favour, if possible, a lower altitude, which benefits the radiometric performance and the launch. These constraints lead to the selection of a frozen Sun-synchronous orbit at a mean altitude of ~674 km with 14 day repeat (i.e., with 14 + 9/14 orbits per day), which provides both site accessibility and variable across-track sampling angles within the repeat cycle.

The analyses for mission planning and operations strategy were performed with the help of a dedicated mission simulator to account for the particular mission, especially regarding the BRDF observations. Based on a first definition of representative user requests, the analyses show that the system can meet the mission objectives, assuming it is capable of attitude manoeuvring that meets the directional sampling requirements (cf. Section 4.3), and that the required average number of BRDF acquisitions per orbit is less than two. This is fully supported by the image acquisition approach, the storage and downlink capabilities, the thermal control and the power generation with good margins.

The satellite definition must cope with a number of challenging and sometimes contradictory mission, system and subsystems constraints. The first mission driver is the directional sampling requirement, leading to the so-called BRDF mode of operation, which dictates that the system must have a strong (rotational) agility. Table 6.1 summarises the results of one of the main trade-offs:

- The satellite will perform the required manoeuvres in pitch and yaw and will ensure the required roll attitude control during image acquisition.
- The roll (i.e. across-track) pointing of the line of sight (LOS) will be performed in the instrument by means of a de-pointing mirror (required also to access the on-board calibration sources). This choice is dictated by the selection of a semi-passive cooling system for the SWIR focal plane for accommodation, reliability and cost reasons, which is incompatible with the attitude variations of the SWIR radiator that would be induced by large satellite roll de-pointing.

De-pointing requirement	Satellite manoeuvre	Instrument de-pointing (by mirror)
Pitch angular range: ± 56° (for ±70° range of the co-elevation angle at site)	Yes	No – Range too large
Pitch control during image acquisition	Yes	No – Difficult implementation and limited accuracy
Roll angular range: ± 35°	No – SWIR radiator constraint	Yes
Roll-limited control during image acquisition	Yes	No – Limited accuracy
Yaw steering during image acquisition	Yes	No – Difficult implementation and limited accuracy

Table 6.1. *The pointing trade-off results.*

The instrument performance and interfaces determine its configuration:

- the spatial registration requirements and the goal of limiting mass and development cost lead to the need to have the largest number of optical elements in common for the various spectral regions: the telescope is common for the whole spectral range and the VNIR and SWIR bands share the same spectrometer
- the above choice is further supported by the selection of a roll de-pointing mirror, well suited to the use of a single telescope
- the radiometric performance in the SWIR band and the related operating temperature are compatible with cooling by means of a passive radiator associated with a Peltier cooler
- the need to avoid image rotations determines the use of an in-plane de-pointing mirror and the associated geometrical configuration of the optical bench, which is located on the Earth-pointing face of the satellite.

The satellite-agility requirements dictate fixed solar arrays and induce requirements on the satellite inertia, so leading to a compact configuration. A good accommodation in the launcher fairing, accounting for the instrument interfaces, leads to an hexagonal configuration with the payload module located on the Earth-pointing face.

The ground-segment definition complies with the dual requirements of maximising the re-use (or heritage) of infrastructures and procedures for cost efficiency and of implementing the ground processing functions. These specific processing requirements are dictated by the various geometrical conditions under which the images will be acquired in the BRDF mode. The baseline is to reuse (as far as possible) the existing ground segment for the command and data-acquisition element (CDAE) and the mission operations and control element (MSCE), and to develop a specific processing and archiving element (PAE) tuned to the needs of the mission.

The LSPIM lifetime is nominally two years. However, the design assumes a four-year lifetime in order to provide margins, e.g. for propellant sizing. The performance values at end-of-life (EOL) quoted in this report also assume a four-year lifetime. These margins have a negligible impact on the cost of the LSPIM space segment.

6.2 Mission Analysis and Operations

This section summarises the results of the mission analysis, focussing on three key aspects:

- the orbital analysis and the selection of the baseline mission profile
- the mission-planning analysis
- the orbital timeline and profile definition.

6.2.1 Orbital Analysis

The first criterion for the orbit selection is to provide access within three days to any sites anywhere in continental regions, assuming cloud-free conditions and subject to the illumination constraints of Chapter 4. The altitude selection is related to the mission operations requirements and to the repeat period, which determines the variation of the across-track de-pointing for consecutive passes over a target site.

Figure 6.2 shows that two altitude domains exist for an acceptable across-track de-pointing angle (< 35°), one around 775 km and the other around 666 km. The main drawback of the orbits at exactly 666 km or 775 km altitude is that the target site is always observed with a constant across-track de-pointing angle. This can be avoided by selecting orbits with a relatively long repetition cycle (far from the 3-day cycle), but providing the full range of across-track de-pointing angles in a period shorter that the complete orbit cycle.

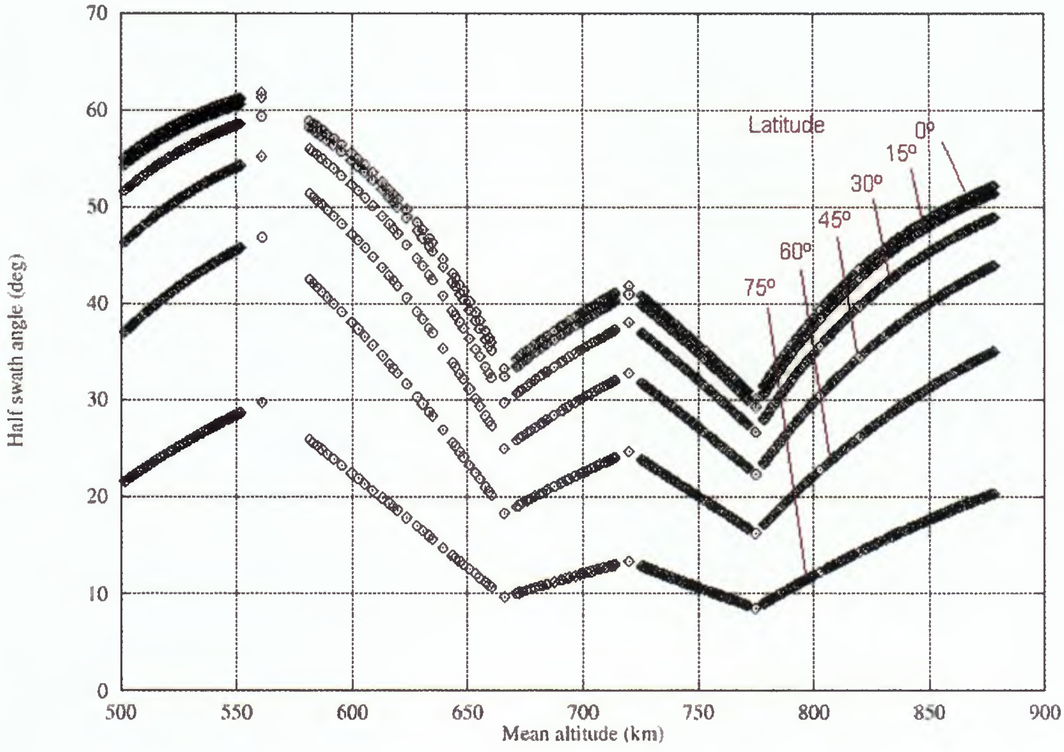

Figure 6.2. *Across-track de-pointing as a function of altitude and of the site latitude.*

Radiometry and launch performance reasons lead to a preferernce for the lowest altitude range, and so finally a frozen Sun-synchronous orbit with a mean altitude of ~674 km and 14 day repeat cycle has been selected (Table 6.2). The baseline local time at the ascending node is 11.00 hours. This orbit guarantees a relatively fast variation of the site observation conditions, while remaining in the acceptable across-track de-pointing range.

	Mean orbital elements
Orbit type	Sun-synchronous, LTAN 11:00 h
Semi-major axis	7051.76 km
Eccentricity	0.001165
Inclination	98.01 deg
Argument of perigee	90.0 deg
Revolutions/day	14 + 9/14
Period (s)	5900.5
Altitude at equator (km)	679.63
Mean altitude (km)	673.62

Table 6.2. *LSPIM orbit parameters.*

The orbit maintenance will require less than 10 kg of hydrazine propellant over 4 years. An orbit manoeuvre at the end of each repeat period will guarantee a ground-track error at the equator within ±10 km. The overall propellant mass (assuming the worst-case launch injection error) is less than 30 kg.

6.2.2 Mission Planning

For mission planning, the applicable LSPIM specific requirements are:

- the mission consists of the acquisition of image sets over a series of well-defined sites, according to a long-term user request scenario
- each image acquisition must be directional, so as to provide observations for BRDF modelling:
  - the following co-elevation angles must be achievable in each satellite pass over the site: ±70°, ±60°, ±45° or ±30°, and an angle as close as possible to nadir
  - hot-spot sampling should be aimed at, compatible with the geometrical constraints; it is therefore desirable to achieve observations at a co-elevation angle in the ranges ±30° to ±45°
  - in the case of conflicts between site acquisitions, those observed in directions close to the hot spot should be preferred in the mission planning.

The hot-spot direction mainly depends on the site latitude and on the epoch of the observation.

Figure 6.3 shows the achievable geometry for BRDF observations over a repeat period (two weeks) for a site in the Northern Hemisphere for co-elevation angles of ±70°, ±60°, ±45° or ±30°, and close to nadir, for March and June.

Further examples of BRDF sampling are shown in Chapter 8. As shown, for example, in Figure 8.6 for the Barrax site (44° latitude, 116° longitude, end June), good hot-spot sampling is obtained with a modified BRDF sequence as ±70°, ±60°, +α, -β, 0°, with α, β selected as close to the hot spot direction as possible. The achievable range for α, β is obviously linked to the satellite manoeuvring capability (this aspect is further discussed in Section 6.4.5 on attitude and orbit control).

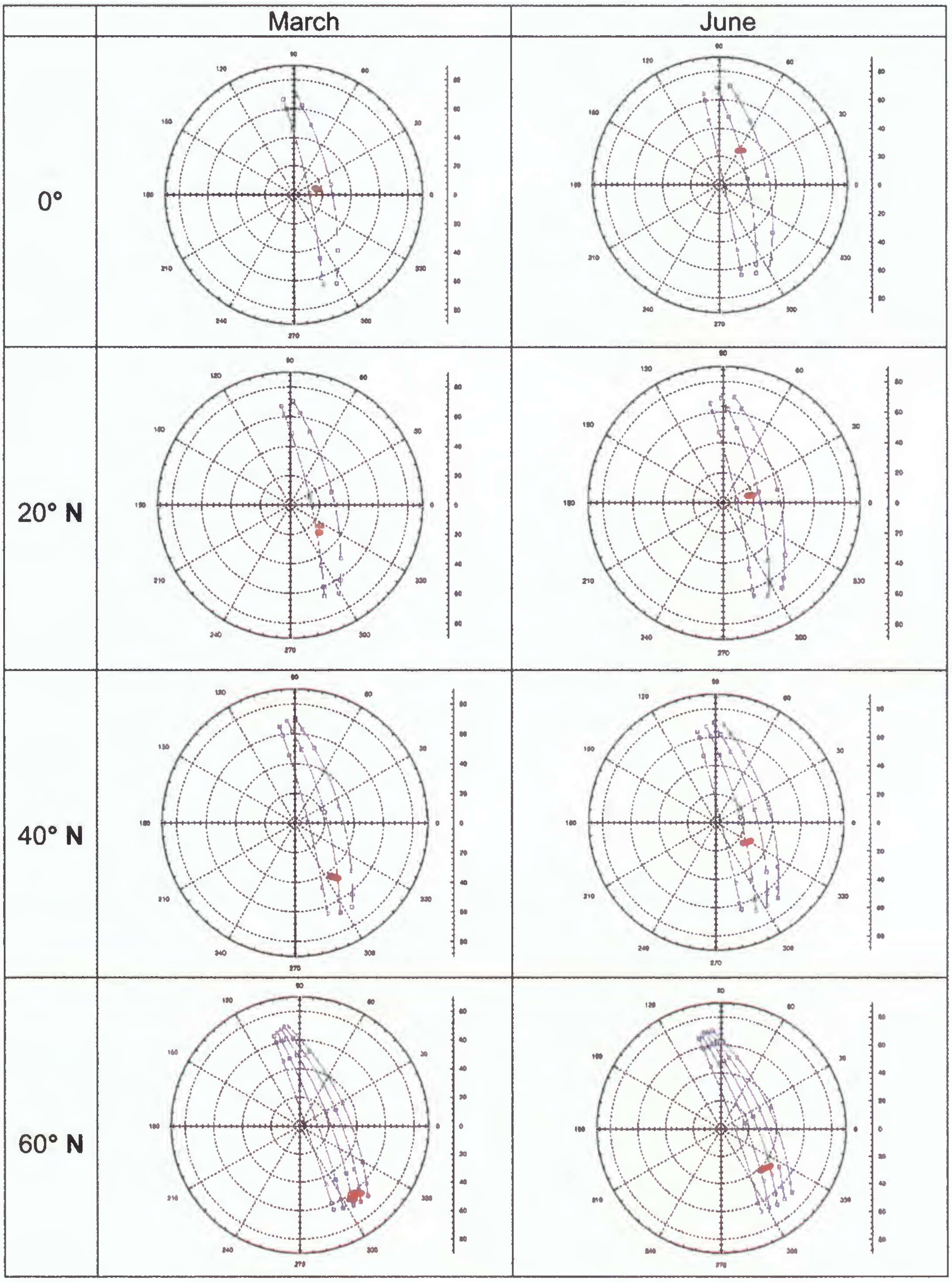

Figure 6.3. *Azimuth angle (with 0°=East) and co-elevation angle (radial co-ordinate) of BRDF acquisitions at ±70°, ±60°, ±45°, and close to nadir, from sites at various latitudes versus hot-spot direction (in red).*

The directional requirement clearly leads to a satellite capable of large and rapid attitude manoeuvres, since implementing the instrument LOS de-pointing entirely within the instrument (e.g. by a mirror system) would imply a very complex opto-mechanical arrangement. BRDF acquisitions are associated with a number of system constraints:

- a single BRDF acquisition occupies an orbital arc of ~25°, and so a clever management of site acquisition conflicts is necessary for regions that include several sites
- the satellite resources must be sized according to a realistic mission profile.

A specific mission simulator has been developed to perform mission planning so as to:

- analyse the performance of the system in response to typical mission-scenario acquisitions
- define the best time-lining for operations
- analyse the directional sampling performance of the system
- analyse the possible use of weather prediction in the mission planning
- provide observational statistics on hot spot sampling capabilities and various technical outputs (on-board resource needs for power, memory, etc.).

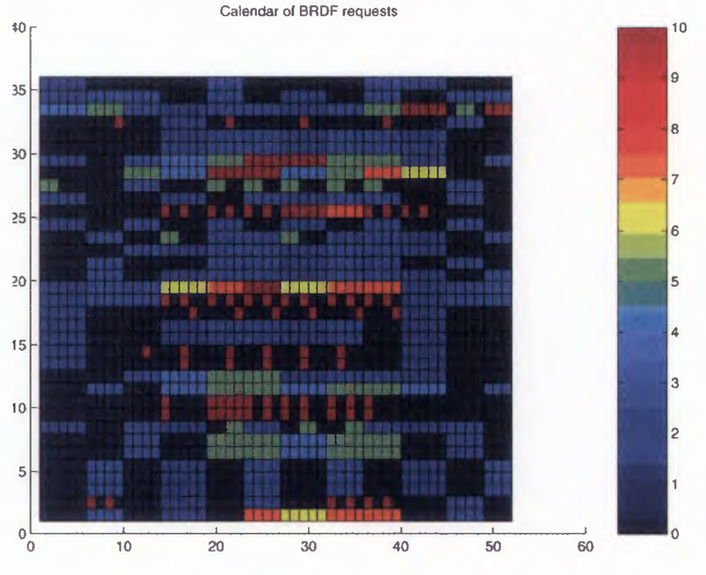

Figure 6.4. *Overview of user requests over a one-year period (horizontal axis: week number; vertical axis: site reference number; colour code: requested observations for each site).*

An input scenario has been defined, with a preliminary but representative set of 36 sites (cf. Fig. 8.4) The simulation accounts for both technical constraints like attitude-control capabilities, memory resources, downlink constraints, and observation requirements such as BRDF and hot-spot sampling constraints. A realistic reference scenario of acquisition requests has been defined as input for planning the site image acquisitions. Figure 6.4 gives an overview of such a scenario, based on the identified sites and their observation requirements. Figure 6.5 shows an example of the simulator output, showing the performance of BRDF acquisition per site versus the requests. It can be seen that all requests are served and spare observation capacity is available.

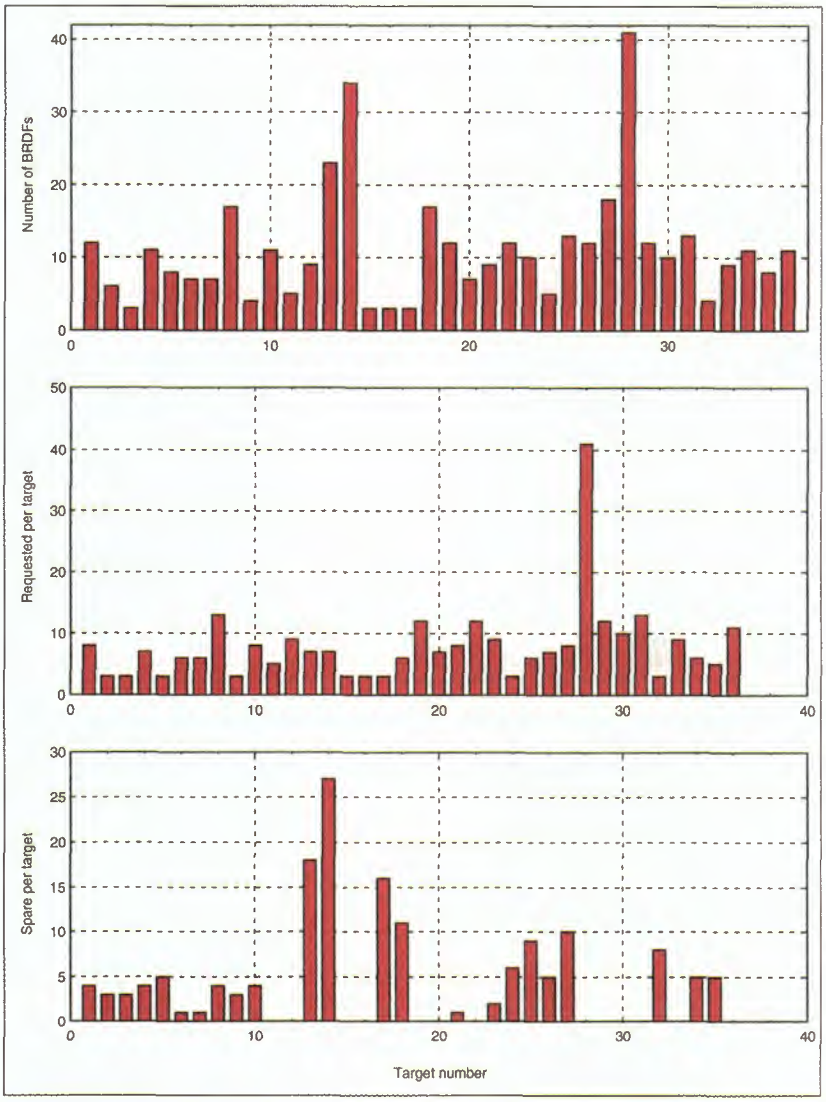

Figure 6.5. Example of mission-planning optimisation output (top: number of BRDF observations per site; middle: number of requested observations; bottom: spare observation capabilities per site).

Background planning over 14 days (the orbit cycle) has been chosen as the baseline, with possible updates and re-planning on a 3-day basis, notably to take into account weather predictions. This can be largely automated, as done (in a very preliminary way) with the simulator, which has proved to be a useful tool for assessing the capabilities of the overall system to cope with various mission scenarios.

6.2.3 Orbital Scenario and Satellite Operation Modes

The mission analysis provides typical orbital scenarios as input for the satellite design. The simulations provide a conservative average value of two BRDF acquisitions per orbit for the selected sites, which has been used to size the on-board mass memory. A single ground station in Kiruna is assumed, so that with the selected orbit typically nine ground station passes per day will be available. Four passes are sufficient for data downlinking even in case of failure of one transmission sequence. The passes can be selected such that they occur consecutively in the same period of the day, which helps to reduce the operation costs. With this approach and with a net downlink rate of 80 Mb/s, some 180 Gb/day can be transmitted, equivalent to approx. 60 BRDF image sets.

In the nominal operating mode, the satellite performs the following operations:

BRDF acquisition: This is performed up to three times during an orbit and lasts about 450 s per site. In line with the directional requirements, the satellite acquires a series of 7 images per site. Each image acquisition lasts about 20 s. The first 10 s are used for performing the TIR relative spatial calibration, needed before each image is recorded for radiometric reasons. The last 10 s are used for the image acquisition proper. Motion compensation by adequate control of the satellite attitude is performed in this period so that this duration corresponds to a 50 km by 50 km image on ground (in the nadir-pointing case). Between two images of a BRDF set, there are about 50 s available for satellite manoeuvres (to re-point along the pitch and yaw directions), and for correcting the roll pointing of the instrument. At the same time, the on-board data processing is performed for the previously acquired image (spectral band selection, data compression and generation of data packets). At the end of a BRDF acquisition, the satellite returns to the Sun-pointing attitude.

TIR acquisition: This is used during eclipse for image acquisition in TIR only. Directional requirements do not apply here.

Sun pointing: During the sunlit part of the orbit, when the satellite is not performing a BRDF acquisition, the attitude is such that the solar arrays are optimally illuminated for battery charging and the thermal fluxes on the SWIR radiator are minimal (to facilitate the detector cooling).

Calibration: When passing above the South Pole, the satellite is Earth-pointed and the instrument is calibrated using Sun illumination on its diffusers. This sequence occurs nominally once per week and lasts about 2 minutes.

Eclipse: During eclipses, the satellite attitude remains approximately inertially fixed. Only a small attitude correction is applied so that the SWIR radiator face is oriented to minimise the Earth thermal flux on it.

Downlink: For data downlinking to the ground station in Kiruna, the satellite attitude is such that Earth flux on the SWIR radiator is kept low and a very coarse pointing of the antenna towards the station is performed.

All of the above operations are performed at points in time that are well known in advance. They can therefore be programmed for on-board autonomous execution with very limited impact on the ground-segment complexity. Figure 6.6 illustrates some of the above operations along an orbit.

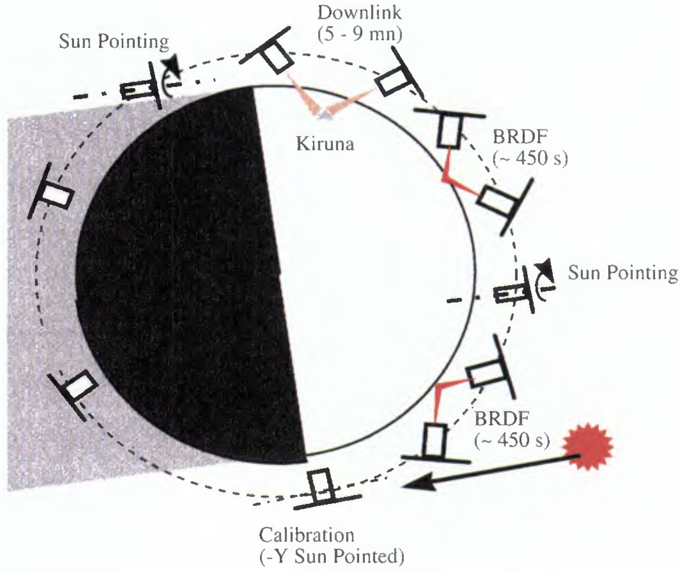

***Figure 6.6.** Typical LSPIM operations along an orbit (with downlinking).*

6.3 The Payload

The payload architecture is defined with the goal of ensuring the required performance and an optimal synergy with the platform functions and accommodation. As noted in previous Chapters, the payload will be composed of a single instrument, the PRISM imaging spectro-radiometer, and auxiliary equipment for data handling and transmission. The following sections briefly describe the principles and the architecture of the PRISM instrument and of the supporting data-handling elements.

6.3.1 Operating Principle and Functional Chains

The operating principle is outlined in Figure 6.7 and a functional block diagram of the entire payload is given in Figure 6.8. PRISM is a push-broom instrument: the extension of the image across the satellite velocity is defined by the instrument field of view (FOV), whereas that along the direction of flight is defined by the duration of the image acquisition.

In Region 1 (VNIR and SWIR), from 0.45 µm to 2.35 µm, PRISM is a hyperspectral imager, with a high spectral resolution (10 to 15 nm) and a high number of bands (144). In Region 2, from 8.0 µm to 9.1 µm, PRISM is a radiometer operating in two spectral bands, namely 8.0 to 8.5 µm and 8.6 to 9.1 µm.

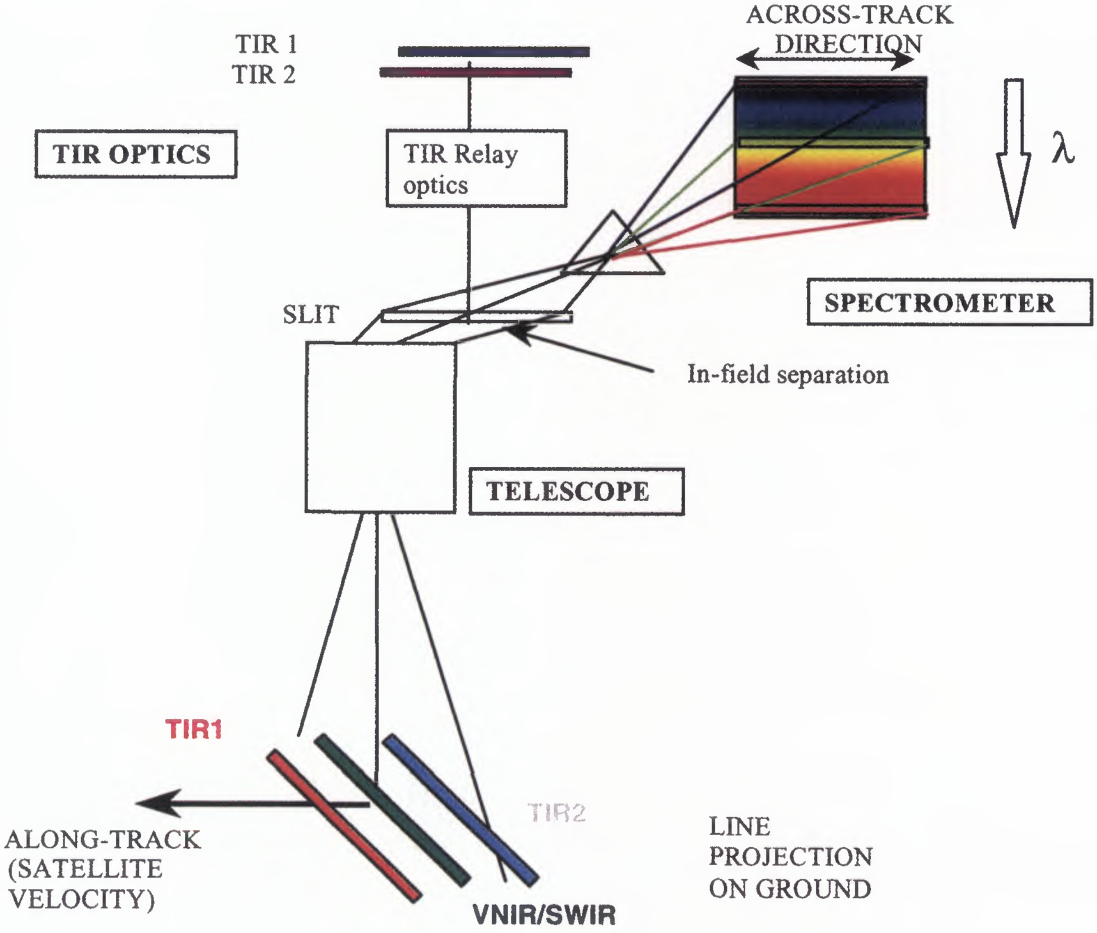

Figure 6.7. Operating principle of PRISM.

The instrument telescope is common to both regions and collects the light at an intermediate focal plane, where it is in-field separated and routed to optics dedicated to each region. The Region 1 optics includes a spectrometer which disperses the light, separating the VNIR and SWIR paths to direct them on the VNIR and SWIR focal planes, which contain two-dimensional detector arrays. The larger dimension (1000 pixels) of each array defines the instantaneous swath and the spectrally dispersed light is collected along the other dimension.

The Region 2 optics include a diffractive relay focusing the incoming light onto two linear detector arrays. Each detector line corresponds to one of the two required spectral bands, the number of pixels per line (1000) defining the instantaneous swath.

During each frame, i.e. during the time corresponding to the sampling of 50 m on-ground, the detectors are illuminated and the pixel information is transferred to the data processing chain. This frame acquisition is repeated 1000 times to generate a set of spectral images of the same scene, with dimensions of 50 km x 50 km (values at nadir). Each frame is read and converted into digital words that are stored in the mass memory unit (MMU). All the spectral bands, 57 spectral bands in VNIR, 85 bands in SWIR and 2 bands in TIR, are acquired and the relative data are transferred to the MMU.

The data are then further processed before the next downlinking. Up to 60 spectral bands in Region 1 are selected, although the possibility exists to retain all the bands (full spectral acquisition). The data are then compressed using a lossless algorithm (to reduce the MMU capacity), formatted and encoded for transmission to ground. The design is cost-effective, powerful and highly flexible, thanks to the implementation of the data processing entirely in the digital domain.

On the ground, further processing is performed according to the following main steps:

- data are decoded and uncompressed to generate 'raw' data (level 0)
- the data are radiometrically and spectrally corrected, using calibration data collected on-board and transmitted with the image data
- the data are geometrically calibrated, which involves:
    - geo-location, to project the acquired images onto a reference map (for both individual images and images acquired during BRDF sequences)
    - further processing to enhance the spatial registration.

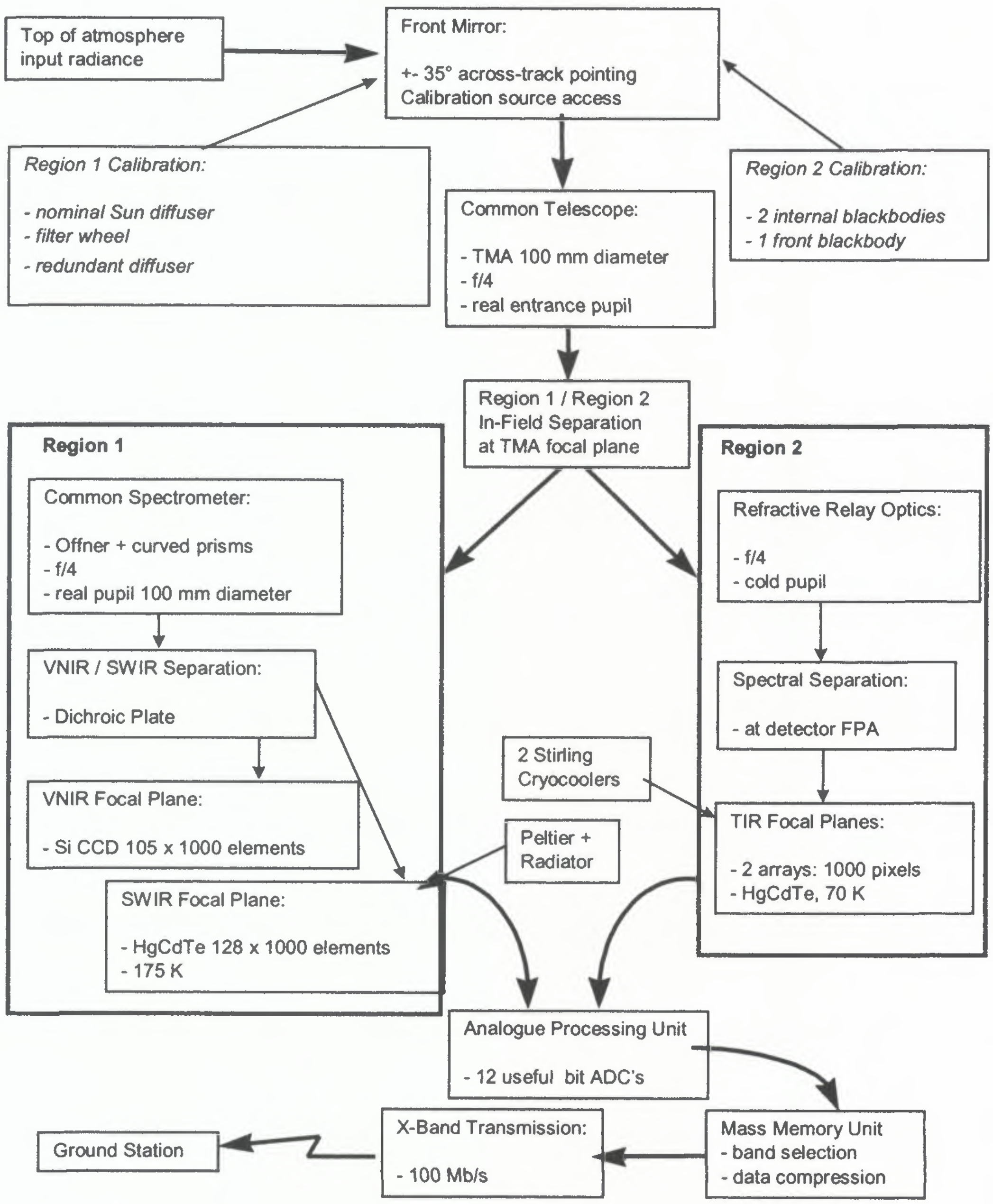

Figure 6.8. *Payload functional block-diagram.*

6.3.2 Optical Architecture

The optical system is modular and involves the following sub-assemblies (see Fig. 6.9): de-pointing mirror, telescope assembly, relay optics, spectrometer, and calibration sub-assemblies.

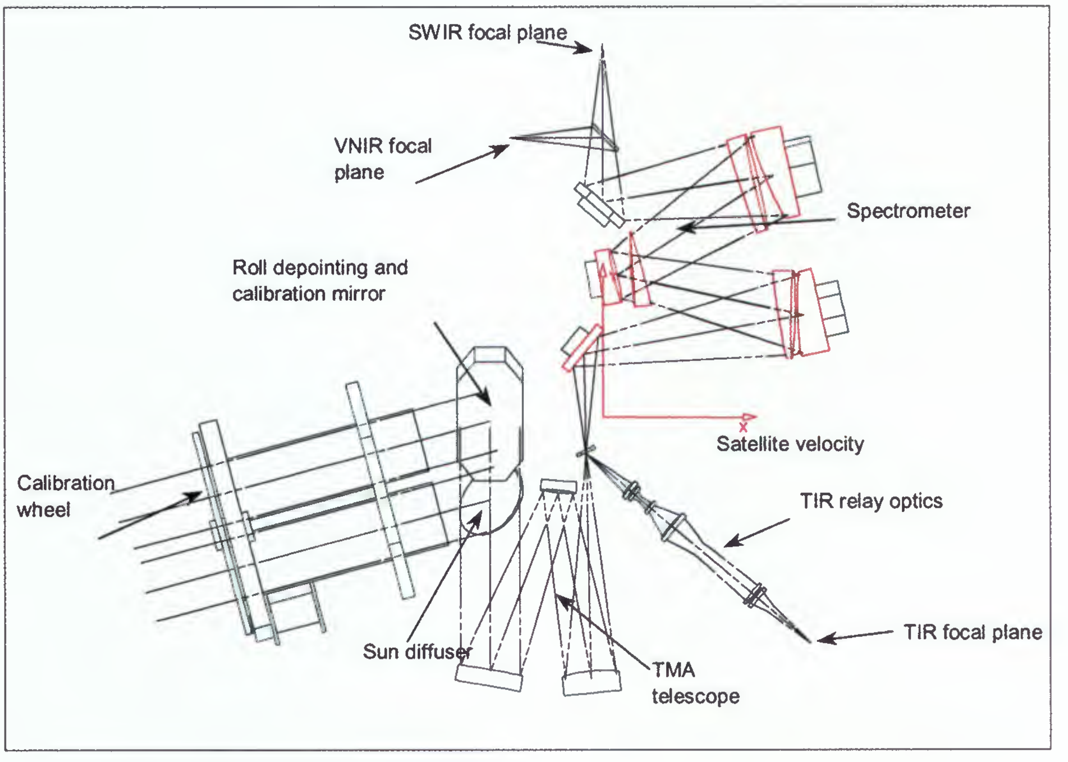

Figure 6.9. Optical architecture.

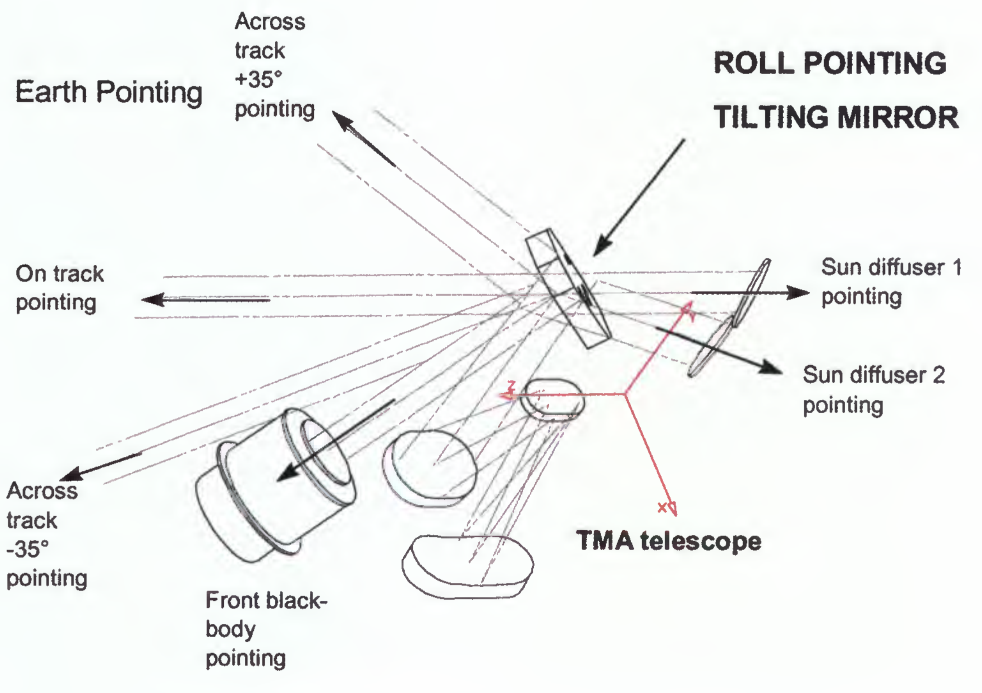

Figure 6.10. De-pointing mirror functions.

The de-pointing mirror, illustrated in the Figure 6.10, provides a dual function by ensuring the roll de-pointing and the accessibility to the front calibration sources. The mirror rotates around an axis in its plane to avoid image rotation problems and does not perform any fine pointing, since this is fully achieved by the satellite attitude control sub-system. The mirror is driven by a stepper motor.

In order to cover the whole spectral range with a very high optical quality, a three-mirror anastigmat (TMA) concept has been selected for the telescope assembly, which is well within the European manufacturing capability. A photo of the telescope breadboard is shown in Figure 6.11. The low entrance diameter (100 mm), focal length (407 mm) and reasonable f-number (4) make the telescope design a very sound one. Low sensitivity to mechanical misalignments has been achieved. The Region 2 relay optics is a state-of-the-art fully refractive system. It provides excellent optical performance (also accounting for mechanical and thermal tolerances) and fits within the required interfaces (dimensions, proximity of cold exit pupil to the focal plane for thermal constraints, etc.).

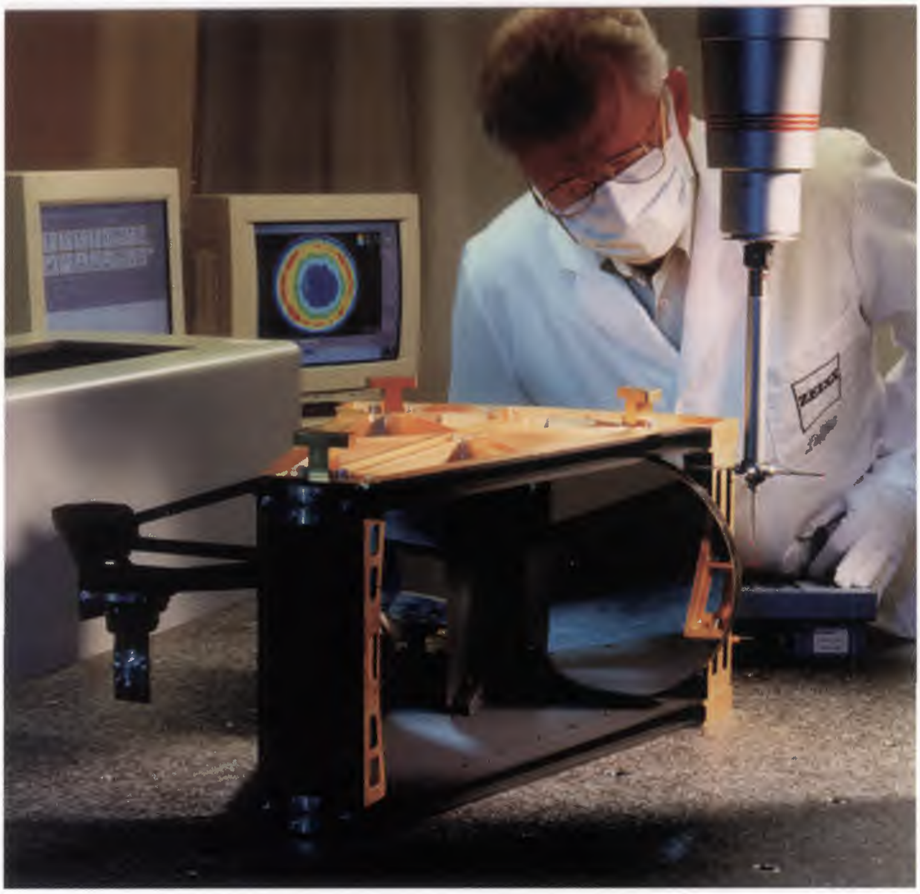

Figure 6.11. *TMA telescope breadboard during optical pre-alignment.*

The spectrometer is the most challenging assembly of the optical system. To ensure its realisation with a limited development effort, the spectrometer design is as simple as possible, while at the same time providing the required performance. The design is based on Offner relay optics and curved silica lenses acting as image correction and dispersing elements. The most critical issue is the spectral registration performance, because of the derived requirements on the positioning accuracy and stability of the optical components. The solutions selected for supporting the lenses and the mirror ensure the highest performance. Critical elements of a similar spectrometer have been manufactured and tested in a breadboard, including the disperser lenses shown in Figure 6.12.

Figure 6.12. *Separate disperser lenses for the spectrometer*

The instrument also includes calibration sub-assemblies to update the radiometric and spectral calibration coefficients on-board, as illustrated in the Figure 6.13. In the Region 1, the radiometric calibration uses two Sun diffusers and a filter wheel. The first diffuser is used routinely to perform the radiometric calibration, while the second is used infrequently to monitor possible long-term changes of the first diffuser. The wheel has three functions: to provide a shutter for characterisation of the detector offset, to provide an adequate level of input Sun irradiance, and to select one of the two diffusers. The spectral calibration is based on a spectral filter doped with a rare Earth element and could be upgraded to more performant spectral sources if needed. In the Region 2, spatial radiometric calibration is performed before each image is taken using internal black bodies. The absolute calibration uses a front black body and cold space viewing.

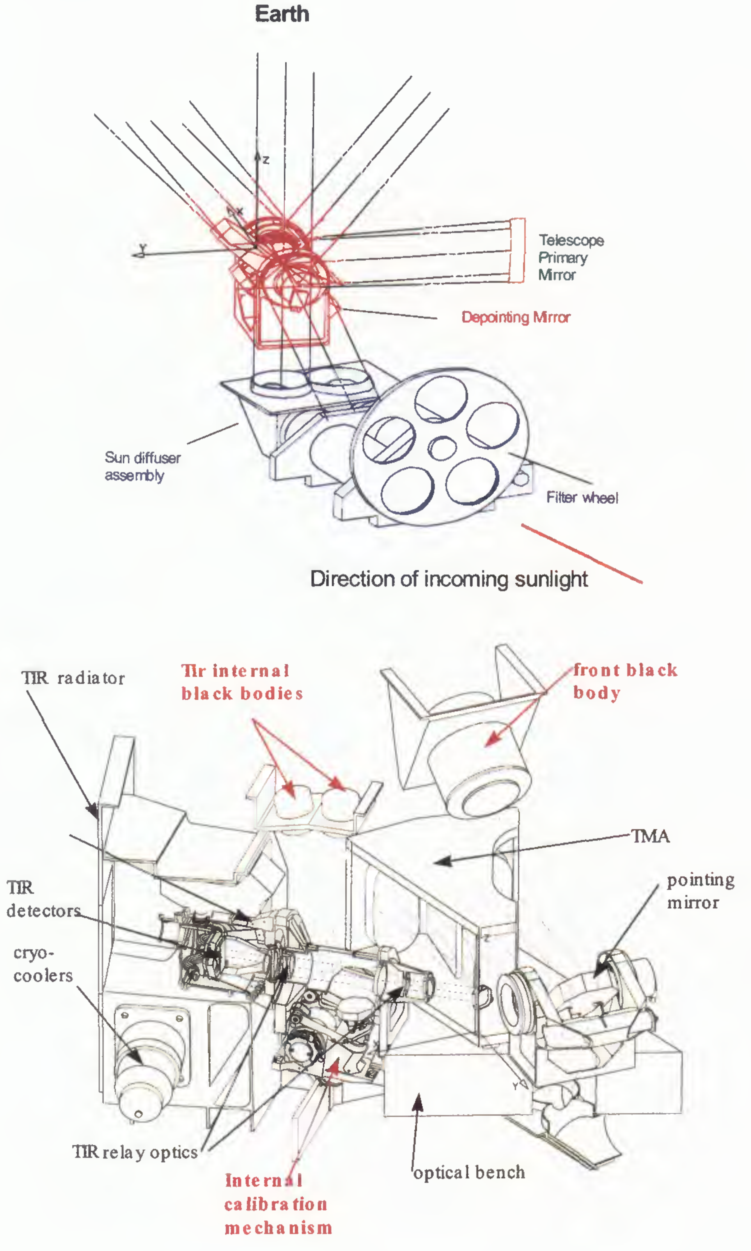

Figure 6.13. *Calibration assemblies (top: Region 1; bottom: Region 2)*

6.3.3 Electrical Architecture

The payload's electrical architecture, illustrated in Figure 6.14, includes the detection chain, the analogue signal processing, and the data handling and instrument control functions.

The detection chain involves three focal-plane detectors and their proximity electronics, which are accommodated on an optical bench:

- the VNIR detector in Si CCD technology operating from 0.45 μm to 1 μm
- the SWIR detector in HgCdTe CMOS technology operating from 1 μm to 2.35 μm
- the TIR detector based in HgCdTe CMOS technology operating from 8 μm to 9.1 μm.

The focal-plane proximity electronics is composed of the VNIR detection unit and the SWIR and TIR proximity interface boxes. The analogue signal processing is performed within the analogue processing unit (APU) located outside the payload module, and includes the amplification, offset correction and analogue-to-digital conversion of the detector outputs. The APU is interfaced to the MMU using standard high-speed IEEE-1355 standard digital links.

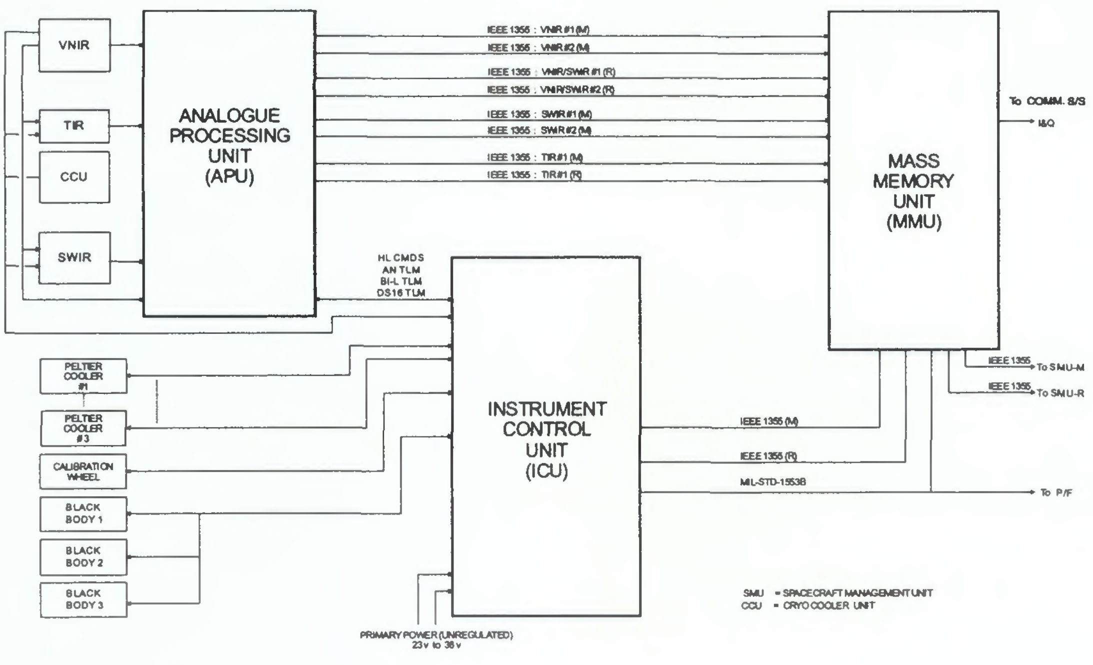

Figure 6.14. Payload electrical architecture.

The data handling includes the MMU, which performs data storage before and after data compression, spectral band selection and formatting. The command and control of the instrument is ensured by the instrument control unit (ICU), interfaced to the overall satellite controller (satellite management unit (SMU)) via a Mil-Std-1553B standard bus.

The ICU performs the instrument telemetry acquisition and controls all the active equipment (thermal heaters, mechanisms, blackbodies, Peltier thermo-electric coolers).

The cryo-cooler control unit (CCU) provides the power supply for the two Stirling-cycle cryocoolers used to cool the Region 2 focal plane to 70 K. The cryo-coolers are mounted in a back-to-back configuration to reduce vibration.

VNIR detector array

The VNIR detector array is a back-thinned Si CCD derived from the MERIS CCD development. The device format corresponds to the so-called 'asymmetric split frame transfer' and is presented in Figure 6.15. The image section consists of 1000 columns by 91 rows of 30 x 30 μm^2 pixels, split so that an equal number of spectral lines are read out of the top and bottom of the device. Because of the spectral pixel summation ('binning') performed in the lower spectral range, there are 62 rows in the short wavelength half of the device and 29 rows in the other half. Additionally about 6 rows in the image sections of each half of the device are required to accommodate the transition regions. The store regions in each half of the device have sufficient rows to accommodate the image region. Dark reference columns are located on each side of the rows. The detector array has four output ports to limit the pixel read-out rate to about 2 MHz, the read-out registers being split into equal parts for transfer in opposite directions.

A large full-well capacity of 1.9 10^6 electrons is required to avoid saturation with an integration time of 10 ms. This is achieved by an increase in the buried channel implant dose, together with a reduction in the thickness of the gate dielectric to increase the field within the structure.

The transfer time of the image zone into the store zone is lower than 70 μs to avoid smear corrections. This is made possible by a combination of the split architecture with very fast two-phase clocking, where the resistance of the electrodes is reduced by the deposition of aluminium tracks ('buttressing').

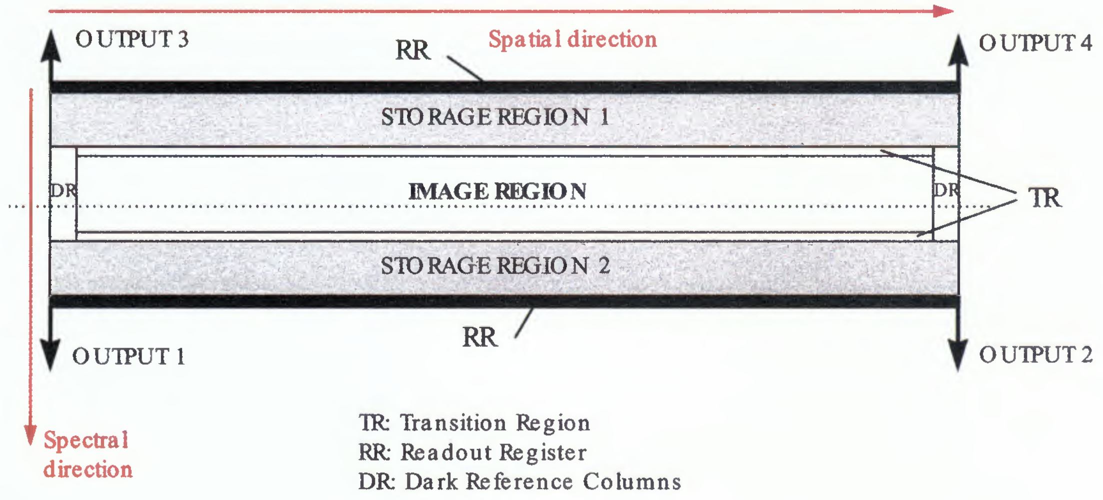

Figure 6.15. *Array organisation of the VNIR detector.*

An acquired image is rapidly transferred to the storage regions and then read out of the device, line by line. While the device is being read out, the next image is being obtained. If each row takes the same amount of time to be read out, the serial registers can operate synchronously. The spectral bands at short wavelength consist of binned rows; therefore these spectral bands take longer to be transferred to the readout register than the single row transfer required to transfer bands at the opposite end of the spectrum. In order to maintain the synchronism of the clocking scheme, the read-out rate is set by the time needed for the spectral band with the highest number of bins (6). An appropriate delay is allowed at the start of the read-out of spectral bands, necessitating less binning.

SWIR detector array

The SWIR detector array has 1000 x 128 pixels of 30 x 30 μm^2 area. The spectral bands cover 105 lines, of which only 79 are to be read out because of the atmospheric absorption gaps in SWIR. The array should operate at 175 K and have a dark current lower than 0.35 pA at this temperature. To get an assessment of the technological capability to realise such a focal plane, two major detector manufacturers have been involved in parallel analysis and design activities. Their proposed designs are rather similar two-dimensional HgCdTe diode arrays connected to CMOS multiplexers in a hybrid technology.

Despite its large size (about 30 x 4 mm^2), the detecting module is expected to be made of a monolith of HgCdTe diodes with a cut-off wavelength near 2.5 µm. The detecting elements are either vertical loophole diodes or planar diodes. The former type of diode is directly hybridised on the CMOS multiplexer during loophole processing, while the latter uses indium-bump hybridisation.

The CMOS multiplexer can also be monolithic, ensuring accurate (to 0.1 µm) alignment of all pixels. Alternatively, the HgCdTe monolithic module can be hybrised on two adjacent half-size mutiplexers with sub-micron accuracy because of the high precision of the hybrid manufacturing technique. However a loss of three blind columns at the interface can be expected in this case.

The input stage to the multiplexer uses buffered direct injection or a trans-impedance amplifier, to provide high injection efficiency, low noise and high bandwidth in low flux conditions. A signal sample-and-hold function is integrated in the pixel, allowing simultaneous 'stare and scan', i.e. integration and readout. At the end of each line, a few additional blind pixels are implemented to enable offset correction. Four outputs are used, with a data rate of 2.1 MHz, allowing one to read out the full set of useful spectral bands within the frame time of 10 ms. The scanning of the rows can also be made programmable, if reading of only a part of the device is requested.

TIR detector array

The TIR focal-plane array is a bi-linear array of 1000 pixels of 30 x 30 μm^2. Spectral filters are located on top of each line to define the spectral responses of the TIR 1 (8.0-8.5 µm) and TIR 2 (8.6-9.1 µm) bands. The operating temperature is 70 K, where mean dark currents lower than 0.06 nA (TIR 1) and 0.18 nA (TIR 2) need to be achieved.

Two leading European manufacturers, as for the SWIR, have been involved in analysing the feasibility of this focal-plane arrangement.

The requirement to have two parallel lines of detectors separated by a distance smaller than 2.5 mm, to minimise mis-registration effects due pointing instability of the satellite, leads to a trade-off between two basic architectures. Separate modules of HgCdTe with tailored cut-off wavelengths for the two bands can be used, with however some minimum distance between the two lines. Alternatively, a single module with the same cut-off wavelength can be produced with very small distances between detector lines. The latter approach is simpler to manufacture, but has the drawback of lower radiometric resolution in channel TIR 1 as the cut-off wavelength is close to 9.4 µm, adapted to TIR 2.

One of the possible designs uses such a monolithic approach where the detector consists of a custom-designed silicon multiplexer with a single monolith element of HgCdTe with a gap of 1 mm between the 2 lines. The process technology for HgCdTe is proposed to be loophole as this gives excellent reliability in long lengths. The spectral filters are deposited on a silicon substrate mounted very close to the detector surface.

The second possible design follows the other route with two lines optimised for each spectral band. It is based on the hybridisation of detecting devices and readout on a common interconnect circuit (indirect hybridisation). The two detecting lines are constituted of two butted sub-arrays of HgCdTe planar diodes. The readout circuits (Si CMOS multiplexers) are hybridised near the HgCdTe modules, with a readout circuit for each HgCdTe sub-array. At the butting interface, approximately 3 pixels are blind (defected pixels). The distance between the two arrays is driven by the dimensions of the HgCdTe modules and the transition zone in the filter and is therefore limited to 2.5 mm.

Direct injection is used in thermal-infrared to inject the diode current into the multiplexer, because the high current in this spectral region allows such a simple input stage to work properly. A sample-and-hold function is integrated in the pixel, allowing simultaneous stare and scan. At the end of each line, a few additional blind pixels can be implemented to enable offset correction.

Each design has redundant detector lines, to allow selection of the best-performance pixels after ground testing. In each spectral band, the best pixel in two or three parallel lines will be selected from a map loaded into the multiplexer memory.

Video processing

The video processing functionally involves the focal-plane proximity electronics and the APU. Table 6.3 summarises the main characteristics of the video processing.

Parameters	VNIR	SWIR	TIR
Typical pixel frequency (MHz)	1,76	2,15	0,1
A/D converter resolution	? 12	? 12	? 12
Temporal noise (LSB)	1,1	0,8	0,5
Absolute gain stability over 7 d (ppm)	± 400	± 400	± 400
Offset stability over 7 d (LSB)	± 0,25	± 0,2	± 0,5
Mean differential non-linearity (LSB)	0,5	0,5	0,5
Global linearity (LSB)	1	1	1

Table 6.3. *Video processing main characteristics.*

The video processing includes four parts:

- the VNIR detection unit (DU) integrated on the optical bench
- the SWIR proximity interface box (PIB1) integrated on the SWIR detector cryostat
- the TIR proximity interface box (PIB2) integrated on the TIR detector cryostat
- the analogue processing unit (APU), including all electronic functions required by the three chains, integrated in the platform module.

The units are visible in the overall satellite electrical architecture shown in Figure 6.26. For cost efficiency, the design is such that all analogue chains share many common functional blocks. The input rate is limited to less than about 2.5 MHz to minimise noise and allow a low-risk development. Correlated double samplers are used for the VNIR CCD detector. The baseline for the analogue processing is to use specific ASICs (under development) in order to comply with the radiometric performance needs.

At APU level the overall video chain of each spectral range (VNIR, SWIR or TIR) is integrated on the same board. This includes the acquisition chains, the sequencer, and the output data interfaces. A common card connected to DU and PIB1 is used for cold redundancy for the VNIR and SWIR. The TIR part is less demanding (since there is only one acquisition chain) and has two video chains in (cold) redundancy.

Instrument control unit (ICU)

The ICU is responsible for the control of the payload. It is monitored and controlled by the SMU, from which it receives high-level commands for execution. The ICU requests and co-ordinates the MMU's data acquisition, processing and storage services.

The ICU functions include:

- image sequencing
- acquisition of payload telemetry
- execution of relevant telecommands
- control of the payload units (including motor drives for actuation of mechanisms)
- payload thermal control
- control of the calibration procedure.

The ICU has its own processor-based module and is internally fully redundant (except for some interface functions).

Mass memory unit (MMU)

The MMU acquires the image data from the APU through high-speed IEEE-1355 links and buffers them. It implements (off-line) spectral band selection (up to 62 out of 144) simply by retaining only the data corresponding to the required spectral bands.

The MMU also performs data compression, generates source packets and stores them for subsequent downlinking. Data compression is lossless and based on the Rice algorithm. To this end, a standard ASIC, the packetising Rice data compressor (PRDC) is used, providing also data packetisation. After format generation, the data is ready for transfer directly to the X-band transmitter under ICU control.

The MMU includes a redundant processor-based module (identical to that used in the ICU) providing also interface and protocol management, processing of operational commands from the ICU and file management. The MMU is highly modular, being composed of a stack of memory modules (baseline size of each module is 16 Gb), accessed via a high-speed switching matrix. The nominal size of the mass memory is 80 Gb, therefore six memory modules are needed (one for redundancy). The size can be increased in steps of 16 Gb with very limited impact on the MMU resource requirements and cost.

6.3.4 Payload Mechanical and Thermal Architecture

The configuration of the payload module combines a very good utilisation of the volume under the launcher fairing with excellent inertial and mechanical properties. The module is located on the Earth face and has the same hexagonal shape as the platform module. This configuration is illustrated in Figure 6.16, where the telescope baffle is visible. The module also accommodates star trackers, antennas, and solar-array locking devices.

The internal accommodation is illustrated in Figures 6.17 and 6.18. The core element is the optical bench, which supports all the optical and focal-plane assemblies and is the main structural element of the spectrometer, the assembly most sensitive to misalignments. To achieve high stability, the bench is made of carbon-carbon composite material. This technology has been developed and tested under previous ESA studies. The telescope, the relay optics, the focal-plane assemblies (with dedicated cryostats for SWIR and TIR) are fixed on the bench with Invar inserts. The bench is isostatically mounted on an interface panel with three specific devices based on memory shape alloy, ensuring both locking and vibration filtering.

The instrument is provided with an adequate thermal environment:

- The optics are controlled to 20° ±1° C and meet special gradient and stability requirements for the Region 2 optics to guarantee radiometric performance.
- The TIR detectors are cooled to 70 K for radiometric performance. Two Stirling-cycle cryo-coolers are mounted on the interface panel and share a dedicated radiator.
- The SWIR detector is cooled to 175 K using a Peltier thermo-electric cooler associated with a double-stage radiator, located on the coldest face of the satellite. This design choice requires specific satellite attitudes when not in image-acquisition mode to improve the thermal flux on the radiator and exclude the possibility to perform also across-track de-pointing with the satellite. On the other hand, it has the advantage of avoiding a second set of cryo-coolers, with important benefits in terms of power consumption, mass, reliability and cost.

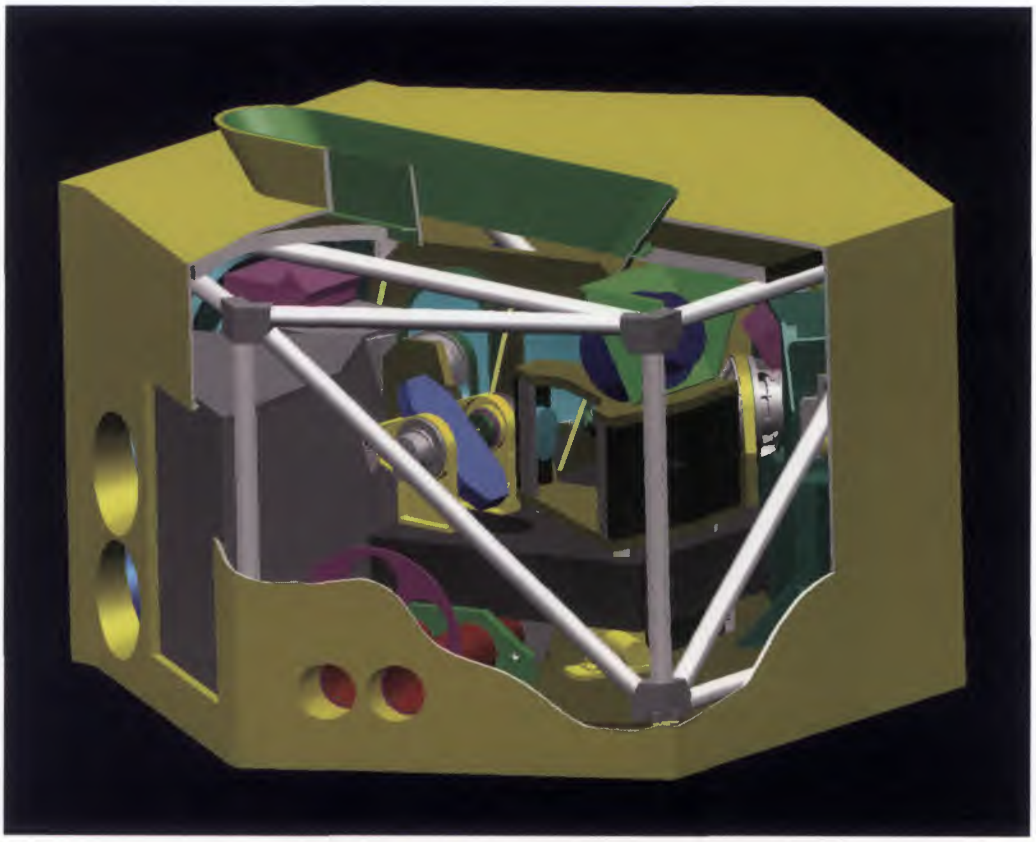

Figure 6.16. *External configuration of the payload module.*

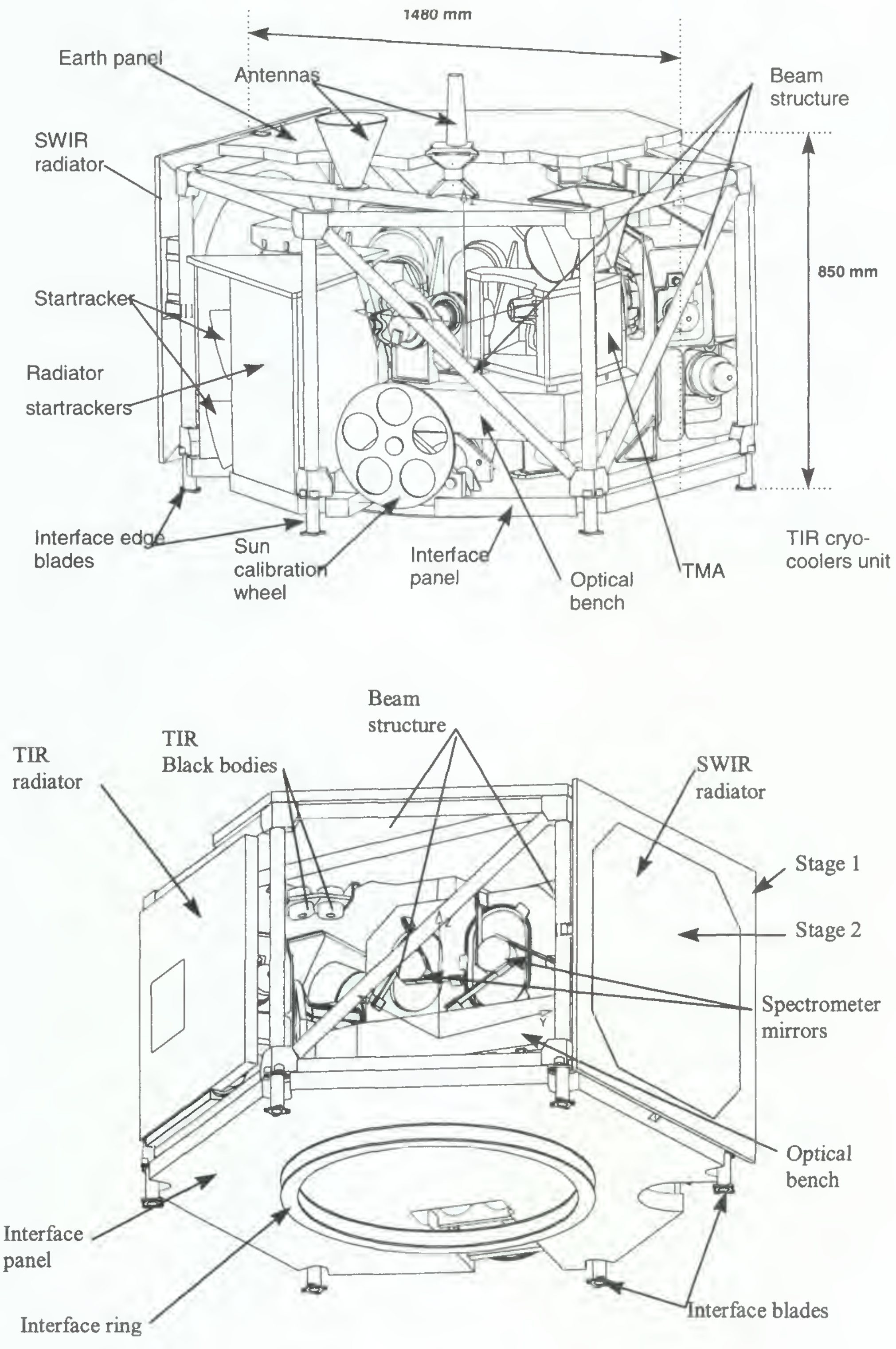

Figure 6.17. *Payload module - exploded views.*

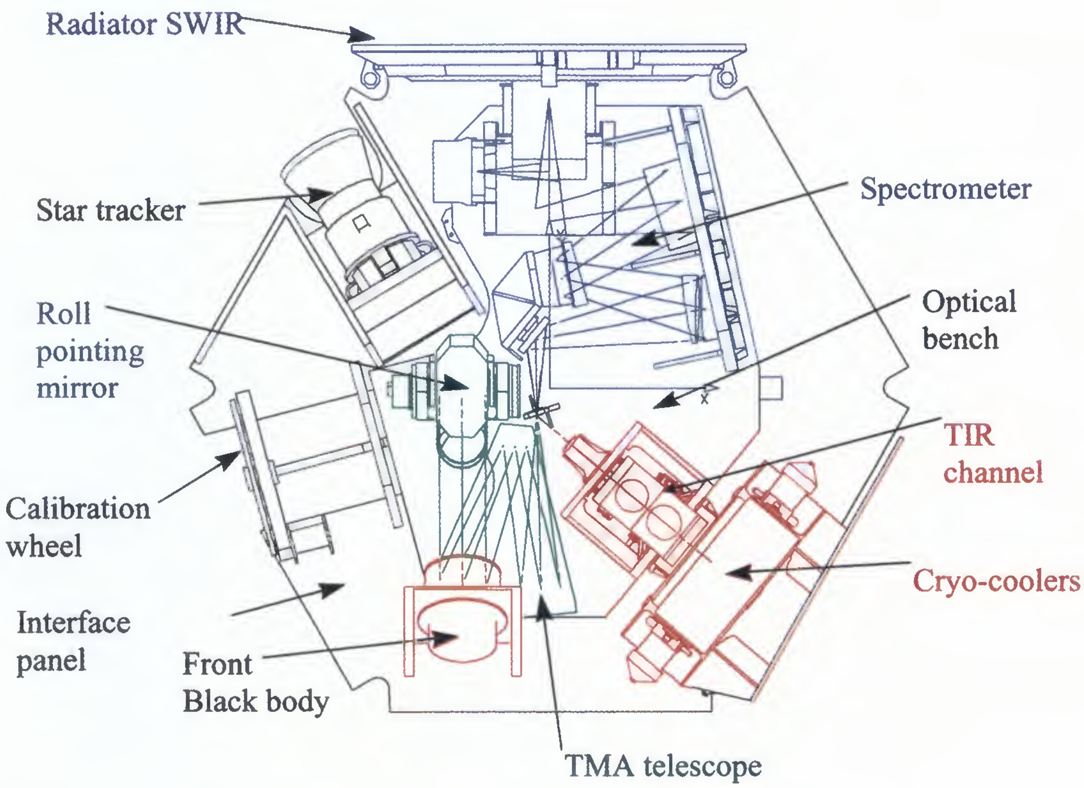

Figure 6.18. Layout of payload module.

6.3.5 Instrument Performance

Radiometric resolution

For the industrial study activities, the radiometric requirements described in Chapter 4 in terms of Neδρ have been translated into a requirement on noise equivalent radiance (NedL) at the top of the atmosphere (TOA). These values have been computed using a range of surface reflectance values for typical observational configurations (spring equinox, continental aerosol visibility of 23 km). The minimum, typical and maximum radiance values and associated NedL values have been computed using standard atmospheric correction models:

- Maximum radiance: equator, tropical conditions, scene reflectance of 1.1 (to take into account the non-Lambertian behaviour of some types of clouds).
- Typical radiance: equator and 60° N, tropical and continental conditions, surface reflectance typical of land scenes composed of 50% sandy surface. The

typical radiances at 60° N and spring equinox represent an average case for typical vegetation scenes.

- Minimum radiance: latitude 60° N, sub-arctic winter conditions, scene reflectance typical of coniferous forest.

The radiometric resolution achieved is compliant with the requirements in both Region 1 and Region 2, following a detailed modelling of the so-called temporal and spatial noises and including relative spatial calibration accuracy. The performance is given in Figure 6.19 and Table 6.4. The performance at end of life (EOL) has been estimated based on results from instruments already flown or on-going development measurements.

The dominant noise contributors in Region 1 are the spatial calibration accuracy, the accuracy of the ground characterisation of the radiance source (Sun diffuser characterisation) and the analogue chain noise. In Region 2, the most important noise contributors are the spatial drifts of optics and black bodies.

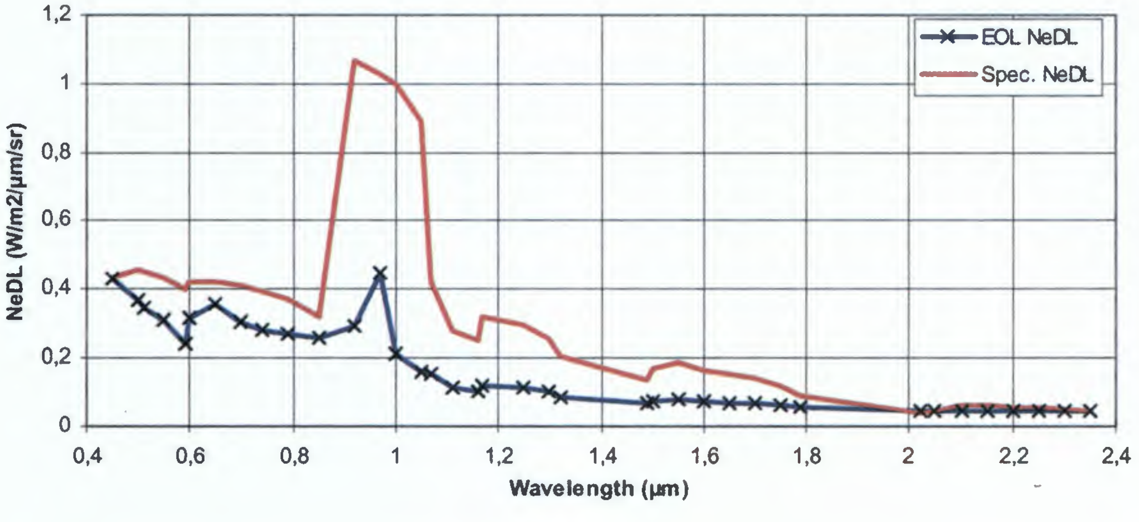

Figure 6.19. *NEdL performance in Region 1 (EOL).*

Absolute radiometric accuracy

The radiometric accuracy goal is 2% for all spectral bands in Region 1. Figure 6.20 shows the calculated performance where all values are within the design goal, the worst figure being 1.9% at 2 µm. The most important errors are the absolute accuracy coefficient error and the non-linearity effect.

The radiometric accuracy in Region 2 was assessed for a typical scene temperature. Table 6.4 shows the results for 300 K. The 1 K requirement is met for both TIR 1 and

TIR 2. The largest error contribution is due to the absolute calibration coefficient caused by the absolute knowledge error of the optical radiance.

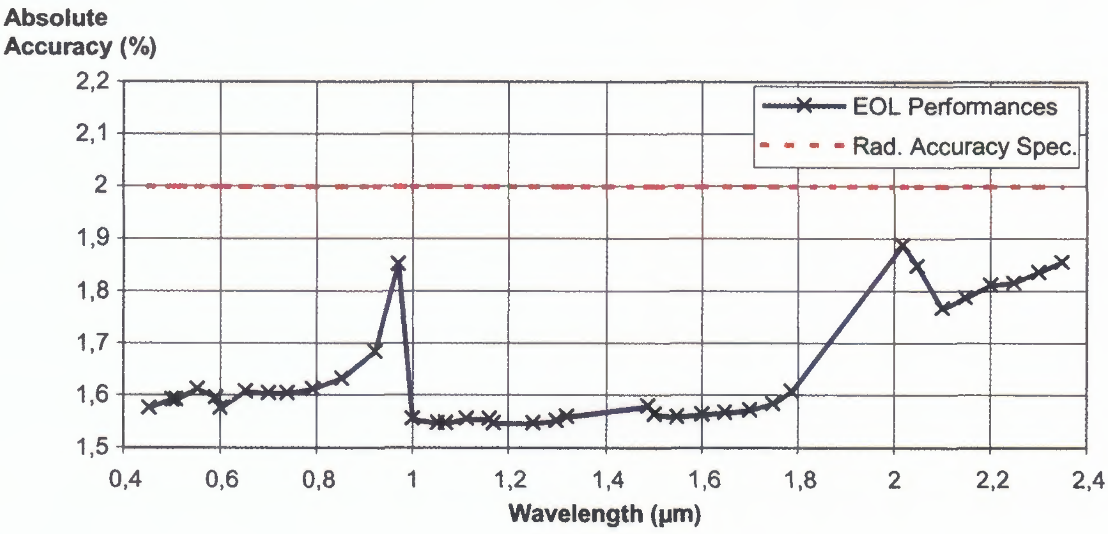

__Figure 6.20.__ Absolute radiometric accuracy in Region 1 (EOL).

TIR 1 accuracy	TIR 2 accuracy	TIR 1 NeDT	TIR 2 NeDT
0.66 EOL	0.80 EOL	0.074 BOL 0.086 EOL	0.097 BOL 0.119 EOL

__Table 6.4.__ Absolute radiometric accuracy (in K) and NeDT (in K) in Region 2.

Spectral performance

The spectral sampling interval (SSI) results from the combination of the spectral dispersion curve of the spectrometer, the geometry of the focal planes in the spectral dispersion direction, and the possible summation of several spectral pixels to improve the radiometric performance. Figure 6.21 shows the SSI achieved. In the VNIR, it is lower than 12 nm except at the edges, where it increases for radiometric reasons, but is still below 14 nm. In the red edge band (680 nm to 769 nm), the SSI is better than 10 nm. Pixel summation is implemented up to 650 nm. In the SWIR, the SSI is exactly within the requirement at about 1300 nm and is lower everywhere else, down to 10 nm at the highest wavelength. No pixel summation is implemented in the SWIR.

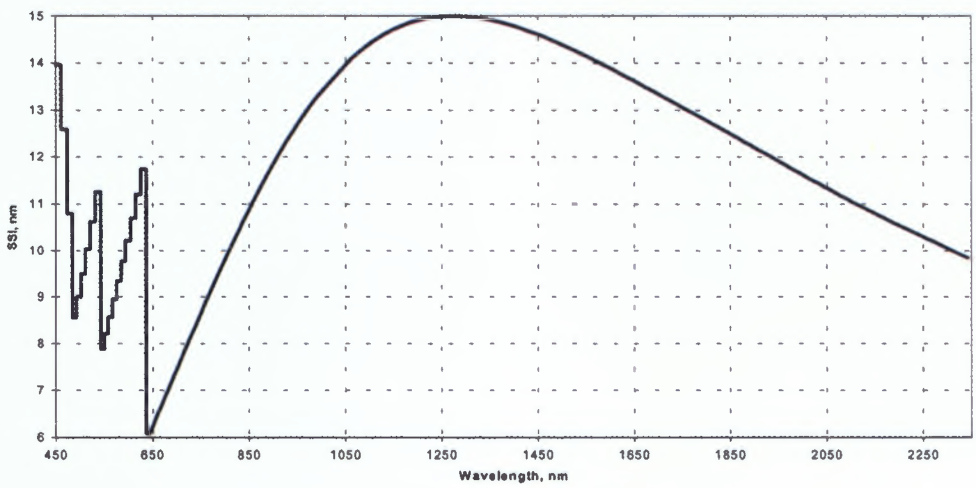

Figure 6.21. *Spectral sampling interval in Region 1.*

The spectral width is defined as the full width at half maximum of the overall instrument spectral response, calculated as the convolution of the spectrometer point-spread function in the spectral direction, of the detector response, and of the slit response. The performance is summarised in Table 6.5.

Wavelength	Centre of field	70% of FOV
450 nm, no pixel summation	2,84	3,04
450 nm, 6 pixels summation	17,04	18,24
700 nm	9,58	10,13
1000 nm	17,45	18,32
1300 nm	19,65	20,46
2350 nm	13,33	13,56

Table 6.5. *Region spectral width.*

The spectral width requirement is 1.5 SSI, i.e. 15 nm for a spectral sampling interval of 10 nm and 22.5 nm for a spectral sampling interval of 15 nm, met in the whole Region 1.

Spectral registration

The spectral registration measures the deviation of the sampled wavelength across the field of view of the instrument for each spectral image acquired. It results from optical residual aberrations, detector realisation error, mechanical instability of the optics and the focal plane assemblies. It puts stringent constraints on all of them.

Table 6.6 shows the estimated maximum spectral misregistration and the accuracy of the knowledge of this misregistration (assuming an on-board wavelength calibration with an accuracy of 0.5 nm). The performance can still be improved with further design optimisation.

Wavelength	0.45 µm	0.69 µm	1.0 µm	1.35 µm	2.35 µm
Spectral mis-registration	0.064	0.206	0.245	0.282	0.188
Knowledge of spectral mis-registration	0.022	0.072	0.089	0.1	0.065

Table 6.6. *Spectral mis-registration and knowledge of it in SSI.*

Wavelength knowledge accuracy

The required 1 nm performance is estimated to be achieved with the present baseline for spectral calibration, which uses a rare Earth spectral filter. Spectral calibration alternatives using hollow cathode lamps as spectral sources or the association of a lamp and a grating acting as a monochromator could be used if the performance is to be increased.

Spectral width knowledge accuracy

No specific on-board hardware is foreseen for the calibration of the spectral width as the requirements are expected to be met by design, thanks to the high thermo-mechanical stability of the spectrometer.

Spatial resolution

The spatial sampling interval is required to be 50 m in the nadir view. The detector geometry and the optical focal length support this performance in the across-track direction. In the along-track direction, the performance is met thanks to the optimal choice of the sampling time associated with partial motion compensation during image acquisition, which improves also the radiometric performance.

The spatial width is the full width at half maximum of the overall point-spread function (PSF) of the instrument. In the across-track direction it corresponds to the convolution of the optical PSF with the detector spatial response, and in the along-track direction to the convolution of the optical PSF with the detector spatial response and with a squared window corresponding to the integration time. The requirement of 1.5 SSI is met at all wavelengths. Figure 6.22 shows an example of the calculated performance at 700 nm.

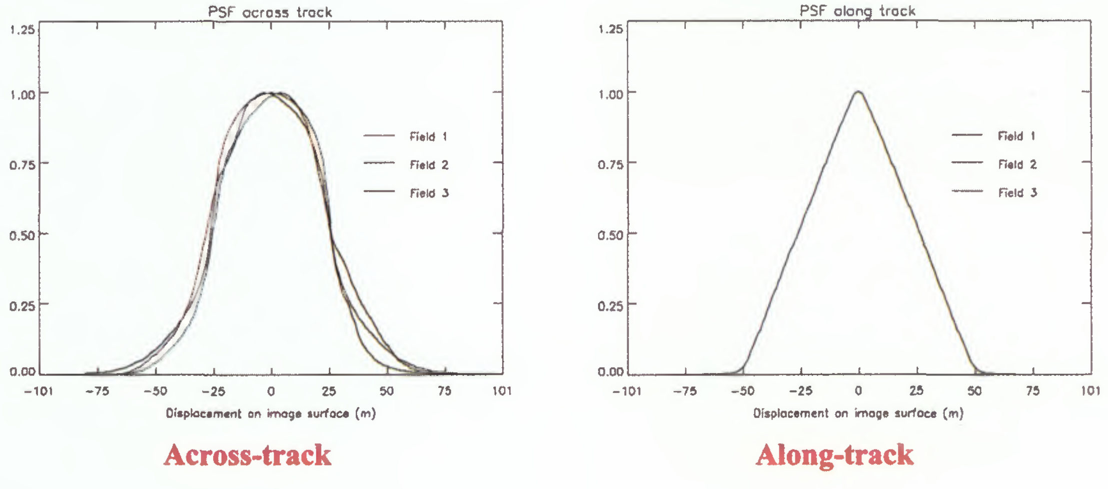

Figure 6.22. *Spatial width at 700 nm.*

Spatial registration

The spatial registration measures the deviation of the localisation on the ground of the pixels seen by each spectral band compared to the theoretical situation in which they should be all co-located. The design effort was put to ensure the best performance on the un-processed images by optimising the instrument mechanical stability and accuracy and guaranteeing an excellent satellite pointing accuracy. Tables 6.7 and 6.8 show the estimated performance within Region 1, Region 2 and between the two regions.

Within VNIR or SWIR, the performance is much better than the requirement. Between VNIR and SWIR, it is degraded, the main cause being the relative positioning and stability errors between the two focal planes. The choice of a single spectrometer covering the two regions improves the achievable optical alignments. In Region 2, the registration between TIR 1 and TIR 2 band is dictated by the geometry of the TIR focal plane, since the two lines are located on the same substrate, in the worst case at about 2.5 mm distance The error contributors correspond to the position accuracy of these two lines during the detector realisation and to the satellite stability. Between Region 1 and Region 2, the performance is about 0.5 pixel.

To further improve the system performance, there is the possibility to use a model of the geometrical characteristics of the instrument and the satellite on the ground to correct the mis-alignments and instabilities.

Spatial Misregistration : within VNIR

Focal plane pixel realisation (X), +/-	1 µm
Optical : theoretical contribution (X), +/-	0.75 µm
Stability of the optical performance (X), +/-	0.5 µm
Overall , +/-	1.3 µm
Performance (fraction of SSI)	**0.09 pixel**
Requirement	**0.2 pixel**

Spatial Misregistration : within SWIR

Focal plane pixel realisation (X), +/-	1 µm
Optical : theoretical contribution (X), +/-	0.75 µm
Stability of the optical performance (X), +/-	0.5 µm
Overall +/-	1.3 µm
Performance (fraction of SSI)	**0.09 pixel**
Requirement	**0.2 pixel**

Spatial Misregistration : between VNIR and SWIR

Performance within VNIR, +/-	1.3 µm
Performance within SWIR, +/-	1.3 µm
Focal plane alignment & stability (VNIR/SWIR), +/-	3.5 µm
Dichroic stability, +/-	1.0 µm
Overall +/-	4.1 µm
Performance (fraction of SSI)	**0.27 pixel**
Requirement	**0.2 pixel**

Spatial Misregistration : VNIR / SWIR with ground correction

Performance of ground processing, +/-	2.5 µm
On-board stability (launch corrected), +/-	0.9 µm
Overall, +/-	2.7 µm
Performance (fraction of SSI)	**0.18 pixel**
Requirement	**0.2 pixel**

Table 6.7. *Spatial registration in Region 1.*

Spatial Misregistration : between TIR1 and TIR2

TIR 1 / TIR2 Relative Pixel positionning (X,Y), +/-	3 µm
Satellite Pointing stability, +/-	2.8 µm
Overall, +/-	4.10 µm
Performance (fraction of SSI)	**0.274 pixel**
Requirement	**0.2 pixel**

Spatial Misregistration : TIR1 / TIR2, with ground correction

Ground processing performance, +/-	2.50 µm
Satellite Pointing stability (restituted), +/-	1.2 µm
Overall, +/-	2.77 µm
Performance (fraction of SSI)	**0.18 pixel**
Requirement	**0.2 pixel**

Spatial Misregistration : between Region 1 and Region 2

Performance within VNIR or SWIR, +/-	1.3 µm
TIR pixel positionning, +/-	1.5 µm
Region 1 / Region 2 positionning (X,Y), +/-	1 µm
Region 1 / Region 2 stability (X,Y), +/-	7.5 µm
satellite Pointing stability, 2sigma,+/-	1.4 µm
Overall +/-	8.0 µm
Performance (fraction of SSI)	**0.53 Pixel**
Requirement	**4 Pixels**

Spatial Misregistration : between Region 1 and Region 2

Processing performance, +/-	2.5 µm
Pointing stability (restituted), +/-	0.7 µm
On-Board stability (launch corrected), +/-	1.5 µm
Overall +/-	3.0 µm
Performance (fraction of SSI)	**0.20 Pixel**
Requirement	**4 Pixels**

Table 6.8. *Spatial registration in Region 2 and between the two regions (without and with ground processing).*

6.3.6 Payload Resource Budgets

The payload mass budget is given in Table 6.9. It includes appropriate margins for each unit, depending on the unit's status of development. Some of the payload electronic units (APU, ICU, MMU and CCU for a total of ~80 kg) are not included, since they are accommodated within the platform module, as shown in Figure 6.26.

The payload power consumption varies according to the modes of operation and ranges from a minimum of 287 W when the satellite is Sun-pointing, to a maximum of 418 W when the PRISM calibration is performed. During BRDF acquisitions, the average power consumption is 380 W. A substantial part of the power (approx.

170 W) is constantly used for the thermal control. Margins according to the maturity factors are included in the figures.

Optics (incl. optical bench)	175 kg
Structure	17 kg
Thermal control	79 kg
Transmission system	14 kg
Total mass	285 kg

Table 6.9. *Payload module mass budget.*

In order to derive a data budget, some assumptions about the image acquisition need to be made. The maximum frame size corresponds to a full spectral band image (total of 144 bands) and is composed of:

- 1000 pixels x 57 bands in VNIR
- 1000 pixels x 85 bands in SWIR
- 1000 pixels x 2 bands in TIR.

These data are acquired every 10 ms, while a full spectral band image (1000 frames) is acquired in 10 s.

The nominal image size to be transmitted to ground corresponds to 62 spectral bands (60 bands in any combination from VNIR, SWIR and 2 TIR spectral bands), i.e. 62 Mpixel/image. In the most demanding case, each pixel requires 14 bit (if 14 bit analogue-to-digital converters are used, presently under assessment). The nominal data volume per orbit corresponds to two BRDF sets (seven images per set) with nominal image size per orbit, i.e. ~12 Gb. Lossless data compression approximately halves the data volumes.

In the nominal case, the data collected over 12 orbits, amounting to ~73 Gb after compression, must be transmitted to ground over three consecutive orbits. A MMU with at least 80 Gb storage capability at EOL is therefore required, which is well within current capabilities. This storage and downlink scenario meets, with ample margins, the observation needs of the preliminary site distribution used in the mission analysis.

6.3.7 Payload Heritage

The design of the PRISM instrument is based on the maximum use of well-known technologies. The optical design involves a TMA telescope, similar to the HRIS (high-resolution imaging spectrometer) telescope already breadboarded. Other similar developments in Europe further support this solution. The spectrometer is a new concept, but it benefits from a number of developments, notably those of ultra-stable structures in carbon-carbon composite material and of the PRISM spectrometer disperser breadboard.

Heritage from MERIS is applicable for the Region 1 radiometric calibration, whereas other on-going European developments ensure the feasibility of the Region 2 calibration. The detection subsystem design is one of the challenging aspects of the instrument. In VNIR, a strong heritage will be available from MERIS, for instance with regard to the CCD detector (Fig. 6.23 shows the MERIS CCD). In SWIR, the detector will have to be customised. The major European manufacturers involved in the studies have a high confidence in the efficient development of this subsystem. In TIR, classical HgCdTe technology is applicable, though some specific aspects, like the implementation of a dual-band focal plane, deserve further study.

The analogue chain is based on existing technology and on ASIC developments that are well within the state-of-the-art. A gain in performance would result from the utilisation of 14 bit high-speed analogue-to-digital converters, currently under radiation-tolerance testing.

The digital system is based on a new generation of mass memory that takes full advantage of the recent development of memory devices and processors. In the proposed baseline, the ICU, MMU and SMU have identical processor modules and operating systems. They are based on the reuse or adaptation of existing units developed under national programmes. The main effort will be linked to the development of the application software. The existing PRDC ASIC is used to perform data compression and formatting. The qualification of this ASIC is an on-going activity.

An alternative solution based on the combination of the ICU and MMU into a single unit has been investigated. It would allow the saving of one (redundant) processor module, since the processor loads are moderate. However, this solution requires some additional effort to space-qualify the new unit and has therefore not been retained. The final choice can be reviewed in later design phases, also in the light of developments for other programmes. The rapid technological advances in this field will increase the range of choices, in particular for the MMU, with advantages in terms of performance and cost.

Finally, many facilities developed within prior optical payload developments will be exploited during the assembly and testing of PRISM, bringing significant cost reductions.

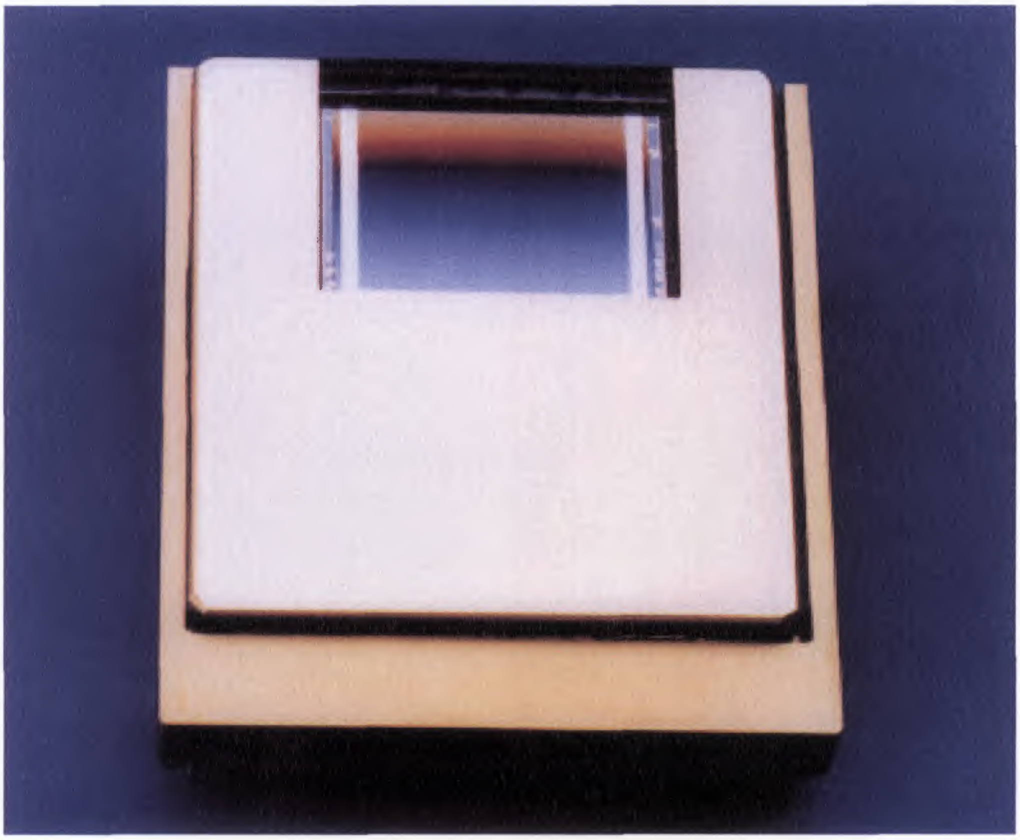

Figure 6.23. The MERIS CCD detector.

6.4 The Satellite

6.4.1 Configuration

As illustrated by the Figure 6.24, the satellite has a compact design for launch compatibility with the largest number of launchers on the market. Its deployed configuration has low moments of inertia (roll: I_{xx} = 301 kgm^2; pitch: I_{yy} = 301 kgm^2; yaw: I_{zz} = 406 kgm^2) and therefore supports the 'agility' requirements imposed on the attitude-control subsystem. Compatibility with several launcher adapters is ensured by the structure/launcher interface ring, which may vary in diameter from 880 mm to 1165.5 mm.

To reduce the development schedule, the satellite is divided into two modules:

- a platform service module (PSM), which houses the units belonging to the platform subsystems (propulsion, power, attitude and orbit control, telemetry and tele-command) as well as the APU, MMU, ICU, CCU and the payload transmission subsystem

– a payload module (PLM), which houses the remaining units of the payload and in particular all the optics.

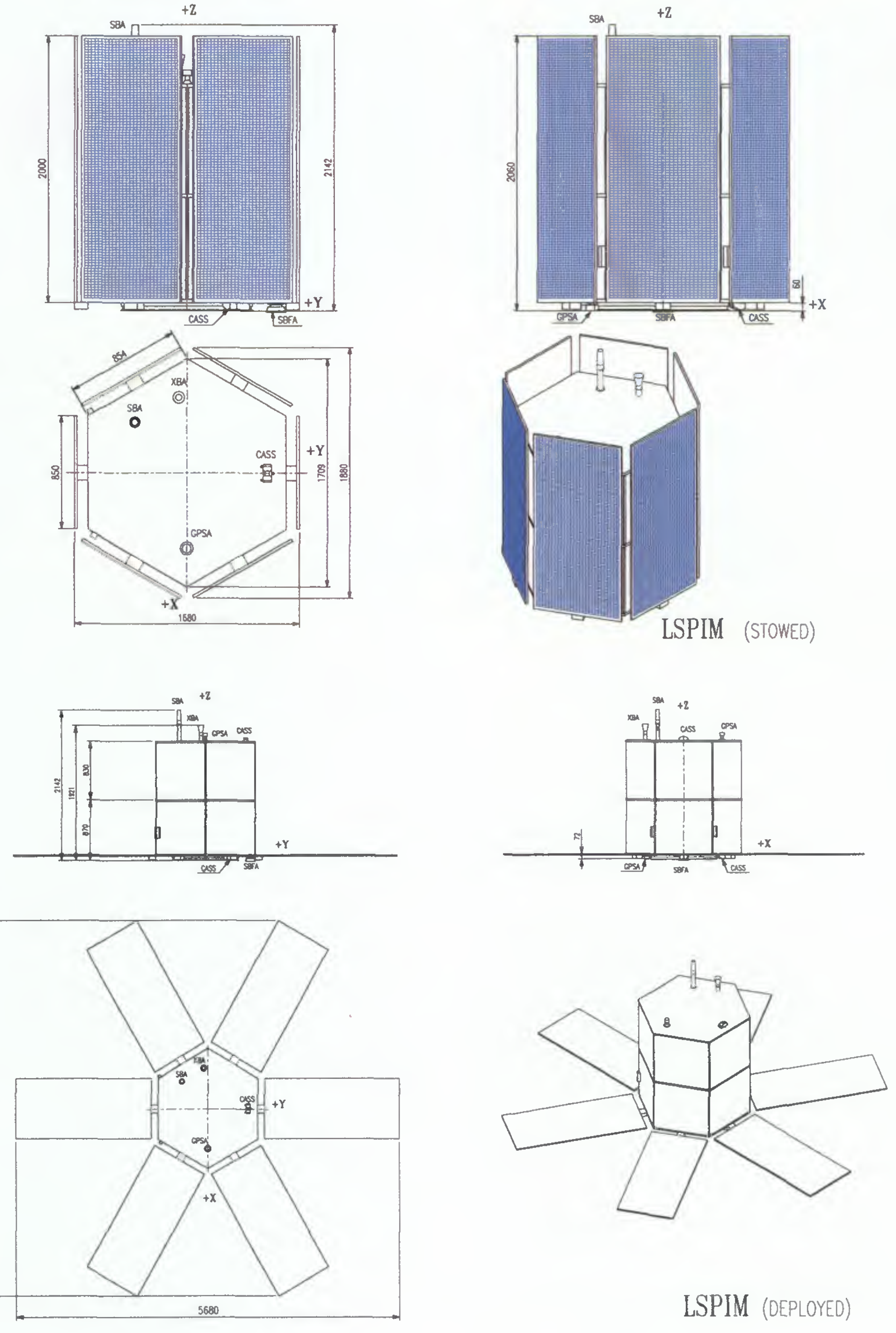

Figure 6.24. LSPIM satellite in stowed (top) and deployed (bottom) configurations.

The PLM is separated from the PSM by a horizontal intermediate deck. The deck rests both on the PSM and on the central cone in order to distribute the loads better. Once assembled, the three modules provide fixation interfaces for the six stowed solar panels, which are hinged at the base of the PSM.

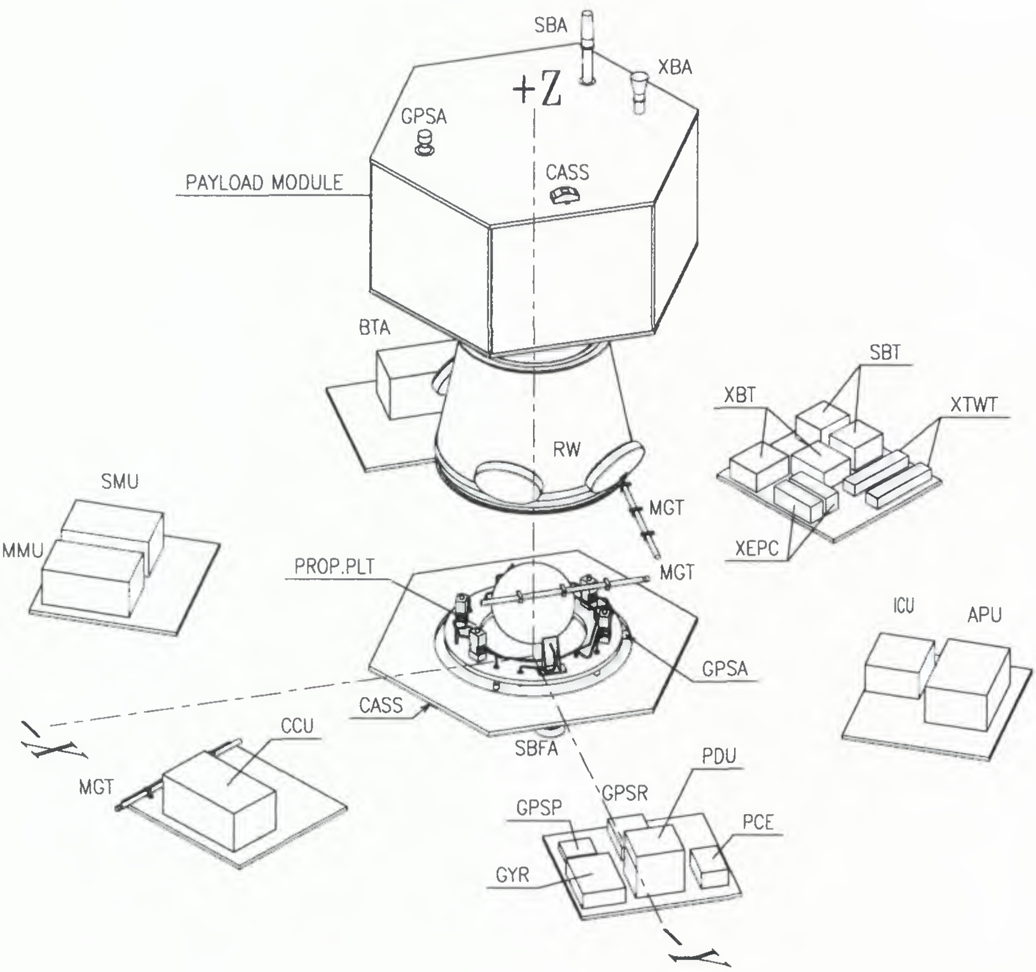

Figure 6.25. *Platform internal layout.*

The internal layout of the PSM is illustrated in Figure 6.25. The units are positioned so as to achieve both low inertia objectives and thermal requirements (e.g. for the dedicated battery panel) and are grouped, as far as possible, per subsystem in the same region. The PSM, including the central cone which houses the propellant tank, constitutes a self-standing assembly, so facilitating the integration and test activities.

6.4.2 Structure

The structural design follows a modular approach. The basic structural elements are honeycomb sandwich panels, which, when assembled, form the modules described above. The main load path goes from the lower internal cone ring (in carbon-fibre reinforced plastic), which interfaces with the launcher adapter, to the upper cone ring, which in turn interfaces with the lower deck of the PLM. The units mounted on the lateral panels introduce loads on the lower and upper decks, which carry them directly to the cone rings. The design complies with the environmental requirements imposed by all the candidate launchers.

6.4.3 Thermal Control

The thermal control also follows a modular design approach. The satellite has different thermal environments that are strongly decoupled:

- A PLM environment, because of the stringent thermal requirements imposed by the payload operation.
- A PSM environment, dedicated to assuring temperature ranges compatible with all the units allocated within the PSM.

The satellite's manoeuvrability implies varying thermal conditions, and so the feasibility of the design for both PLM and PSM environments has been verified in detail with appropriate thermal models. The PLM thermal environment is controlled by means of temperature sensors and heaters, managed by the ICU. Detailed analyses have been performed to make sure that the 175 K operating temperature of the SWIR detectors can be achieved with the proposed approach (Peltier thermo-electric cooler and radiators). The PSM uses passive means to ensure an internal temperature within –20° C and 45°C, using in particular flexible second surface mirrors on the external faces of the lateral panel, trimmed with multi-layer insulation (MLI). The interior is painted black in order to couple all surfaces and favour a homogeneous thermal environment. The battery is placed on a 'cold' panel (+Y face) and thermally decoupled from the internal environment with a dedicated MLI, since its operating range is somewhat lower than the PSM average environment. Heaters, MLI, thermistors and thermostats are used according to specific unit requirements.

6.4.4 Electrical Architecture

The overall electrical architecture, including the payload, is shown in the Figure 6.26. The main functional chains are:

- the satellite data handling and control, which includes the spacecraft management unit (SMU), the ICU and the MMU (described in Section 6.3.4)

- the communication subsystem
- the electrical power subsystem.

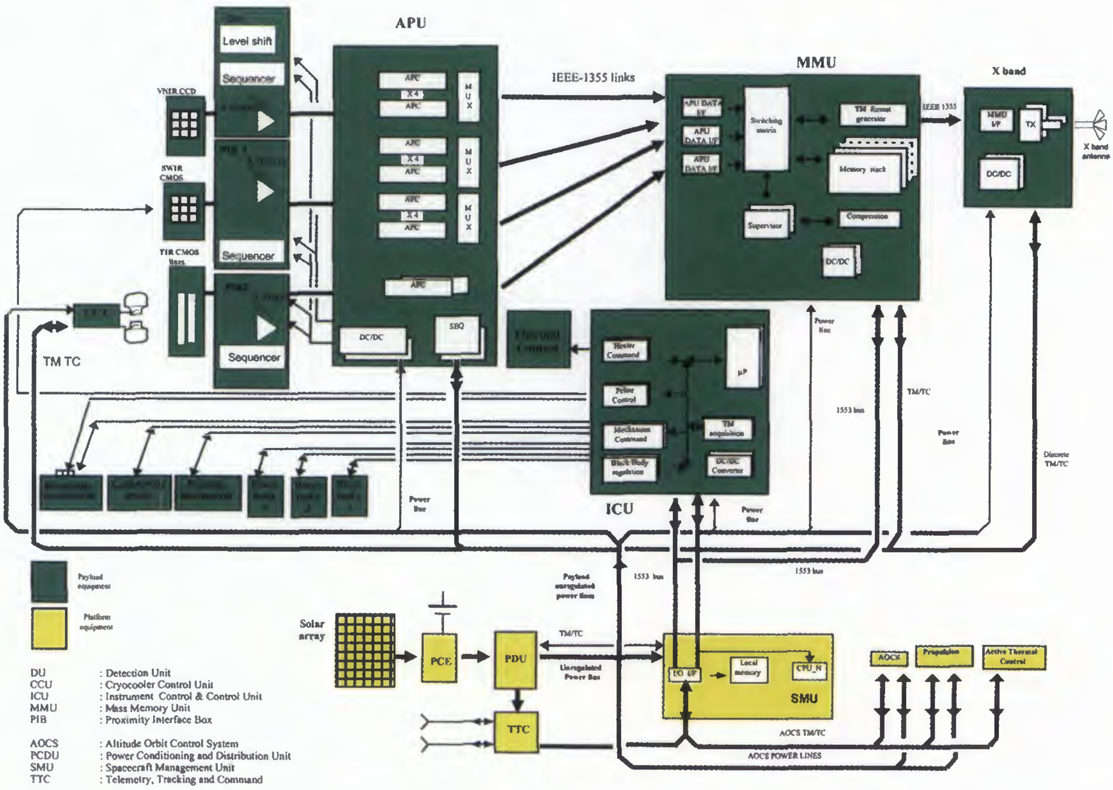

Figure 6.26. *Overall satellite electrical architecture.*

Satellite data handling and control

The architecture of the data handling and control is based on proven design concepts and readily available hardware. It is based on the SMU, which is the platform controller, integrating attitude and orbit control subsystem (AOCS) and data-handling functions.

This design reduces the interfaces between the PLM and the PSM and allows largely independent developments for platform and payload software and parallel development, integration and testing of the PLM and PSM.

Complete configuration control and on-board status observability is provided to the ground segment, including control of on-board autonomy, such as enabling/disabling alarms or recovery actions to be executed on specific alarms, redundant unit configuration, etc.

The SMU controls the satellite operations and runs the AOCS, collects and stores telemetry, maintains the on-board time and interfaces to the payload through the ICU. The SMU also provides the main synchronisation events for the payload timeline as well as all platform control and monitoring interfaces to subsystem/units not directly interfacing to the Mil-Std-1553B bus (including AOCS sensors and actuators, power subsystem and thermal subsystem).

The SMU functions include:

- telecommand management, including storage, verification, execution of telecommands addressed to the SMU, dispatching of telecommands addressed to units interfaced via 1553 bus (e.g., MMU and ICU)
- telemetry data acquisition for monitoring purposes
- telemetry management, including formatting various type of source packets
- autonomous failure detection, isolation and recovery services (e.g. dispatching of pre-stored sequences of commands for re-initialisation or switch-over to redundant unit)
- resource management (e.g. for the power subsystem)
- reference time distribution (through the 1553 bus) and synchronisation service to ICU
- payload timeline generation and related high-level commands to the ICU, e.g. start of calibration, start of image acquisition, start of data transmission.

The SMU is internally redundant and comprises the following modules:

- telecommand and telemetry module
- processor module
- reconfiguration module
- attitude-control electronics module
- power converter module.

Communication subsystem

Two dedicated communication assemblies are foreseen, one for payload data downlinking (in X-band) and one for the telemetry and telecommand (in S-band).

The telemetry and telecommand assembly provides a telecommand uplink rate of 4 kb/s, which is ample for the mission needs. The required telemetry rate is 8 kb/s, convolutionally encoded. This is achieved with ample margins by the assembly. Two S-band antennas ensure a quasi-omni-directional coverage. Two receivers and one transmitter are active at the same time for hot redundancy.

The payload data is downlinked in X-band (8.5 GHz) at a rate of 100 Mb/s, including source-packet layer overhead. The net data rate is ~80Mb/s. The data will be Reed-Solomon coded and will meet the ESA telemetry-channel coding standard. A wide coverage horn antenna is used, so as to avoid the need for precise pointing during the transmission of payload data. The transmitted power is 20 W. A traveling-wave-tube power amplifier is baselined for efficiency reasons.

Electrical power subsystem

The electrical power subsystem is composed of:

- a solar array (6 wings)
- power-conditioning electronics (PCE)
- a battery, determining the bus voltage (non-regulated and between 23 and 36 V)
- the power distribution unit (PDU).

The design is based on the use of a single battery permanently connected to the power bus. The management of the battery charge is ensured by a digital series regulator (DSR) in the PCE. During sunlit phases, the DSR adapts the current provided by the solar array to the satellite needs. This is controlled by the SMU, which commands the connection/disconnection of solar-array sections on the bus based on various measurements, including account battery voltage, temperature and current. The switching is performed in the PCE.

Electrical power is generated by six fixed and rigid panels. Each panel has an area of 1.7 m^2 and contains 18 parallel lines of 51 GaAs cells. The array is capable of delivering 1660 W at EOL. The solar-panel sizing has also taken into account the profiles of attitude manoeuvres to be performed by the satellite.

The energy is stored in a 40 Ah NiCd battery, which will undergo 21000 cycles over 4 years with a depth of discharge below 30%. The reliability of this technology has been proven for 40000 cycles at 40% depth of discharge.

The power distribution is centralised (via the PDU) and under SMU control. It also includes switching and protections for release devices and thruster valves.

6.4.5 Attitude and Orbit Control Subsystem (AOCS)

Design criteria and requirements

The main driver for the AOCS design is the attitude manoeuvring capability associated with the BRDF mode. The observations require pitch pointing, adaptation of the yaw angle and limited guidance of the roll angle during image acquisition. These requirements demand good platform agility, which leads to a relatively large attitude control bandwidth (0.25 Hz) and therefore to an increased sensitivity to sensor noise.

Another important design driver is the pointing requirement, driven by the relative TIR 1-TIR 2 detector line registration, as shown in Figure 6.27. Since the TIR 1 and TIR 2 images are acquired with 0.83 s delay (in the worst-case separation of 2.5 mm among the detector lines), the AOCS must ensure roll and pitch stability to better than $2.2\ 10^{-4}$°/s (3σ, from 0 to 5 Hz) to guarantee the overlapping of the TIR images. In addition, the yaw guidance law must ensure the alignment of the image column with the velocity vector to better than 0.015° (3σ).

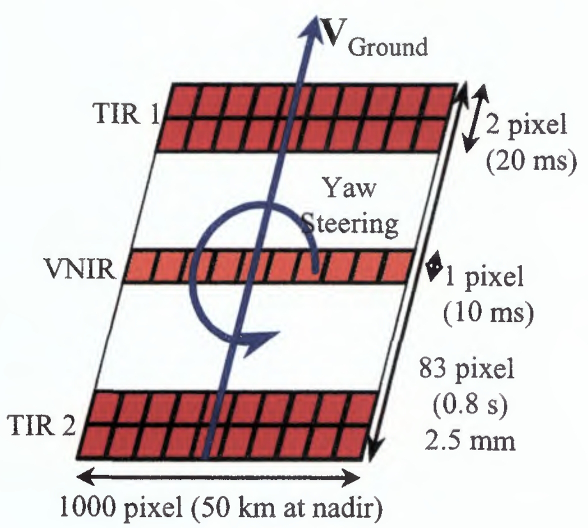

Figure 6.27. *Ground projection of detector lines.*

AOCS modes

The requirements lead to the design of an agile and accurate normal operation mode (NOM) assuming high-quality attitude sensors and high-torque actuators. The reference for the attitude estimation is a large field-of-view star-tracker mounted close to the satellite Y-axis in order to provide the best accuracy along the yaw axis. The large stability and the possibility to lose the star reference during manoeuvres (e.g. because of Earth obstruction) lead to the use of fibre-optic gyroscopes with low noise and drift. The actuation capability is provided by four reaction wheels mounted in an optimised skewed configuration so as to provide a maximum 1.25 Nm torque capability on the pitch axis. The momentum off-loading is performed by magneto-torquers.

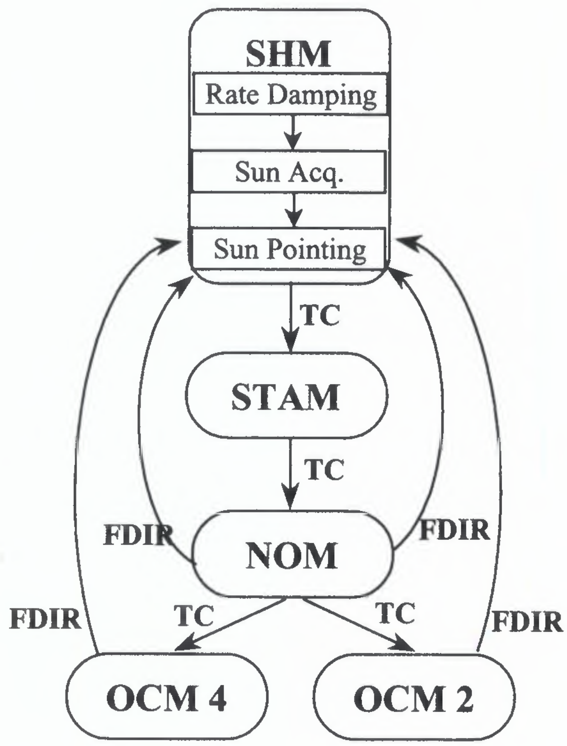

Figure 6.28. *AOCS modes and transition logic.*

This mode is supported by complementary AOCS modes necessary for acquisitions, for orbit control and for safety. The Sun-acquisition manoeuvre is intended to orient the solar array towards the Sun and to set the satellite into a safe attitude whatever the initial attitude. This is performed within the safe hold mode (SHM) of the satellite, which is based on a robust attitude estimation using coarse Sun sensors and magnetometers as sensors and magneto-torquers as actuators. After Sun acquisition, the satellite, set into a slow spin, can wait for ground control to command the transition to the inertial reference acquisition.

The purpose of the star acquisition mode (STAM) is to ensure inertial reference acquisition in order to be able to enter the NOM. The orbit control is performed by four thrusters, properly tilted, with the possibility of a redundant or fine two thruster operation. During these orbital control modes (OCM 4 and OCM 2, respectively), the attitude estimation is performed in the same way as in the NOM.

The transition between different modes is triggered by telecommands (TC) or by the fault detection, isolation and recovery (FDIR) functions, as shown in Figure 6.28.

Normal operation mode

While in the normal operation mode, the attitude estimation is based on gyroscope and star-tracker measurements. Because of the frequent star-tracker unavailability during BRDF acquisitions, the estimator can propagate the attitude using gyroscope data only when star-tracker data is unavailable. The estimator is tuned to reduce the star-tracker noise and the sensitivity to gyro drift.

Attitude-profile generation is based on optimised jerk profiles that minimise the torque requirement and excitation of the bending modes. During image acquisition, the guidance profiles are polynomials, computed on the ground based on the observation plan and then uploaded to the satellite and stored in the SMU.

The digital control law combines a high-gain proportional-derivative (PD) controller with filtering of the solar-array bending modes. A control bandwidth of 0.25 Hz is necessary to reduce the time for vibration damping after attitude manoeuvres to a maximum of 4 s. The bending mode filters are tuned to provide sufficient stability margins. A feed-forward command of the attitude profile during a manoeuvre, combined with gyroscopic torque compensation, augments the above (feedback) controller. The commanded torque is distributed to each wheel in an optimal way. The magneto-torquers are used for reaction-wheel off-loading, except during image acquisition when they are disabled to improve attitude stability.

A single-frequency GPS receiver is used for on-board real-time position and time determination.

Figure 6.29 shows an example of attitude and angular rate during BRDF acquisition. Figure 6.30 illustrates the estimation and control concept in normal operation mode.

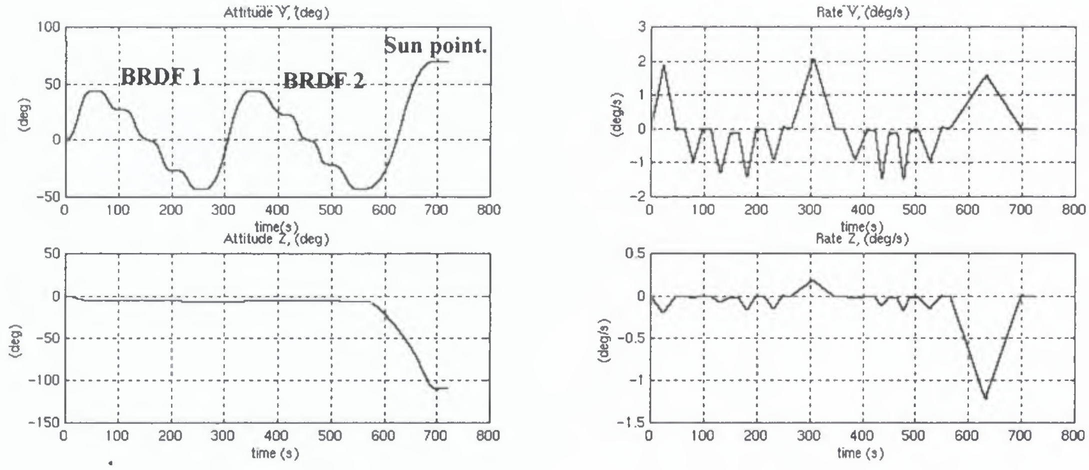

Figure 6.29. Typical pitch attitude and rate evolution during BRDF acquisition.

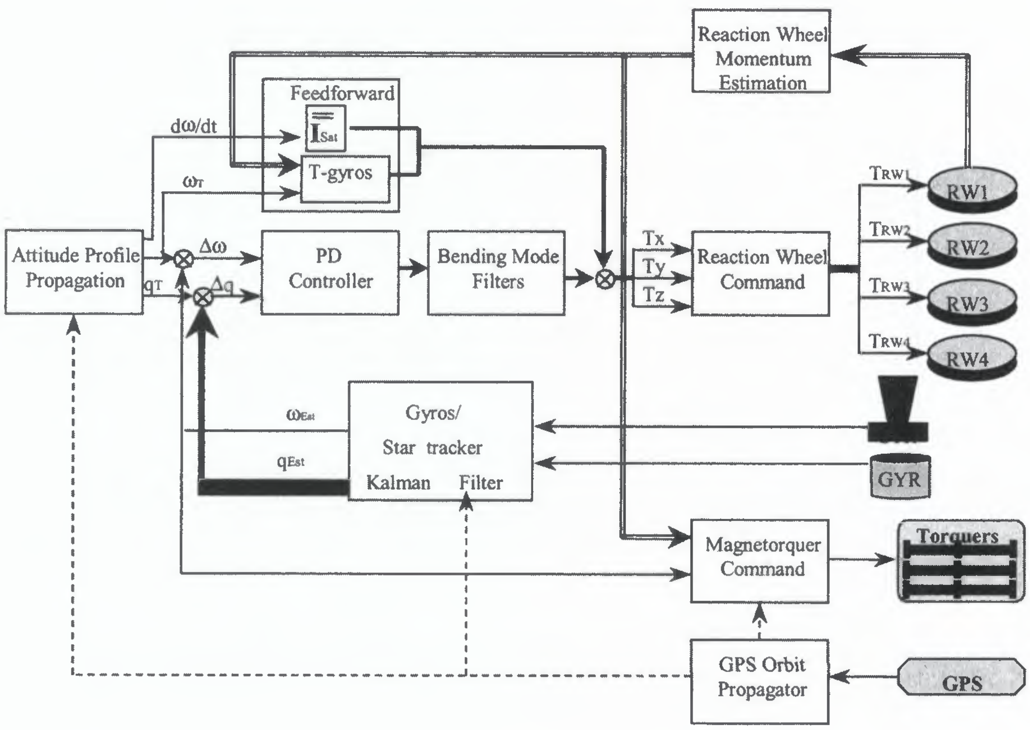

Figure 6.30. Estimation and control in normal operation mode.

AOCS performance

The above design provides excellent agility. The most critical manoeuvre in BRDF mode is the one required to re-point after a (near) nadir observation. In a BRDF sequence passing through a nadir view, the satellite can handle the required co-elevation angles, with excess performance with respect to the requirement of covering the ranges ±30° to ±45°. Any angle in the range -45° to -25°, and in the range 25° to 45° is feasible, as illustrated in Figure 6.31, so improving the hot-spot sampling for a large number of site observations.

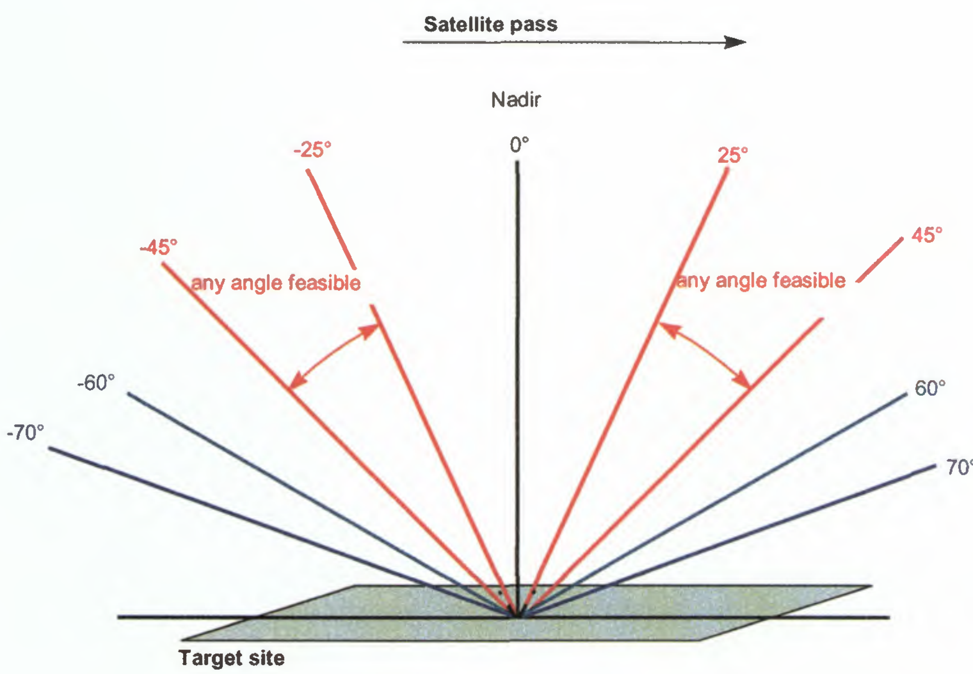

Figure 6.31. *Agility performance (nadir viewing): all required co-elevation angles are feasible.*

The pointing performance is met with good margins, leading to a 675 m pointing accuracy at nadir. The pointing stability supports the TIR 1/TIR 2 on-board registration by achieving a 3σ error of 0.165 spatial sampling interval. The attitude-restitution requirements are also met with good margins.

6.4.6 Satellite Mass and Power Budgets

The maximum mass of the satellite is 788 kg, including propellant and margins (both at unit level, depending on the development maturity, and at system level (10%)). The maximum total power consumption is 806 W, also including margins at unit level and at system level.

MASS SATELLITE BUDGET	NOMINAL TOTALS (kg)	MARGIN (kg)	MAXIMAL MASS (kg)
Payload			
Optical Bench	155.6 kg	19.1	175 kg
Payload Units inside Platform	68.3 kg	11.2	79 kg
Payload Module Thermal Control	74.0 kg	5.2	79 kg
Payload Module Structure	14.8 kg	2.2	17 kg
Payload Telemetry	12.0 kg	2.4	14 kg
Payload Total	324.7 kg	40 kg	365 kg
Platform			
Power Supply	58.5 kg	5.0	63 kg
AOCS	46.5 kg	3.5	50 kg
TMTC RF	6.9 kg	0.7	8 kg
Data Handling	11.0 kg	1.1	12 kg
Solar Arrays	46.5 kg	4.7	51 kg
Structure PF	78.0 kg	7.8	86 kg
Thermal Control PF	15.0 kg	3.0	18 kg
Harness PF	15.0 kg	3.0	18 kg
Propulsion	7.0 kg	0.9	8 kg
Assembling	0.0 kg		0 kg
Balance	0.0 kg		0 kg
Platform total	284.4 kg	30 kg	314 kg
DRY SATELLITE MASS	609.1 kg	70 kg	679 kg
PROPELLANT	28 kg		28 kg
Launcher Adapter	9 kg		9 kg
	NOMINAL		MAXIMUM
LAUNCH MASS without system margin	**646 kg**		**716 kg**
LAUNCH MASS with system margin (10 %)			**788 kg**

Table 6.10. *Satellite mass budget.*

	Sun pointing (38'-60')	**BRDF acquisition (7')**	**TIR acquisition**	**Eclipse (35')**	**Calibration (1'-2')**	**Data downlink (7'-10')**
Payload	287.3	379.5	318.7	292.8	418	326.9
Platform	242.1	321.7	271.7	270.7	249.7	317.4
Satellite total	529.4	701.2	590.4	563.5	667.7	644.3
Satellite total, 15% margin	608.8	806.3	678.9	648	767.8	741

Table 6.11. *Satellite power budget.*

6.5 Launchers

An important requirement is that the satellite should be launched by a small or intermediate-size launcher to minimise cost. Table 6.12 lists some candidate launchers and gives the performance for a launch into the selected orbit (the adapter mass must be subtracted from the launcher payload mass).

Launcher name and supplier	**Payload mass, adapter mass [kg]**	**Usable fairing size [cm]§**	**Adapter [D,h**]**	**Launch site**	**Static unbal. [mm]**
Athena 2 /LMLV Lockheed Martin	1085, 52	198 by 197	944, 0	Vandenberg	51
Cosmos (SL-8) Cosmos (USA)	840, NA	220 by 192	NA	Pletsesk	10
Rockot Eurockot Launch Service	980 , 15	222 by 361 242 by 361	937, 100	Pletsesk	30
PSLV / Antrix ISRO (India)	1130, NA	290 by 274	937, 0	Shriarikota	10
Taurus OSC (USA)	830, 3,5	140 by 279 205 by 344	943.6, 0	Vandenberg	25.4
VEGA K FiatAvio, Aerospatiale	≅1000, NA	215 by 224	NA	Kourou	NA
§ - fairing size is given as diameter by length of cylindrical section ** - adapter protrusion within considered envelope					

Table 6.12. *Candidate launchers.*

For both technical and cost reasons, Rockot is the reference launcher. However, the baseline satellite design is compatible with all the identified candidates, as illustrated in Figure 6.32. The launcher interface can also be easily adapted to any of the above launchers. The final choice can therefore be made in Phase-B, based on cost and risk.

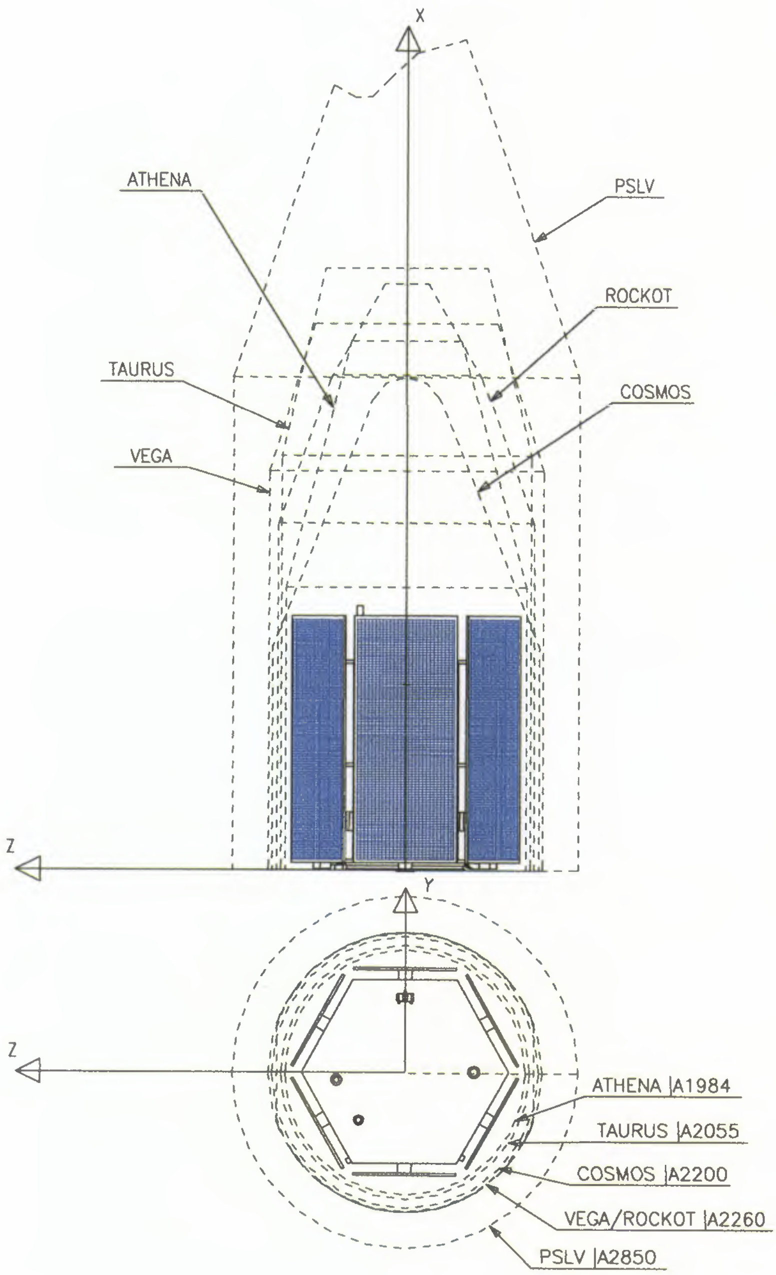

Figure 6.32. *LSPIM satellite on candidate launchers.*

6.6 Ground Segment

6.6.1 Architecture

The LSPIM ground-segment (GS) elements interface the supporting ground station(s) and the external entities, including the users with the satellite. The GS comprises four major elements:

- the command and data-acquisition element (CDAE), in charge of the telemetry and telecommand (TT&C) links with the satellite and of the acquisition of the scientific data from the satellite
- the mission operations and control element (MSCE), in charge of mission operations and satellite planning and control
- the processing and archiving element (PAE), in charge of data pre-processing and quality control
- the scientific data centre (SDC), representing the users.

An overview of the ground segment is provided in Figure 6.33, with the main functions allocated to each element.

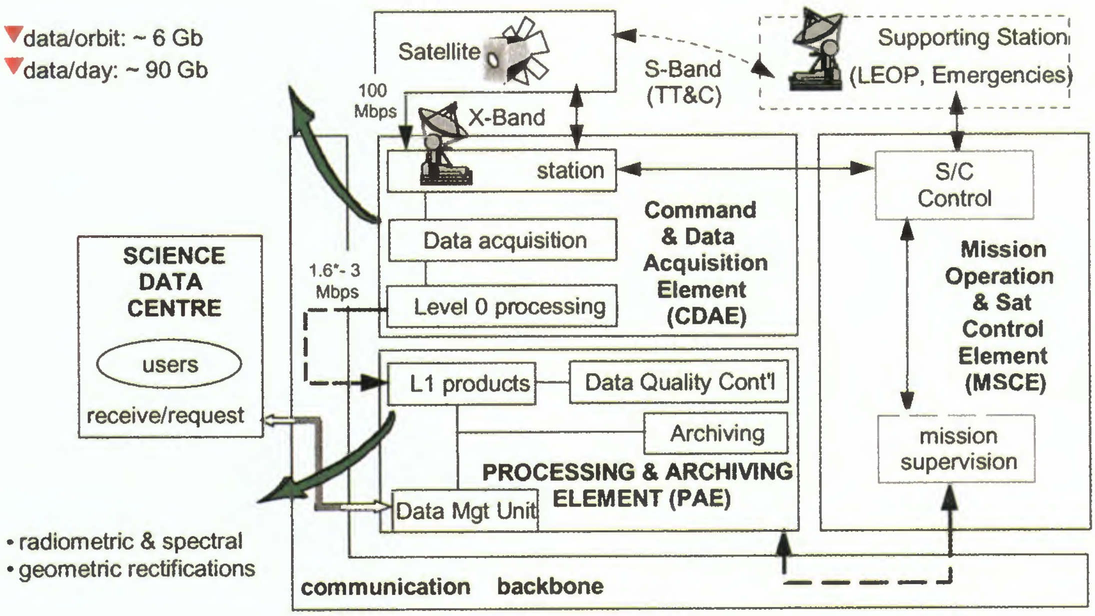

Figure 6.33. Overview of the ground segment.

The key requirement for the GS design is a cost-effective approach, through judicious re-use of existing infrastructure and use of the expected advances in computer technology. Cost efficiency will not be achieved at the expense of performance nor of user-friendliness.

The existing acquisition facilities can be shared with other missions for the CDAE, particularly in the case of Envisat. The possibility to implement this without impacting on the Envisat mission has been studied and confirmed. As a complement to the

CDAE, the MSCE that will be used to control the Envisat satellite can also be extended to control the LSPIM. In contrast, processing and archiving need to be customised for the LSPIM objectives and therefore a dedicated PAE has to be developed.

6.6.2 Command and Data Acquisition Element

The CDAE is in charge of TT&C communications and of the scientific data acquisition. The CDAE consists of a single ground station at high latitude for nominal operations. For the launch and early orbit phase (LEOP) and for emergencies, the existing network of TT&C stations will be used.

The CDAE operations can be largely automated and do not require significant operator involvement. This is mainly devoted to preventive and corrective maintenance for acquisition and TT&C equipment, limited media handling for the archive subsystem and for the supervision of the CDAE operation. The CDAE can be implemented at Kiruna. As noted earlier, the communication contacts will be limited to a maximum of four per day in a single work shift so as to reduce operation costs. The two S/X band antennas (15 m dish and 13 m dish, respectively) can be used and the required TT&C and payload data rates can be supported with adequate margins. The compatibility with the operation of Envisat has been satisfactorily checked.

6.6.3 Mission Operations and Satellite Control Element

The MSCE is in charge of the mission planning and operations and of the satellite control.

The baseline for the MSCE is to follow, with adaptations linked to the LSPIM mission, the GS control concept used for Envisat. The proposed architecture is depicted in the Figure 6.34.

The breakdown in subsystems corresponds to the following existing facilities (with small adaptations):

- Mission management subsystem: to implement tools for mission preparation and analysis.
- Mission planning subsystem: in charge of analysing feasibility and implementation of user requests.
- Ground-segment control subsystem: in charge of overall coordination with external subsystems, production control, and ground-segment configuration management.

– Flight dynamics, spacecraft scheduling, spacecraft control and analysis, satellite simulator: classical control centre tasks, which will be implemented in the frame of existing ESOC products (Spacecraft Operation System (SCOS) 2000, ORATOS).

– Mission quality monitoring subsystem.

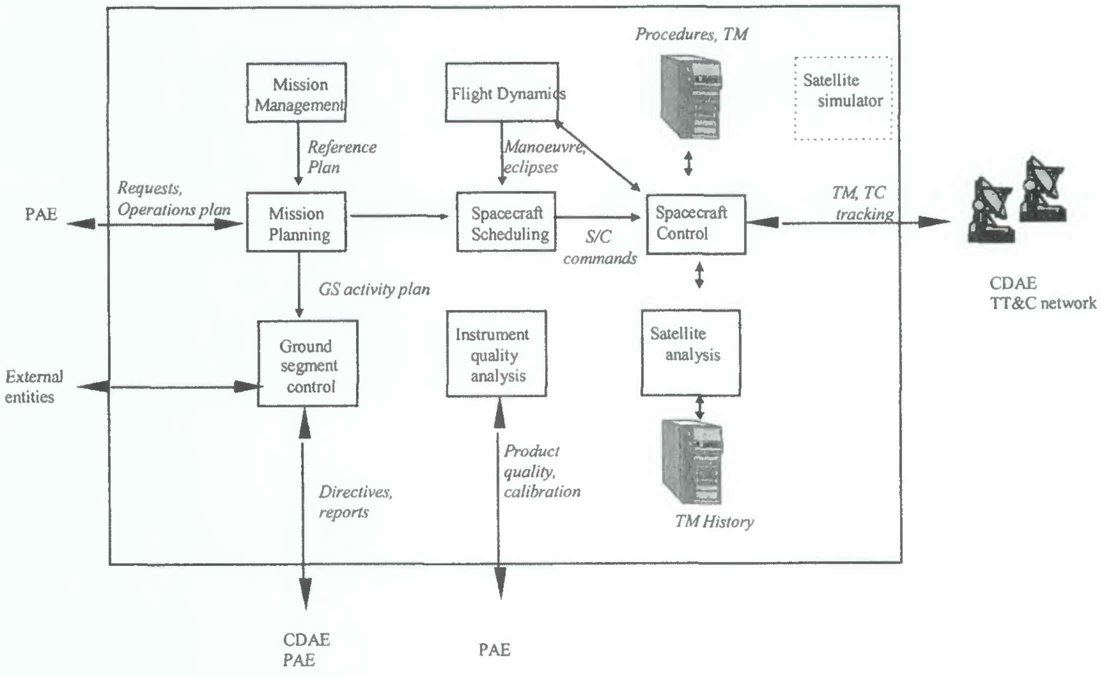

Figure 6.34. *MSCE overview.*

6.6.4 Processing and Archiving Element

The PAE is in charge of data processing to level 1b, data archiving, high-level mission planning and user services.

Processing to level 1b includes the steps described in Section 7.1. It starts with the ingestion of the level 0 data provided by the CDAE. The computing performance for the various level 1 processing steps has been estimated. The worst-case requirements range from 10 kFLOPS/sample for the background routine processing to 300 kFLOPS/sample for the advanced processing, which is only required on some images every six months. Near-real-time online and offline processing options have been traded-off considering expected advances in computing performance for the post-2000 horizon. Though there is no requirement for near-real-time processing, the analysis shows it will be less expensive than off line processing. Near-real-time in the context of the LSPIM means that all data downlinked in one pass are processed to level 1b within the next orbital period.

Online quality control will be embedded in the routine data processing with the aim of monitoring the quality of incoming data (data losses, glitches, saturation, anomalous pointing, etc). In addition, there will be off line quality control on sample products and products rejected by users. Reports will be issued to the MSCE for appropriate action.

Despite the high data rate of the instrument during image acquisition, the operational strategy of the LSPIM means that only a moderate volume of data is generated. It is estimated that 8 terabytes of data would have to be archived per year if all level 0 and level 1 data were included. This is the proposed approach, which can be implemented with commercial off-the-shelf equipment.

Concerning the relation with the users, the PAE will provide directory, guide and bulletin-board services, inventory and catalogue/browse services. It is estimated that the size of the browse products and the expected number of accesses to the catalogue browse service will be moderate. Interaction via Internet is therefore the baseline.

The PAE also interfaces with the users for planning the LSPIM observations. A long-term mission planning will be established in order to take also into account the interactions with the field segment. The PAE will receive the user requests and, after elaboration, it will forward the mission-planning changes to the MSCE.

The processing and archiving functions are proposed to be co-located with the CDAE to reduce costs and enhance timeliness. User services will be located at the PAE.

6.7 Technical Concept Summary

The technical concept proposed for the LSPIM space segment has been defined to meet the mission objectives, exploiting well-established technical solutions so as to enable a cost-effective and low-risk development. The analysis shows that the mission requirements can be met with a system requiring a very low number of specific developments optimised for this mission.

The following table summarises the key aspects of the system.

Ground segment

CDAE	Strong re-use of existing facilities
MSCE	Strong re-use of existing facilities
PAE	Developed to account for specific processing and archiving needs

Mission management

Planning timeline	– 14 days background – 3 days re-planning possible
Orbital timeline	– 2 BRDF sets per orbit on average – 3-4 passes used for downlink to Kiruna – 3 BRDF sets max. per orbit

Satellite

Mechanical configuration	– hexagonal shape – two modules, platform and payload – optimised inertia
Data handling and control	– decentralised management: SMU and ICU – MMU as storage and processing element – spectral band selection (full spectrum or 62 arbitrary bands) – lossless data compression
AOCS	– manoeuvring satellite in pitch and yaw – high pointing accuracy and stability – large equipment re-use
Power generation	– fixed and stiff solar panels – GaAs cells – Sun pointing when not in image acquisition

Payload

Optical architecture	– single telescope for VNIR, SWIR and TIR – single spectrometer – depointing mirror (for across-track access)
Mechanical architecture	– very high stability – use of known technologies
Detection	– equipment heritage in VNIR – development needed in SWIR – adaptation of design in TIR
Analogue chain	– known technologies and performance – 14 b ADC will further improve performance
Thermal control	– TIR: active Stirling-cycle coolers – SWIR: passive radiator and Peltier cooler
Calibration	– strong heritage in radiometric calibration – challenging but feasible spectral calibration

7 Data Processing

7.1 Data Pre-Processing

Two kinds of data products are delivered by the PRISM system, as illustrated in the Figure 7.1:

- Level 0 data products represent unprocessed compressed payload data in chronological order at full space/time resolution with all supplementary information for subsequent processing (e.g. orbit data, payload health information, time conversion, etc.).
- Level 1 data products represent pre-processed geo-located data in chronological order at full space/time resolution with all corrections (radiometric, geometric, etc.) applied.

The first part of the pre-processing activity is applied performing radiometric calibration. This is followed by spectral calibration, to arrive at the Level 1a images. These images are then processed to perform geometrical calibration and to obtain Level 1b images. The geometrical calibration accounts for the specificity of LSPIM with respect to:

– Its multiple spectral regions: a specific ground processing work has been proposed to improve the co-registration between the spectral regions, based on the elaboration and peridic update of a static and dynamic model of the LOS geometry. This allows access to accurate knowledge of the relative position of each pixel and leads to a series of information products:
  - geometrical information can be delivered, for instance to be directly assimilated into production of Level 1a data and in thematic processing leading to Level 2 products
  - spatially co-registered, re-sampled images can be delivered as data products corrected for static misalignments and attitude as well as for dynamic misalignments caused by vibrations;

– The various configurations of the image acquisition geometry, notably in BRDF mode. It is possible to obtain spatially co-registered, geo-located and re-sampled images to which static corrections and possibly also dynamic corrections have been applied.

Several processes are involved in the geometric calibration:

- Correlation: automated measurement of relative shifts between two images by pattern recognition.

- Geometric modelling: identification of a dynamic image acquisition model so as to correct geometrical image distortions and determine an optimised geometric model taking into account the correction of these distortions.
- Re-sampling: projection of the image in a new reference frame, usually a ground reference system.
- Ground-control-points extraction: determination of the location of reference points (tie points) between an image and a ground map.
- Attitude and orbit restitution: processing of ancillary image data in order to accurately determine the location of the satellite and the orientation of the LOS.

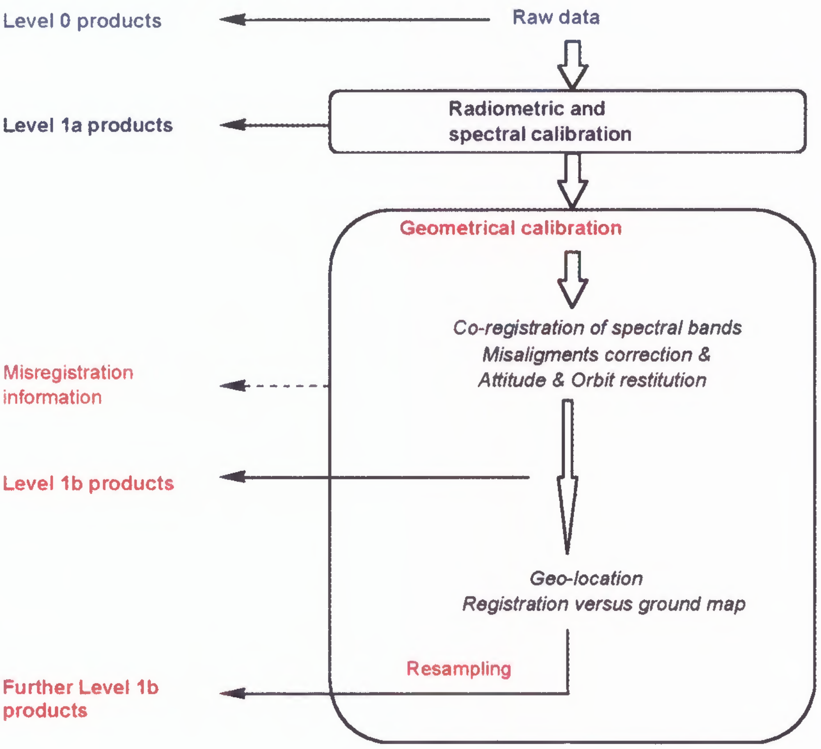

***Figure** 7.1. Outline of LSPIM data products.*

7.2 The Concept of Higher Level Data Processing and Assimilation

This section describes how Level 1b data, which are geometrically and radiometrically calibrated top of the atmosphere radiances (TOA), are converted to the land-surface variables, and how these are then ingested and assimilated into land-surface process models. As the analyses in Chapters 3 and 4 have already revealed, the spectral, directional and thermal-radiance measurements of the proposed LSPIM allow the estimation of the key land-surface variables.

A general outline of the data processing and assimilation chain, which leads to the final land-surface process description, is given in Figure 7.2.

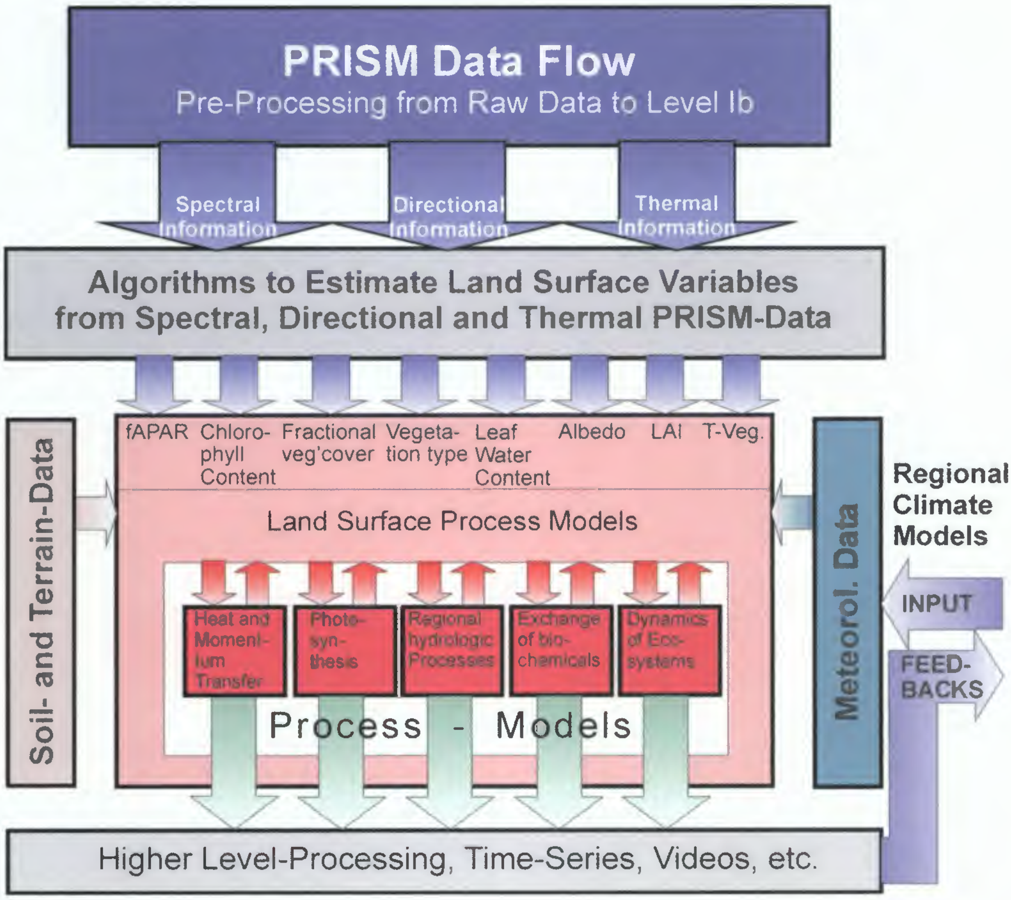

***Figure** 7.2. Schematic of the data-processing concept for the PRISM data.*

From calibrated and geometrically corrected top-of-atmosphere radiances, land-surface variables are estimated by applying the algorithms, described in Chapter 4. In Figure 7.2 important land-surface variables as (identified in Table 3.1) are shown as being retrieved from Level 1b PRISM data, namely:

- fAPAR
- chlorophyll content
- vegetation type
- fractional land cover
- leaf water content

- albedo
- leaf area index
- leaf surface temperature
- atmospheric water content.

It is intended to provide the scientific user community with higher level products (Level 2 variables) on a systematic and regular basis.

7.2.1 Representative Retrieval Algorithms

The enhancement of retrieval algorithms (as described in Chapter 4) is presently the subject of intense research activities. Since it is not possible to describe the retrieval techniques for all variables that will be provided by LSPIM in this report, this section will mainly focus on the state of the art of some retrieval algorithms that could benefit from the improved spectral and directional sampling capability provided by the PRISM instrument. They exemplify the principles used for the retrieval of the land-surface variables. The section explores how each algorithm works, explores their capacity to be used routinely over large sets of images, and presents a few results that demonstrate their capability to estimate the geo/biophysical and geochemical key variables listed in Chapters 3 and 4.

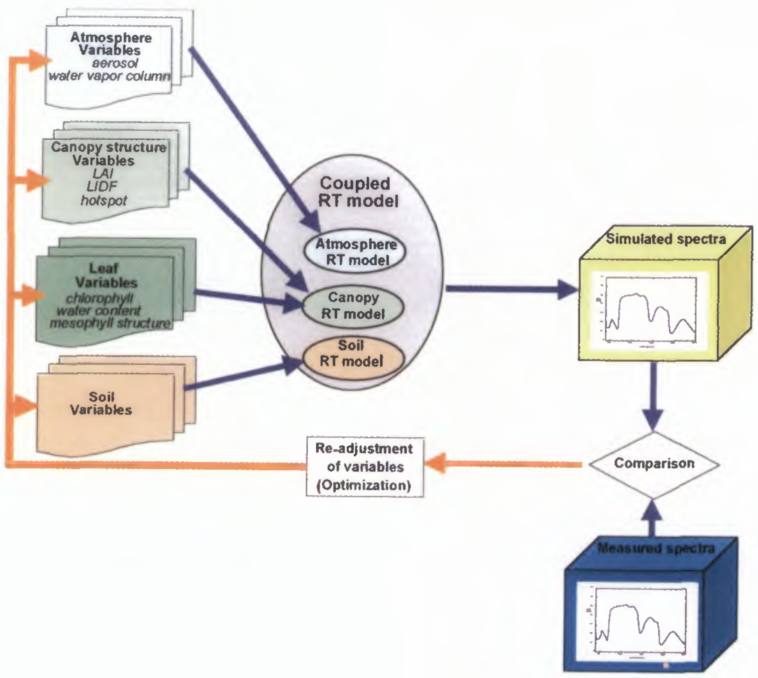

__Figure__ 7.3. Schematic of the spectral matching procedure applied to retrieve simultaneously atmosphere, canopy, leaf and soil variables.

The examples presented relate to the estimation of albedo, surface temperature, and plant water content. A general scheme for such a retrieval approach is displayed for the separation of atmosphere and leaf water in Figure 7.3.

Albedo

The albedo at the top of the canopy may formally be computed as:

$$a = \frac{1}{\pi} \frac{\int\limits_{\lambda=300nm}^{\lambda=3000nm} E_O(\lambda) \int\limits_{\theta=0}^{\theta=\pi/2} \int\limits_{\varphi=0}^{\varphi=2\pi} \rho(\theta,\varphi,\lambda)\cos\theta \; s\sin\theta \; d\theta \; d\varphi}{\int\limits_{\lambda=300nm}^{\lambda=3000nm} E_O(\lambda)} \tag{7.1}$$

where $E_o(\lambda)$ is the top of canopy irradiance for wavelength λ and $\rho(\theta,\varphi,\lambda)$ is the Bidirectional Reflectance Factor (BRF) for directions (θ,φ). Since the sensor only samples a limited number of directions and spectral bands, the full BRF has to be reconstructed from the view directions recorded and the reflectance spectra from the set of bands provided by the instrument.

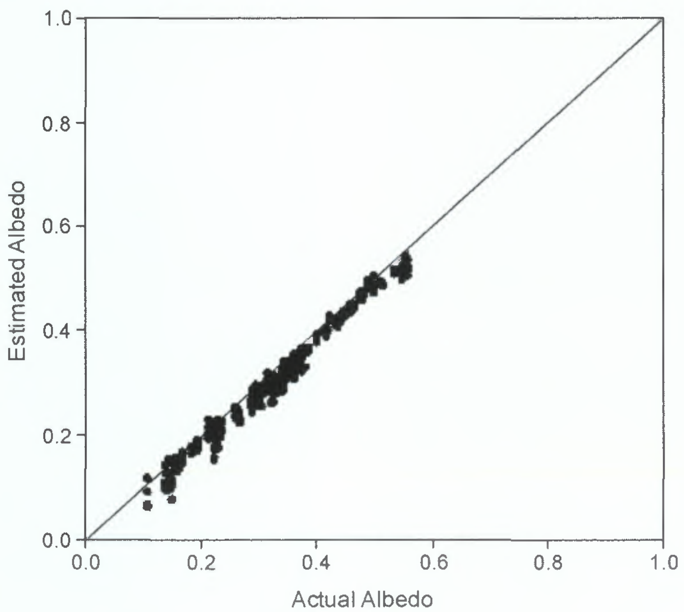

Figure 7.4. *Comparison of the actual albedo with the one estimated from PRISM data spectral and directional sampling scheme using the algorithm developed by Weiss et al., 1999a.*

The reconstruction of the full hemisphere from a limited set of directional measurements can be done using BRDF models as proposed by Rahman (1998), Lucht et al. (1998), Privette et al. (1997), Wanner and Strahler (1997) and Weiss (1998). The relative accuracy achieved using these techniques is estimated to be about 5% (Fig. 7.4). These techniques require preliminary atmospheric corrections. However, several techniques that do not require atmospheric correction have been developed, particularly for such sensors as MISR (Martonchik et al., 1998) or POLDER (Leroy et al., 1997). Menenti and Verhoef (1998) showed that the direct use of TOA radiance within a coupled atmospheric/ canopy model allows accurate estimation for the top of canopy albedo.

Canopy and Soil Temperature

Algorithms used to retrieve the canopy and soil temperature from the top of the atmosphere thermal-infrared radiances have to take into account the effects of atmosphere and of surface emissivity.

Separation of the vegetation and ground temperature is required for heat- and mass-exchange models based on SVAT models. The retrievals of the surface temperature from the top of the atmosphere thermal-infrared radiances using single TIR bands are based on two principles:

- They assume that the emissivity is known accurately. This is applied to single-channel atmospheric corrections. Potential uncertainties due to the unkown emissivity remain.
- They try to mitigate the impact of emissivity uncertainty on T_s extraction. Algorithms of this type are most often Split-Window (SW) algorithms used in the 10.5-12.5 µm window, or derive from the SW approach (linear combination of top of atmosphere thermal-infrared radiances).

Caselles et al. (1998) developed an algorithm derived from the split-window technique within a LSPIM Phase-A study. This algorithm is based on the use of two channels [8.0-8.5µm] and [8.6-9.1µm]. The canopy emissivity is written as:

$$\varepsilon = \varepsilon_v \cdot fCover + \varepsilon_g \cdot (1 - fCover) + d\,\varepsilon \tag{7.2}$$

where ε_v is the emissivity of vegetation, ε_g the emissivity of soil, *fCover* the vegetation cover fraction and $d\varepsilon$ a correcting term accounting for cavity effects. The cover fraction is derived from estimates using the visible and near-infrared information. It was shown that this algorithm provides estimates of canopy brightness temperature with an accuracy of ±1.1 K.

The separation between vegetation temperature and soil temperature is more complex and requires directional observation in order to exploit the information on the canopy structure. Sobrino and Caselles (1990) developed a geometric description of the canopy structure. Using estimates of the cover geometry, the soil and vegetation emissivity, and the downward atmospheric radiation, the inversion of the geometric model for two view directions allows the separation of vegetation and soil temperature. More recently, Djepa et al. (1998) developed a similar approach using a turbid medium radiative transfer model. The algorithm needs knowledge of the leaf area index (LAI) and the leaf angle distribution function (LIDF) and the emissivity of the soil and vegetation. The inversion of this canopy radiative-transfer model using directional measurements provides estimates of the vegetation and soil temperature. It should be emphasised that directional measurements are essential, as well as concurrent estimates of canopy variables such as the cover fraction, the leaf area index and the leaf angle distribution, which can be estimated from the visible and near-infrared spectra.

An actual case study (Djepa et al., 1998) of the separation of soil and foliage temperatures within a heterogeneous target was carried out using dual-angle observations of thermal infrared spectral radiances. These observations were obtained with the ATSR-1 imaging radiometer aboard the ERS-1 satellite. Two data sets, acquired on 9 July and 19 August 1991 were used for this study. The study was conducted in the frame of the Hei He International Field Experiment (HEIFE) (Wang et al.,1994) and focused on the large, flat oasis of Zhang-Ye. It is ideally suited because the temperature of dense vegetation within the oasis and the surrounding desert are well known. Even though the low spatial resolution of the ATSR observations is not well suited to studying such land targets, the case study illustrates an approach applicable to LSPIM observations. The retrieval is based on a radiance interaction model of the target, the principle of which is decribed in Chapter 4.

Radiometric observations can be used to derive either directional spectral radiance, or directional radiometric temperature. The first approach avoids the difficult estimation of effective emissivity for a heterogeneous target, but requires accurate characterisation of the atmosphere. The advantage of the second approach is that split-window algorithms may be applied, although an estimate is necessary for the effective emissivity. In Table 7.1 the effective radiometric temperatures, as determined at the oasis and the surrounding desert, are given and compared to the measurements at two local weather stations. It is clear that the approach give satisfactory estimates for the effective radiometric temperatures for both test sites.

Observations	Oasis	Desert	AWS013	AWS015
ATSR-1	307.2	318.2	323.2	322.2
Ground	306.6	318	318.4	320.2

Table 7.1. *Effective radiometric temperatures of Zhang-ye Oasis - Gansu P.R. China and the surrounding desert; AWS = Automatic Weather Stations located in the desert.*

The estimated radiometric temperatures of foliage can also be compared with field observations (Table 7.2). No field observations of the radiometric temperature of the soil underneath the vegetation canopy were available.

Observations	T_f	T_s
ATSR-1 Directional Spectral Radiances	306.9	311.4
ATSR-1 Split window	306.7	310.9
Observed oasis	306.2	

Table 7.2. *Radiometric temperatures of foliage and bare soil in Zhang-ye Oasis, Gansu P.R. China determined with ATSR-1 using two different approaches for data analysis and ground measurements (T_f = foliage temperature, T_s = soil temperature).*

The estimation of the foliage and soil temperatures of heterogeneous targets has the potential for solving a fundamental problem in modelling the heat transfer at heterogeneous land surfaces by improving the parametrisation of heat-transfer resistances (Anderson et al., 1997).

Primary production: Canopy structure and composition characteristics

As was seen in Chapter 4, canopy attributes have frequently been retrieved from remotely sensed data through the inversion of radiative-transfer models. As an example, this section will show how the leaf water content could be retrieved from hyperspectral data in the SWIR domain. Leaf water content could be indirectly used to assess the leaf biomass assuming some knowledge of the relative water content which generally changes slightly with time for living tissues. Leaf water content, can also be used as a way to adjust some key parameters of canopy functioning models within an assimilation approach.

Water content can be estimated using knowledge of the specific absorption features of the water molecule. When this spectral signature is sufficiently sampled by a hyperspectral imaging sensor, coupled models of radiative transfer in the soil, the leaves, the canopy and the atmosphere can be inverted to provide estimates of atmosphere, canopy and leaf attributes, including leaf water content, leaf area index, and atmosphere water vapour column.

This approach was applied on AVIRIS data sets, gathered during the MAC'91 campaign, for the Barrax study area in Spain. An iterative optimisation method was applied to the coupled models in order to estimate leaf and atmosphere water contents, simultaneously with other canopy and soil variables. This is possible due to the large amount of spectral information provided by the airborne AVIRIS hyperspectral sensor in the SWIR domain where liquid water has absorption features. The optimisation technique consists thus in adjusting leaf, soil, canopy and atmosphere variables in such a way that the simulated reflectance spectra best match the measured spectra (see Fig. 7.3).

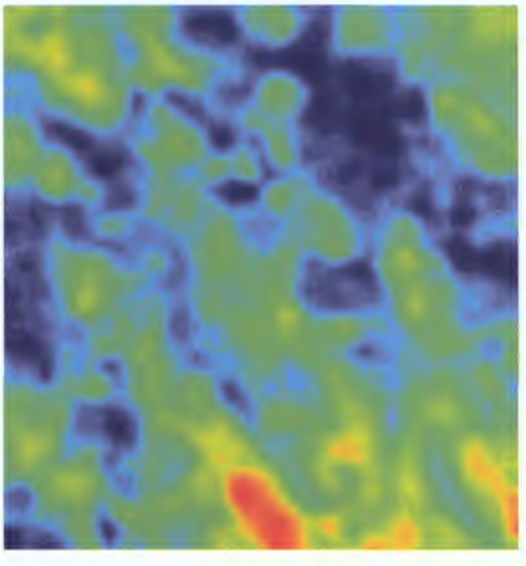

Atmospheric water vapour

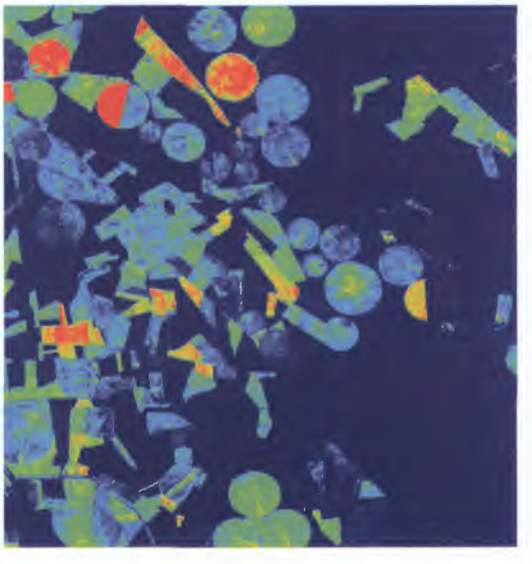

Canopy water content

Figure 7.5. *Atmospheric water vapour and canopy water content estimated by inversion of radiative-transfer models using AVIRIS MAC'91 data over the Barrax site in Spain.*

Results show that the estimated atmospheric water vapour has a completely different spatial structure compared to the canopy water content that matches closely the field boundaries as expected (Fig. 7.5). The accuracy of the retrieval was validated on a complementary experiment conducted in 1998 over the same site, but using data acquired by the DAIS instrument. Canopy water content could be estimated with an accuracy of ±100g.m^{-2}. This value is equivalent to a relative retrieval error of 30%. Although the principle of simultaneous estimation of leaf and atmospheric water content is validated, improvements are still expected from enhanced sensor performances in terms of radiometric accuracy and spectral and directional sampling, more accurate radiative-transfer models, better constraints on the inversion process and advanced inversion techniques.

7.2.2 Alternative Methods of Retrieval

The methods described so far in this section work well for small amounts of data. However, as they are based on computationally expensive non-linear optimisations, they are not well suited to handling, on a pixel-by-pixel basis, the enormous volumes of data that will be generated by a hyperspectral imager. Alternative techniques, using look-up tables or neural networks, are envisaged as part of the standard processing chain for this mission. These are quick and efficient when properly calibrated and implemented.

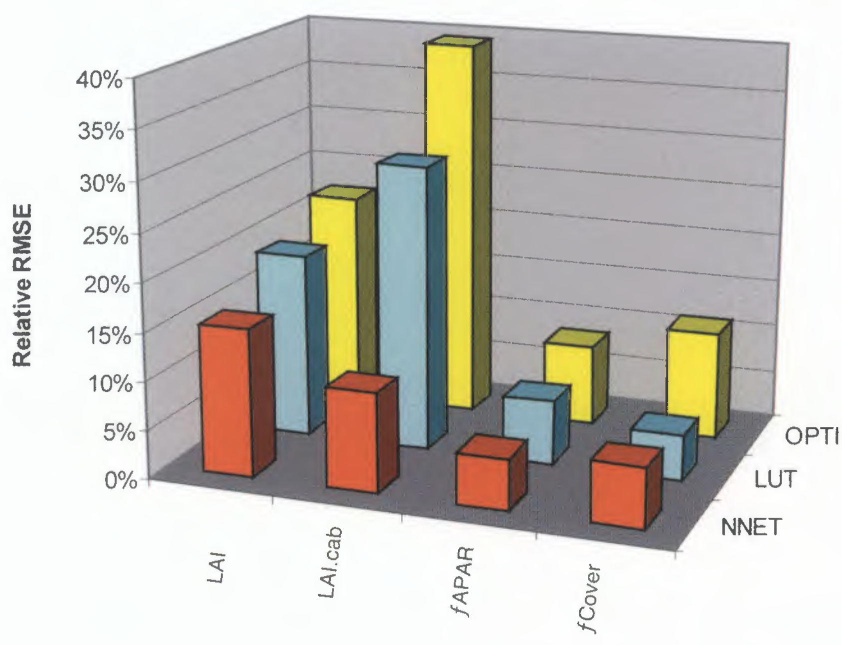

***Figure 7.6**. Comparison of retrieval algorithm performances (optimisation (OPTI), look-up tables (LUT), and neural network (NNET)) for the retrieval of four biophysical variables: leaf area index (LAI), canopy chlorophyll content (LAI.Cab), fraction of photosynthetically active radiation absorbed by the canopy (fAPAR), and fractional cover (fCover). The performances are expressed in relative root-mean-square error (RMSE) terms (Baret et al., 1999).*

A comparison between these techniques in terms of retrieval performances was investigated through a study conducted for the preparation of the LSPIM mission (Baret et al., 1999). The result is shown in Figure 7.6. It displays clearly that neural networks perform better than optimisation techniques in the situations investigated.

Neural networks are increasingly used in the interpretation of remote-sensing data (Smith, 1993; Baret et al., 1995; Buelgasim et al., 1998). They are recognised as a universal approximator of surface responses (Hornik, 1989 and 1991; Leshno et al., 1993), i.e. they allow inferences to be made linking any input variable to any output variable, assuming that those variables are related through a given process. In remote-sensing applications, neural networks are trained to invert radiative-transfer models, i.e. to relate the output variables (the reflectance or radiance field) to the input variables (the biophysical variables of interest). Back-propagation neural networks are generally used in this case. They are defined by their architecture, i.e. the number of layers, the number of neurones per layer and the type of neurones, as is illustrated in Figure 7.7.

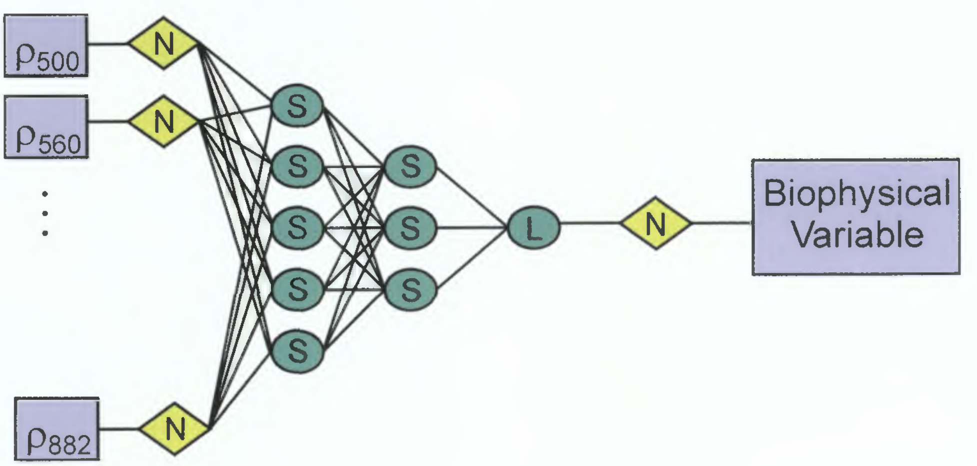

***Figure** 7.7. Schematic of the neural network architecture. N stands for the normalisation process. S and L stand, respectively, for tangent-sigmoid and linear transfer function of the neurones.*

The neural network has to be calibrated (trained) using carefully chosen training data sets. This data set must sample the space of actual canopy characteristics, by generating the appropriate distribution and co-distribution of the biophysical variables. A radiative-transfer model is then used to compute the corresponding reflectance field. In this way, the training can be focussed on particular biomes by choosing the appropriate distribution and co-distribution of the variables, as well as the type of radiative-transfer model in order to better represent the biome of interest and improve the retrieval performances. In the same way, neural networks allow one to account for the particular radiometric performances of the sensor (i.e. its radiometric resolution and absolute accuracy), to provide more robust estimates of the biophysical variables (Fig. 7.8). Additionally, neural networks gain from being trained over coupled atmosphere-canopy radiative-transfer models, to provide a more direct link between canopy characteristics and top-of-atmosphere radiance (Fourty and Baret, 1997).

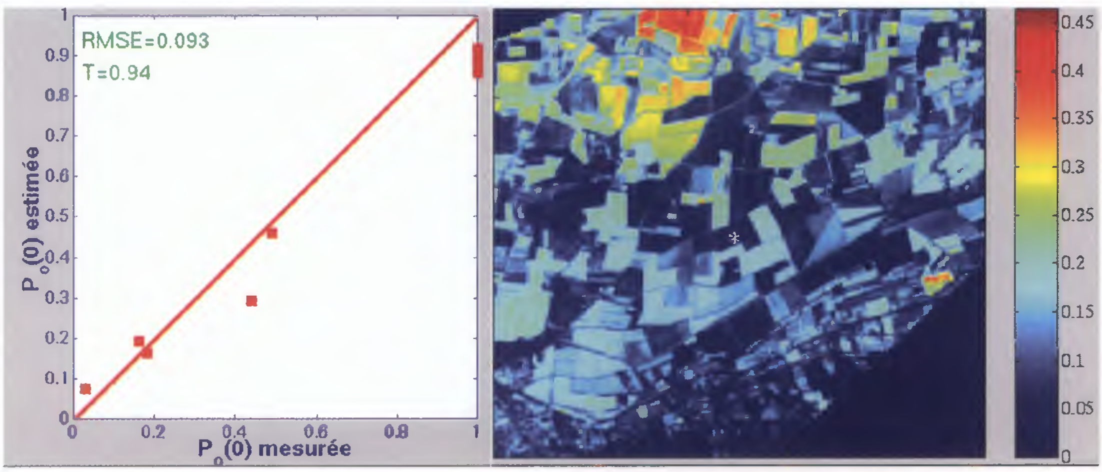

Figure 7.8. *Comparison of cover fraction estimated using a neural network from the airborne POLDER data ($P_o(0)$ estimée) and that actually measured in the field of the ReSeDA experiment ($P_o(0)$ mesurée). The figure on the right is an airborne POLDER image in the near-infrared band from which the cover fraction was estimated. It shows the strong bi-directionality of the canopies, with the hot-spot feature clearly observed at the top of the image (Weiss, 1998).*

7.3 Representative Process Models

As indicated in Figure 7.2, Level 2 data are currently being used in a Geographical Information System (GIS) structure which drives the land-surface processes models. This GIS structure is responsible for spatial data management, the assimilation of the retrieved fields of variables and information flow. Within the GIS structure, the remote-sensing derived variables, are fused with other spatial data such as physical properties of the land surface, topography and meteorological inputs (incident shortwave radiation, air temperature, humidity, wind speed, rainfall). Meteorological inputs can either originate from interpolations of point observations, from the established meteorological networks, or estimated from mesoscale atmosphere models.

In the following section selected model results of typical process investigations are presented, which demonstrate the data assimilation and information flow involved in the analysis of Level 2 data. The examples are given for key land-surface processes related to heat and mass transfer as well as primary production and photosynthesis.

7.3.1 Heat and Mass Transfer – Evapotranspiration

The assimilation of variables derived from hyperspectral measurements into land-surface process models is demonstrated using DAIS hyperspectral and thermal data acquired within the frame of the Large Scale Facility (LSF) of the European Union. DAIS was flown over the test-site of Weilheim/Bavaria on 31 May 1996 (Ludwig et al., 1998). In this experiment it was shown how model variables derived from combined hyperspectral and thermal measurements can improve the quality of land-surface process modelling in comparison with conventional inputs taken from a GIS based on ground survey. Evapotranspiration serves as a representative land-surface process because it is complex and it connects the energy balance of the land surface with the physiology of the different vegetation covers. The physically based soil-vegetation-atmosphere-transfer (SVAT) scheme PROMET (**PR**ocess-**O**riented **M**ultiscale **E**vapo**T**ranspiration model, (Mauser, 1991; Mauser and Schädlich, 1998)) is chosen as a typical representative of spatially distributed land-surface process models.

PROMET is based on the Penman-Monteith equation (Monteith, 1965), which determines the actual evapotranspiration as a function of water availability, radiation balance and the physiological regulation mechanisms of heterogeneous plant stands. The model architecture closely follows Figure 7.2 and consists of the following coupled modules:

- a radiation module, which determines the radiation balance for each proxel (see Fig. 2.6) depending on time, topographic position, illumination angle and cloud cover
- a one-dimensional soil water module to determine the soil moisture balance, as a function of infiltration, exfiltration and capillary rise
- a plant module, which determines the water transport in the plant, governed by its morphological (LAI, height, biomass) and physiological properties (stomatal resistances as function of environmental conditions and water availability) for different canopy layers
- an aerodynamic module, which describes the transport of water vapour away from the land surface.

The model requires topographical information, a digital soil map and meteorological inputs. Plants are described through a set of variables, which are either static and species dependent (e.g. stomatal resistence) or dynamic and general. The species-dependent variables determining the potential transpiration rates are taken from literature. The dynamic variables describing the development of the plants are leaf area index (LAI), plant height, albedo, and root depth. The classical approach to spatial modelling of land-surface processes takes values for these variables from standard growth curves, which can be found in literature. These values are then distributed in space using a conventional GIS-system, which consists of the field boundaries of each land-use class and the land-use type. For the test-site in the Bavarian Alpine Foreland, this classical approach results in the data set shown in Figure 7.9 and Table 7.3.

	Landuse	LAI	Plant Height [cm]	Albedo [%]
	Barley	3.05	51	14.3
	Wheat	4.00	78	14.0
	Corn	0.4	33	18.5
	Grassland	0.9	14	23.2
	Other	-	-	-
	Settlement	-	200	40

Tab. 7.3: Conventional plant-morphological variables taken from literature

Fig. 7.9: Digital land use map compiled through ground survey

Table 7.3 and Figure 7.9. *Land-use map of the Weilheim test area derived from ground survey and values of plant-morphological variables taken from standard growth tables.*

It can be seen that land use and the spatial variables are treated as spatially homogeneous within each field since there is no information available on spatial heterogeneity. Nevertheless, there is a certain spatial differentiation within the scene, which reflects actual land use.

Alternatively, as described in Chapter 4, hyperspectral and directional measurements of the reflected shortwave solar radiation allow the leaf area index, albedo and plant height to be estimated if the cover type is known. Applying retrieval algorithms to Level 1b hyperspectral radiance data converts the calibrated radiation measurements into spatially distributed input variables for PROMET. The spatial distribution of the variables derived from DAIS data is compared with the conventional GIS-based results in Figure 7.10.

Figure 7.10 illustrates that in comparison with the GIS-based results, the data derived from remote-sensing measurements show a considerable variation of the plant-morphological variables within each field and across the entire test site. This is due to different growth conditions originating from the soil and random variations in fertiliser application by the farmers. Both sets of variables are used as input to PROMET to determine the distribution of the Evapo Transpiration (ET) at the time of the DAIS-overflight. Figure 7.11 shows a comparison of the resulting modelled ET patterns of the two resulting PROMET runs. For the left side of Figure 7.11 PROMET was run using the conventional GIS-based spatial distributions of plant-morphological variables (see Fig. 7.10 (top)); on the right side of Figure 7.11 the actual distributions derived from Figure 7.10 (bottom) were used.

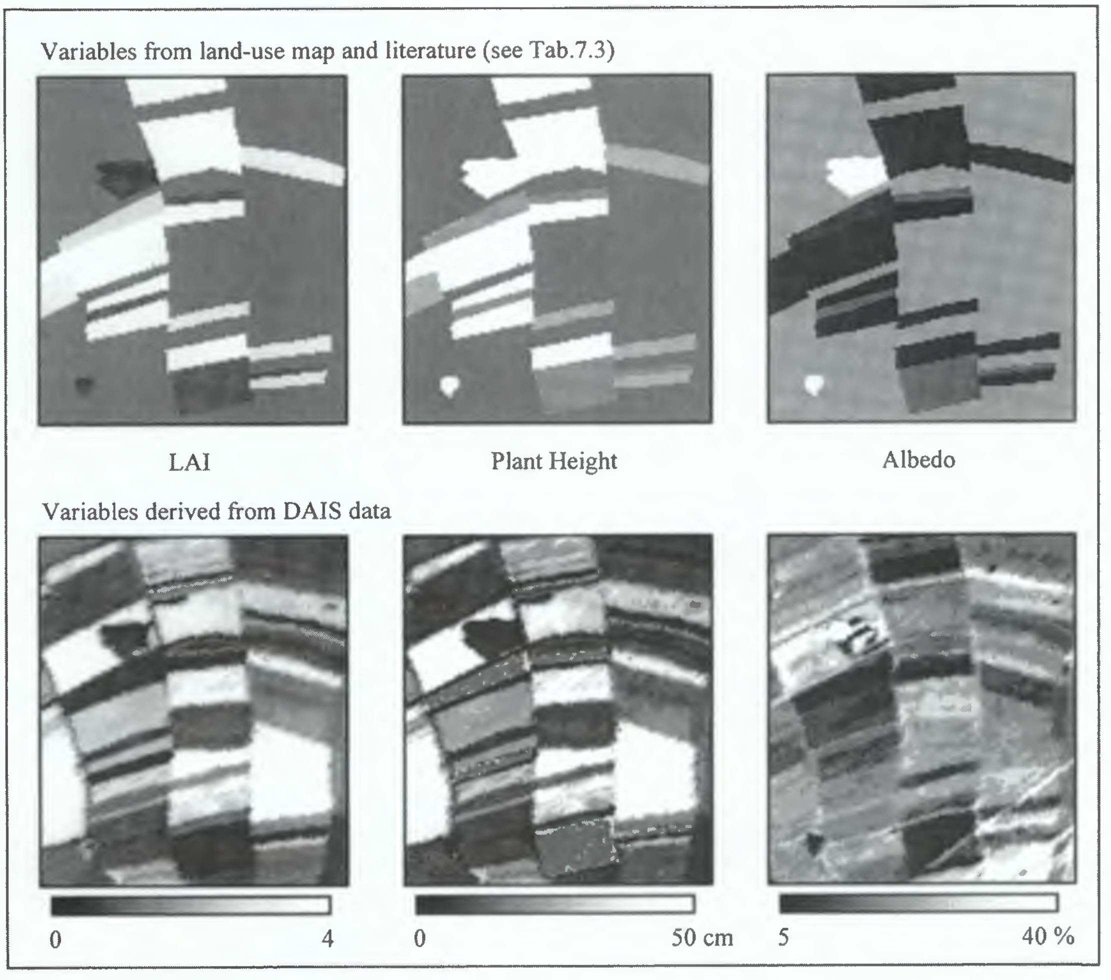

Figure 7.10. *Comparison of GIS-layers from literature data (top) and spatially distributed fields of variables derived from hyperspectral DAIS data for May 31, 1996, 11 a.m (bottom) as input to the SVAT-model PROMET.*

There are clear differences between the results from the two approaches, evidenced both in the spatial patterns and in the absolute values of estimated ET. The differences in the absolute ET values reflect the impact of early drought conditions in 1996, which caused a deviation in the actual growth of vegetation from the standard literature values used in Figure 7.11 left. The GIS results do not describe correctly the difference in air temperature between the ground (retrieved from the DAIS measurements) and the air (from a nearby meteorological station). Surface temperature is determined by the relative magnitude of net radiation, sensible, latent and soil heat flux. Net radiation is mainly determined by albedo, sensible and latent fluxes by surface roughness (closely related to canopy height) and soil heat flux by fractional vegetation cover. Spatial heterogeneity in these variables implies spatial heterogeneity of surface temperature.

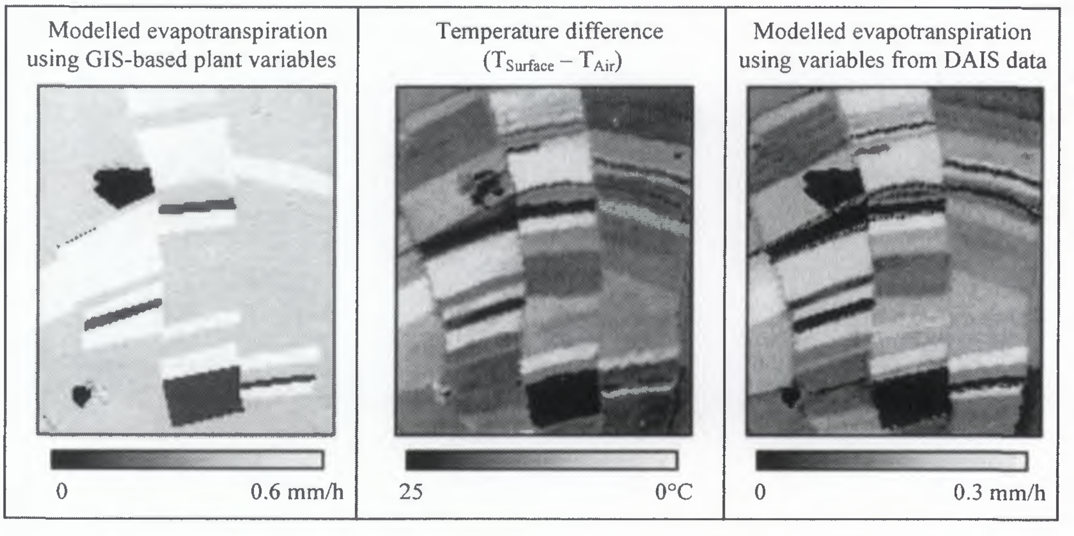

Figure 7.11. *Comparison of evapotranspiration patterns modelled with PROMET using conventional GIS- (left) and hyperspectral remote-sensing (right) based distributions of plant-morphological variables with the measured difference of surface and air temperature (centre).*

The spatial distribution of ET values obtained with the GIS procedure (Fig. 7.12 top) is fully uncorrelated with the spatial distribution of the difference between surface (pixelwise) and air (weather station) temperature. The ET values obtained with the DAIS data are clearly correlated with this difference.The GIS-based result is due to a lack of information on the spatial variability of the input variables within the fields, which leads to almost constant ET values within each land-use. This in turn cannot explain the differences in surface temperatures within the fields. This clearly demonstrates that the consideration of the spatial heterogeneity of the input variables, which can be derived using advanced remote-sensing data, is a crucial step in the improvement of spatial land-surface process models.

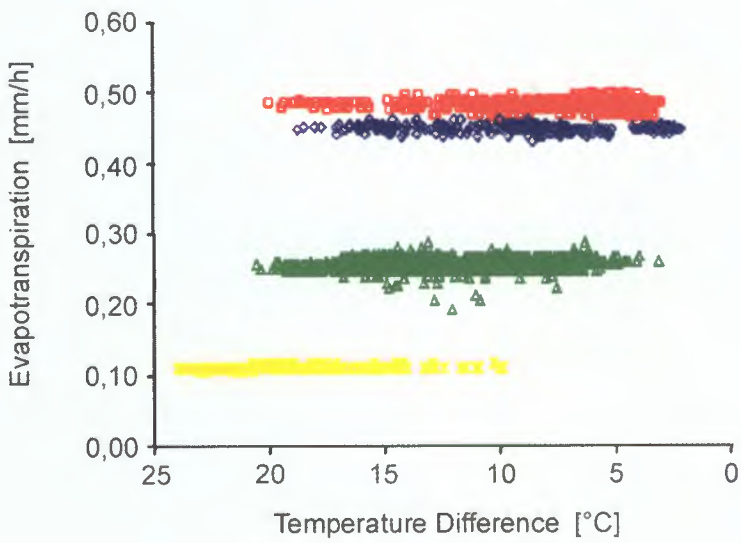

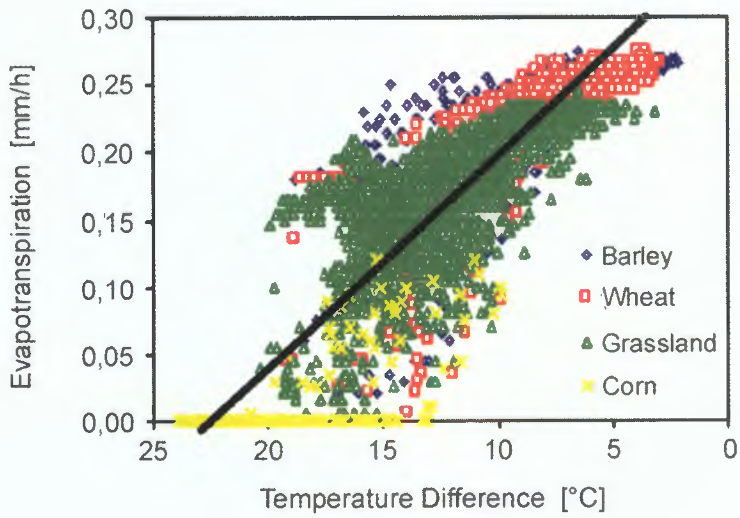

Figure 7.12. Surface-air temperature difference versus modelled evapotranspiration using conventional GIS-based input data (top) and remote-sensing-based input data using the imaging spectrometer DAIS (bottom).

7.3.2 Primary Production and Photosynthesis – Modelling of Plant Growth

Plant growth and evapotranspiration are closely coupled processes which are determined to a large degree by using the same environmental variables. As an example of a spatially distributed plant growth model, the **Pro**cess-oriented **M**odular **E**nvironmen**t**al - **V**egetation model (PROMET-V, Schneider, 1999) was chosen. It directly couples all major plant growth processes (photosynthesis, respiration, allocation, senescence), hydrological processes (transpiration, evaporation, interception, soil water balance) and nitrogen transformations and fluxes. For this purpose, in addition to the modules necessary for ET-modelling, the following modules are integrated into an overall data structure similar to that of Figure 7.2:

- a plant growth module
- a nitrogen flux module
- a soil temperature module
- an agricultural management module.

PROMET-V uses remote-sensing data for three different purposes:

- as input to define initial values of model variables
- to adapt and update model variables
- to validate model results.

Initial conditions are defined by the variables plant type, fractional vegetation cover/plant density and leaf area index. Additionally, data on fAPAR, chlorophyll content and leaf water content may be used to define functional variables related to photosynthesis to determine the state and health of the vegetation.

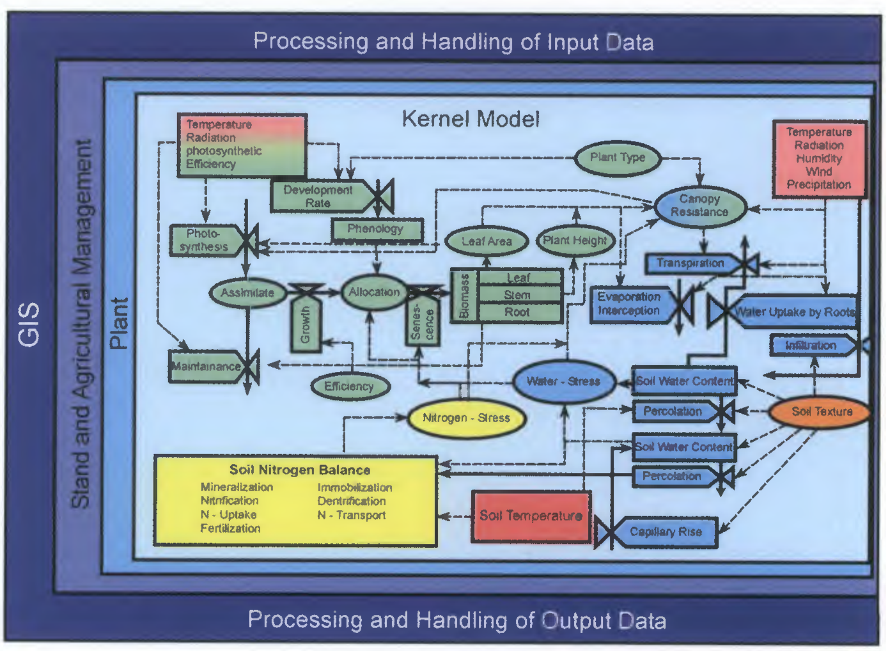

Figure 7.13. *Representation of plant growth, water and nitrogen fluxes with PROMET–V.*

Plant growth is calculated for different land-use types (cereals, corn, meadows, forest). Feedback mechanisms exist between water, CO_2 and nitrogen fluxes. Figure 7.13 gives an overview of the processes considered within PROMET-V as well as their interactions and feedback.

PROMET-V was tested at the Ammer watershed catchment in the Bavarian Alpine Foreland. It is a very heterogeneous region with regard to climate, soil, elevation and vegetation. It covers 709 km^2 with elevation differences exceeding 1100 m.

Validation of the model with independent ground-truth measurements indicates that a major source of uncertainty regarding the biomass production is related to agricultural management variables which may vary significantly in the spatial and temporal domains. For cereals and corn, the plant density and the date of sowing have a strong impact upon the model results. For meadows, the date of cutting is a crucial variable, and for forests the stand density reveals large spatial variations. The validation of the model on the field scale proves that it accurately models plant growth, water and nitrogen fluxes and biomass if related management variables are known. However, additional influences such as unpredictable cutting dates for meadows, which are chosen by the farmers, unknown plant densities for cereals and corn, pests, diseases, wind damage, drought and other unpredictable events result in spatial heterogeneties that cannot be modelled appropriately and require spatial observations.

A simple example, using Landsat TM data, shows how remotely sensed data can be assimilated into the PROMET-V model to reduce the uncertainties caused by these unknown management decisions. Values of LAI calculated in PROMET-V are used to predict surface radiances, which are then compared to atmospherically corrected values from the satellite data. This is illustrated in Figure 7.14. If the discrepancy between observations and model is sufficiently large, the model variables are tuned in the following way:

- For meadows, the last cutting date is iteratively chosen so that the temporal development of the LAI in the model produces radiance values which match the measured radiances at the sensor overpass. For meadows, the cutting date is the crucial unknown.
- For corn and cereals, the first remote-sensing observation in the growing season is used to adjust the plant density in the same manner as for meadows, while all additional observations are used to adapt the LAI.
- For forests, the LAI is estimated and adjusted from the measured radiances.

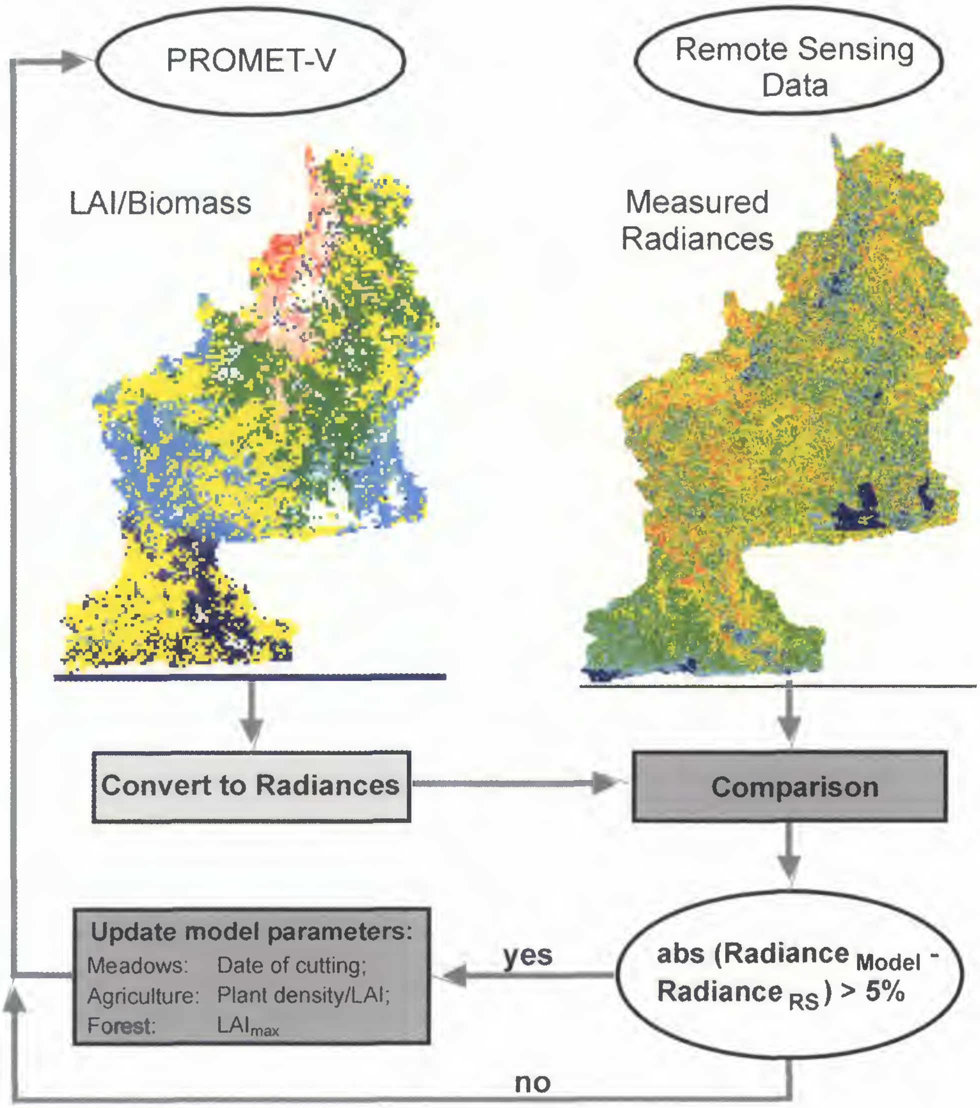

***Figure 7.14**. The use of remote sensing for variable updating in PROMET-V.*

The modelled and measured biomass of a meadow using standard cutting dates (broken lines) and remote sensing data, which is used in the way described above to adjust LAI within PROMET-V (full line), is compared in Figure 7.15. The squares show the ground measurements of the biomass. Without the assimilation of remote-sensing data, a RMS-error for the modelled vs. the measured biomass of 114 g/m^2 was calculated. Through the use of remote-sensing data, the RMS decreased to 38 g/m^2.

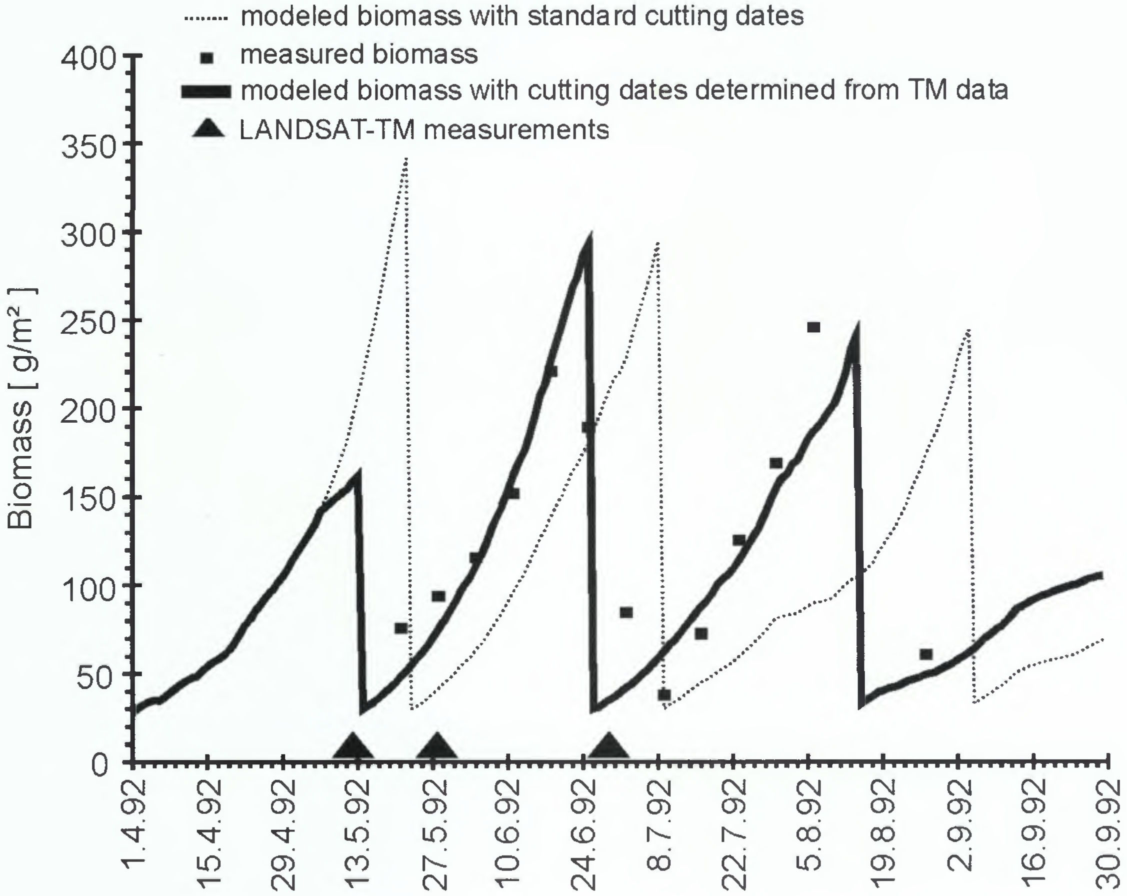

Figure 7.15*. Comparison of the modelled and measured biomass for meadows.*

As the model results indicate, the combination of both process-based models and remote-sensing observations significantly improves the representation and accuracy of the spatial heterogeneity of biomass production. However, due to the currently limited availability and quality of appropriate remote-sensing data, the full potential of this data source to adapt and update model variables has not been exploited yet.

7.4 Spatial Scale and Non-Linearity: Observational Aspects

7.4.1 Definition and Estimation of Length-Scales in Heterogeneous Landscapes

The theoretical argument about the importance of scale for land-surface processes developed in Chapter 2.4 can be illustrated by an example based on data sets acquired at the Barrax site (E1.1 in Table 5.1). The landscape at this site is characterised by a well defined length-scale: the size of central pivot irrigation systems (see Fig. 7.5).

Irrigation leads to large differences between the irrigated plots and the dry surface between them.

The example presented here relates to heat and mass fluxes. Models and observations should provide the same estimates of the amount of energy exchanged between the land surface and the atmosphere, irrespective of the spatial resolution of the models and observations (Fig. 2.8). Heat transfer is a non-linear process. This constraint implies that the domain A (see Chapter 2.4) must be homogeneous. Thus, the heterogeneity of its spatial distribution must be considered. Information is required on:

- the dominant length-scales of the landscapes, and
- the errors due to the area-averaged observation.

Over distances smaller than the dominant length-scale, the heterogeneity term V (see Chapter 2.4) is negligible. To estimate the length scale the extent of variability as a function of spatial sampling must be estimated. A systematic analysis of the amount of variability observed at different spatial sampling intervals provides an estimate of the dominant length-scales in heterogeneous landscapes. The dominant length-scale is here defined as that spatial sampling interval where variability of the signal is largest. The concept and tools of multi-resolution analysis (Mallat, 1989) provide a robust and precise context for the quantitative studies of heterogeneous land surfaces envisaged for the LSPIM. The wavelet transform is used because it measures the local structure of signals (Lindsay et al., 1996). Using a wavelets series gives a measure of variability (values of wavelets coefficients) as a function of resolution, i.e. the *lengths* of the terms in the series. The largest value of the wavelet coefficients indicates the resolution at which variability is largest and, therefore, provides an estimate of the dominant *length-scale.*

In the example presented here, a Discrete Wavelet Transform (DWT) (Lindsay et al., 1996) was used to decompose an image data set into an equally large set of wavelet coefficients. Each wavelet coefficient corresponds to a wavelet ψ of the scale Level j and the position k. The Haar wavelet was used. The coefficient corresponding to the Haar scaling function is the mean value for the scale j and the position k. The variance of the coefficients is an estimate of the term V. By relating values of V to the length of the wavelets the required relation between the extent of the spatial variability and the spatial sampling can be established.

The method was applied to estimate the dominant length scale of the Barrax test site. Multi-spectral observations acquired by the Thematic Mapper airborne Simulator (TMS) during the EFEDA 1991 campaign were used for this purpose. In Figure 7.16 it is shown that wavelet variance changes with the resolution and peaks between 600 m and 1200 m, comparable with the size of the circular irrigated plots. This gives an estimate of the dominant length-scale of the Barrax site. It also demonstrates that heterogeneous landscapes may be characterised by a dominant length-scale, but significant variability is present in a range of length-scales.

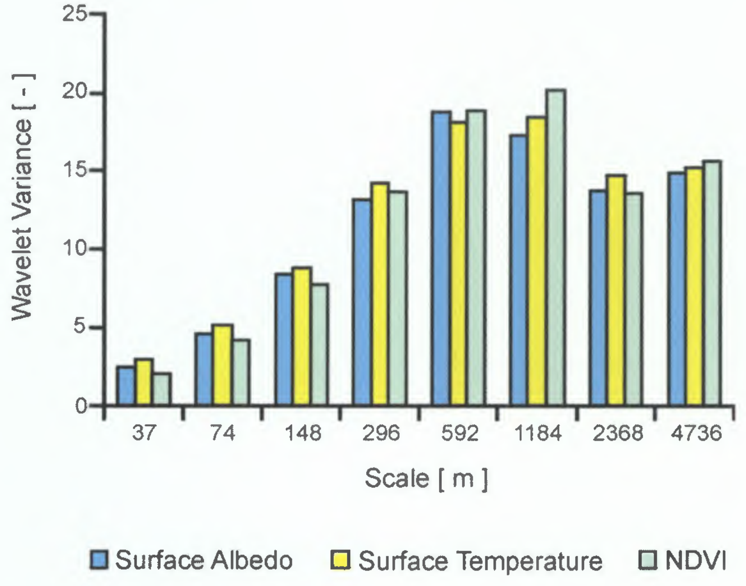

Figure 7.16. *Wavelet variance of land-surface characteristics (courtesy of H. Pelgrum).*

7.4.2 A Case-Study on Up-Scaling of Heat Fluxes

The discussion above provides an answer to the question of how the dominant-length scale of a heterogeneous land surface is defined and how it can be estimated. The error on estimates of the heat released from a landscape in the case where the spatial resolution is not adequate for the landscape under investigation can be estimated. Adequate in this case means a spatial sampling interval smaller than the smallest length-scale estimated in the landscape; for this case each homogeneous element in the landscape where the term V=0 is correctly sampled.

This experiment can be simulated by stepwise degrading the actual resolution of the TMS-data (18 m). This mimics the use of observations at increasingly lower resolution. At each step the heat fluxes are determined, the integral over domain A calculated and the result compared with the reference value obtained with the 18 m data. The value of V will be $\neq 0$ for that fraction of the landscape where the current (degraded) resolution is not adequate. The objective of the experiment is to estimate the relation between the cumulative (up to a given sampling interval) error of aggregation and the cumulative (up to a given length-scale) variance of the wavelets coefficients. Sensible and latent heat fluxes were calculated with the surface energy balance index method described by Menenti and Choudhury (1993).

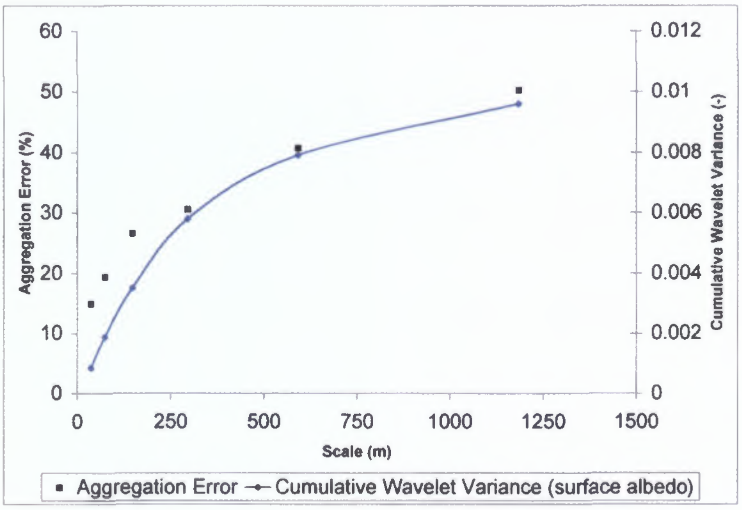

***Figure** 7.17. Estimation error of the evaporative fraction due to the different aggregation (courtesy of H. Pelgrum).*

Because of the heterogeneity of the landscape, the error of aggregation becomes very large at sampling intervals comparable with the ones provided by sensors such as AVHRR and ATSR (see Fig. 7.17). It indicates that with a spatial sampling interval of some 100 m, the aggregation error alone is around 10%. The results indicate that the variance of the wavelet coefficients is a useful measure of heterogeneity.

7.5 Summary

The above case studies have clearly demonstrated the steps involved in the challenging retrieval, processing and assimilation of spectral, spatial, directional and multitemporal reflection measurements. They demonstrate:

- how Level 1b PRISM data, which represent top-of-atmosphere radiance values, can be converted into complex bio-geophysical variables of the key processes of plant production, water and nutrient fluxes
- how these retrieval methodologies can be applied to large amounts of data
- how the variables can be assimilated in land-surface process models to produce outputs of the key ecosystem state and rate variables
- how the expected LSPIM remote-sensing inputs can significantly improve model results

and thereby cover the whole data-utilisation chain aimed at by the proposed LSPIM.

The case studies provide evidence of the feasibility and focus of the overall mission objectives. At the same time they give a flavour of how data from the proposed LSPIM and the derived products will be assimilated and used in land-surface processes and interactions models to:

- improve their performance
- improve the underlying modelling approaches
- analyse land-surface processes and interactions on a previously unknown level of spatial detail and realism
- explore options of environmental planning and
- thereby provide important data developing environmental and agricultural decision support systems.

8 Mission Performance and Mission Requirements

8.1 Retrieval Accuracy of Key Variables

This Chapter summarises how the proposed LSPIM concept will achieve the mission objectives as inferred from the scientific issues described in Chapter 2, specified in Chapter 3 and detailed in the form of corresponding observational requirements in Chapter 4. It will be demonstrated first that the space segment (see Chapter 6) is able to meet the requirements put forward in Chapter 4. All of the essential mission elements as described in Chapter 5 will be considered in this evaluation. Secondly, it will be demonstrated that it is feasible to retrieve the geophysical variables identified in Chapter 3 with the required accuracy using the algorithms, models and data-processing techniques (Chapter 7) described earlier in this report.

Finally, the impact of the mission on the better understanding of the land-surface processes is discussed here. Therefore this Chapter closes the loop by giving examples of the feasibility of performing the variable retrievals and thus process investigations that were identified originally in Chapter 2.

The LSPIM aims at providing a complex set of observations necessary to further our understanding and to improve models of land-surface processes. Five categories of processes have been identified as well as 18 relevant variables. Since it is difficult to assess mission performance for all processes and all variables, the performance assessment presented here focuses on the two dominant processes, heat and mass transfer and primary production.

The observation requirements set out in Chapter 4 imply that in order to meet its objectives, the LSPIM space-, field- and ground segment must:

> *provide accurate observations of the two fundamental radiometric state variables: the spectral BRDF and the TDD that are required to effectively perform the retrieval of the process variables and deliver the products and services needed by the scientific community.*

The science objectives of the mission focus on the understanding of land-surface processes and the bio-geophysical variables involved, which are needed for process modelling and analysis (Table 4.1). By closing the data gap between field- and large-scale observations, the space segment of this mission will meet its major objectives and thus contribute to more accurate modelling and understanding of land-surface processes and their interactions with the atmosphere.

In the following, the mission performances are set against their requirements enabling the assessment of the expected retrieval accuracy taking due account of the mission constraints, such as are imposed by the geometry of observation arising from orbit design and mission operation and the spectro-radiometric properties the sensor system and the target response.

Concerning the TDD, the proposed LSPIM will provide, for the first time, multi-directional observations at high spatial resolution of thermal-infrared radiances and, as such, has a clear potential for innovative exploration. Similar measurements have only been achieved in a limited number of field experiments and no sensor system exists today with the capability of providing these observations (see Table 5.2). The instruments ATSR-1 and -2 have been providing measurements, but at low spatial resolution and for only two observation angles. As a consequence, the development of algorithms to exploit this capability is an emerging field of research and an assessment of the mission performance has to be based on the experience derived from field-, laboratory- and airborne campaign experiments.

The fundamental radiometric quantity is the spectral BRDF (Fig. 8.1). This is a continuous function of view and illumination angles and, as such, cannot be observed directly (see also Figs. 3.1, 4.3 and 4.5). The accuracy of the reconstruction of the BRDF using a limited sample of observations is critical for a quantitative radiometric retrieval. Once the BRDF is reconstructed with satisfactory accuracy, algorithms are used to estimate process variables. In Chapter 4 and 7 the chain of process models and retrieval algorithms linking the science objectives of the mission with the radiometric observations to be provided by PRISM has been described (Chapter 4) and examples of actual use presented in some detail (Chapter 7).

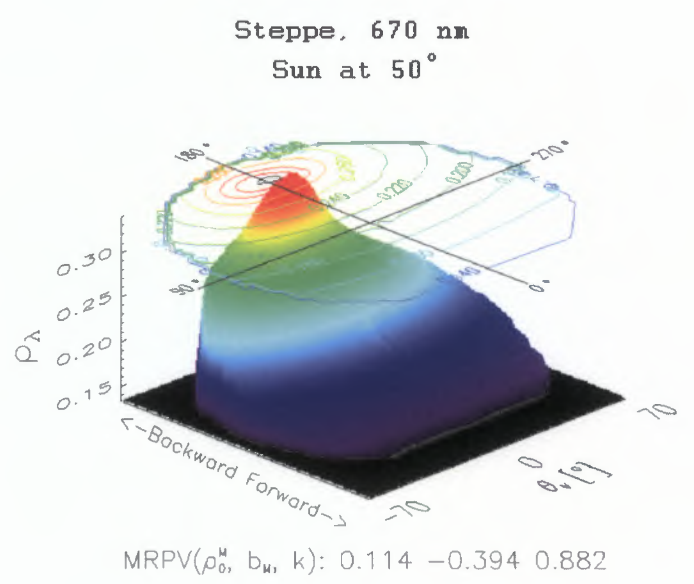

Figure 8.1. *Reference BRDF of a steppe obtained by assuming the values of the MRPV model (for details on the approach see Engelsen et al., 1996).*

Spectral Sampling and Accuracy

As far as the spectral sampling and the related accuracy are concerned, the achievement of the expected performance (Chapter 4 and 6) is mandatory to enable the retrieval of the required variable by separating their characteristic absorption features. This can only be achieved if the data exhibit a high degree of spectral accuracy. Too coarse a spectral resolution, (i.e. below the level postulated for this mission) means that a separation of important spectral absorption features (such as plant water content and atmospheric water vapour) could not possibly be achieved (Fig. 8.2). Likewise, the position of such an absorption feature needs to be determined with a high degree of accuracy as even a slight shift in the spectrum will lead to large radiometric errors (Green, 1998).

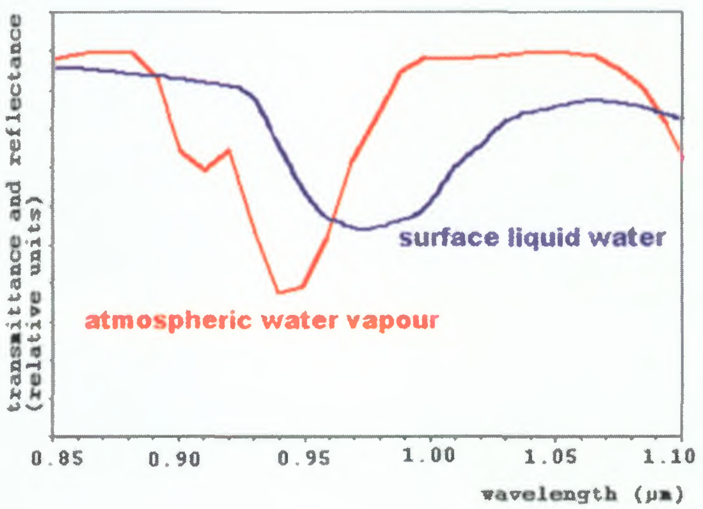

Figure 8.2. *Illustration of the spectral resolution required to separate the atmospheric water vapour effects and the surface liquid water effects in the retrievals of 'water content' from hyperspectral data (courtesy of J. Moreno).*

Radiometric Range and Accuracy

The radiometric performance as expected for this mission will enable the retrieval of process variables over a large dynamic range. Canopy features in dense vegetation, showing a comparatively low radiometric response, will be analysed as well as soil features showing bright reflectance levels. The required radiometric accuracy is necessary to retrieve key canopy variables such as leaf and canopy water content (Fig. 8.3). A performance below the mandatory level as described in Chapters 4 and 6 would hamper the quantitative derivation of process variables.

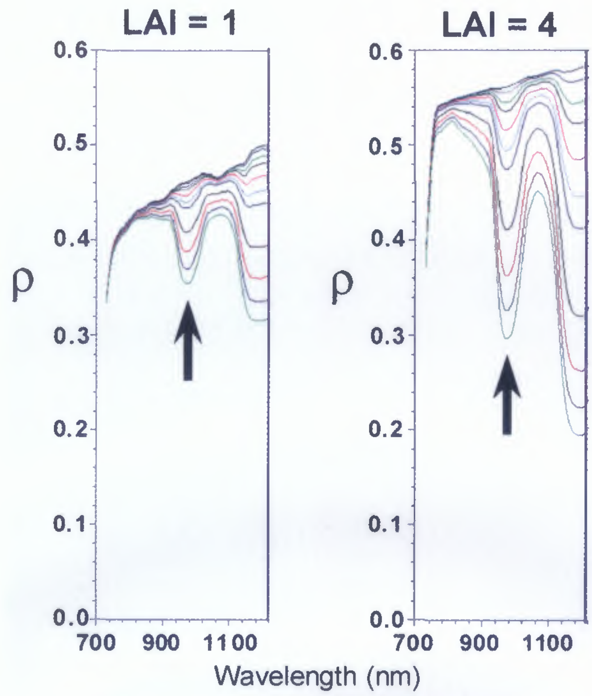

Figure 8.3. *Changes in canopy reflectance as varying leaf liquid water content, for two cases of LAI values. Changes are due to multiple scattering effects. Compensation of these effects are needed for estimation of leaf water content from canopy spectra (courtesy of J. Moreno).*

The same sequence of process models and algorithms can be exploited to evaluate directional and spectral sampling schemes for the retrieval of the variables listed in Tables 3.1 and 4.1. In preparation of this mission a few such sampling studies have been carried out. Some of these studies have been mentioned earlier in this report (see Chapters 4 and 7). These studies led to the identification of specific sampling schemes and tentative estimates of errors. They provide useful indications of achievable accuracy and on the combination of spectral and directional observations.

The error estimates shown in Table 8.1 are based on an analysis of the statistics of retrieval performance based on a large number of combinations of target properties, atmospheric conditions and observation geometry. To some extent they all depend on the selection of cases to be considered and are all based on certain procedures for modelling the observations. The assessment provided on leaf water content for example is based on two field experiments. The feasibility of the approach is demonstrated, but cannot provide any generally valid indications on absolute accuracy. The leaf water algorithm will require a focused effort in the framework of the LSPIM data exploitation. When comparing Table 4.1 with Table 3.2, the algorithms evaluated so far show promise of the possibility of delivering an accuracy better than the one aspired to in Chapter 3. As noted earlier in the report, the development of robust algorithms for scientific studies of the land surface is an active area of research and significant improvements may be expected in the next few years.

Variable	Requirement	Error	Comments
Albedo	7%	1.4%	Menenti and Verhoef, 1998.
Long-wave spectrally integrated exitance	2.5%	14%	Preliminary case study, error increases with thermal heterogeneity of targets; (Nery, F. personal communication)
Surface temperature	1 K	1.1 K	Caselles et al., 1998
Soil and canopy temperature	2 K soil 1 K vegetation	2 K soil; 4 K vegetation	Retrievable with other large forward view angle; accuracy TBD
Cover fraction	10%	5%	Weiss and Baret, 1999
fAPAR	10%	10%	Weiss and Baret, 1999
LAI	20%	15%	Weiss and Baret, 1999
Leaf chlorophyll content x LAI	20%	10%	Weiss and Baret, 1999
Leaf water content	20%	30%	Moreno and Green, 1996

Table 8.1. *Summary of relative error assessments on key variables documented by case.*

In summary, the figures provided above must be considered encouraging, but not as final estimates, and further studies on the accuracy of algorithms have to be performed in Phase-B.

A key step in the path from radiometric observations to processes is, therefore, the estimation of the two key radiometric-state variables, i.e. the BRDF and the TDD. The versatile platform designed for this mission (see Chapter 6) has unique capabilities in this sense. The latter is essential to the successful realisation of the experiment plan outlined in Chapter 5. The analysis of performance presented in this Chapter, therefore, focuses on the capability of the mission to deliver useful spectral BRDF data for the sites where experiments take place (Chapter 5).

8.2 Observability of the Spectral BRDF and TDD: Temporal and Geometric Aspects

8.2.1 Approach

As far as the sampling strategy of the LSPIM is concerned issues, to be addressed include:

- Does the mission have the capability to support a set of experimental sites such as included in the experiment plan?
- Is it feasible to meet the temporal requirements emerging from the ensemble of these experiments?
- Is the directional sampling of the BRDF provided by the LSPIM sufficient to meet the requirements on the accuracy of process variables?

All three questions have been addressed by the mission simulator (MOSAP-L) developed as part of the Phase-A study.

The LSPIM mission profile (see also Chapter 6) has been studied under the following constraints:

- Selection of a (for the processes to be investigated) representative set (Fig. 8.4) of globally distributed experiment sites from the full set of sites included in the experiment plan.
- Schedule of actual acquisitions, i.e. after discounting loss of viewing opportunities due to clouds, defined for each site.
- Selection of an orbital altitude for a 3-day revisit time, repeat cycle (14+9/14) orbits day^{-1} and global access with an Across Track de-Pointing (ATP) angle of $\pm 34.7^0$.
- Minimum Sun elevation 10^0.
- Along-track de-pointing for directional measurements: 70^0, 60^0, 45^0, 0^0, $-\alpha$, -60^0, -70^0; where α is user-selectable for better BRDF sampling, with the restriction that each angular step is consistent with the manoeuverability of the platform.

Figure 8.4. *Selected sites for mission simulation.*

8.2.2 Selected Sites and Schedule of Required Acquisitions

On the basis of information provided by the site coordinators, the following tentative data acquisition schedule was prepared. The frequency of observations indicated in Table 8.2 is an estimate of actual user requirements, i.e. after discounting missed viewing opportunities due to clouds.

tentative LSPIM acquisition schedule													
site	process	jan	feb	mar	apr	may	june	july	aug	sep	oct	nov	dec
AF2	photosynthesis		1-7; 14-21		one obs.		one obs		1-7; 14-21	1-7; 14-21		one obs.	
AF4_4	ecosystems		one obs.		one obs.		one obs.		one obs.		one obs.		one obs.
AF4_6	ecosystems		one obs.		one obs		one obs.		one obs.		one obs.		one obs.
AF5_1	biochemical		one obs.		one obs.		one obs		one obs		one obs.		one obs.
E1_1	heat momentum				1-7;	weekly	1-7; 14-21	1-7; 14-21	1-7; 14-21	1-7;			
E1_2	heat momentum				1-7;	weekly	1-7; 14-21	1-7; 14-21	1-7; 14-21	1-7;			
E3_1	heat momentum	one obs.			14-21;	14-21	14-21	14-21	14-21		one obs.		
E3_2	heat momentum	one obs.		14-21	14-21;	14-21	14-21	14-21	14-21		one obs.		
E4_1	biochemical	one obs.			one obs.	one obs	one obs.	one obs.	one obs		one obs.		
E4_3	heat momentum	one obs.			one obs.	one obs	one obs.	one obs.	one obs		one obs		
E5_3	photosynthesis	one obs			21-28;	21-28;	21-28;	21-28;	21-28;	21-28;	one obs.		
E7	heat momentum	one obs.	one obs	one obs	1-7; 14-21	1-7; 14-21	1-7; 14-21	1-7; 14-21	1-7; 14-21	1-7; 14-21	one obs	one obs	one obs
E9	photosynthesis	one obs	one obs.	one obs	three obs	three obs.	four obs	three obs	three obs.	three obs	one obs	one obs	one obs.
NA11	hydrology		one obs		one obs.	one obs.	one obs	one obs.	one obs	one obs	one obs		one obs.
NA16	hydrology		one obs.			one obs	one obs	one obs.	one obs	one obs		one obs	
NA17	ecosystems			one obs.	one obs.	one obs	one obs	one obs.	one obs	one obs.	one obs.		
NA23	ecosystems	one obs.		one obs.		one obs		one obs		one obs.		one obs.	
NA24	ecosystems				1-7; 14-21	1-7; 14-21	1-7; 14-21	weekly	three obs.	1-7; 14-21	1-7; 14-21		
NA26	ecosystems	one obs.			one obs.		one obs.	one obs.	one obs.	one obs.		one obs.	
NA5	heat momentum			two obs.	two obs	weekly	weekly	two obs.	two obs	three obs	three obs.		
NA7	ecosystems				one obs.	one obs	one obs.	one obs.	one obs	one obs.	one obs		
NA8	photosynthesis				one obs.	one obs.	one obs	one obs.	one obs.	one obs	one obs.		
NA9	photosynthesis		21-28;		one obs	14-21;		14-21;		14-21;		one obs	
OC1	biochemical	two obs.	two obs	one obs.	one obs.	one obs.	one obs.	one obs	one obs.	two obs	weekly	7-21;	weekly
OC2_3	heat momentum	one obs.	one obs.	one obs.		one obs.		one obs.		one obs		one obs	one obs.
OC3	photosynthesis	one obs.				one obs.				one obs.	one obs.		
SA1_1	biochemical	weekly	weekly	one obs	one obs	one obs	one obs	one obs	weekly	weekly	weekly	one obs	one obs.
AF1_1	heat momentum		one obs		one obs.		three obs	three obs.	three obs	three obs		one obs	
AS1_2	heat momentum			one obs.		two obs	two obs	two obs	two obs	two obs.		one obs.	
AS3	photosynthesis	one obs.		one obs.	one obs.	15-31;	one obs	15-31;	15-31;	one obs	one obs.	one obs	
E15_1	hydrology		one obs		two obs	two obs.	two obs.	two obs	two obs	two obs	two obs.		one obs.
E16	heat momentum			one obs.	two obs	two obs.	two obs.	one obs	one obs	one obs	one obs		
NA2	hydrology		one obs		1-14;	one obs.	one obs.	1-14;	one obs.	one obs.	one obs.		one obs.
NA3_1	biochemical	1-14;		one obs.		1-14;	1-14;	1-14;	1-14;	1-14;		one obs	
NA6_3	heat momentum	one obs.		one obs.	two obs.	two obs.	weekly	weekly	two obs.	two obs.	one obs.		one obs.

Table 8.2. *Calendar of data acquisitions required by users.*

The simulator generates data sets containing the calculated actual view angles for each acquisition at each site. These data were then used to:

A. Determine the values of the parameters of the MRPV model (Engelsen et al., 1996).
B. Estimate selected process variables.

Regarding A, performance is measured by the deviation between the true (assigned a-priori) BRDF of the land cover at the site of interest and the BRDF reconstructed with the set of view angles computed by means of MOSAP-L. Regarding B, performance is measured by the deviation between the true (assigned a-priori) value of the selected process variable.

8.3 Results of Mission Simulation: Statistics on Feasible Acquisitions

The LSPIM simulator has been used first to identify opportunities for site viewing to maximise the number of observations in the vicinity of the hot spot. Each white trace in Figure 8. 5 indicates the displacement of the spacecraft during the acquisition of the full seven view angle set of observations. The sensor is pointed westward only, i.e. Line Of Sight (LOS) is close (nearly parallel for one observation) to the Line Of Illumination (LOI). Segments are on adjacent or subsequent orbits. Repeated observations during an orbital cycle give a directional pattern of the type shown in Figure 8.6.

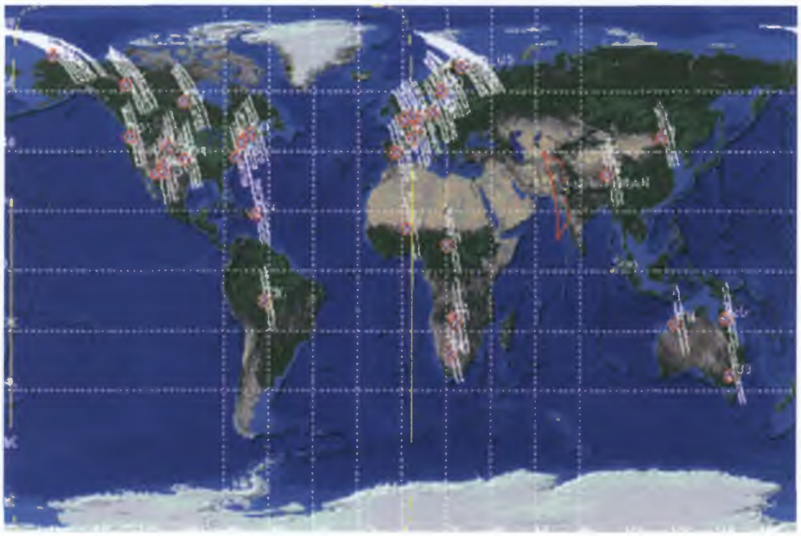

Figure 8.5. *Optimisation of viewing direction to maximise observations in the vicinity of the hot spot.*

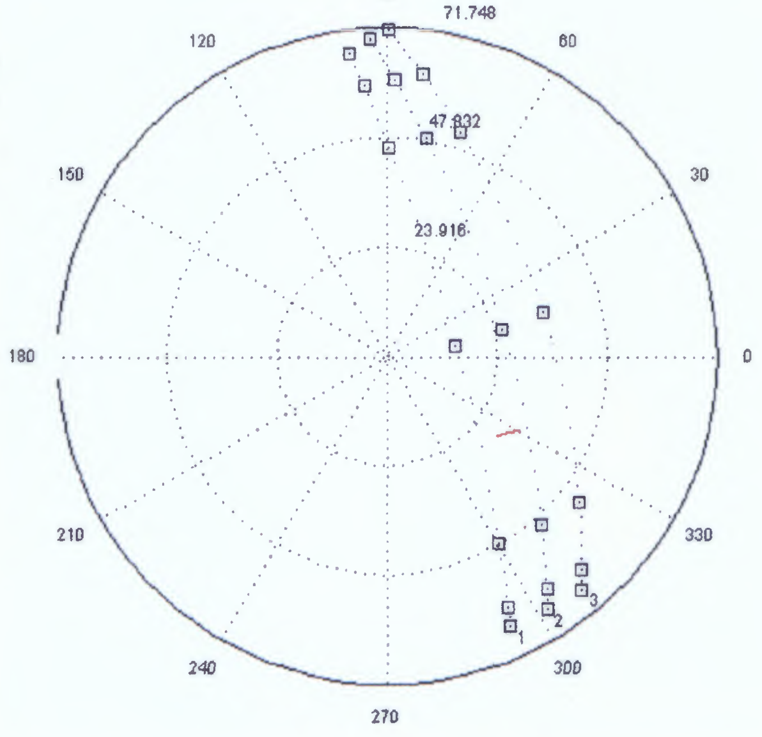

Figure 8.6. *Polar diagram of subsequent BRDF sampling during a single orbital cycle(15-29 June) and for a specific site (E1.1 Barrax). Squared dots indicate the actual position of observations. Red dots indicate Sun position. The sequence is taken during the ascending orbit (from bottom to top of figure).*

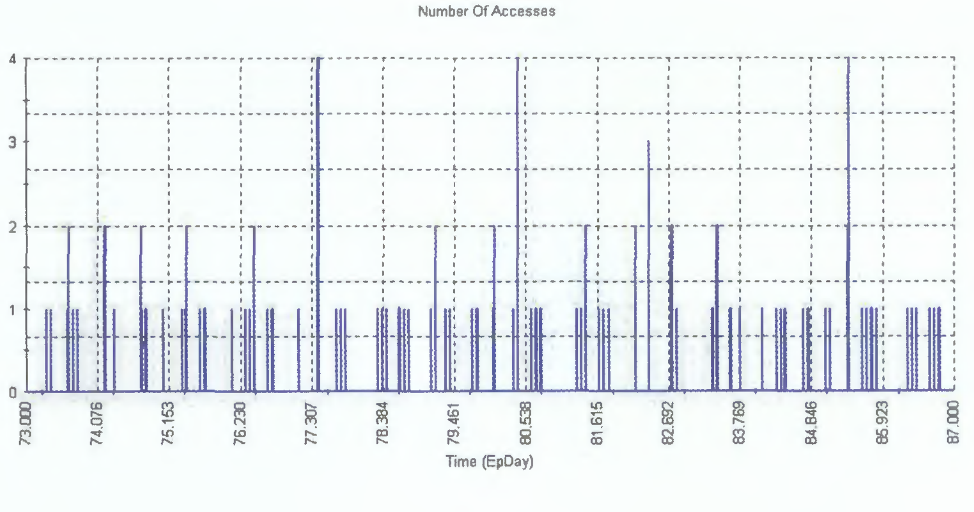

Figure 8.7. *Number of acquisitions during an orbit cycle.*

During each orbit the number of acquisitions may vary (i.e. from 1 to 4 – Fig. 8. 7), implying lower requirements for higher level data-processing capacity. The overall number of BRDF acquisitions can be estimated using statistics produced by a larger number of orbits. The total number of acquisitions for all sites addressing a specific type of land-surface process (see Table 5.1) can be considered as a concise indicator of mission performance (Fig. 8.8).

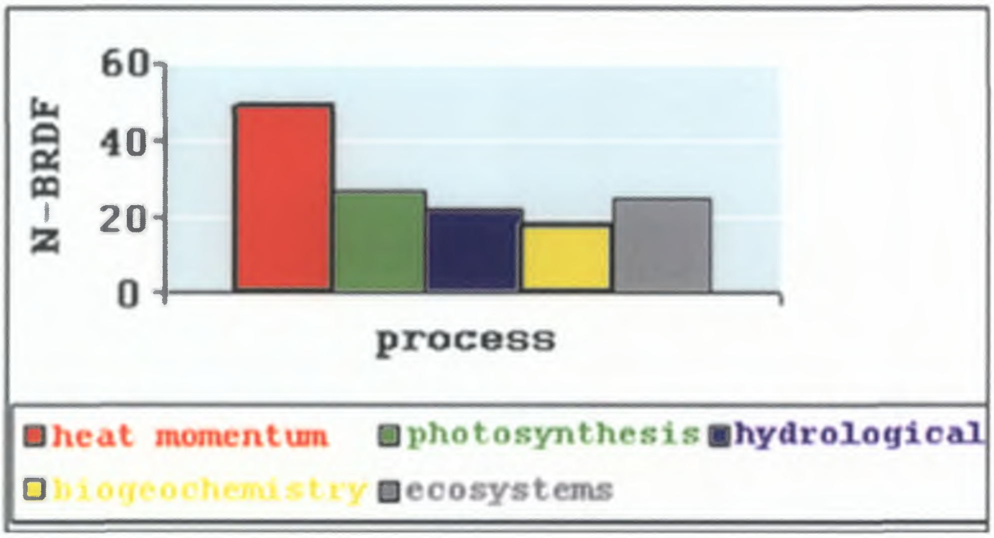

Figure 8.8. *Total number of directional acquisitions over two months (June and July) by process.*

This simulation was carried out by adding an additional constraint to take into account loss of acquisition opportunities due to cloudiness. When a site can be accessed on the basis of geometry, a 40% threshold is applied on the probability of having a cloud-free acquisition. If the cloud climatology indicates a probability lower than the threshold, the acquisition opportunity is discarded. The total number of acquisitions is higher than the total number of requested acquisitions for June and July (see Table 8.2).

It can be concluded that the mission has the capability of fulfilling the expectations of the investigator teams. During mission operation, the MOSAP-L will be used in a somewhat different way. Weather forecasts will be used instead of climatology to schedule data-takes. It is expected that this will increase the number of cloud-free acquisitions. Specific simulation studies are also recommended to be carried out during Phase-B. The present simulation exercises have demonstrated that the number and geographical distribution of sites do not exploit the technical capabilities of the space and ground segments to the fullest extent possible. Ways to address this issue will be discussed later in this chapter.

8.4 Feasible Versus Required Sampling

The directional sampling of the mission has the capability of providing a reasonably large number of directional observations within a single orbit cycle. These observations may be performed in the vicinity of the hot spot, or away from it when mission planning is developed under constraints different from the hot-spot viewing. A simulation study was carried out to evaluate the accuracy of the reconstructed BRDF for a given sampling scheme. The reference data set generated for representative land cover types using the parametric BRF model of Engelsen et al., (1996). Values of the parameters are assigned on the basis of previous experimental and modeling studies (Engelsen et al., 1996). A particular directional sampling will give estimated values of the three model parameters, and therefore a different BRDF.

The error assessment was carried out by using the actual LSPIM view angles as computed by MOSAP-L (e.g. Fig. 8.5), and demonstrated by using the simulated view angles for the site IMGRASS (AS3). This site is representative of the steppe in Inner Mongolia (P.R. China). The reference BRDF is shown in Figure 8.1.

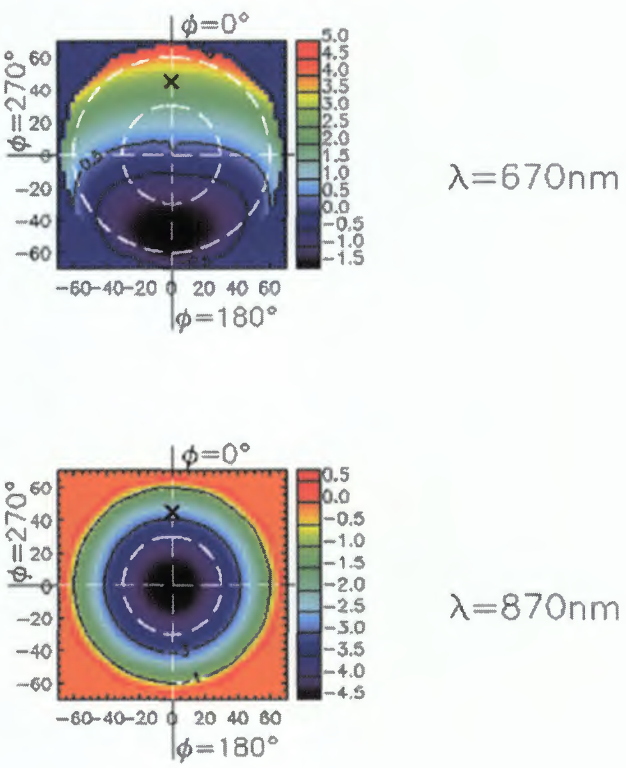

Figure 8.9. Error on the reconstructed spectral BRDF using the set of directional observations given by the simulated (MOSAP-L) sampling scheme and the parametric BRF model of Engelsen et al. (1996); IMGRASS (AS3); orbit cycle 15-29 june (courtesy of P. Vogt).

In the following step the error of reconstructing the BRDF with the sample of observations provided by LSPIM can be computed in the same way as done earlier for generic set of observations. It appears that the parameters of the MRPV model can be estimated with sufficient accuracy (Fig. 8. 9).

As a consequence, the performance in the retrieval of the spectral hemispherical reflectance (9 wavebands in the solar domain) was evaluated (Fig. 8.10). The neural network approach described in Chapter 7.2 was used, with the values of the values of the MRPV parameters as input data. Two sampling schemes generated by means of MOSAP-L for the site Barrax (E1.1) were used:

(i) planning aimed at sampling the BRDF in the vicinity of the hot-spot,
(ii) planning aimed at maximising the number of acquisitions.

The latter sampling strategy tends to give larger view angles than the former. It appears that the sampling aimed at the hot-spot gives a slightly lower error. In any case the mean error meets the objective indicated in Table 3.2.

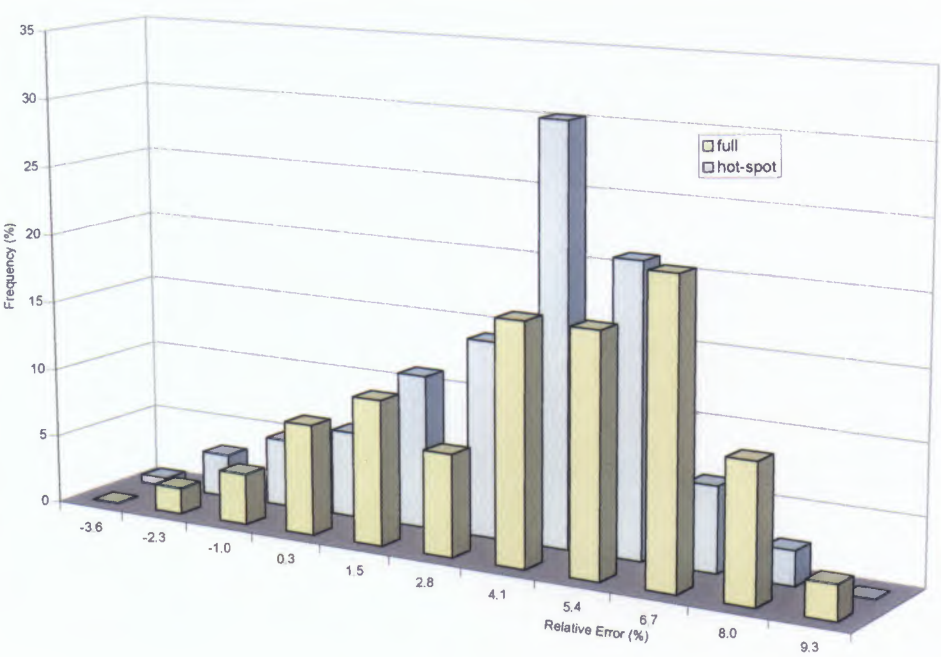

Figure 8.10. *Relative error on the reconstructed spectral hemispherical reflectance; orbit cycle 15-29 June. The test case is the maize data set as described by Weiss et al., (1999) ; relative error=[(actual-estimated) / actual]*100.*

Although rather limited, the comparison of performance with requirements presented here is encouraging and suggests ways to exploit the flexibility of mission operation and the versatility of the platform to optimise sampling in view of the key-process variables required at each site.

8.5 Concluding Remarks

The simulation and analysis studies, performed in the framework of investigating the requirements for and capabilities of the LSPIM, have clearly demonstrated that:

- The mission has clearly defined and focussed objectives.
- The mission can meet the requirements of the mission experiment plan.
- The instrument proposed for the mission can meet the required retrieval accuracy for variables needed to significantly contribute to process understanding and up-scaling of land-surface processes.

The currently studied scenario is based on rather conservative assumptions with regard to the capabilities of the space and ground segments. Improvements in the overall performance of the system are indeed expected and should, just taking the example of the global distribution of sites and their acquisition, be pursued in two ways:

A. Allow for more frequent requests of acquisitions.
B. Increase the number of sites.

Regarding A, teams of identified potential investigators have indicated their satisfaction with the assumed schedule. In some cases, however, they have expressed interest in shorter intervals between acquisitions, particularly when changes in land-surface properties are expected to happen over a shorter time-scale. The scope for increasing the number of sites is evident (Fig. 8.4) for Asia and South America. The number of sites is limited in Africa, although in this case the size of the scientific user community is also limited.

This leads to the overall conclusion that the LSPIM is to be regarded as a truly global mission:

- First and foremost, to cover all relevant terrestrial ecosystems, including those outside Europe in terms of comprehensive process research and analysis.
- Second, to guarantee effective exploitation of an unparalleled focussed observing capability, forming a unique tool to support biospheric process research and provide much-needed observations for process modelling at various scales.

Data from the LSPIM will significantly further the ability of the scientific community to model the cycles of water, energy and carbon. The global nature of this mission means that fluxes of biochemicals to and from all the World's major biomes can be estimated more accurately. Only when these fluxes are known with a higher degree of accuracy can a better picture be constructed of the global distribution of, for example, the net sources and sinks of carbon.

9 Programmatics

9.1 Development Approach

The development schedule as proposed by the industrial team at the end of Phase-A is shown in Figure 9.1. The work plan assumes that the 12-month Phase-B is started in July 2000, including early breadboard and testing of key items as shown in Section 9.2. Phase-C/D follows three months after completion of Phase-B. The launch can take place at the end of 2004. The LSPIM can therefore be the first Earth Explorer Core Mission.

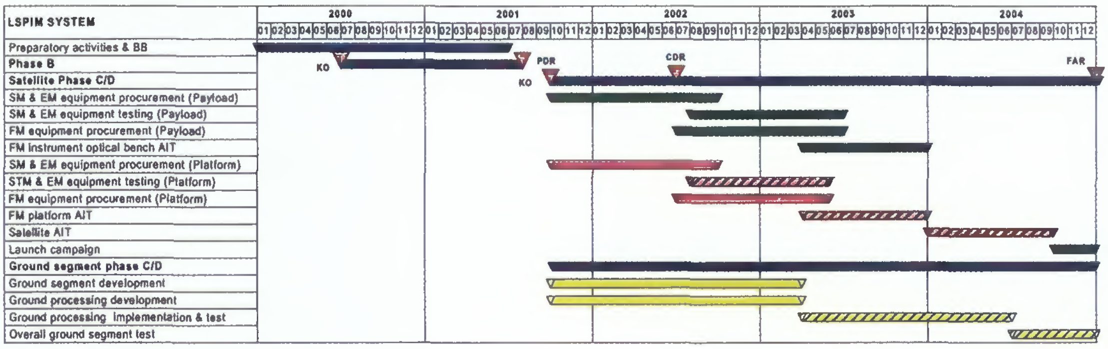

Figure 9.1. LSPIM development schedule.

For the above schedule to be met, it is necessary to continue the technology developments already started and to strengthen them in Phase-B. The interaction between development flow and validation work is highlighted in Figure 9.2.

The model philosophy is defined considering the main issues identified in Chapter 6 and summarised in Section 9.2, and taking into account financial and time development constraints. The issues identified are of low to moderate criticality, but imply long-lead items thus the development should start already in Phase-B. It is proposed to continue the ongoing development of the SWIR detectors and initiate in Phase-B the customisation of the VNIR and TIR detectors, the development of the opto-mechanical breadboard (optical bench and spectrometer) and the analogue processing unit. For the Phase-C/D, it is proposed to have a proto-flight approach for the platform and to manufacture a structural-thermal model (STM) and an EQFM for the PRISM instrument.

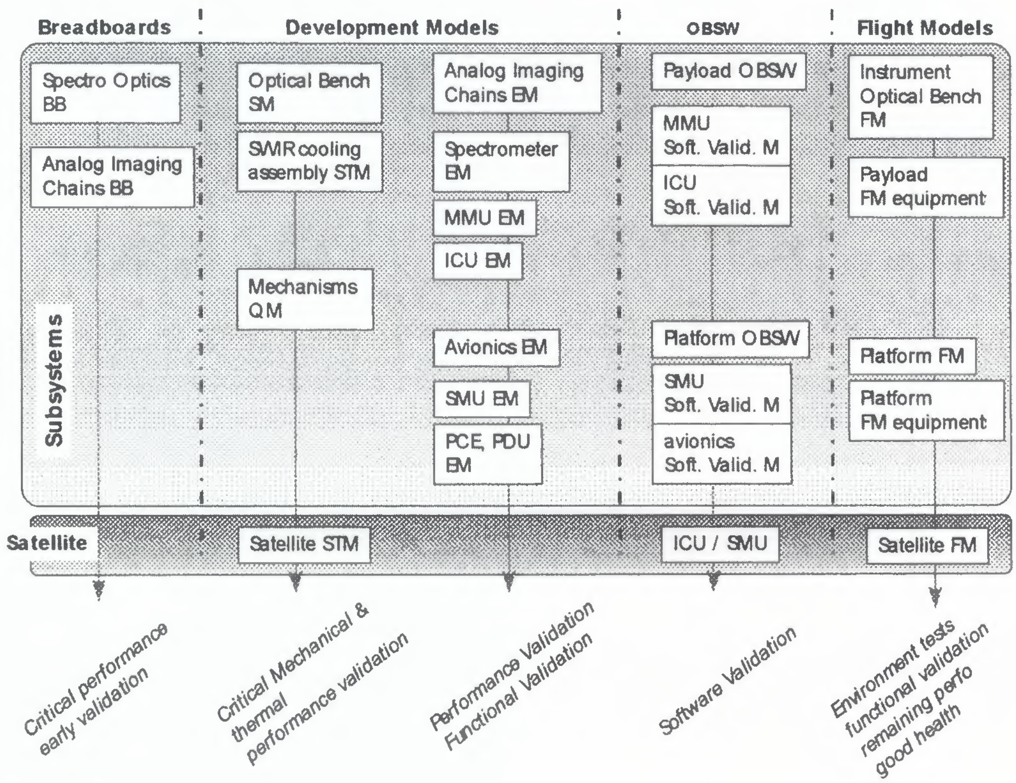

Figure 9.2. *LSPIM development flow*

9.2 Heritage, Critical Areas and Risks

Table 9.1 summarises the implementation of the space, ground and field segments and indicates the relevant heritage.

	Implementation	Heritage
	Instrument PRISM	
Mirror	Common mirror for access to calibration sources and for roll pointing	Classical, all scanners
Telescope	TMA	HRIS, other , tools available
TIR relay optics	All germanium lenses	Classical
Spectrometer	Offner, all silica lenses	New concept, partial breadboard already
Separation VNIR/SWIR	Dichroic	Classical
Optical bench	C-C	Military, TRP, proven

VNIR focal plane	CCD, higher well, faster line transfer	MERIS, other, customisation
SWIR focal plane	CdHgTe detectors, 175 – 180 K	HRIS, customisation
TIR focal plane	CdHgTe detectors 8.0 – 9.1 microns	HRTIR, customisation
Calibration VNIR/SWIR	Radiometric: Diffusers, filter wheel, mechanism Spectral: Rare Earth doped glass	Classical, MERIS
Calibration TIR	Two black bodies each image, frontal blackbody every month	Classical
Video processing unit	Proximity electronics, analogue processing unit	MERIS
Analogue/Digital Converter	12 or 14 bit considered	Commercial, testing ongoing
Mass Memory Unit	80 Gb, including band selection and lossless compression	Development for the PRIMA platform ongoing, PRDC ASIC developed
Instrument Control Unit	ERC-32 based	New processor, used in Ariane 5, Columbus, PROBA, etc.
Thermal	Cryocoolers for TIR, passive radiator-Peltier cooler for SWIR	Classical thermal equipment
Platform and launcher		
Configuration	Compact, integrated	
Structure	CFRP cone, sandwich panels	Classical
Thermal	Passive and heaters, margin radiator area	Classical
Propulsion	30 kg hydrazine, 4 x 1 N thrusters	Classical, PRIMA, Proteus platforms
Power	6 panels, GaAs cells, 1660 W, 40 Ah NiCd battery, unregulated	Standard components, Proteus regulation and distribution
Data handling	Central computer, ERC-32 processor, MIL 1553 command / control bus	PRIMA
AOCS	Gyros, star sensors, GPS Reaction wheels, magnetotorquers	Proteus equipment, Helios, PROBA guidance, estimation and control
Communications	2 kb/s TC, 8 kb/s HK TM in S-band 100 Mb/s science data X-band	Classical

<table>
<tr><td colspan="2">Launcher</td><td>Rockot</td><td>SS19 and Breeze on Proton, demo flights in 1999 for proposed configuration</td></tr>
<tr><td colspan="4"></td></tr>
<tr><td colspan="4">Field segment</td></tr>
<tr><td colspan="2">Experiment sites</td><td>Instrumented sites around the World</td><td>Large number of sites, growing</td></tr>
<tr><td colspan="4"></td></tr>
<tr><td colspan="4">Ground segment</td></tr>
<tr><td rowspan="3">Ground segment facilities</td><td>CDAE</td><td>Kiruna</td><td>ERS, Envisat</td></tr>
<tr><td>MSCE</td><td>Operations and satellite control</td><td>Very large</td></tr>
<tr><td>PAE</td><td>Processing and archiving</td><td>Very large</td></tr>
</table>

Table 9.1. *Implementation solutions and heritage*

Table 9.1 shows that there is very strong heritage for nearly every item. The novelties are in the spectrometer, the focal planes and the analogue processing unit at instrument level and in the AOCS at satellite level. The areas of risk are summarised in Table 9.2 which also includes the proposed risk-reduction measures.

	Critical areas	**Risk reduction measures**
	Instrument PRISM	
Mirror	No critical area	
Telescope	No critical area	
TIR relay optics	No critical area	
Spectrometer	Manufacturing, alignment, stability	Opto-mechanical breadboard in Phase-B
Separation VNIR/SWIR	No critical area	
Optical bench	Manufacturing, alignment, stability	Opto-mechanical breadboard in Phase-B
VNIR focal plane	Minor criticality, aluminum buttressing	Breadboard Phase-B, fall-back solution available
SWIR focal plane	Long-lead item, performance versus temperature	Development started in Phase-A, two sources available, breadboard Phase-B
TIR focal plane	Long-lead item but no critical area.	Development in Phase-B, two sources available
Calibration VNIR/SWIR	No critical area	
Calibration TIR	No critical area	

Video processing unit	Common design for VNIR, SWIR and TIR, moderate risk	Breadboard in Phase-B
Analogue/Digital Converter	Radiation	Testing ongoing
Mass Memory Unit	Flight demonstration in 2002. No critical area at design or component level.	Several alternatives available
Instrument Control Unit	No critical area	
Thermal	In relation with SWIR focal plane	See SWIR focal plane, fall back to mechanical cooling available

Table 9.2. *Critical areas and risk-reduction measures.*

There are no critical areas at platform level. The thermal control, the electric power and the AOCS subsystems will require more analysis than usual due to the satellite's manoeuvrability, but this will be normal project work. The ground and field segments do not have critical areas.

The proposed implementation concept has a limited number of critical areas, which are anyway of low to moderate criticality. The technical risk is limited. From the technical and programmatic points of view, LSPIM is feasible and mature.

9.3 Related Missions, International Cooperation Possibilities and Timeliness

Following the failure of the Lewis mission, NASA are planning to fly a similar VNIR-SWIR spectrometer on NMP-EOS. Developments are announced, often with commercial orientation, and hence very different mission objectives, such as ARIES. However, no other mission concept offers the combination of spatial, spectral, radiometric and directional capabilities of the LSPIM. The LSPIM is a unique mission.

LSPIM is also very complementary to other missions, in particular SAR missions such as Envisat and the Japanese ALOS with its land-oriented L-band SAR. LSPIM is also very complementary to other optical missions such as MERIS on Envisat, HRV and Vegetation on SPOT.

International cooperation is inherent in LSPIM. The observation sites are distributed around the World and run by and for international scientific programmes.

From the technical programmatic points of view 2004, is very timely. Further development of the building blocks for which critical areas have been identified does not make sense in abstract, but in the context of customisation to a project. The 2004 launch allows overlap with the complementary missions, which is not only convenient to enhance the scientific return, but also to reduce the cost. The 2004 launch date will also ensure seamless building on the developments of Envisat, SPOT VEGETATION. The LSPIM will also be very timely for providing the technologies, techniques and underlying science required for a range of applications as indicated in Section 9.4.

9.4 Enhancement of Capabilities and Application Potential

The uniqueness of the LSPIM implies that it contributes to the enhancement of European capabilities, first of all at system level since it is the first European hyperspectral mission. It also contributes to developing the technology to the level of utilisation in space, thus bringing several years of technology development for detectors (VNIR, SWIR, TIR), electronics (analogue and digital), data-handling architectures and processing techniques to a successful culmination.

The LSPIM has high application potential. Several proposals received in response to an ESA call for outline proposals for (application-oriented) Earth Watch missions were based on multispectral systems. LSPIM would contribute to developing the underlying science and extend the application fields because of its richer spectral content.

References

Aber, J.D., 1992: Terrestrial Ecosystems. In: K.E. Trenberth (Ed.). Climate System Modelling, Cambridge Univ. Press: 173-200.

Anderson, M.C., J.M. Norman, G.R. Diak, W.P. Kustas and J.R. Mecicalski, 1997: A two-source time-integrated model for estimating surface fluxes using thermal infrared remote sensing. *Remote Sensing of the Environment*, 60: 195-216.

Avissar, R., and R. A. Pielke, 1989: A parameterization of heterogeneous land surfaces for atmospheric numerical models and its Impact on regional meteorology. *Monthly Weather Review*, 117, 2113-2136.

Bach, H., 1998: Yield Estimation of Corn based on Multitemporal LANDSAT-TM Data as Input for an Agrometeorological Model. Pure and Applied Optics, Vol. 7, 809-825.

Bach, H., and W. Mauser, 1994: Modelling and model verification of the spectral reflectance of soils under varying moisture conditions: IGARSS'94, 2354-2356.

Bach, H., Mauser, W., Hounam, D., Nithack, J., and Smullius, C., 1996: Combination of Synthetic Aperture Radar (SAR) and Optical Spectroradiometer Data in Aggregated Models, Final report of the ESA contract AOP/WK/334415.

BAHC, 1993: Biospheric Aspects of the Hydrological Cycle. The Operational Plan, Edited by BAHC Core Project Office, Berlin. IGBP Report 27, IGBP Secretariat.

Balick, L. K., B. A. Hutchinson, J. A. Smith and M. J. Mc Guire, 1987: Directional thermal exitance distributions of a deciduous forest in summer: *IEEE Transactions on Geoscience and Remote Sensing*, 25, 410-412.

Barbier, E. et al., 1994: Paradise lost? The ecological economics of biodiversity, Earthscan Publications Ltd., London.

Baret, F., and G. Guyot, 1991: Potentials and limits of vegetation indices for LAI and APAR assessment: *Remote Sensing of the Environment*, 35, 161-173.

Baret, F., and S. Jacquemoud, 1994: Modelling canopy spectral properties to retrieve biophysical and biochemical characteristics., in J. Hill, and J. Megier, eds., Imaging spectrometry as a tool for environmental observations., Brussels and Hamburg, Kluwer Academic Publishers, 145-167.

Baret, F., and T. Fourty, 1998: Estimation of leaf water content and specific leaf weight from reflectance and transmittance measurements: *Agronomie*, 17, 455-464.

Baret, F., J. G. P. W. Clevers, and M. D. Steven, 1995: The robustness of canopy gap fraction estimates from red and near infrared reflectances: a comparison of approaches. *Remote Sensing of the Environment*, 54, 141-151.

Baret, F., M. Weiss, et al., 1999: Evaluation of model inversion techniques. Application to the retrieval of key biophysical variables, Avignon (France), INRA/ESA: 18.

Bastiaanssen, W.G.M., H. Pelgrum, M. Menenti and R.A. Feddes, 1996: Estimation of surface resistance and Priestley-Taylor alpha-parameter at different scales. In: J. Stewart et al. (eds.). Scaling up in hydrology using remote sensing. J. Wiley & Sons, 93-111.

Becker, A., and Bugmann, H, (Ed.), 1997: Predicting Global Change Impacts on Mountainous Hydrology and Ecology: Integrated Catchment Hydrology/Altitudinal Gradient Studies, IGBP Report 43, IGBP Secretariat, Stockholm.

Becker, F. and Z.L. Li, 1995: Surface temperature and emissivity at various scales : definition, measurement and related problems. *Remote Sensing Reviews*, 12, 225–253.

Begue, A., 1992: Modelling hemispherical and directional radiative fluxes in regular clumped canopies. *Remote Sensing of the Environment*, 40, 219-230.

Bertero, M., and P. Boccacci, 1998: Introduction to Inverse Problems in Imaging. Institute of Physics Publishing, Philadelphia.

Beven, K.J. and A.M. Binsley, 1992: The future of distributed models: model calibration and uncertainty predictions. *Hydrol. Processes*, 6:279 – 298.

Biard, F., and F. Baret, 1996: Crop residue estimates using multiband reflectance data: *Remote Sensing of the Environment*, 59, 530-536

Bicheron, P., and M. Leroy, 1999: A method of biophysical parameter retrieval at global scale by inversion of a vegetation reflectance model: *Remote Sensing of the Environment*, 67, 251-266.

Bonan, G.B., Pollard, D. and S.L. Thompson, 1992: Influence of subgrid-scale heterogeneity in leaf area index, stomatal resistance, and soil moisture on grid scale land-atmosphere interactions. *J. Climate*, 6, 1882-1897.

Borel, C.C., S.A. W. Gerstl, and B.J. Powers, 1991: The radiosity method in optical remote sensing of structured 3-D surfaces. *Remote Sensing of the Environment*, 36, 13-44.

Bouman, B.A.M., 1992: Linking physical remote sensing models with crop growth simulation models applied for sugar beet. *International Journal of Remote Sensing*, 13, 2565-2584.

Bowler, I.R. (Ed.), 1992: The Geography of Agriculture in Developed Market Economies, Longman Scientific & Technical.

Briggs, S., J. Settle, F. Gallager, G. Groom, and F. Wyatt, 1995: spatial resolution of PRISM, Final report, ESA study 135/015.

Brisson, N., B. Mary, D. Ripoche, M. H. Jeuffroy, F. Ruget, B. Nicoullaud, P. Gate, F. Devienne-Barret, R. Antonioletti, C. Durr, G. Richard, N. Beaudoin, S. Recous, X. Tayot, D. Plenet, P. Cellier, J. M. Machet, J. M. Meynard, and R. Delécolle, 1998: STICS: a generic model for the simulation of crops and their water and nitrogen balances. I. theory and parameterization applied to wheat and corn. *Agronomie*, 18, 311-346.

Buelgasim, A. A., S. Gopal, et al.,1998: Forward and inverse modelling of canopy directional reflectance using a neural network, *International Journal of Remote Sensing,* 19(3): 453-471.

Caselles, V., J.A. Sobrino, and Becker, F., 1988: Determination of the effective emissivity and temperature under vertical observation of a citrus orchard: application to frost nowcasting. *International Journal of Remote Sensing*, 9, 715-727.

Caselles, V., C. Coll, E. Rubio, E. Valor, U. del Bello, and P. Merheim-Kealy, 1996: Study on thermal band selection for high resolution land-surface processes mission, Valencia, ESA/University of Valencia.

Caselles, V., E. Rubio, C. Coll and E. Valor, 1998: Thermal band selection for the PRISM instrument. 3. Optimal band configuration. *J. Geophys. Res.*, 103 (D14): 17057-17067

Cernusca, A., Bahn, M., Chemini, C., Graber, W., Siegwolf, R., Tappeiner, U., and Tenhunen, J. ,1998: ECOMONT: a combined approach of field measurements and process-based modelling for assessing effects of land-use changes in mountain landscapes. *Ecol. Modelling*, 112, 167-178.

Cramer, W. and C.B. Field (Eds.), 1999: The Potsdam NPP Model Intercomparison. *Global Change Biology*, 5(1): 1-76.

Dickinson, R. E., 1983: Land Surface Processes and Climate - Surface Albedos and Energy Balance: *Advances in Geophysics*, 25, 305-353.

Dickinson, R.E, 1995: Land Processes in Climate Models. *Remote Sensing of the Environment*, 51:27-38.

DIVERSITAS, 1996: An international Programme of biodiversity science, Operational Plan. IUBS, Paris.

Djepa, V., M. Menenti and G.J. Roerink, 1998: Estimation of soil and vegetation temperatures with directional thermal infrared observations : a case study on the Gobi Desert with ATSR observations. In: G. Roerink and M. Menenti (Eds.). Climate and Hydrology at Mesoscale: the contribution of future sensor systems; Bridging Phase. Final Report. BCRS NUSP 98-01: 31-39

Doerffer, R. and H. Schiller, 1997: Pigment index, sediment and gelbstoff retrieval from directional water leaving radiance reflectances using inverse modelling techniques. MERIS Algorithm Theoretical Basis Document 2.12: 83 p

Duchemin, B., J. Goubier, and G. Courrier, 1999: Monitoring phenological key stages and cycle duration of temperate deciduous forest ecosystems with NOAA/AVHRR data: *Remote Sensing of the Environment*, 67, 68-82.

Ellingson, R.G. (1995): Surface longwave fluxes from satellite observation: A critical review. *Remote Sensing of the Environment*, 51: 89-97.

Ellingsby, R.G., 1995: Surface Longwave Fluxes from Satellite Observations: A Critical Review: *Remote Sensing of the Environment*, 51:89-97.

Engelsen, O, B. Pinty, M.M. Verstraete and J.V. Martonchik, 1996: Parametric Bidirectional Reflectance Factor Models: Evaluation, Improvements and Applications. Technical Report EUR 16426. Joint Research Centre. 114 p.

Esaias, W.E., 1996: Algorithm Theoretical Basis Document for the MODIS Annual Ocean Primary Productivity Product (MOD-24). NASA. 44 p

Escadafal, R., and A. R. Huete, 1992: Soil optical properties and environmental applications of remote sensing.: *Int. Arch. Photogramm. Rem. Sens*., v. XXVII, p. 709-715.

España, M., F. Baret, F. Aries, M. Chelle, B. Andrieu, and L. Prévot, 1999: Modelling maize canopy 3D architecture. Application to reflectance simulation: Ecological Modelling, in press.

European Community, 1999: Energy Environment and sustainable Development, Programme for Research, Technology Development and Demonstration under the Fifth Framework Programme; Work Programme, Brusselles.

Famiglietti, J.S., and Woods, E.F., 1992: A Catchment Scale Water Balance Model for FIFE. *J. Geophys. Res.*, 97(D17) 18, 997 – 19,007.

Fisher, A., L. Kergoat, and G. Dedieu, 1997: Coupling satellite data with vegetation functional models: review of different approaches and perspectives suggested by the assimilation strategy: *Remote Sensing Reviews*, 15, 283-303.

Fourty, T. and F. Baret, 1997: Vegetation water and dry matter contents estimated from top of the atmosphere reflectance data: a simulation study, *Remote Sensing of the Environment*, 61: 34-45.

François, C., C. Ottlé, and L. Prévot, 1997: Analytical parameterization of canopy directional emissivity and directional radiance in the thermal infrared. Application on the retrieval of soil and foliage temperatures using two directional measurements: *International Journal of Remote Sensing*, 18, 2587-2621.

Franks, S.W. and K.J. Beven, 1997: Bayesian estimation of uncertainty in land surface – atmosphere flux predictions. *J. Geophys. Res.* 102: D20:23991-23999.

Galloway. J.N., and Melillo, J.M. (Ed.), 1998: Asian Change in the Context of Global Climate Change, International Geosphere-Biosphere Programme Book Series No.3, Cambridge University Press.

Gao, B. C., and A. F. H. Goetz, 1990: Column atmospheric water vapor and vegetation liquid water retrievals from Airborne Imaging Spectrometer data: *J. Geophys. Res.,* 95, 3549-3564.

Gastellu-Etchegorry, J. P., V. Demarez, V. Pinel, and F. Zagolski, 1996: Modelling radiative transfer in heterogeneous 3-D vegetation canopies: *Remote Sensing of the Environment*, 58, 131-156.

Gobron, N., B. Pinty, and V. M.M., 1997a: Theoretical limits of the estimation of the leaf area index on the basis of visible and near infrared remote sensing data: *IEEE Trans. Geoscience and Remote Sensing*, 35, 1438-1445.

Gobron, N., B. Pinty, M. M. Verstraete, and Y. Govaerts, 1997b: A semi-discrete model for the scattering of light by vegetation: *J. Geophys. Res*., 102, 9431-9446.

Goel, N. S., D. E. Strebel, and R. L. Thompson, 1984: Inversion of vegetation canopy reflectance models for estimating agronomic variables. II. Use of angle transforms and error analysis as illustrated by the Suits model: *Remote Sensing of the Environment*, 14, 77-111.

Gordon, H.W. and W.M. Balch, 1999: Algorithm Theoretical Basis Document for the MODIS Detached Coccolith Concentration Product (MOD-23). NASA 30 p

Govaerts, Y. M., and M. M. Verstraete, 1998: Raytran: a Monte Carlo ray tracing model to compute light scattering in three dimensional heterogeneous media: *IEEE Trans. Geoscience and Remote Sensing*, 36, 493-505.

Govaerts, Y., and M. M. Verstraete, 1995: Modelling the Scattering of Light in Three-Dimensional Canopies: Contribution of a Monte Carlo Ray Tracing Approach, Proceedings of the Second Topical Symposium on Combined Optical-Microwave Earth and Atmosphere Sensing, 3-6 April 1995, Atlanta, p. 31-34.

Green, R., 1998: Spectral calibration requirement for Earth-looking imaging spectrometers in the solar-reflected spectrum, *Applied Optics*, 37 (4), 683 – 690.

Hadfield, M. G., W. R., Cotton, and R. A., Pielke, 1991: Large eddy simulation of thermally – forced circulations in the convective boundary layer, Part I: a small-scale circulation with zero wind. *Boundary Layer Meteo*. 57:79-114.

Hall, F.G., K.F. Huemmrich, S.J. Goetz, P.J. Sellers and J.E.Nickeson, 1992: Satellite remote sensing of surface energy balance: success, failures and unresolved issues in FIFE. *J. Geophys. Res*., 97(D17): 19061-19089

Hall, D.K., V.V. Salomonson and G.A. Riggs, 1998: Algorithm Theoretical Basis Document for the MODIS Snow-, Lake Ice- and Sea Ice-Mapping Algorithms. (MODIS-10). NASA 49 p

Heal, O.W., Menaut, J.-C., and Steffen, W. (Ed.), 1995: Towards a Global Terrestrial Observing System (GTOS): Detecting and Monitoring Change in Terrestrial Ecosystems, IGBP Report 26.

Henderson-Sellers, A. and A.J. Pitman, 1992: Land surface schemes for future climate models: specification, aggregation and heterogeneity. *J. Geophys. Res*., 93 (D3): 2687-2696.

Hoogenboom, H.J., A.G. Dekker and IJ.A. Althuis, 1998: Simulation of AVIRIS sensitivity for detecting chlorophyll over coastal and inland waters. *Remote Sensing of the Environment,* 65: 333-340

Hornik, K., 1989: Multilayer feedforward networks are universal approximators, *Neural Networks,* 2: 359-366.

Hornik, K., 1991: Approximation capabilities of multilayer feedforward networks. *Neural Networks,* 4: 251-257.

Houghton, R.A., 1995: In: Encyclopaedia of Energy Technology and the Environment, John Wiley & Sons, Inc., New York. pp 491-504.

IGBP, 1990: The International Geosphere-Biosphere Programme: A Study of Global Change (IGBP). The Initial Core Project, IGBP Report 12, IGBP Secretariat, Stockholm.

IPCC – Intergovernmental Panel on Climate Change, 1996a: Climate Change 1995: Impacts, Adaptations and Mitigation of Climate Change: Scientific-Technical Analysis. Cambridge, New York; Cambridge University Press.

IPCC – Intergovernmental Panel on Climate Change, 1996b: Climate Change 1995: The Science of Climate Change. Cambridge , New York; Cambridge University Press.

Irons, J. R., R. A. Weismiller, and G. W. Petersen, 1989: Soil reflectance, in G. Asrar (Ed.), Theory and Applications of Optical Remote Sensing, Wiley Interscience, 66-106.

Jacquemoud, S., 1993: Inversion of the PROSPECT+SAIL canopy reflectance model from AVIRIS equivalent spectra: theoretical study. *Remote Sensing of the Environment*, 44, 281-292.

Jacquemoud, S., F. Baret, and J. F. Hanocq, 1992: Modelling spectral and directional soil reflectance. *Remote Sensing of the Environment*, 41, 123-132.

Joffre, R., D. Gillon, P. Pardenne, R. Agneessens, and R. Biston, 1992, The use of near infrared reflectance spectroscopy in litter decomposition studies. Annales des Sciences Forestieres, v. 49.

JSC (Joint Scientific Committee of WCRP), 1998: Annual review of the World Climate Research Programme. WMO/ TD-No.929. WMO, Geneva: 98 pp.

Kaufman, Y. J., 1989: The Atmospheric Effect on Remote Sensing and its Correction, in G. Asrar, ed., Theory and Applications of Optical Remote Sensing, New York, John Willey, p. 336-428.

Kimes, D. S., and A. Kirchner, 1983: Directional radiometric measurements of row crop temperatures: *International Journal of Remote Sensing*, 4, 299-311.

Kimes, D. S., R. F. Nelson, M. T. Manry, and A. K. Fung, 1998: Attributes of neural networks for extracting continuous vegetation variables from optical and radar measurements: *International Journal of Remote Sensing*, 19, 2639-2663.

King M.D. (Ed.), 1999: EOS – Science Plan, The State of Science in the EOS Program, NASA.

Knyazikhin, Y. V., A. L. Marshak, and R. B. Myneni, 1992: Interaction of Photons in a Canopy of Finite-Dimensional Leaves: *Remote Sensing of the Environment*, 39, 61-74.

Knyazikhin, Y., J. V. Martonchik, R. B. Myneni, D. J. Diner, and S. W. Running, 1998b: Synergistic algorithm for estimating vegetation canopy leaf area index and fraction of absorbed photosynthetically active radiation from MODIS and MISR data: *Journal of Geophysical Research*, 103, 32257-32275.

Kuusk, A., 1991: The inversion of the Nilson-Kuusk canopy reflectance model, a test case: Int. Geosci. and Remote Sens. Symp. (IGARSS'91), 1547-1550.

Lavabre J., D. Sempere-Torres and F. Cernesson, 1993: Changes in the hydrological response of a small Mediterraean basin a year after a wildfire. *J. Hydrol.* 142: 273-299

Leprieur, C., M. M. Verstraete, and B. Pinty, 1994, Evaluation of the performance of various vegetation indices to retrieve vegetation cover from AVHRR data: *Remote Sensing Reviews*, 10, 265-284.

Leroy, M., J. L. Deuzé, F. M. Bréon, O. Hautecoeur, M. Herman, V. Buriez, D. Tanré, S. Bouffiès, P. Chazette, and J. L. Roujean, 1997: Retrieval of atmospheric properties of surface bidirectional reflectances over land from POLDER: J. Geophys. Res., 102, 17023-17037.

Leshno, M., V. Ya Lin, et al., 1993: Multilayer feedforward networks with non polynomial activation function can approximate any function, *Neural Networks,* 6: 861-867.

Li, X., and A. H. Strahler, 1985: Geometric-Optical Modelling of a Conifer Forest Canopy: *IEEE Trans. Geoscience and Remote Sensing*, GE-23, 705-721.

Liang, S., and A. H. Strahler, 1993a: An analytical BRDF model of canopy radiative transfer and its inversion: *IEEE Trans. Geoscience and Remote Sensing*, 31, 1081-1092.

Liang, S., and A. H. Strahler, 1993b: Calculation of the Angular Radiance Distribution for a Coupled Atmosphere and Canopy: *IEEE Trans. Geoscience and Remote Sensing*, 31, 491-502.

Lindsay R.W., D.B. Percival, and D.A. Rothrock, 1996: The discrete wavelet transform and the scale analysis of the surface properties of sea ice, *IEEE Trans. Geoscience and Remote Sensing* 34 (3), 771-787.

Lucht, W., C. B. Schaaf, A. H. Strahler, J. P. Muller, B. Hu, P. Lewis, Y. Liu, A. H. Hyman, X. Li, M. J. Barnsley, N. C. Strugnell, and R. P. d'Entremont, 1998: At launch status of the MODIS BRDF/albedo algorithm: implementation, AVHRR-based prototyping, and future plans: IGARSS'98

Ludwig, R., Bach, H., Grüner, V., Mauser, W. ,1998: The Use of Imaging Spectrometer Data to Determine Vegetation Parameters for SVAT-Modelling, Proceedings of the EARSel Workshop on Imaging Spectroscopy, Zurich, 263-270.

Mackin, S., 1997: Study to investigate land degradation applications using a high resolution land-surface processes mission, ESTEC/ESA.

Mahfouf, J.F. et al., 1987: The influence of soil and vegetation of development of mesoscale circulation, *J. Appl. Meteor.*, 26, 1483-1495.

Mallat, S. A, 1989: Theory for multiresolution signal decomposition: The wavelet representation, *IEEE Trans. Pattern. Anal. Mach. Intel.,* 11(7), 674-693.

Mallat, S., 1993: A theory for multiresolution signal decomposition: The wavelet representation, *IEEE Trans. Pattern. Anal. Mach. Intel.,* 11(7), 674-693.

Marshak, A. L., 1989, The Effect of the Hot Spot on the Transport Equation in Plant Canopies: *Journal of Quantitative Spectroscopy and Radiation Transfer*, 42, 615-630.

Martonchik, J. V., D. J. Diner, et al., 1998: Determination of land and ocean reflective, radiative and biophysical properties using multiangle imaging, IEEE Transactions on Geoscience and Remote Sensing 36(4): 1266-1281.

Martonchik, J. V., D. J. Diner, R. A. Kahn, T. P. Ackerman, M. M. Verstraete, B. Pinty, and H. R. Gordon, 1998: Techniques for the retrieval of aerosol properties over land and ocean using multiangle imaging: *IEEE Trans. Geoscience and Remote Sensing*, 36, 1212-1227.

Mauser, W., 1991: The Use of Multitemporal TM- and SPOT-Data in a Geographical Information System to Model the Spatial Variability of Evapotranspiration, Proc. IGARSS'91, Helsinki, 59-62.

Mauser, W., 1997: Mesoscale Modelling of Evapotranspiration using Remote Sensing Data. SPIE Proceedings Series 2959:108-118.

Mauser, W., H. Bach and M. Rast., 1999: Remote Sensing - What will we get?. In: (J. Tenhunen and P. Kabat (Eds.). Integrating Hydrology, Ecosystem Dynamics and Biogeochemistry in Complex Landscapes. J. Wiley & Sons, Chichester, UK: 61-89

Mauser, W., and Schädlich, S., 1998: Modelling the Spatial Distribution of Evapotranspiration on Different Scale using Remote Sensing Data, *J. Hydrol.* (Special BAHC Issue), 212-213(1998)250.

Menenti, M. and B.J. Choudhury, 1993: Parameterization of land-surface evaporation by means of location dependent potential evaporation and surface temperature range. *IAHS publ.* 212: 561-568.

Menenti, M. and W. Verhoef, 1998: Spatial and Spectral Scales of Spaceborne Imaging Spectro-radiometers (SASSSIS), ESA contract, No. 12072/96/NL/CN, 289.

Menenti, M. and W.G.M. Bastiaanssen, 1997: Mesoscale climate hydrology: the potential of new Earth Observation Systems, Report 106. DLO- Winand Staring Centre, Wageningen, The Netherlands: 197 pp.

Menenti, M., and J. C. Ritchie, 1994: Estimation of effective aerodynamic roughness of Walnut Gulch watershed with laser altimeter measurements: *Water Resources Research,* 30, 1329-1337.

Mölders, N., and Raabe, A., 1998: Landscape Changes Over a Region in East Germany and Their Impact Upon the Processes of its Atmospheric Water-Cycle. *Meteorol. Atmos. Phys.* 68, 79-98.

Mölders, N., U. Strasser, K. Schneider, W. Mauser, A. Raabe, 1997: A Sensitivity Study on the Initialization of Surface Characteristics in Meso-b/g-modelling using Digitized vs. Satellite derived Landuse Data. Contrib. *Atmos. Phys.,* 70:173-187.

Monteith, J.L. and M.H. Unsworth, 1991: Principles of Environmental Physics, 2nd edition. Hodder and Stoughton, London.

Monteith, J.L., 1965: Evaporation and the environment. *Symp. Soc. Expl. Biol.,* 19: 205-234

Moreno, J.F. and R.O. Green, 1996: Surface and atmospheric retrieval from AVIRIS data: the importance of non-linear effects. Proceedings AVIRIS workshop. JPL, Pasadena, Ca.: 175-184

Moulin, S., A. Bondeau, and R. Delecolle, 1998: Combining agricultural crop models and satellite observations: from field to regional scales: *International Journal of Remote Sensing,* 19, 1021-1036.

Myneni, R. B. M. S. I. J., J. L. Privette, N. Gobron, B. Pinty, D. S. Kimes, M. M. Verstraete, and D. L. Williams, 1995: Optical Remote Sensing of Vegetation: Modelling, Caveats, and Algorithms: *Remote Sensing of the Environment*, 51, 169-188.

Myneni, R. B., and G. Asrar, 1993: Radiative Transfer in 3-Dimensional Atmosphere Vegetation Media: *Journal of Quantitative Spectroscopy and Radiative Transfer*, 49, 585-598.

Myneni, R. B., and J. Ross, 1991: Photon-vegetation interactions. Applications in optical remote sensing and plant ecology: Berlin Heiderberg New York, Springer Verlag, 565 p.

NASA, 1988: From Pattern to Process: The Strategy of the Earth Observing System, Eos Science Steering Committee Report, Volume II.

National Science Foundation, 1992: Our Changing Plant, 1-16.

Nilson, T., and A. Kuusk, 1989: A reflectance model for homogeneous plant canopy and its inversion: *Remote Sensing of the Enviroment*, 27, 157-167.

Noble, I.R., 1999: Effect of Landscape Fragmentation, Disturbance and Succession on Ecosystem Function, in: Integrating Hydrology, Ecosystem Dynamics, and Biogeochemistry in Complex Landscapes (Ed. J. Tenhunen & P. Kabat), 297-313, John Wiley & Sons

Norman , J. M., and J. L. Chen, 1990: Thermal emissivity and infrared temperatures dependence on plant canopy architecture and view angle: IGARSS'90, 1747-1750.

O'Neill, R.V., Hunsacker, C.T., Jones, K.B., Riitters, K.H., Wickham, J.D., Schwartz, P.M., Goodman, I.A., Jackson,B.L., Baillargeon, W.S., 1997: Monitoring Environmental Quality at the Landscape Scale, *BioScience*, 47, 8, 513-519.

Otterman, J., 1990: Inferring parameters for canopies non-uniform in azimuth by model inversion. *Remote Sensing of the Environment*, 33: 41-53

Painter, T.H., D.A. Roberts, R.O. Green and J. Dozier, 1998: The effect of grain size on spectral mixture analysis of snow-covered area from AVIRIS data. *Remote Sensing of the Environment,* 65: 320-332

Peltoniemi, J., 1993: Radiative Transfer in Stochastically Inhomogeneous Media: *Journal of Quantitative Spectroscopy and Radiation Transfer*, 50, 655-671.

Pernetta, J.C., Milliman, J.D., (Ed.), 1995: Land-Ocean Interaction in the Costal Zone. Implementation Plan, IGBP Report 33, IGBP Secretariat, Stockholm.

Pielke, R.A., G.Dalu and J.S.Snook et al., 1991: Nonlinear influence of mesoscale land use on weather and climate, *J. Climate*, 4, 1053-1069.

Pielke, R.A., Liston, G.E., Lu, L., and Avissar, R. 1999: Land-surface Influences on Atmospheric Dynamics and Precipitation: in: Integrating Hydrology, Ecosystem Dynamics, and Biogeochemistry in Complex Landscapes (Ed.: J. Tenhunen & P. Kabat), pp.105-117, John Wiley & Sons.

Pinty, B., and M. M. Verstraete, 1991: Extracting information on surface properties from bidirectional reflectance measurements: *J. Geophys. Res.,* 96, 2865-2874.

Pinty, B., and M. Verstraete, 1992: GEMI: A non linear index to monitor global vegetation from satellites: *Vegetation*, 101, 15-20.

Pinty, B., M.M. Verstraete, and R.E. Dickinson, 1989: A physical model for predicting bidirectional reflectances over bare soils: *Remote Sensing of the Environment*, 27, 273-288.

Pinty, B., M.M. Verstraete, and R.E. Dickinson, 1990: A physical model of the bidirectional reflectance of vegetation canopies. 2. Inversion and validation: *J. Geophys. Res.*, 95, 11767-11775.

Pitman A.J. et al. (39 authors), 1993: PILPS results from off-line control simulations (phase 1a) IGPO Publication Series No. 7, 47pp.

Prata, A.J., and R. P. Cechet, 1999: An assessment of the accuracy of land-surface temperature determination from the GMS-5 VISSR: *Remote Sensing of the Environment*, 67, 1-14.

Price, J.C., 1990: On the information content of soil reflectance spectra: *Remote Sensing of the Environment*, 33, 113-121.

Price, J.C., 1994a: A band selection procedure for multispectral scanners: *Applied Optics*, 33, 3281-3288.

Price, J., 1994b: How unique are spectral signatures?: *Remote sensing of the Environment*, 49, 181-186.

Privette, J.L., T. Eck, and D.W. Deering, 1997: Estimating spectral albedo and nadir reflectance through inversion of simple BRDF models with AVHRR/MODIS-like data: *J. Geophys. Res.*, 102, 29529-29542.

Privette, J.L., W.J. Emery, and D.S. Schimel, 1996: Inversion of a vegetation reflectance model with NOAA AVHRR data: *Remote Sensing of the Environment*, 58, 187-200.

Rahman, H., 1998: Inferring spectral surface albedo from bidirectional reflectance measurements: *Geocarto International*, 13, 41-46.

Renders, J.-M., and S. p. Flasse, 1996: Hybrid Methods Using Genetic Algorithms for Global Optimization: *IEEE Trans. Systems, Man, and Cybernetics*, 26, 243-258.

Ross, J., 1981: The Radiation Regime and Architecture of Plant Stands: Boston, W. Junk.

Ross, J., and A.L. Marshak, 1988: Calculation of the Canopy Bidirectional Reflectance Using the Monte-Carlo Method: *Remote Sensing of the Environment*, 24, 213-225.

Rossow W.B., P.J. Gardner and A. Walker, 1988: International Satellite Cloud Climatology Project (ISCCP) documentation on cloud data, Rep. WMO/TD n°26, 78 pp, World Meteorogical Organisation, Geneva, Switzerland,

Schädlich, S., and Mauser, W., 1996: Spatial evapotranspiration calculation on a microscale test site using the GIS-based PROMET-model. In: Application of Geographic Information Systems in Hydrology and Water Resources Management (ed. by Kovar, K. & Nachtnebel, H.P.), IAHS Publ. No. 235:649-657.

Schneider, K., 1999: Spatial Modelling of Evapotranspiration and Plant Growth in a Heterogeneous Landscape with a coupled Hydrology-Plant Growth Model utilizing Remote Sensing. Proc. Internat. Conf. on Spatial Statistics for Production Ecology Vol. 4 (in press).

Segal, R. Avissar, M. C. McCumber and R. A. Pielke, 1988: Evaluations of vegetation effects on the generation and modification of mesoscale circulations. *J. Atmos. Sci.,* 45, 2268-2292.

Sellers, P.J., 1985: Canopy reflectance photosynthesis and transpiration: *International Journal of Remote Sensing*, v. 3, p. 1335-1372.

Sellers, P. J., 1987: Canopy reflectance, photosynthesis and transpiration. II. The role of biophysics in the linearity of their dependence: *International Journal of Remote Sensing*, 21, 143-183.

Shultis, J. K., and R. B. Myneni, 1988: Radiative Transfer in Vegetation Canopies With Anisotropic Scattering: *Journal of Quantitative Spectroscopy and Radiation Transfer*, 39, 115-129.

Simmer, C., and S.A. Gerstl, 1985: Remote Sensing of Angular Characteristics of Canopy Reflectances: *IEEE Trans. Geoscience and Remote Sensing*, GE-23, 648-658.

Smith, J.A., 1992: LAI inversion from optical reflectance using neural network trained with multiple scattering model.: IGARS'92, 757-759.

Smith, J.A., 1993: LAI inversion using backpropagation neural network trained with multiple scattering model, *IEEE Trans. Geoscience and Remote Sensing*, 31(5): 1102-1106.

Smith, J.A.a nd S.M. Goltz, 1995: A thermal exitance and energy balance model for forest canopies. *IEEE Trans. Geosc. Remote Sensing*. 32(5): 1060- 1066

Smith, T.M., Shugart, H.H., Woodward, F.I. (Ed.), 1997: Plant Functional Types, International Geosphere-Biosphere Programme Book Series No.1, Cambridge University Press.

Sobrino, J.A., and V. Caselles, 1990: Thermal infrared model for interpreting the directional radiometric temperature: *Remote Sensing of the Environement*, 33, 193-199.

Steffen, W., et al. (Ed.), 1992: Global Change and Terrestrial Ecosystems: The Operational Plan. IGBP Report 21, IGBP Secretariat, Stockholm.

Suits, G. H., 1972: The calculation of the directional reflectance of a vegetative canopy: *Remote Sensing of the Environment*, 2, 117-125.

Tarantola, A., 1987: Inverse problem theory. Methods for data fitting and model parameter estimation, Elsevier Science Publisher B.V.

Tenhunen, J.D., Geyer, R., Valentini, R., Mauser, W., and Cernusca, A., 1999: Ecosystem Studies, Land-use Change, and Resource Management, in: Integrating

Hydrology, Ecosystem Dynamics, and Biogeochemistry in Complex Landscapes (Ed.: J. Tenhunen & P. Kabat), pp. 117-147, John Wiley & Sons.

Tenhunen, J.D., Valentini, R., Köstner, B., Zimmermann, R., and Granier, A., 1998: Variation in Forest Gas Exchange at Landscape to Continental Scales, *Ann. Sci. For.*, 55, 1-11.

Tsai, F and W. Philpot, 1998: Derivative analysis of hyperspectral data. *Remote Sensing of the Environment,* 66: 41-51.

Turner, B.L. II, et al. (Ed.), 1995: Land-Use and Land-Cover Change. Science/Research Plan. IGBP Secretariate Stockholm, HDP Secretariat, IGBP Report 35/HDP Report 7.

United Nations, 1997: Comprehensive Assessment of the Freshwater Resources of the World, New York.

Valentini, R., Baldocchi, D.E., Tenhunen, J.D., 1999: Ecological Controls of Land-Surface Atmospheric Interactions, in: Integrating Hydrology, Ecosystem Dynamics, and Biogeochemistry in Complex Landscapes (Ed.: J. Tenhunen & P. Kabat), 117–147, John Wiley & Sons.

Verhoef, W., 1984: Light scattering by leaf layers with application to canopy reflectance modelling: the SAIL model: *Remote Sensing of the Environment*, 16, 125-141.

Vermote, E.F., D. Tanré, J.L. Deuzé, M. Herman, and J.J. Mocrette, 1997: Second simulation of the satellite signal in the solar spectrum, 6S: an overview: *IEEE Trans. Geoscience and Remote Sensing*, 35, 675-686.

Verstraete, M.M., B. Pinty, and R.E. Dickinson, 1990: A physical model of the bidirectional reflectance of vegetation canopies. 1. Theory: *J. Geophys. Res.,* 95, 11755-11765.

Verstraete, M.M., B. Pinty, and R. Myneni, 1996: Potential and limitations of information extraction on the terrestrial biosphere from satellite remote sensing: *Remote Sensing of the Environment*, 58, 201-214.

Verstraete, M.M., and B. Pinty, 1996: Designing optimal spectral indexes for remote sensing applications: *IEEE Trans. Geoscience and Remote Sensing*, 34, 1254-1265.

Vine, P., C. Puech and J.M. Gresillon, 1999: Mapping vegetation re-growth by remote sensing to interpret the hydrological impact of fire. In : A. Pietroniro (ed.). *Applications of Remote Sensing in Hydrology* (in press).

Walker, B.H., and Steffen, W. (Ed.), 1996: Global Change and Terrestrial Ecosystems, International Geosphere-Biosphere Programme Book Series No.2, Cambridge University Press.

Walker, B.H., and Steffen, W. (Ed.), 1999: The Terrestrial Biosphere and Global Change: Implications for Natural and Managed Ecosystems, IGBP Book Series No.4, Cambridge University Press.

Wan, Z.M. and W. Snyder, 1996: MODIS Land-Surface Temperature Algorithm Theoretical Basis Document (MOD-11-LST). NASA. 73 p.

Wang, J.M. and Y. Mitsuta, 1992: Evaporation from the desert: Some preliminary results of HEIFE. *Boundary-Layer Meteor.,* 59, 413-418.

Wang, J.M., Y. Hu, K. Sakashi and Y. Mitsuta, 1994: Outline of HEIFE field observations. In: Y. Mitsuta (ed.). Proc. Intern. Symp. on HEIFE. Disaster Prevention Research Institute. Kyoto University: 22- 29.

Wanner, W., A. H. Strahler, et al., 1997: Global retrieval of bidirectional reflectance and albedo over land from EOS MODIS and MISR data: Theory and algorithm, *J. Geophys. Res.,* 102(D14): 17143-17161.

Waring, R.H., and Running, S.W., 1999: Remote Sensing Requirements to Drive Ecosystem Models at the Landscape and Regional Scale, in: Integrating Hydrology, Ecosystem Dynamics, and Biogeochemistry in Complex Landscapes (Ed.: J. Tenhunen & P. Kabat), pp. 23-39, John Wiley & Sons.

Waring, R.H., Running, S.W., 1998: Forest Ecosystems. Analysis at multiple Scales, Academic Press, San Diego, 370.

Weiss, M., 1998: Développement d'un algorithme de suivi dela végétation à large échelle: PhD thesis , Ecole des Mines de Paris/ INRA Bioclimatologie Avignon, 174 pages.

Weiss, M., and F. Baret, 1999: Evaluation of canopy biophysical variables retrieval performances from the accumulation of large swath satellite data: *Remote Sensing of the Environment,* v. in press

Weiss, M., F. Baret, M. Leroy, A. Begué, and R. Santer, 1999a: Hemispherical reflectance and albedo estimates from the accumulation of across track sun synchronous satellite data: *J. Geophys. Res.,* v. in press

Weiss, M., F. Baret, R. Myneni, A. Pragnère, and Y. Knyazikhin, 1999b: Investigation of a model inversion technique for the estimation of crop charcteristics from spectral and directional reflectance data: *Agronomie,* v. in press.

Wood, E.F. and E. Lakshmi, 1992: Scaling water and energy fluxes in climate systems: Three land atmospheric modelling experiments. *J. Climate,* 6, 839-857.

Xue,Y., and J. Shukla, 1993: The influence of surface properties on Sahel climate. Part I: desertification, *J.Climate*, 6, 2232-2245.

GLOSSARY

Abbreviations and acronyms:

ADC	Analogue to Digital Converter
ADEOS	Advanced Earth Observation System
Airborne BIRD	Bi-spectral Infrared Detection
AirMISR	Airborne Multi-angle Imaging Spectro-Radiometer
AISA	Airborne Imaging Spectrometer for different Applications
Albedo	Spectrally integrated hemispherical reflectance of sunlight
ALOS	Advanced Land Observation System
AOCS	Attitude and Orbit Control System
APEX	Airborne PRISM Experiment
APU	Analogue Processing Unit
ARIES	Australian Resource Information and Environment Satellite
ASAS	Advanced Solid-State Array Spectroradiometer
ASIC	Application Specific Integrated Circuit
ASTER	Advanced Spaceborne Thermal Emission and Reflection Radiometer
ATP	Across Track de-Pointing
ATSR	Along Track Scanning Radiometer (onboard ERS-1/2)
AVHRR	Advanced Very High Resolution Radiometer
AVIRIS	Airborne Visible/Inrared Imaging Spectrometer
BAHC	Biospheric Aspects of the Hydrological Cycle (Core Project of IGBP)
BOREAS	BOReal Ecosystem-Atmosphere Study
BRDF	Bi-directional Reflectance Distribution Function
BRF	Bi-directional Reflectance Function corresponds to BRFD sampling
CASI	Compact Airborne Spectrographic Imager
CBL	Convective Boundary Layer
CCD	Charge-Coupled Device
CCSDS	Consultative Committee for Space Data Systems
CCU	Cryocooler Control Unit
CDAE	Command & Data Acquisition Element
CdHgTe	Cadmium Mercurium Tellurium
CEOS	Committee on Earth Observation Satellites
CERES	Clouds and Earth's Radiant Energy System
CHRIS/PROBA	Compact High Resolution Imaging Spectrometer/ Project for On-Board Autonomy
CMOS	Complementary Metal Oxide Semiconductor
CSS	Coarse Sun Sensor
DAIS 7915	Digital Airborne Imaging Spectrometer
DC	Direct Current (0 Hz)

DH&C	Data Handling and Control
DIVERSITAS	Internal Programme on Biodiversity
DOD	Depth of Discharge
DSR	Digital Series Regulator
DU	Detection Unit
DWT	Discrete Wavelet Transform
EFEDA	European Field Experiment in Desertification-threatened Area
EMC	Electro-Magnetic Compatibility
EOL	End of Lifetime
EQFM	Engineering and Qualification Module
ERBE	Earth Radiation Budget Experiment
ESF	Engineering Support Facilities
ESOC	European Space Operation Centre
ET	Evapo-Transpiration
fAPAR	Fractional Absorbed Photosynthetic Active Radiance
FDIR	Failure Detection, Isolation and Recovery
FIFE	First ISLSCP Field Experiment
FOV	Field Of View
FPA	Focal Plane Array
GCM	General Circulation Model
GCOS	Global Climate Observation System
GCP	Ground Control Point
GCTE	Global Change and Terrestrial Ecosystems
GERB	Geostationary Earth Radiation Budget experiment
GEWEX	Global Energy and Water Cycle Experiment
GIS	Geographical Information Systems
GS	Ground Segment
GSP	Global System Planning
GTOS	Global Terrestrial Observation System
HAPEX	Hydrology-Atmospheric Pilot Experiment
HEIFE	Hei He Field experiment
HYDICE	Hyperspectral Digital Imagery Collection Experiment
ICSU	International Council of Scientific Unions
ICU	Instrument Control Unit
IECF	Instrument Engineering Calibration Facility
IEEE	Institute of Electrical and Electronics Engineers
IEOS	International Earth Observing System
IFOV	Instantaneous Field Of View
IGBP	International Geosphere Biosphere Programme
IHDP	International Human Dimensions Programme
ISLSCP	International Satellite Land-Surface Climatology Project
LAI	Leaf Area Index
Landsat ETM	Land Remote Sensing Satellite – Enhanced Thematic Mapper

LBA	Lambada Baterista Abracos
LEOP	Launch and Early Orbit Phase
LIDF	Leaf Inclination Distribution Function
LIDF	Leaf Inclination Distribution Function
LOI	Line Of Illumination
LOICZ	Land Ocean Interaction in the Coastal Zone
LOS	Line Of Sight
LSE	Land Surface Emissivity
LSF	Large Scale Facility
LSPIM	Land-Surface Processes and Interactions Mission
LST	Land Surface Temperature
LUCC	Land Use and Land Cover Change
MAC'91	Multisensor Airborne Campaign 1991
MAG	Magnetometer
MAS	MODIS Airborne Simulator
MASTER	MODIS/ASTER Airborne Simulator
MCF	Monitoring & Control Facility
MERIS	Medium Resolution Imaging Spectrometer
METOP	Meteosat Operational Programme
MISR	Multi-angle Imaging Spectro-Radiometer
MIVIS	Multispectral Infrared and Visible Spectrometer
MMU	Mass Memory Unit
MODIS	Moderate Resolution Imaging Spectrometer
MPS	Mission Planning System
MSCE	Mission Operations and Control Element
MTB	Magneto-Torquer Bars
MTF	Modulation Transfer Function
NEDL	Noise Equivalence Difference Radiance
NEDT	Noise Equivalence Difference Temperature
NEMO	Naval Earth-Map Observer
NiCd	Nickel Cadmium
NIR	Near Infra-Red
NOM	Normal Operation Mode
NPP	Net Primary Production
OCM	Orbit Control Mode
PAE	Processing and Archiving Element
PAF	Processing and Archiving Facility
PCE	Power Conditioning Electronics
PD	Proportional-Derivative
PDS	Payload Data Segment
PDU	Power Distribution Unit
PIB	Proximity Interface Box
PILPS	Project for Intercomparison of Land-surface Parameterisation Schemes
Pixel	Picture Element

PLM	Payload Module
POLDER	Polarization Directionality of the Earth's Reflectance
PRDC	Packetizing Rice Data Compressor
PRISM	Processes Research by an Imaging Space Mission (the Space Segment of the LSPIM)
PROMET	Process-Oriented Multiscale Evapo-Transpiration model
Proxel	Process Element
RGT	Reference operation plan Generation Tool
RMS	Root Mean Square
ROSIS	Reflective Optics System Imaging Spectrometer
SAR	Synthetic Aperture Radar
SCARAB	Scanner for Earth Radiation Budget
SCOS	Spacecraft Operation System
SDC	Scientific Data Centre
SHM	Safe Hold Mode
Si	Silicon
SMIFTS	Spatially Modulated Imaging Fourier Transform Spectrometer
SMU	Satellite Management Unit
SNR	Signal to Noise Ratio
SPOT HRV	Systeme Probatoire d'Oberservation de la Terre, High Resolution Visible
SPOT Vegetation	VEGETATION onboard SPOT 4, SPOT 5
SRB	Surface Radiation Budget
SSI	Spectral Sampling Interval
STR	Star Tracker
SVAT	Soil Vegetation Atmosphere Transfer
SW	Split Window
SWIR	Short Wave Infra-Red (1300 – 2500nm)
TDD	Temperature Directional Distribution
TIMS	Thermal Infrared Multispectral Scanner
TIR	Thermal Infra-Red
TM/TC	Telemetry and Telecommand
TMA	Three Mirror Anastigmat
TOA	Top Of Atmosphere
TT&C	Telemetry and Telecommand
UNEP	United Nations Environmental Programme
VNIR	Visible/Near Infra-Red
WCRP	World Climate Research Programme

Land-surfaces processes terminology:

Albedo	Fraction of the total solar radiation incident on a body that is reflected by it.
Biomass	The total dry organic matter or stored energy content of living organisms that is present at a specific time in a defined unit (community, ecosystem, etc.) of the Earth's surface.
Biome	Biotic community of plants and animals.
Carbon Cycle	Sequence of conversion processes from matter into energy. All reservoirs and fluxes of carbon; usually thought of as a series of the four main reservoirs of carbon interconnected by pathways of exchange (atmosphere, terrestrial biosphere, oceans and sediments). Carbon is exchanged from reservoir to reservoir by various chemical, physical, geological, and biological processes.
Climatology	Quantitative spatio-temporal analysis of meteorological variables characterising the climate of a given location or region.
Ecosystem	The unit of ecology is the ecosystem, which includes the plants and animals occurring together plus that part of their environment over which they have an influence.
Emissivity	The ratio of radiative energy (power) emitted by a body to that emitted by a blackbody at the same temperature.
Hot Spot	Also called 'opposition effect': local maximum (zero phase angle) in the BRDF corresponding to shadowing function equal to one.
Imaging Spectrometry	The simultaneous acquisition of images in many (often contiguous) spectral bands.
Modelling	An investigative technique that uses a mathematical or physical representation of a system or theory that accounts for all or some of its known properties. Models are often used to test the effects of changes of system components on the overall performance of the system.

Parameter	A quantity which is constant (as distinct from the ordinary variables) in a particular case considered, but which varies in different cases.
Photosynthesis	The conversion of inorganic matter into organic matter by plants, using light as the energy source.
Primary Production	The accumulation of organic matter, carbon, or energy.
Primary Productivity	Rate at which the primary production occurs.
Spectrometer	A device to detect, measure and analyse the spectral content of the incident radiation by dispersing it into spectral intervals (bands).

Acknowledgements

We are grateful for the valuable contributions from U. del Bello, M. Berger, A. Caramagno, C. Jacobs, J.-Y. Labandibar, J. Moreno, H. Pelgrum, W. Verhoef, P. Vogt and M. Weiss

Thanks are also extended to C. Readings, M.L. Reynolds and A. Tobias for their time and effort in reviewing the document, and to D. Reinprecht for preparing the document for publication.

European Space Agency
Agence spatiale européenne

Contact: ESA Publications Division
c/o ESTEC, PO Box 299, 2200 AG Noordwijk, The Netherlands
Tel. (31) 71 565 3400 - Fax (31) 71 565 5433